Formation of bioscorodite for stabilization of arsenic species derived from bio-mineral processing

田中, 雅仁

https://doi.org/10.15017/1931893

出版情報：Kyushu University, 2017, 博士（工学）, 課程博士
バージョン：
権利関係：

KYUSHU
UNIVERSITY

Formation of bioscorodite for stabilization of arsenic species derived from bio-mineral processing

by

Masahito Tanaka

Department of Earth Resources Engineering
Graduate School of Engineering
Kyushu University
Fukuoka, Japan

A thesis submitted to Kyushu University
for the degree of Doctor of Engineering

March 2018

Abstract

Bio-mineral processing (bioleaching and biooxidation) is considered as one of the most effective approaches to recover valuable metals (i.e. Cu, Au, Ag), especially from low-grade refractory mineral ores and concentrates. Arsenic (As) is a major impurity contaminated in metal refinery wastewaters including those deriving from bio-mineral processing, and its economically-viable and environmentally-friendly removal technique is needed. This thesis firstly demonstrated the applicability of biooxidation of highly refractory As-bearing Au-ore concentrates, and secondly investigated the factors that enable effective bioscorodite ($FeAsO_4 \cdot 2H_2O$) crystallization using the thermo-acidophilic Fe(II)-oxidizing archaeon, *Acidianus brierleyi* from dilute As(III)-bearing acidic solutions (3.3–20 mM): i.e. (i) $[Fe(II)]_{ini}/[As(III)]_{ini}$ molar ratios, (ii) initial pH values, (iii) seed-feeding, (iv) SO_4^{2-} ions. Moreover, in order to evaluate microbial effect on bioscorodite crystallization, the utility of different thermo-acidophilic Fe(II)- and sulfur-oxidizing archaeal strains (*Sulfolobus metallicus* Kra23, *S. tokodaii* 7, *S. acidocaldarius* 98-3 and *Metallosphaera sedula* TH2) was also evaluated.

In **chapter 1**, background information about As properties, current As immobilization techniques and scorodite synthesis methodologies (abiotic/biotic approaches) were overviewed. Based on these backgrounds, the motivation and objectives of this thesis were presented.

In **chapter 2**, methodologies used in this work were described.

In **chapter 3**, effectiveness of different pure and mixed cultures of three moderately thermophilic bacterial strains (*Acidimicrobium ferrooxidans* ICP, *Sulfobacillus sibiricus* N1 and *Acidithiobacillus caldus* KU) were investigated for biooxidation of As-bearing highly refractory polymetallic Au-ore concentrates. Despite of the complex mineralogy and the presence of a mixture of potentially inhibitory metals and metalloids, the concentrates were readily dissolved in defined mixed cultures including both iron and sulfur oxidizers, releasing as much as 80% of soluble Fe and 61% of soluble As at 45°C. Partial As was immobilized as amorphous ferric arsenate, but not as crystalline scorodite. Applying the biooxidation pretreatment improved the recovery of both Au (from 1.1% to 86%) and Ag (from 3.2% to 87%), which was shown to be one of the most effective options compared with other abiotic

pretreatment approaches (roasting, pressure oxidation, and alkali dissolution).

From **chapter 4** to **chapter 6**, bioscorodite crystallization tests were conducted using *Ac. brierleyi* at 70°C. In **chapter 4**, a range of dilute As(III) solutions (3.3–20 mM) with varying $[Fe(II)]_{ini}/[As(III)]_{ini}$ molar ratios (0.8–6.0) were tested. Bioscorodite was crystallized in the $[Fe(II)]_{ini}/[As(III)]_{ini}$ ranges of 0.8–2.0. Generally, 94–99% of As was successfully removed as crystalline bioscorodite by setting the $[Fe(II)]_{ini}/[As(III)]_{ini}$ molar ratios at 1.4–2.0. Molar ratio of over 2.5 resulted in the formation of amorphous ferric arsenate or jarosite. Lowering the initial pH from 1.5 to 1.2 using bioscorodite seeds lead to a steady and continuous formation of bioscorodite particles, but As removal remained relatively incomplete at pH 1.2 (91%), compared to at pH 1.5 (98%). Formation of amorphous precursors at pH 1.5 played an important role to achieve the maximum As removal from dilute As(III) solutions by inducing two-stage As and Fe precipitations.

In **chapter 5**, the effect of seed-feeding on bioscorodite crystallization from dilute 4.7 mM As(III) solution was investigated from the viewpoint of morphological and structural differences of two types of scorodite seeds; (i) bioscorodite seeds (lower-density, finer particles) and (ii) chemical scorodite seeds (higher-density, coarse particles). Feeding bioscorodite seeds enabled effective As removal from dilute As(III) solution (98% final As removal at day 21). When bioscorodite seeds were fed, hollow seed particles became increasingly filled with newly formed scorodite. On the other hand, solid chemical seeds induced their surface to be thoroughly coated with new scorodite precipitates. TCLP (Toxicity Characteristic Leaching Procedure) leachabilities of final bioscorodite products formed on bioscorodite or chemical scorodite seeds were 0.59 ± 0.08 mg/l or 1.86 ± 0.05 mg/l, respectively. The values satisfied the regulatory limit of As set by the US EPA (United States Environmental Protection Agency). Utilization of seed crystals with highly positive surface charge, such as hematite (+ 60 mV at pH 2) and bioscorodite (+ 50 mV at pH 2), enabled effective bioscorodite crystallization, owing to their property as absorbent of anionic As(V) ($H_2AsO_4^-$) and less positively charged *Ac. brierleyi* cells (+ 5 mV at pH 2).

In **chapter 6**, behavior of SO_4^{2-} ions during bioscorodite formation was investigated by liquid/solid characterization analyses, and the mechanism of bioscorodite crystallization process (2-stage process consisting of precursor formation and transformation into crystalline scorodite) was elucidated. During the 1st-stage

As-removal, brown-colored amorphous precursors were formed by precipitation of mixture of basic ferric sulfate ($MFe_x(SO_4)_y(OH)_z$) and ferric arsenate ($FeAsO_4 \cdot (2+n)H_2O$). During the following equilibrium state (induction period), the cycle of dissolution and recrystallization of the above precursors likely proceeded: As a result, higher solubility basic ferric sulfate and ferric arsenate particles mostly dissolved and released Fe(III), which were able to further react with the remaining As(V) ions in bulk solution. These precipitates formed a passivation layer on the surface of precursor particles, followed by bioscorodite crystallization (2nd-stage As-removal). Since the above bioscorodite crystallization process was made possible only in the presence of SO_4^{2-} ions, formation of intermediate basic ferric sulfate was thought to be the key trigger for effective As removal.

In **chapter 7**, the alternative archaeal strains were tested for bioscorodite crystallization; *S. metallicus* Kra23, *S. tokodaii* 7, *S. acidocaldarius* 98-3 and *M. sedula* TH2. Partial As(III) oxidation was observed only in *M. sedula* TH2 culture in the presence of Fe(II) and elemental sulfur. Bioscorodite was successfully crystallized in *M. sedula* culture containing 6.5 mM As(III), 9 mM Fe(II) and 0.1% (w/v) elemental sulfur at pH 1.5 on day 23. In the absence of Fe(II), microbial As(III) oxidation was not observed regardless of the presence/absence of elemental sulfur and yeast extract. This result implied that the presence of Fe(II) induced microbial As(III) oxidation ability of *M. sedula* TH2.

In **chapter 8**, the main conclusions of this work were summarized.

要旨

主要有価金属の世界的な需要増大、およびこれらを含む高品位鉱石の枯渇に伴い、特にその毒性が問題視されるヒ素 (As) を含有するような低品位・難処理性鉱石に対する有効な資源処理プロセスの開発が必須となってきている。微生物反応を利用して鉱物溶解を促進するバイオミネラルプロセッシングは上記課題に対する有効な方法の一つとして期待されている。本博士論文は、バイオミネラルプロセッシングにより発生した亜ヒ酸含有酸性製錬廃液を対象とした、バイオスコロダイト ($FeAsO_4 \cdot 2H_2O$) 法によるヒ素回収に関する研究論文である。

第 1 章では、湿式製錬による溶液中へのヒ素の混入およびその不動化に関する研究内容について総括した。酸性溶液からのヒ素不動化法として、化学的および微生物学的スコロダイト生成に関する先行研究をまとめ、微生物学的手法を用いる利点および今後の課題について述べた。それを踏まえ、低濃度 As(III)溶液からのバイオスコロダイト生成における各種条件検討および生成メカニズムの解明を本研究の目的とした。

第 2 章では、本論文中の実験方法および分析方法について記述した。

第 3 章では、異なる生理学的特徴をもつ中度好熱好酸性・鉄硫黄酸化細菌 3 種を組み合わせ、アラスカ産難処理金鉱石に対するバイオオキシデーションの効率化及び有効性の検討を行った。3 種の細菌株の組み合わせにより、難処理金鉱石の浸出率は顕著に向上した。バイオオキシデーションを前処理としたシアンリーチングでは、最終金銀回収率は、Au 1.2%から 91%、Ag 3.3%から 89%へと大幅に向上し、他の 3 種の前処理方法と比較してその優位性が示された。浸出した一部の As(III)は非晶質 ferric arsenate ($FeAsO_4 \cdot nH_2O$) として不動化していたが、結晶性スコロダイトの生成は微視的に確認されるに留まった。

第 4 章では、好熱・好酸性鉄硫黄酸化古細菌 *Acidianus brierleyi* を利用したバイオスコロダイト生成における、初期[Fe(II)]/[As(III)]モル比および初期 pH の影響について評価した。対象 As(III)濃度 3.3–20 mM において、初期[Fe(II)]/[As(III)]モル比 0.8–2.0 にてバイオスコロダイト生成が行われた。また、モル比を 1.4–2.0 に設定することで最終 As 不動化率 95%以上を達成した。モル比を 2.5 以上に設定した場合、非晶質 ferric arsenate および jarosite ($KFe_3(SO_4)_2(OH)_6$) の生成が確認され、低濃度 As(III)溶液からのバイオスコロダイト生成における初期[Fe(II)]/[As(III)]モル比設定の重要性が示された。pH の影響として、初期 pH 1.5 の場合は通常前駆体生成を伴った典型的な 2 段階の As 濃度減少が見られたが、初期 pH 1.2 の場合は、前駆体生成が行われずに速やかにバイオスコロダイトが生成した。しかし、最終 As 不動化率は 98%から 91%へと却って減少する結果となり、前駆体生成が最終 As 不動化率改善に影響を及ぼすことが示された。

第 5 章では、種結晶添加の影響として、異なる結晶性および形状を持つスコロダイト種結晶について評価を行った。高比表面積で空隙を持つバイオスコロダイト種結晶を使用することにより、バイオスコロダイト生成が促進されることが明らかとなった。使用した種結晶によって結晶成長過程に次のような違いが見られた。高密度の化学合成スコロダイト種結晶を用いた場合は、種結晶表面を覆うようにバイオスコロダイトが生成していたが、バイオスコロダイト種結晶を用いた場合はその空隙を埋めていくように結晶が成長した。毒性評価溶出試験 (TCLP; Toxicity Characteristic Leaching Procedure) による最終産物の安定性評価を行ったところ、As 溶出量は米国環境保護庁 (US EPA; United States Environmental Protection Agency) が設定した基準値未満であり、バイオスコロダイトの十分な安定性が確認された。また、バイオスコロダイトやヘマタイトのように正に帯電した種結晶を利用することで、負電荷を持つヒ酸および *Ac. brierleyi* 細胞の吸着材として作用し、バイオスコロダイトが速やかに生成することが示された。

第 6 章では、硫酸イオンがバイオスコロダイト生成に及ぼす影響およびバイオスコロダイト生成機構について考察を行った。放射光分析等の結果を総合的に解釈すると、黄褐色の非晶質前駆体が 2 種類の沈殿により構成されることが示された。まず、1 段階目の As 濃度減少では、塩基性硫酸第二鉄 ($MFe_x(SO_4)_y(OH)_z$) を主とする前駆体が生成し、その溶解・再結晶による定常状態が数日継続した。これに伴い、非晶質ヒ酸塩の結晶成長が起こり、最終的に結晶性バイオスコロダイトが形成されることによって、2 段階目の As 濃度減少が認められたと考えられる。低 As(III)濃度域においては、硫酸イオン非存在下で沈殿が生成しないことから、塩基性硫酸第二鉄を含む前駆体の生成がバイオスコロダイト生成に大きく寄与していることが示された。

第 7 章では、*Ac. brierleyi* の近縁種である、好熱好酸性・鉄硫黄酸化古細菌 4 株を利用した亜ヒ酸酸化およびバイオスコロダイト生成を試みた。*Metallosphaera sedula* TH2 株を利用したバイオスコロダイト生成実験 (初期 As(III)濃度 6.5 mM) において、速やかに Fe(II)酸化が行われた後、緩やかな As(III)酸化が観察され、23 日以内にバイオスコロダイトの生成が確認された。As(III)酸化機構について、Fe(II)未添加では As(III)酸化が行われなかった。Fe(III)–As(III)の化学的酸化還元カップリング反応が疑われるものの、他の古細菌株では As(III)酸化が見られなかったことから、*M. sedula* TH2 による微生物学的 As(III)酸化が行われたことが示唆される。

第 8 章では、本博士論文の結論として、各実験結果の総括を行い、難処理金鉱石への前処理プロセスとしてバイオオキシデーション法が、また低濃度 As(III)含有廃液からのヒ素不動化プロセスとしてバイオスコロダイト法が有効であることを示した。

Contents

Chapter 2

List of Tables

List of Figures

Abbreviations

Ac.	*Acidianus*
Am.	*Acidimicrobium*
At.	*Acidithiobacillus*
As(III)	arsenite (H_3AsO_3)
As(V)	arsenate ($H_2AsO_4^-$)
ATR-FTIR	attenuated total reflection-Fourier transform infrared spectroscopy
BET	Brunauer–Emmett–Teller
EPA	environmental protection agency
EPS	extracellular polymeric substances
HBS	heterotrophic basal salts
IAP	ion activity products
ICP-OES	inductively coupled plasma optical emission spectrometry
M.	*Metallosphaera*
Fe(II)	ferrous iron (Fe^{2+})
Fe(III)	ferric iron (Fe^{3+})
FT-IR	Fourier transform infrared spectrometer
PCR	polymerase chain reaction
S.	*Sulfolobus*
Sb.	*Sulfobacillus*
SEM	scanning electron microscope
SSA	specific surface area
TCLP	toxicity characteristic leaching procedure
TG-DTA	thermo gravimetry differential thermal analysis
w/v	weight per volume
XRD	X-ray diffraction
XAFS	X-ray absorption fine structure
XANES	X-ray absorption near-edge structure
[ ]	concentration of ion species
$[\ ]_{im}$	immobilized concentration of ion species in solid
$[\ ]_{ini}$	initial concentration of ion species in solution

Chapter 1

Introduction

1.1 Introduction

Arsenic (As) is the 20th most abundant element in the earth's crust. As belongs to a metalloid group, and it had been used in various fields such as herbicides and insecticides. However, As has the risks for human health. Since As is a carcinogen, the World Health Organization (WHO) revised the environmental regulation for arsenic exposure from 0.050 to 0.010 mg/L in 1993 (Leist et al., 2000; WHO, 2001). The occurrence of As includes natural sources and anthropogenic sources. Natural sources is derived from the dissolution of As in minerals as a long-term consequence of rock weathering, downstream transport and sediment deposition of arsenic-rich minerals (Oremland and Stolz, 2005). The influence of microorganisms is also considerable on the kinetics. The dissolution of unwanted metals/metalloids in nature is depending on the difference of redox potential by microbial metal oxidation or reduction (Harrington et al., 1998). As a result, serious groundwater arsenic problems are reported in many part of world such as Argentina, Bangladesh, Chile, China, Hungary, India (West Bengal), Mexico, Romania, Taiwan, Vietnam and many parts of the USA (Boyle and Jonasson, 1973; Smedley and Kinniburgh, 2002). Anthropogenic origin is derived from human activities such as mining, manufacturing, wood processing, glassmaking industry, electronics industry, chemical weapons and so on (Lièvremont et al., 2009). In metallurgical operation, As is a common impurity because it is associated with sulfide minerals of sulfur, iron, copper, gold, silver, etc. Depending on the processing of these sulfide minerals, As is contaminated to the refinery wastewaters. Due to preventing the arsenic effluent, it is necessary to treat properly processing wastewater. Hence, As removal and immobilization from mining wastewater and groundwater has become an important issue from the viewpoint of the increase of its toxicity and byproduct amount.

1.2 Contamination of arsenic in aqueous solutions

1.2.1 Aqueous speciation of arsenic

Arsenic can exist in four oxidation states (3, 0, +3, +5). Specifically, trivalent arsenite (+3, As(III)) and pentavalent arsenate (+5, As(V)) is the predominant aquatic forms (Riveros et al., 2001). As shown in Figure 1, As(III) exists in the no valence form of H_3AsO_3 under neutral and acidic conditions (pK_{a1} = 9.23). In case of As(V), the species $HAsO_4^{2-}$ is predominant in acidic solutions, and main in neutral one. Under extremely acidic condition such as refinery wastewaters, no valence H_3AsO_4 is the predominant species. This is the reason why the mobility of As(III) is greater than As(V) because of difference of oxidation state (Cullen and Reimer, 1989; Lièvremont et al., 2009). As(III) is highly toxic compared to As(V) because As(III) binds to the sulfhydryl groups of the enzymes and then induces functional impairments (Matschullat, 2000; Lièvremont et al., 2009).

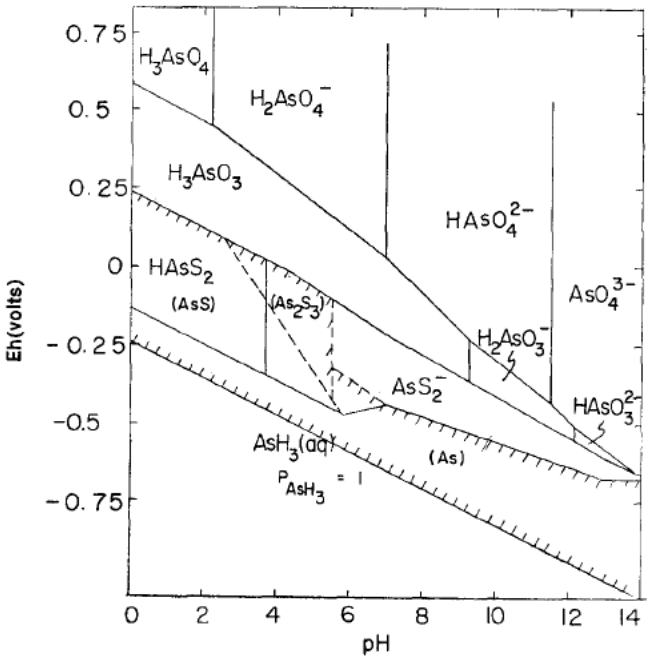

Figure 1.1 Eh-pH diagram for As species at 25°C and 1 atmosphere with total arsenic 10^{-5} mol/l and total sulfur 10^{-3} mol/l. (Ferguson and Gavis, 1972).

1.2.2 Arsenic-containing minerals and dissolution in metallurgical operation

There are over 300 arsenic-bearing minerals (Gonzalez and Monhemius, 1988). Common arsenic minerals frequently found in sulfide base metal (Fe, Cu, etc.) ores and concentrates such as arsenopyrite (FeAsS), enargite (Cu_3AsS_4), and tennantite ($(Cu,Fe)_{12}As_4S_{13}$) (Mandal and Suzuki, 2002). With the increasing the metal resources, the utilization of low-grade, As-bearing refractory metal ores (Table 1.1) are increasing in metallurgical operations. According to the dissolution of these copper minerals associated with As in hydrometallurgical operation, As is contaminated in process solutions after the electrowinning and bleed streams are operated to keep As at less than 20 g/L. As is mainly dissolved in the form of As(III) from ores. Refinery bleed streams is commonly recycled to and adjacent solvent extraction operation. (Riveros et al., 2001). Contamination of As in acidic refinery wastewaters is becoming a great concern in terms of operation cost and environmental impact. The worldwide arsenic consumption has decreased from 25 to 5 thousand metric tons, while its production has increased up to 60 thousand metric ton since 2004 (Kelly et al., 2010). Therefore, it is imperative to develop the stable As treatment technologies.

Table 1.1 Arsenic minerals considered as primary mineral (Tomioka et al., 2005).

Mineral name	Composition
Native arsenic	As
Arsenopyrite	FeAsS
Realger	AsS
Orpiment	As_2S_3
Cobaltite	CoAsS
Enargite	Cu_3AsS_4
Tennantite	$(Cu,Fe)_{12}As_4S_3$
Loellingite	$FeAs_2$
Niccolite	NiAs
Rammelsbergite	$NiAs_2$
Smaltite	$CoAs_2$
Seligmannite	$PbCuAsS_3$
Proustite	Ag_3AsS_3
Domeykite	Cu_3As
Safflorite	$(Co,Fe)As_2$

1.2.3 Biological leaching techniques for low-grade and refractory metal ores

These low-grade and refractory metal ores are usually processed by hydrometallurgical metal recovery process rather than pyrometallurgy in economically viable aspect. As one of the hydrometallurgical process, microbiological techniques such as bioleaching (extraction of metals from low-grade metal ores via microbial Fe(II)- and sulfur-oxidation) and biooxidation (a pre-treatment technique for refractory gold ores prior to chemical cyanide leaching using the same mechanism of bioleaching) have been developed in mining area (Figure 1.2) with the advantages in low cost and low environmental impact (Acevedo, 2002; Brierley and Brierley, 2001; Panda et al., 2015; Pradhan et al., 2008).

Heap bioleaching is the technique for extraction of metals such as copper, iron, zinc, nickel and cobalt from low-grade mineral ore using microbial iron- and

sulfur-oxidation activity (Figure 1.3). The metal-bearing leached solutions are regularly collected and sent to electrowinning process. The capital cost of heap bioleaching depends on the ore grade and total cash cost was calculated as 109.6 US$/ton for ore grade of 0.4%, 64.9 US$/ton for 1.2%, which accounts for 50% of conventional smelting or refining operation cases (William, 2004). Annual operation cost is also within the range of 67–135 US$/ton Cu in case of several bioleaching projects such as Collahausi, Chuquicamata and Salvador (William, 2004). Therefore, bioleaching can be applied even for low grade ore, while copper price is 5000–7000 US$/ton.

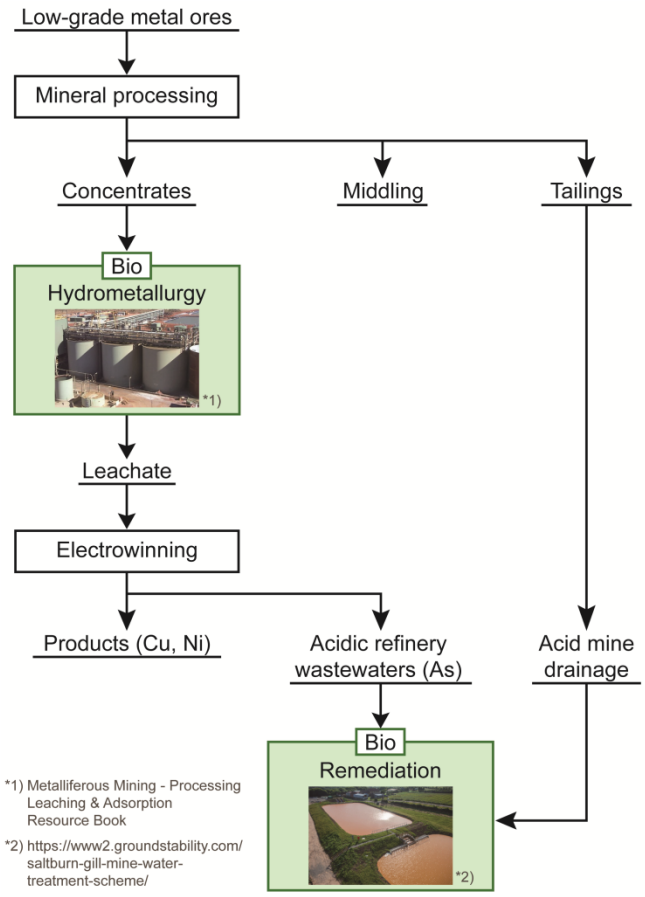

Figure 1.2 Process flow chart of metal production from low-grade ores and the applicable area of biological techniques.

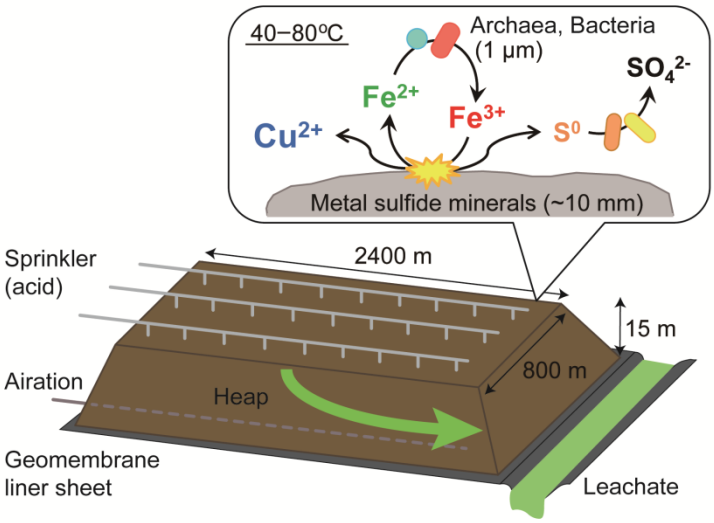

Figure 1.3 Schematic image of heap bioleaching and the mechanism of indirect bioleaching.

Tanaka (2017) compared the operating heap bioleaching sites in Chile and Finland in terms of historical background, economic and environmental points in order to search for the factors affected on biotechnology installation. Although Chile and Finland are different economic scale, both countries were financially supported by foreign capitals through the mining development projects in the 1970s–1990s (Gentina and Acevedo, 2013, 2016). Developing Chilean economy strongly depends on copper mining industry, and major operators consist of domestic and foreign companies such as major international mineral resources companies which have wide experiences in mining operation in the world and stably obtain large benefits (Panda et al., 2015). This indicates these companies' business strategies affect the application of bioleaching. Although mining industry accounts for only the small amount of total GDP in Finland, the bioleaching technologies were developed by the support from European Commission's project (d'Hugues et al., 2007, 2008) which aimed to define the novel mining techniques for environmentally-friendly development together with high economic performance. The mining policy and environmental protection act in Finland

were revised in 2010 and 2014 to intensify the environmental measures in Finnish industry (Jogmec, 2016). These revisions possibility lead to install the new technology such as bioleaching in mining. In order to install bioleaching system, withstanding low profits and minute researches for stable operation are required regardless of the political economic scale. The business strategies of mining operators strongly affect the selection of latest technologies installation, especially in developing countries. In developed countries, environmental perspective also possibly affected as well as profitable technology. Therefore, environmentally-friendly heap bioleaching technologies are developed and selected in mining industry.

Although bioleaching is definitely environmentally- friendly compared to conventional processes, there are concerns that toxic chemicals (e.g. As, Cr) are leached and it possibly leads the inhibition of bacterial activities and environmental pollution, once the operation is started, bioleaching reaction cannot be stopped immediately. To prevent the environmental problems, proper treatments of toxic chemical are required.

1.3 Current techniques used for removal of arsenic

Current arsenic removal techniques from aqueous solutions can fall into the following categories; ion exchange, adsorption on activated alumina and carbon, ultrafiltration, reverse osmosis, and precipitation or adsorption by metals followed by coagulation (Leist et al., 2000). As(III) exist as uncharged state under acidic and neutral condition (Figure 1.1). This characteristic is one of the factors that As(III) is more difficult to form the precipitates than As(V). Then, the conventional As remediation procedures generally set the first chemical As(III) oxidation step using strong chemical oxidants such as ozone, hydrogen peroxide, manganese compounds

and so on (Bissen et al., 2003; Dabekaussen et al., 2001; Kim and Nriagu,2000; Molnár et al., 1994) as shown in Eq. 1.1.

$$H_3AsO_3\ (aq) + H_2O_2\ (aq) \rightarrow H_3AsO_4\ (aq) + H_2O \qquad \text{(Eq. 1.1)}$$

1.3.1 Membrane and adsorption process

Membrane process is categorized to reverse osmosis and ultrafiltration. Reverse osmosis are widely used as a method for drinking water secured from sea water or contaminated water. Osmosis membrane is usually based on the fact that water molecules move spontaneously from low concentration to high concentration liquid. By contrast, reverse osmosis is the phenomenon that water molecules move into the diluted solution side from the concentrated solution by applying larger pressure than the osmotic pressure to the concentrated solution side. Two types of reverse osmosis are used to remove As from water; nanofiltration and hyperfiltration. Arsenic removal test was conducted using this two reverse osmosis types. Less than 2 μg/L As was permeated from the water containing 39-154 μg/l fed with 38-86 psi ($2.6\text{-}5.9 \times 10^5$ Pa) (nanofiltration), and 36-92 μg/l fed with 92-115 psi ($6.3\text{-}7.9 \times 10^5$ Pa) (hyperfiltration), respectively (Kartinen Jr and Martin, 1995). Reverse osmosis is more effective to remove As(V) than As(III). Other pilot study reported that 96-99% of As(V), and 46-84% of As(III) could be removed (Ning, 2002). Negatively charged ultrafiltration membranes remove As(V) by electrostatic repulsion with opening the pore structure (Brandhuber and Amy, 2001).

Adsorption process consists of activated alumina/carbon and ion exchange. Huang and Vane (1989) researched metal-treated activated carbon for As removal. As was adsorbed on the carbon surface. As a result, 99% of As was removed from the

solution containing 2 x 10^{-4} M (15 mg/l) As(V).

Ion exchange column is also studied to remove As from drinking water. Ninety eight percent of As(V) was exchanged in the pH range 3.5 to 7.0 (Ruixia et al., 2002). However, these membrane and adsorption process is more effective for treatment of low As concentration (level of μg/l) such as drinking water (Leist et al., 2000).

1.3.2 Lime precipitation

The neutralization of As(V) with lime (CaO, $Ca(OH)_2$) produces calcium arsenate compounds such as $Ca_4(OH)_2(AsO_4)_2 \cdot 4H_2O$, $Ca_5(AsO_4)_3OH$, and $Ca_3(AsO_4)_2 \cdot 3.6H_2O$ (Bothe and Brown, 1999; Moon et al., 2004). However, it was reported that all calcium arsenate compounds have high solubility of As. This is caused by the presence of CO_2.

$$Ca_3(AsO_4)_2 + 3CO_2 + 3H_2O \rightarrow 3CaCO_3 + 2H_3AsO_4 \quad \text{(Eq. 1.2)}$$

By contrast, calcination process contributes the transformation of the amorphous calcium arsenate into crystalline compounds at more than 700°C (Riveros et al., 2001). However, this calcination process is no longer economic.

$$Ca_3(AsO_4)_2 \cdot Ca(OH)_2 = Ca_3(AsO_4)_2 + CaO + H_2O \quad \text{(Eq. 1.3)}$$

1.3.3 Precipitation or adsorption using Fe(III) followed by coagulation

Precipitation is most effective for arsenic removal for small quantities of highly concentrated arsenic waste (Leist et al., 2000). Poorly crystalline hydroxides have large surface area, so that As(V) is easily adsorbed (Bowell, 1994). The common

industrial approach is co-precipitates with ferrihydrite ($Fe_5HO_8 \cdot 4H_2O$) (Fuller et al., 1993; Jambor and Dutrizac, 1998; Klaus et al., 1998; Twidwell et al., 2005; Waychunas et al., 1993, 1995; William et al., 2004). Ferrihydrite is classified two types; 2-line ferrihydrite, and 6-line ferrihydrite which depend on the number of characteristic XRD peaks. That is, 6-line ferrihydrite is better crystalline than 2-line ferrihydrite. The structure of ferrihydrite is similar to that of the FeOOH-type minerals. According to rapid neutralization of the solution containing Fe(III), ferrihydrite forms and precipitates (Jambor and Dtrizac, 1998). When AsO_4^{3-} and AsO_3^{3-} are dissolved with ferrihydrite, these adsorbs as follows.

$$Fe^{3+} + (3+x)H_2O = FeO(OH)(H_2O)_{1+x} + 3H^+ \quad \text{(Eq. 1.4)}$$

$$FeO(OH)(H_2O)_{1+x} + AsO_4^{3-} = AsO_4^{3-} \cdot FeO(OH)(H_2O)_{1+x} \quad \text{(Eq. 1.5)}$$

The optimum pH range for effective arsenical ferrihydrite precipitation is 4-7. The stability of arsenical ferrihydrite was studied. It passed the standard EPA TCLP test because of low solubility of less than 0.5 mg As/l (Fe/As = 9), and 1-2 mg As/l (Fe/As = 2.3) (Twidwell et al., 1999). Therefore, Fe/As molar ratios of more than 3 were most stable for long terms storage (Riveros, 2001). This arsenical ferrihydrite process was regarded as Best Developed Available Technology (BDAT) by US EPA, and it is applied to the actual operations (Harris, 2003).

Under acidic condition, schwertmannite ($Fe_8O_8(OH)_{5.5}(SO_4)_{1.25}$), goethite (FeOOH), and jarosite ($MFe_3(SO_4)_2(OH)_6$; $M = Na^+$, K^+, NH_4^+) precipitate instead of ferrihydrite (Asta et al., 2009; Duquesne et al., 2003). Arsenic incorporation in jarosite is shown as follows (Dutrizac et al., 1987).

$$xHAsO_4^{2-} + KFe_3(SO_4)_2(OH)_6 \rightarrow KFe_3(SO_4)_{2-x}(HAsO_4)_x(OH)_6 + xSO_4^{2-} \quad \text{(Eq. 1.6)}$$

$$xAsO_4^{3-} + xH^+ + KFe_3(SO_4)_2(OH)_6$$
$$\rightarrow KFe_3(SO_4)_{2-x}(AsO_4)_x(OH)_{6-x}(H_2O)_x + xSO_4^{2-} \quad \text{(Eq. 1.7)}$$

However, these precipitations with Fe(III) are necessary to be higher Fe/As molar ratios than 3. This indicates the compounds are high volume. Furthermore, the separation of arsenic ferrihydrite from the liquid is inefficient because of its poorly crystalline.

1.4 As immobilization as scorodite

1.4.1 Characteristics of scorodite

Scorodite ($FeAsO_4 \cdot 2H_2O$) is the orthorhombic compounds (Figure 1.4) of ferric iron (Fe(III)) and arsenate (As(V)). It is found in weathering environment as a result of the dissolution of As-bearing minerals such as arsenopyrite (FeAsS) and enargite (Cu_3AsS_4) by microbial Fe(II)-oxidation activity (Swash et al., 2000). Under the extremely acidic condition (pH < 2.24), As(V) can exist in the form of H_3AsO_4 (Figure 1.1). Then, scorodite precipitates quickly in highly concentrated solutions of Fe^{3+} as follow (Dove and Rimstidt, 1985);

$$Fe^{3+} + H_3AsO_4 + 2H_2O = FeAsO_4 \cdot 2H_2O + 3H^+ \quad \text{(Eq. 1.8)}$$

Scorodite is one of the effective arsenate phases for As treatment owing to its thermodynamic stability, lower iron demand than adsorption compounds with iron, compactness with 30% wt of As, and high density (Bluteau and Demopoulos, 2007;

Riveros et al., 2001; Robins, 1987; Langmuir et al., 2006). The solubility and stability was studied. Scorodite has low stability at pH 2.8-5.3 less than 0.5 mg/l (Krause and Ettel, 1989). It was also found to be most stable at pH 3-6 by leaching test (Fujita et al., 2012). The solubility product K_{sp} value was calculated as $10^{-25.83}$ (Langmuir et al., 1999), $10^{-25.4}$ (Bluteau and Demopoulos, 2007). These results showed that it was suitable for disposal form of As. The following sections show the study of the scorodite synthesis.

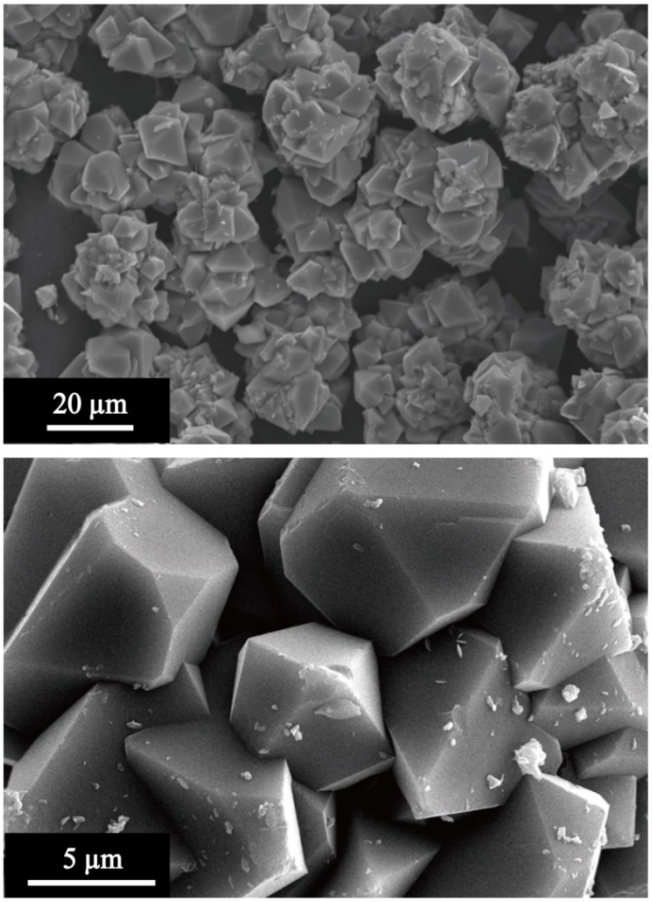

Figure 1.4 SEM images of scorodite synthesized from $[As(V)]_{ini}$ = 267 mM and $[Fe(II)]_{ini}$ = 358 mM at 70°C.

1.4.2 Abiotic scorodite synthesis

1.4.2.1 Hydrothermal scorodite synthesis

One of the major scorodite synthesis methods utilizes hydrothermal treatment by autoclaving. Dutrizac et al. (1987) and Dutrizac and Jambor (1988) showed that crystalline scorodite was synthesized from 25 g/l As(V) solution and 0.3 M $Fe(NO_3)_3$ (17 g/l Fe(III)) at pH less than 0.7 by hydrothermal method. Temperature was maintained at 160°C using autoclave. Other research showed that greater than 95% of As was immobilized at over 150°C from the solution containing 13 g/l As(V) and 10.5, 16, and 21 g/l Fe(III). TCLP test showed that the solubility of arsenical precipitates was less than 5 As mg/L in pH-buffered acetate solution, which is one of the most stable forms of arsenic immobilization (Monhemius and Swash, 1999).

Weert and Droppert (1994) described the aqueous processing of arsenic trioxide (As_2O_3) to crystalline scorodite. Arsenic trioxide is a common by-product (roaster dusts) in pyrometallurgical operations, and its oxidation state of arsenic is trivalent. Then, it is necessary to oxidize As(III) to As(V) before precipitating with Fe(III). The experiment was conducted in a total volume of 1.5 l containing 0.25 M As_2O_3 (37.5 g/l As(III)), 0.5 M $Fe(NO_3)_3$ (28 g/l Fe(III)), and 2.5 M HNO_3. The solution was brought to 160°C, 12 $\times 10^5$ Pa, and maintained for 4 hours in autoclave. With the increasing temperature up to 130°C, As_2O_3 was dissolved and oxidized to As(V) by HNO_3. Continuously, As(V) and Fe(III) were converted into crystalline scorodite at 160°C. This study had achieved the As(III) oxidation and immobilize in continuous process.

The advantages using hydrothermal scorodite crystallization for arsenic removal was summarized as follows; (i) simplicity (autoclave or pipe reactor), (ii) low volume of solid arsenical residue, (iii) good settling and filtration characteristics in

precipitates, (iv) crystalline materials with low surface areas, (v) low-solubility solids produced, (vi) high-grade arsenic residue produced, (vii) capability to treat many different arsenical materials (Monhemius and Swash, 1999). However, autoclave method is capital intensive because of high temperature demand. At temperature below 100°C, the amorphous iron hydroxide precipitates (ferrihydrites) which adsorbed As(V) (Monhemius and Swash, 1999). Temperatures greater than 125°C are needed for good crystallinity of scorodite (Dutrizac and Jambor, 1988). Therefore, this process can be employed only for arsenic stabilization operated concurrently with the processing of valuable materials such as gold-bearing pyrite or copper concentrates (Filippou and Demopoulos, 1997).

1.4.2.2 Scorodite precipitation under atmospheric pressure

Alternative arsenic removal process was studied as a substitute for hydrothermal method. Scorodite precipitates were synthesized at lower temperature (< 100°C) than the above method and under atmospheric pressure by supersaturation-control approach. Neutralization by controlling pH was conducted so that the critical supersaturation line of arsenic was not exceeded. The reaction of scorodite crystallization was shown as following. $Mg(OH)_2$ or $Ca(OH)_2$ was added as a neutralizing agent.

$$2H_3AsO_4\ (aq) + Fe_2(SO_4)_3\ (aq) \rightarrow 2FeAsO_4{\cdot}2H_2O\ (s) + 3H_2SO_4\ (aq) \qquad \text{(Eq. 1.9)}$$

$$H_2SO_4\ (aq) + Mg(OH)_2\ (s) \rightarrow MgSO_4\ (aq) + 2H_2O \qquad \text{(Eq. 1.10)}$$

Slow pH increasing within the limits of the working range contributes the crystal growth of scorodite, while precipitation of amorphous compounds was caused by

increasing pH too quickly. Filippou and Demopoulos (1997) showed that crystalline scorodite was formed from the solution containing 10 g/l or 50 g/l As(V), Fe(III) at Fe/As molar ratio of 1.1-1.2, and 25 g/l H_2SO_4 under atmospheric pressure condition (95°C). As a result, more than 90% of arsenic was immobilized in three hours. The precipitates were also tested by TCLP leaching experiment, and it was found to be very stable with the dissolution of only 0.5-2.2 ppm As. Other researches showed scorodite crystallization from 0.5 l solution containing 10 g/l As(V) and 7.5 g/l Fe(III) at 95°C with neutralizing. About 95% of As was immobilized in the culture with addition of scorodite seed crystals, and its leachability was less than 5 mg/L As (Singhania et al., 2005; Singhania et al., 2006). As a role of scorodite seed crystals, the supersaturation level of ferric arsenate was kept low. Other research showed that precipitation of crystalline scorodite was possible at even low temperature (80ºC) by addition of seed crystals. This research also showed that the presence of SO_4^{2-} ion in the solutions inhibited the crystallization of scorodite (Demopoulos et al., 1995).

In practical hydrometallurgical situation, this supersaturation control was undesirable because of the requirement of a lot of neutralizing agents such as $Mg(OH)_2$ and $Ca(OH)_2$. In addition, gypsum ($CaSO_4 \cdot 2H_2O$) was mixed into the precipitates by using $Ca(OH)_2$. This leads to decreasing the As immobilization efficiency. In another perspective, ferrous iron (Fe(II)) is generally contaminated into the process wastewaters according to the dissolution of iron-sulfide minerals. From these points, Fujita et al. (2008a, 2008b, 2009) showed that stable scorodite particles were synthesized without gentle neutralization. These researches focused on the oxidation of Fe(II) during the scorodite precipitation. Oxygen gas was introduced (4 l/min) into a reactor containing 4 L of 50 g/l As(V) and 56 g/l Fe(II) solution (Fe/As molar ratio of 1.5) for oxidation of Fe(II). Solution was adjust to extremely acidic condition (initial

pH 1.1), and It was stirred with 800 rpm at 95°C for 1-7 hours. The reaction is described as follow;

$$4H_3AsO_4 + 4FeSO_4 + O_2\,(g) + 6H_2O \rightarrow 4FeAsO_4 \cdot 2H_2O + 4H_2SO_4 \qquad \text{(Eq. 1.11)}$$

Fe(II) was readily oxidized to Fe(III) by oxygen gas. As a result, 97% of As was immobilized as crystalline scorodite. The report suggested that this Fe(II) oxidation was the primary factor controlling the oversaturation (Fujita et al., 2009). In this research, the negative effect of SO_4^{2-} ion on the scorodite crystallization was avoided. This technology developed by Dowa Metals & Mining Co. Ltd. has been named Dowa Mining Scorodite Process (DMSP®) (Fujita et al., 2012; Kubo et al., 2010).

However, these scorodite synthesis methods under hydrothermal or atmospheric pressure have a downside that As remains about 1 g/l in the solution containing high concentration of As. Previous researches showed that 0.6 g/l (Monhemius and Swash, 1999), 0.5 g/l (Singhania et al., 2005), and 1.4 g/l As (Fujita et al., 2009) remained, which are not satisfied the environmental standard. It is difficult to remove arsenic completely from the process solutions. Therefore, it is required to develop the alternative scorodite formation methods from the solution containing diluted concentration of As.

1.4.3 Microbiological scorodite crystallization

1.4.3.1 Microbial Fe(II) oxidation by thermoacidophilic Fe(II)-oxidizing archaea

In case of As removal in low concentration range, it is eligible to be energy, space, and cost saving treatment. One technique to achieve these conditions includes the treatment using microorganisms. The influence of microorganisms is considerable

on the kinetics of soil metal ions. There is possibility to accelerate the dissolution of unwanted metals/metalloids in nature depending on the difference of redox potential by microbial metal oxidation or reduction (Chapter 2). On the other hand, these oxidation or reduction ability can utilize for mining area. Actually, bioleaching has been applied for metal extraction from copper ore using Fe(II)-oxidizing microorganisms. It can oxidize Fe(II) under extreme environment condition such as low pH. In addition, there are many species which can grow at hot temperature such as 45-95°C. These microorganisms called extremophiles have possibility to be applied to the treatment of highly acidic refinery wastewaters.

Gonzalez-Contreras et al. (2010) succeeded the crystallization of biogenic scorodite using thermoacidophilic iron-oxidizing archaeon *Acidianus sulfidivorans* (DSM 18786) isolated from a sulfur rich acidic edge of a hot spring. This archaeon is able to grow and oxidize Fe(II) under highly acidic (pH 0.35-3.0) and hot (45-83°C) condition. Experiments were carried out in 100 mL of serum bottles as reaction vessels in duplicate. The growth medium containing 0.75 g/l Fe(II) and 1 g/l As(V) (Fe/As molar ratio of 1.0) was adjusted initial pH to 0.8, and *Ac. sulfidivorans* was inoculated to the medium. The serum bottles were shaken incubated at 150 rpm and 80°C for 16 days. As a result, Fe(II) was biologically oxidized to Fe(III) by *Ac. sulfidivorans* (Fe(II) oxidizing rate of 0.04 g/l·day), followed by decreasing the concentrations of Fe and As. The biogenic precipitate was identified as crystalline scorodite, and it was low solubility and high stability (Gonzalez-Contreras et al., 2010). The experiments were scaled up from batch test to bioreactor (CSTRs and airlift reactor). A mixed microbial culture was adopted which consisted of *Sulfolobales* (*Acidianus brierleyi* (98-99%), *Metallosphaera sedula* (1-2%), *Sulfolobus* spp. (very small numbers)) originally taken from a hot, sulfur rich coal dump. Their Fe(II) oxidation rate was researched as 1.5

g/l·day at pH 1.1 and 72°C (Gonzalez-Contreras et al., 2012a). When using CSTRs under the condition of pH 1.2, 72°C, 2.8 g/l As(V), and 2.4 g/l Fe(II), the arsenic removal efficiency was achieved higher than 99% (Gonzalez-Contreras et al., 2012b, 2012c).

1.4.3.2 Microbial As(III) and Fe(II) oxidation by *Acidianus brierleyi*

In metallurgical operations, As is generally dissolved from sulfide concentrates in the form of As(III). Therefore, these previous researches have to oxidize As(III) to As(V) using strong chemical oxidants such as H_2O_2 and O_3 as first step, followed by immobilization step. For improving As(III) oxidation step, microbial As(III) oxidation was studied by Okibe et al. (2013). The physicochemical property of the industrial refinery wastewater is highly acidic (pH 1-2), and hot (50-80°C). Then, thermoacidophilic iron-oxidizing archaeon *Acidianus brierleyi* (DSM 1651) was focused on. This process solution is suitable for optimal growth of *Ac. brierleyi* which possess the optimal pH 1.5-2.0 and temperature 70°C. This study found that *Ac brierleyi* could oxidize As(III) to As(V). Further study revealed that 1 g/L As(III) was oxidized to As(V) in the presence of yeast extract. Additionally, As(III) oxidation progressed much more rapidly and completely in the culture plus Fe(II) (Okibe et al., 2014).

This microbial As(III) oxidation was found to be progressed for not energy obtaining but detoxification. As a following As immobilization experiment, synthetic copper refinery wastewater containing 1 g/l As(III) and 1 g/l Fe(II) was tested, whereas Gonzalez-Contreras et al. (2010, 2012b, 2012c) used As(V) and Fe(II) as starting reactants. *Ac. brierleyi* was inoculated in 500 ml Erlenmeyer flasks containing 200 mL of growth medium with 13 mM (1 g/l) As(III), 18 mM (1 g/l) Fe(II), and 0.01% (w/v)

yeast extract. Flasks were incubated shaken at 100 rpm and 70°C for 14 days. Fe(II) and As(III) were readily oxidized and 86-100% of As was immobilized as biogenic scorodite (Okibe et al., 2014) (Figure 1.5).

Actual copper refinery wastewater contaminates different dissolved metals such as As(III), Fe(II), and Cu(II) on the process. Cu(II) has been concerned about affecting microorganisms negatively in terms of inhibition of enzymatic activity. However, Cu(II) inhabitation was alleviated when scorodite seed crystals were added into the solutions as immediate support for microbial colonization (Okibe et al., 2017). From these results, microbial scorodite synthesis is considered to be one of the most effective As immobilization methods from diluted As wastewater after chemical treatment.

The advantages of biological scorodite crystallization compared to chemical crystallization process was summarized as follows; (i) the features of biogenic scorodite are very similar to the mineral, (ii) supersaturation can be controlled on microscale by biological Fe(II) oxidation, (iii) it does not need the utilization of strong chemical oxidants, (iv) at least of 1 g/l As can be treated, (v) the solid can be separated from the solution in terms of crystal and agglomerate size (Gonzalez-Contreras et al., 2010). However, biological scorodite techniques have challenges to be solved. These require long term for crystallization of biogenic scorodite compared to chemical crystallization process. Operation cost may run up due to maintain hot condition around 70-80°C for a few weeks. Therefore, condition improvement is required for such as shorten the reaction time, and crystallization at Intermediate temperature range.

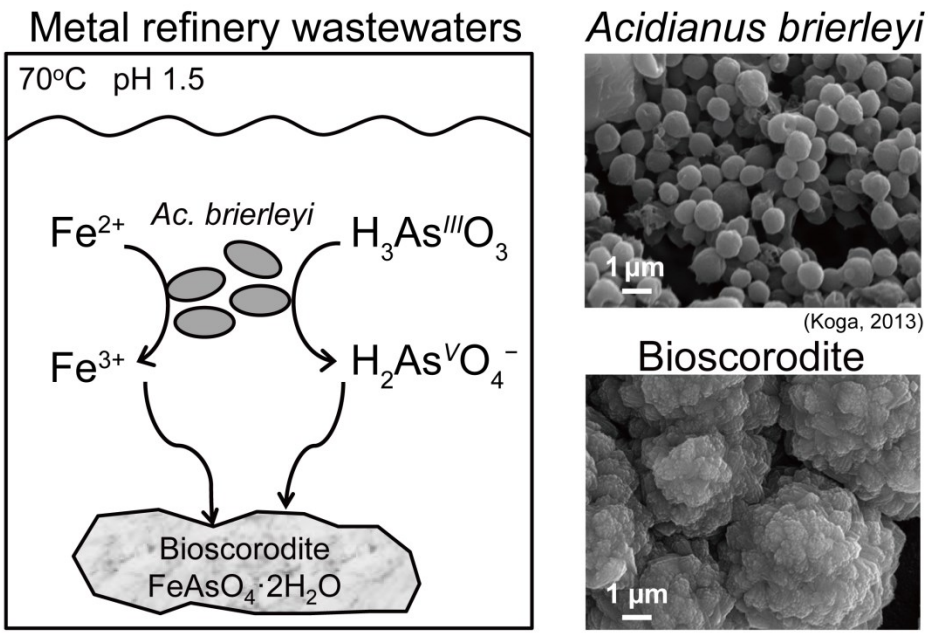

Figure 1.5 Schematic illustration of bioscorodite crystallization using *Ac. brierleyi*.

1.5 Objective of this thesis

Bio-mineral processing is considered as one of the most effective approaches to recover valuable metals, especially from low-grade refractory mineral ores and concentrates. As is a major impurity contaminated in metal refinery wastewaters including those deriving from bio-mineral processing, and its economically-viable and environmentally-friendly removal technique is needed. This thesis firstly demonstrated the applicability of biooxidation of highly refractory As-bearing Au-ore concentrates. There are also cases that dilute As(III) solutions (up to 25 mM) are produced in metallurgical operations, such as from solid-liquid separation followed by Cu recovery after enargite concentrate leaching, wherein chemical scorodite synthesis turns ineffective (JX Nippon Mining & Metals Co. Ltd.; personal communication). Whilst scorodite crystallization becomes more difficult at more dilute As concentrations under milder temperature condition, exploiting factors to enable such reaction is of great importance to broaden the applicability of the scorodite method for a wide range of

As(III)-contaminated waters. Initial solution Fe/As ratios and initial pH are affecting factors (Fujita et al. 2009b): In hydrothermal scorodite synthesis at 150°C, the rate of As precipitation decreased with increasing initial solution Fe(III)/As(V) molar ratios from 1.0 to 1.5 and 2.0 (Monhemius and Swash 1999). Our previous bioscorodite study also found that the form of As precipitation changes at different initial solution Fe(II)/As(III) ratios (Okibe et al. 2014). From studies of conventional abiotic scorodite synthesis, seed feeding (scorodite or other heterogeneous crystals) was shown one of the influential factors to promote scorodite formation (Singhania et al. 2005; Caetano et al. 2009; Demopoulos et al. 1995).

Based on that, the aim of this study was set to find factors that enable effective bioscorodite crystallization from dilute As(III)-bearing solutions (3.3-6.5 mM; so far undescribed by scorodite studies). In chapter 4, optimization of bioscorodite crystallization condition was conducted focusing on initial [Fe(II)]/[As(III)] molar ratios (0.8–6.0) and initial pH (1.5 or 1.2). In chapter 5, the effects of seed-feeding were investigated. Bioscorodite and chemical scorodite particles were produced to compare their characteristics, and their effectiveness as seed crystals was evaluated for the bioscorodite crystallization reaction from dilute 4.7 mM As(III) solution. Additionally, stability of the resultant bioscorodite products was evaluated by the toxicity characteristic leaching procedure (TCLP) test.

Generally, metal refinery wastewater contains high concentrations of sulfate (SO_4^{2-}) ions due to extremely high pH and dissolution of sulfide minerals. The effects of SO_4^{2-} ions on scorodite synthesis have been reported in chemical methodologies (Demopoulos et al., 1995, Gomez et al., 2011). Bioscorodite crystallization progresses through second As concentration decrease (1st-stage As-removal at ~day 4; 2nd-stage As-removal at day 10~) (Okibe et al., 2017). At the 1st-stage As-removal,

brown-colored amorphous precipitates (precursors) formed, and then it was transformed into scorodite at 2nd-stage As-removal. However, this transformation mechanism is still unclear. Therefore, this thesis also focused on the effect of SO_4^{2-} ions on bioscorodite crystallization process in chapter 6.

Finally, in chapter 7, the alternative archaeal strains were tested for bioscorodite crystallization using four kinds of thermophilic acidophilic archaea strains, Fe(II)-oxidizers: *Sulfolobus metallicus* strain Kra23, *Sulfolobus tokodaii* strain 7, *Sulfolobus acidocaldarius* strain 98-3, and sulfur- and Fe(II)-oxidizer *Metallosphaera sedula* strain TH2 in bioscorodite crystallization experiment and the elucidation of As(III) oxidation mechanism.

Contents shown in section 1.2.3 were partially included in the paper accepted as:
Tanaka, M., 2017. A comparison study of heap bioleaching sites in Chile and Finland for further development of biotechnology for mining. *Evergreen*, 4(4), 1-7.

Chapter 2

Methodology

2.1 Culture medium and chemical reagents

2.1.1 Heterotrophic basal salts (HBS)

Heterotrophic basal salts solutions for acidophilic microorganisms were prepared as 50X concentrates (Johnson et al., 2008). The chemical reagents as shown in below list were added into distilled water and acidified to pH 1.5 with H_2SO_4. The HBS solutions were filter-sterilized through 0.22 μm polyethersulfone membranes (Steritop, Millipore), and stored at 4°C.

Heterotrophic basal salts solutions (50X)

$(NH_4)_2SO_4$	22.5 g/l
KCl	2.5 g/l
KH_2PO_4	2.5 g/l
$MgSO_4 \cdot 7H_2O$	25.0 g/l
$Ca(NO_3)_2 \cdot 4H_2O$	0.7 g/l
Na_2SO_4	7.1 g/l

2.1.2 Chemical reagents

20 g/l Fe(II) stock solutions

$FeSO_4 \cdot 7H_2O$ (Wako Pure Chemical Industries) was added into acidic distilled water and adjusted to pH 1.5 with H_2SO_4. The stock solutions were filter-sterilized through 0.22 μm polyethersulfone membranes (Steritop, Millipore), and stored at 4°C.

20 g/l Fe(III) stock solutions

$Fe_2(SO_4)_3 \cdot nH_2O$ (n = 5–7; Wako Pure Chemical Industries) was added into distilled water and acidified to pH 1.5 with H_2SO_4. Based on the measured Fe(III) concentrations by *o*-phenanthoroline method, the Fe(III) stock solutions were diluted to 20 g/l with acidic distilled water. The stock solutions were filter-sterilized through 0.22 μm polyethersulfone membranes (Steritop, Millipore), and stored at 4°C.

10 g/l As(III) stock solutions

$NaAsO_2$ (Sigma-Aldrich) was added into distilled water and acidified to pH 1.5 with H_2SO_4. The stock solutions were filter-sterilized through 0.22 μm polyethersulfone membranes (Steritop, Millipore), and stored at 4°C.

10 g/l As(V) stock solutions

$Na_2HAsO_4 \cdot 7H_2O$ (Junsei Chemical) was added into distilled water and acidified to pH 1.5 with H_2SO_4. The stock solutions were filter-sterilized through 0.22 μm polyethersulfone membranes (Steritop, Millipore), and stored at 4°C.

Sterilized elemental sulfur powder

Elemental sulfur powder (Wako Pure Chemical Industries) was heat-sterilized in dry oven (SG600, Yamato Scientific) at 110°C for 40 minutes. This sterilization was operated once a day for three days, and stored in sterilized bottle.

2.1.3 Media preparation for cultivation and experiments

For cultivation and experiments, 4 ml of HBS (50×) stock solution and 40 mg of yeast extract powder (Sigma-Aldrich) were added into 500 ml Erlenmeyer flask containing adequate amount of pure water (pH 1.5 with H_2SO_4). Silicone rubber with continuous bubbles (SILICOSEN T-type, Shin-Etsu Polymer) was utilized as culture plugs. Flasks containing media were heat-sterilized by autoclave (120°C, 20 min; ES-215, TOMY). The filter-sterilized stock solutions of Fe(II), Fe(III), As(III) and As(V) were added into heat-sterilized HBS media. Final solution volume was set to 200 ml using pure water (pH 1.5 with H_2SO_4).

2.2 Microorganisms cultivation

2.2.1 Moderately thermophilic, acidophilic bacteria

2.2.1.1 *Acidimicrobium ferrooxidans*^{T} strain ICP (DSM 10331)

Am. ferrooxidans ICP (Clark and Norris, 1996) was maintained in 500 ml Erlenmeyer flask containing 200 ml of HBS medium (pH 1.5 with H_2SO_4) with 10 mM Fe(II) and 0.02% (w/v) yeast extract. Flasks were incubated at 45°C, shaken at 100 rpm (G·BR-200, Taitec).

2.2.1.2 *Sulfobacillus sibiricus*^{T} strain N1 (DSM 17363)

Sb. sibiricus N1 (Melamud et al., 2003) was maintained in 500 ml Erlenmeyer flask containing 200 ml of HBS medium (pH 1.5 with H_2SO_4) with 10 mM Fe(II) and 0.02% (w/v) yeast extract. Flasks were incubated at 45°C, shaken at 100 rpm (G·BR-200, Taitec).

2.2.1.3 *Acidithiobacillus caldus*^{T} strain KU (DSM 8584)

At. caldus KU (Hallberg and Lindström, 1994) was maintained in 500 ml Erlenmeyer flask containing 200 ml of HBS medium (pH 1.5 with H_2SO_4) with 5 mM sodium tetrathionate and 0.02% (w/v) yeast extract. Flasks were incubated at 45°C, shaken at 100 rpm (G·BR-200, Taitec).

2.2.2 Thermo-acidophilic archaea

2.2.2.1 *Acidianus brierleyi*^{T} (DSM 1651)

Ac. brierleyi (Segerer et al., 1986) was maintained in 500 ml Erlenmeyer flask containing 200 ml of HBS medium (pH 1.5 with H_2SO_4) with 18 mM Fe(II), 13 mM As(III), and 0.02% (w/v) yeast extract. Flasks were incubated at 70°C, shaken at 100 rpm (RGS-20-TH-V, Sanki Seiki).

2.2.2.2 *Metallosphaera sedula*^{T} strain TH2 (DSM 5348)

M. sedula TH2 (Huber et al., 1989) was maintained in 500 ml Erlenmeyer flask containing 200 ml of HBS medium (pH 1.5 with H_2SO_4) with 9 mM Fe(II), 6.5 mM As(III), 0.1% (w/v) elemental sulfur and 0.02% (w/v) yeast extract. Flasks were incubated at 70°C, shaken at 100 rpm (RGS-20-TH-V, Sanki Seiki).

2.2.2.3 *Sulfolobus tokodaii*^{T} strain 7 (DSM 16993)

S. tokodaii 7 (Suzuki et al., 2002) was maintained in 500 ml Erlenmeyer flask containing 200 ml of HBS medium (pH 1.5 with H_2SO_4) with 9 mM Fe(II), 6.5 mM As(III), and 0.02% (w/v) yeast extract. Flasks were incubated at 70°C, shaken at 100 rpm (RGS-20-TH-V, Sanki Seiki).

2.2.2.4 *Sulfolobus metallicus*^{T} strain Kra 23 (DSM 6482)

S. metallicus Kra 23 (Huber and Stetter, 1991) was maintained in 500 ml Erlenmeyer flask containing 200 ml of HBS medium (pH 1.5 with H_2SO_4) with 9 mM Fe(II), 6.5 mM As(III), 0.1% (w/v) elemental sulfur and 0.02% (w/v) yeast extract. Flasks were incubated at 70°C, shaken at 100 rpm (RGS-20-TH-V, Sanki Seiki).

2.2.2.5 *Sulfolobus acidocaldarius*^{T} strain 98-3 (DSM 639)

S. acidocaldarius 98-3 (Brock et al., 1972) was maintained in 500 ml Erlenmeyer flask containing 200 ml of HBS medium (pH 1.5 with H_2SO_4) with 9 mM Fe(II), 6.5 mM As(III), 0.1% (w/v) elemental sulfur and 0.02% (w/v) yeast extract. Flasks were incubated at 70°C, shaken at 100 rpm (RGS-20-TH-V, Sanki Seiki).

2.3 Sampling procedures

2.3.1 Liquid samples

Liquid samples were taken from the experimental cultures in clean bench (CCV-1300E, Hitachi) after compensation of water evaporated with sterilized distilled water. The solutions were filtered through 0.20 μm cellulose acetate membrane (Advantec) to monitor the concentrations of total soluble Fe, As, Fe(II) and As(III), pH and Eh vs SHE. Average cell number per square was direct-counted using Thoma counting chamber and phase-contrast microscopy (BX-51, Olympus), and then it was multiplied by 2.0×10^7 to calculate the cell density (cells/ml).

2.3.2 Solid samples

Precipitates were separated by filtration through 0.20 μm mixed cellulose ester membrane (Advantec) using aspirator (A-1000S, EYELA) and stored at −20°C. Pre-frozen precipitates were freeze-dried overnight (FDU-2110, EYELA).

2.4. Analytical methods

2.4.1 Liquid analysis

2.4.1.1 pH and Redox potentials (Eh vs SHE)

Culture pH and redox potentials (ORP values) were measured using multi-function water quality meter (MM-43X, TOA-DKK). Measured ORP values were converted to Eh vs. standard hydrogen electrode (SHE) by adding the value of 206 (25°C).

2.4.1.2 Determination of Fe(II) concentrations

Soluble Fe(II) concentrations were determined by *o*-phenanthroline method (Caldwell and Adams 1946). A 100 µl of diluted samples (max. Fe(II) 0.5 mM with pH 1.5 distilled water) were added into a disposable cuvette and mixed with 100 µl of 1 M HCl, 100 µl of 5 mM *o*-phenanthroline ($C_{12}H_8N_2 \cdot H_2O$) solution, and 50 µl of 2 M sodium acetate (CH_3COONa) solution. Total volume was set to 1 ml by distilled water, and gave 30 minutes for stable equilibrium. The absorbance at 510 nm was measured against a full reagent blank using spectrophotometer (NanoPhotometer Pearl, Implen).

Standard curve was obtained with 10 mM ferrous sulfate ($FeSO_4 \cdot 7H_2O$, pH 1.5, completely reduced by adding L(+)-ascorbic acid sodium salt) over the range of 0–0.9 mM (0–50 ppm) (Figure 2.1).

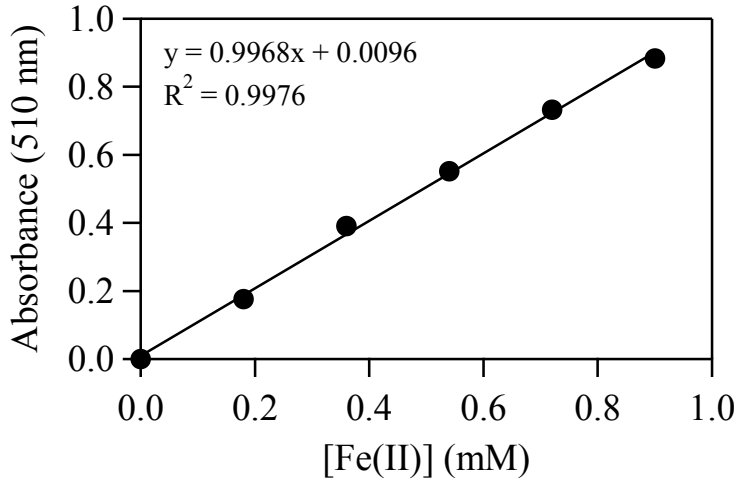

Figure 2.1 A typical standard curve for Fe(II) assay using *o*-phenanthroline method. The equation of the fitted line is $y = 0.9968x + 0.0096$. $R^2 = 0.9976$.

2.4.1.3 Determination of As(III) concentrations

Soluble As(III) concentrations were determined by stripping voltammetric method using Nano-band explorer (GL sciences). After thin film plating of carbon electrode using 200 ppm Au solution in 0.1 M HCl (1000 ppm gold standard solution, Kanto Chemical), 50 ml of diluted samples in 0.1 M HCl were measured under the condition of clean time 0.1 second and plate time 10 second.

Standard curve was obtained with 20 ppm sodium metaarsenite ($NaAsO_2$, pH 1.5) over the range of 0–40 ppb (Figure 2.2). Measurement at each concentration was carried out in triplicate.

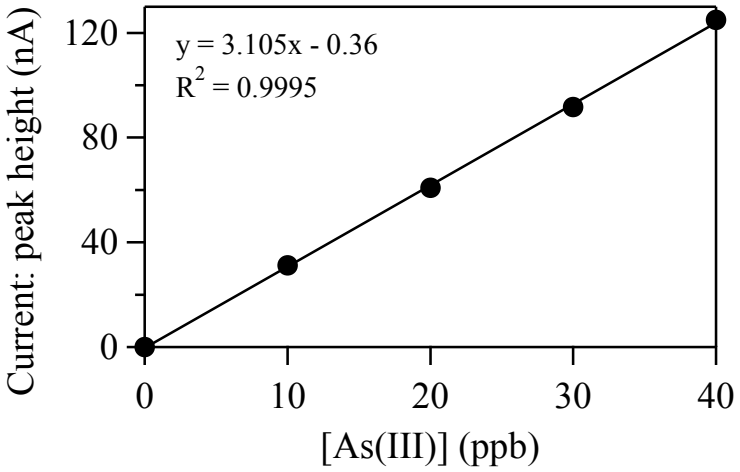

Figure 2.2 A typical standard curve for As(III) assay using stripping voltammetric method. The equation of the fitted line is $y = 3.105x - 0.360$. $R^2 = 0.9995$.

2.4.1.4 Determination of total soluble Fe, As and S concentrations

Total soluble Fe, As and S concentrations were determined by Inductively Coupled Plasma Optical Emission Spectrometry (ICP-OES; Optima 8300, PerkinElmer). Filtered samples were diluted using 0.1 M HCl. All the measurements were carried out in triplicates and the values were averaged. Wavelengths measured for each metal were described as follows; Fe: 238.204, 239.562, 259.939 nm, As: 188.979, 193.696, 197.197 nm, S: 180.669, 181.975, 182.563 nm.

Standard curve was obtained with 1000 ppm iron standard solution, 1000 ppm arsenic standard solution and 1000 ppm sulfur standard solution (Wako Pure Chemical Industries) over the range of 0–20 ppm (Fe, As) and 0–100 ppm (S).

2.4.2 Solid analysis

2.4.2.1 X-ray diffraction (XRD)

XRD measurement was performed using Ultima IV (Rigaku) with Cu-Kα radiation as an X-ray source. The accelerating voltage and current were 40 kV and 40 mA, with a scanning speed of 2°/min and scanning step of 0.02°. Obtained XRD patterns were identified based on International Centre for Diffraction Data (ICDD) using powder diffraction analysis software PDXL (Rigaku).

2.4.2.2 Scanning electron microscope (SEM)

Surface geometry: Dried samples were fixed on carbon tape and Au-Pd magnetron-sputtered (MSP-1S, Vacuum Device) prior to observation of secondary electron images (VE-9800, Keyence).

Cross-section views: Precipitates were embedded in an epoxy resin (SpeciFix-20, Struers) and polished using 2000 and 4000 grit emery papers on a polishing machine (Doctor Lap ML-182, Maruto) and carbon-sputtered (JEC-560, JEOL) prior to observation of backscattered electron images (ULTRA55, ZEISS).

2.4.2.3 Fourier transforms infrared spectroscopy (FT-IR)

FT-IR spectra of precipitates were obtained by KBr pellet method (sample 1% (w/v)) using FT/IR-670 (JASCO) in the range of 360–4000 cm^{-1} (resolution: 4 cm^{-1}). $Fe_2(SO_4)_3 \cdot nH_2O$ (Fe(III); Wako Pure Chemical Industries), $Na_2HAsO_4 \cdot 7H_2O$ (As(V); Junsei Chemical), chemically-synthesized scorodite ($FeAsO_4 \cdot 2H_2O$) and dried *Ac. brierleyi* cells were utilized as standard substances. The Fe(III) (20 mM $FeCl_3 \cdot 6H_2O$; Wako Pure Chemical Industries) and SO_4^{2-} (20 mM Na_2SO_4; Wako Pure Chemical Industries) solutions (pH 1.5 with HCl) were examined using the attenuated total

reflection Fourier transform infrared spectroscopy (ATR-FTIR) using ZnSe crystal. Overlapped peaks were determined by the curve-fitting program PeakFit ver. 4.12 (Systat Software) with the mixed Gaussian and Lorentzian function (Maddams, 1980).

2.4.2.4 X-ray absorption fine structure measurement (XAFS)

XAFS spectra of As K-edge and Fe K-edge for precipitates were collected in transmission mode on Kyushu University beam line (BL06) at Kyushu Synchrotron Light Research Center (SAGA-LS; 1.4 GeV storage ring). Energy selection was accomplished by a double crystal Si (1, 1, 1) monochromator. $FeSO_4 \cdot 7H_2O$ (Fe(II); Wako Pure Chemical Industries), $Fe_2(SO_4)_3 \cdot nH_2O$ (Fe(III); Wako Pure Chemical Industries), $NaAsO_2$ (As(III); Sigma-Aldrich), $Na_2HAsO_4 \cdot 7H_2O$ (As(V); Junsei Chemical) and chemically-synthesized scorodite ($FeAsO_4 \cdot 2H_2O$) were utilized as standard substances. All samples were diluted with boron nitride (BN; Wako Pure Chemical Industries) in appropriate ratios and then formed into tablets with a diameter of 1 cm. The experimental data was analyzed using the IFEFFIT software package ver. 0.9.25 (ATHENA) (Ravel and Newville, 2005).

2.4.2.5 Thermo gravimetry differential thermal analysis (TG-DTA)

TG-DTA analysis of precipitates was carried out using TG-DTA analyzer (2000SA, Bruker) to calculate the water content in precipitates. A 5 mg of samples in Pt-sample-pan was heated from room temperate to 800°C at 10°C/min with an N_2 gas flow rate of 100 ml/min. α-Al_2O_3 powder was used as reference substances.

2.4.2.6 Particle size distribution

Particle size distribution of precipitates and seed scorodite was measured using laser diffraction particle size analyzer (Partica LA-950, Horiba). Samples were dispersed in water. Refractive index of scorodite was adopted as 1.797 (Ondrus et al., 1997).

2.4.2.7 Specific surface area (BET method)

Specific surface area of seed scorodite (bioscorodite and chemical scorodite) was measured using BET (Brunauer–Emmett–Teller) theory (BEL-Max, MicrotracBEL) based on adsorption isotherms using N_2 gas at −196°C. Adsorbed water and gases were removed under vacuum at 80°C for 50 hours prior to measurement. The pore size distributions of seed scorodite were calculated using the Barrett–Joyner–Halenda (BJH) equation.

2.4.2.8 Zeta-potential measurement

Zeta-potentials of *Ac. brierleyi* cells (5.0×10^7 cells/ml) or precipitates (0.2% (w/v)) were measured in 10^{-3} M KCl or 10^{-2} M NaCl solutions using Zetasizer Nano ZS (Malvern) at pH values ranging from 2.0 to 5.0 (adjusted with HCl and KOH). All measurements were conducted at least in triplicate.

2.5 Stability evaluation of bioscorodite/chemical scorodite

2.5.1 Toxicity characteristic leaching procedure (TCLP)

The TCLP test was conducted by following the EPA method 1311 (EPA, 1992). Original scorodite seeds formed in chapter 4 "*4.2.1 Preparation of bioscorodite and chemical scorodite as seed crystals*" and final bioscorodite produces formed in

"*4.2.2 Bioscorodite crystallization experiment fed with seed crystals*" (using $[As(III)]_{ini}$ = 4.7 mM and $[Fe(II)]_{ini}$ = 9.5 mM) were transferred into 25 ml vials containing 10 ml acetate buffer (pH 4.93) at a pulp density of 5% (w/v) (solid : liquid = 1 : 20) and incubated at 25°C, rotated at 30 rpm for 18 hours. Liquid samples were filtered (0.45 μm glass fiber) to measure total soluble Fe and As concentrations. Tests were conducted in duplicates.

Acetate buffer at pH 4.93 was prepared following the protocol: 5.7 ml glacial CH_3COOH and 64.3 ml 1 N NaOH were added to 500 ml of distilled water and diluted to a volume of 1 l.

2.5.2 Japanese leaching test No. 46 (JLT46)

The JLT46 test was conducted by following the Japan Environment Agency Notification No. 46. Original scorodite seeds formed in "*4.2.1 Preparation of bioscorodite and chemical scorodite as seed crystals*" were transferred into 5 ml vials containing 5 ml distilled water (pH 5.8–6.3 adjusted with HCl) at a pulp density of 10% (w/v) (solid : liquid = 1 : 10) and shaken at 200 rpm for 6 hours. The leachate was allowed to stand for 10 min and centrifuged at 3000 rpm for 20 min. The supernatants were filtered (0.45 μm membrane filter) to measure total soluble Fe and As concentrations. Tests were conducted in duplicates.

2.6 Ion activity product (IAP) calculation

The IAP of bioscorodite was calculated as Eq. 2.1, based on its congruent dissolution (Eq. 2.2). Ionic activities of Fe(III) and As(V) were calculated from Eq. 2.3 and 2.4, using the measured pH values ($a_{H^+} = 10^{-pH}$) and total soluble concentrations of Fe(III) and As(V) (M), respectively. The hydrolysis constants (K_i) at 70°C were

calculated using the van't Hoff equation (Table 2.1 and Eq. 2.5; Dove and Rimstidt, 1985; Gonzalez-Contreras et al., 2010).

$$\mathrm{IAP_{scorodite}} = (a_{\mathrm{Fe^{3+}}})(a_{\mathrm{AsO_4{}^{3-}}}) \quad \text{(Eq. 2.1)}$$

$$\mathrm{FeAsO_4{\cdot}2H_2O\ (scorodite) \rightleftarrows Fe^{3+} + AsO_4^{3-} + 2H_2O} \quad \text{(Eq. 2.2)}$$

$$a_{\mathrm{Fe^{3+}}} = \frac{\mathrm{Fe(III)_{total}}}{1+\frac{K_{\mathrm{Fe1}}}{a_{\mathrm{H^+}}}+\frac{K_{\mathrm{Fe1}}K_{\mathrm{Fe2}}}{(a_{\mathrm{H^+}})^2}+\frac{K_{\mathrm{Fe1}}K_{\mathrm{Fe2}}K_{\mathrm{Fe3}}}{(a_{\mathrm{H^+}})^3}+\frac{K_{\mathrm{Fe1}}K_{\mathrm{Fe2}}K_{\mathrm{Fe3}}K_{\mathrm{Fe4}}}{(a_{\mathrm{H^+}})^4}} \quad \text{(Eq. 2.3)}$$

$$a_{\mathrm{AsO_4{}^{3-}}} = \frac{\mathrm{As(V)_{total}}}{1+\frac{a_{\mathrm{H^+}}}{K_{\mathrm{As3}}}+\frac{(a_{\mathrm{H^+}})^2}{K_{\mathrm{As2}}K_{\mathrm{As3}}}+\frac{(a_{\mathrm{H^+}})^3}{K_{\mathrm{As1}}K_{\mathrm{As2}}K_{\mathrm{As3}}}} \quad \text{(Eq. 2.4)}$$

Table 2.1 Hydrolysis constants of Fe(III) and As(V) at 25°C (Dove and Rimstidt, 1985) and 70°C.

		p*K* (25°C) Dove and Rimstidt, 1985	p*K* (70°C) van't Hoff Equation
Ferric iron; Fe(III)			
$Fe^{3+} + H_2O = Fe(OH)^{2+} + H^+$	K_{Fe1}	2.19	2.18
$Fe(OH)^{2+} + H_2O = Fe(OH)_2^{+} + H^+$	K_{Fe2}	3.48	3.47
$Fe(OH)_2^{+} + H_2O = Fe(OH)_3 + H^+$	K_{Fe3}	6.33	6.31
$Fe(OH)_3 + H_2O = Fe(OH)_4^{-} + H^+$	K_{Fe4}	9.6	9.57
Arsenate; As(V)			
$H_3AsO_4 = H_2AsO_4^{-} + H^+$	K_{As1}	2.24	2.27
$H_2AsO_4^{-} = HAsO_4^{2-} + H^+$	K_{As2}	6.86	6.94
$HAsO_4^{2-} = AsO_4^{3-} + H^+$	K_{As3}	11.49	11.51

$$-\ln K_{70°C} = -\ln K_{25°C} + \frac{\Delta H_r{}^0}{R}\left(\frac{1}{T_{70°C}} - \frac{1}{T_{25°C}}\right) \quad \text{(Eq. 2.5)}$$

, where ΔH_r^0; standard reaction enthalpy (kJ/mol), T; temperature (K), R; gas constant = 8.314 (J/mol·K).

Concentrations of Fe(III) and As(V) were determined as the activity of various dissolved ion species as shown in Eqs. 2.6 and 2.7.

$$\mathrm{Fe(III)_{total}} = a_{\mathrm{Fe^{3+}}} + a_{\mathrm{Fe(OH)^{2+}}} + a_{\mathrm{Fe(OH)_2{}^{+}}} + a_{\mathrm{Fe(OH)_3}} + a_{\mathrm{Fe(OH)_4{}^{-}}} \quad \text{(Eq. 2.6)}$$

$$\mathrm{As(V)_{total}} = a_{\mathrm{AsO_4{}^{3-}}} + a_{\mathrm{HAsO_4{}^{2-}}} + a_{\mathrm{H_2AsO_4{}^{-}}} + a_{\mathrm{H_3AsO_4}} \quad \text{(Eq. 2.7)}$$

The equations for hydrolysis of Fe(III) (Eqs. 2.8–2.11) and As(V) (Eqs. 2.12–2.14) are based on the reactions shown in Table 2.1. Activities of Fe(III) and As(V) (Eqs. 2.3 and 2.4, respectively) are obtained by applying Eqs. 2.8–2.11 and 2.12–2.14 to Eqs. 2.6 and 2.7, respectively.

$$K_{\mathrm{Fe1}} = \frac{[\mathrm{Fe(OH)^{2+}}][\mathrm{H^+}]}{[\mathrm{Fe^{3+}}]} \quad \text{(Eq. 2.8)}$$

$$K_{\mathrm{Fe2}} = \frac{[\mathrm{Fe(OH)_2{}^{+}}][\mathrm{H^+}]}{[\mathrm{Fe(OH)^{2+}}]} \quad \text{(Eq. 2.9)}$$

$$K_{\mathrm{Fe3}} = \frac{[\mathrm{Fe(OH)_3}][\mathrm{H^+}]}{[\mathrm{Fe(OH)_2{}^{+}}]} \quad \text{(Eq. 2.10)}$$

$$K_{\mathrm{Fe4}} = \frac{[\mathrm{Fe(OH)_4{}^{-}}][\mathrm{H^+}]}{[\mathrm{Fe(OH)_3}]} \quad \text{(Eq. 2.11)}$$

$$K_{\mathrm{As1}} = \frac{[\mathrm{H_2AsO_4{}^{-}}][\mathrm{H^+}]}{[\mathrm{H_3AsO_4}]} \quad \text{(Eq. 2.12)}$$

$$K_{\mathrm{As2}} = \frac{[\mathrm{HAsO_4{}^{2-}}][\mathrm{H^+}]}{[\mathrm{H_2AsO_4{}^{-}}]} \quad \text{(Eq. 2.13)}$$

$$K_{\mathrm{As3}} = \frac{[\mathrm{AsO_4{}^{3-}}][\mathrm{H^+}]}{[\mathrm{HAsO_4{}^{2-}}]} \quad \text{(Eq. 2.14)}$$

Chapter 3

Biooxidation of gold-bearing highly refractory sulfide concentrates

3.1 Introduction

To enhance gold recovery by cyanidation, refractory gold ores which are recognized as invisible gold incorporated in pyrite (FeS_2) and arsenopyrite (FeAsS) generally require a pyrometallurgical or hydrometallurgical pretreatment process. Biooxidation of refractory gold ore has become a preferred pretreatment technology prior to cyanidation for gold recovery.

Biooxidation process is based on microbial activities to oxidize and dissolute unnecessary sulfide mineral matrix to expose occluded gold. Upon dissolution of arsenopyrite, As is dissolved in the form of As(III) (Breed et al., 1996; Mandl et al., 1992). It was reported that oxidation of As(III) to As(V) by Fe(III) is mediated during mineral dissolution by the presence of pyrite as an electron mediator (Barrett et al., 1993; Wiertz et al., 2006). Since As(III) is highly toxic and mobile compared to As(V) especially at acidic pH (Cullen and Reimer, 1989; Matschullat, 2000), biooxidation microbes would benefit from the oxidation reaction of As(III) to As(V) in order to maintain their activity. In this sense, mineral-oxidizing microbes possessing As(III) tolerance as well as As(III) oxidation ability would have advantages during biooxidation. However, As(III) oxidizing abilities in moderately thermophilic, extremely acidophilic bacteria are yet largely unknown.

Microbial oxidative dissolution of minerals is often accompanied with formation of passivation (a layer of secondary mineral precipitates) on the mineral surface. Secondary minerals such as jarosite and elemental sulfur are generally considered to hinder biooxidation/bioleaching efficiencies. Optimization of the metal recovery, therefore, requires understanding of major passivation reactions involved during the biooxidation.

Most studies on arsenopyrite oxidation by pure cultures have been done with

a mesophile *Acidithiobacillus ferrooxidans* (e.g., Ehrlich, 1964; Fernandez et al., 1995; Mandl et al., 1992; Tuovinen et al., 1994), whereas other studies used mesophilic *Leptospirillum ferrooxidans* (Corkhill et al., 2008) and thermophilic *Sulfolobus acidocaldarius* (Escobar et al., 2000). Mixed microbial cultures can be considered more robust than pure cultures as they meet different physico-chemical conditions during biooxidation. In fact, they are often significantly more effective in sulfide mineral dissolution (Johnson, 1998).

Precise comparison studies on pure and mixed cultures have clarified this trend for biooxidation of ground rock pyrite using moderate thermophiles (*Leptospirillum* sp. MT6, *Am. ferrooxidans, At. caldus, Alicyclobacillus* sp. Y004, three *Sulfobacillus* spp. and *Ferroplasma* sp. MT17): A mixed culture comprising *Leptospirillum* MT6, *At. caldus* and *Ferroplasma* MT17 was the most efficient of all of those tested, followed by an almost comparable mixed culture of *Am. ferrooxidans* and *At. caldus* (Okibe and Johnson, 2004). The advantages of mixed cultures were also noted for arsenopyrite biooxidation using moderately thermophilic *At. caldus* strains and *Sulfobacillus thermosulfidooxidans* by Dopson and Lindström (1999). The well-known BIOX™ process also utilizes a mixed population of *At. ferrooxidans, Acidithiobacillus thiooxidans* and *L. ferrooxidans* (van Aswegen et al., 2007).

Although biooxidation is now recognized as an alternative to conventional pretreatment techniques (e.g., roasting and pressure oxidation) and alkali dissolution, few literatures are available which compared different pretreatment options for the process screening purpose (but see technical papers available from the Xstrata ALBIO PROCESS™ website; Aylmore and Jaffer, 2012; Hourn et al., 2005). Hourn et al. (2005) reported that the Au recovery was greater with the Albion™ process (alkali dissolution; 92%) and pressure oxidation (94%), than with biooxidation (78%). The Ag

recovery was significantly lower with biooxidation (25%) and pressure oxidation (4%) than with the Albion™ process (75%), although detailed methodologies used are unknown.

This study compared pure and defined mixed cultures of three moderately thermophilic, extremely acidophilic bacterial strains (*Am. ferrooxidans* ICP, *Sb. sibiricus* N1, *At. caldus* KU) for their efficacy in biooxidation of highly refractory polymetallic gold ore concentrates. Factors to affect mineral dissolution efficiencies, such as microbial As(III) oxidation ability, formation of different secondary mineral precipitates, and microbial population dynamics during biooxidation, were also investigated. For the initial process screening purpose, effectiveness of biooxidation using the defined mixed cultures was finally compared to that of three other abiotic pretreatment options for the recovery of Au and Ag after cyanidation.

3.2 Materials and Methods

3.2.1 Minerals

The gold-, silver-, and antimony-bearing sulfide ore concentrate from Alaska used in this study was shown highly refractory (total Au and Ag recovery of only 1.1% and 3.2%, respectively, without any pretreatment), with complex mineralogy. Its elemental and mineral compositions are shown in Tables 3.1 and 3.2, respectively. During the flotation process, the gold ore was subjected to the flotation collectors (AERO® 6697 promoter; 42% sodium diisobutyl monothiophosphate, 3.0% sodium diisobutyl dithiophsphate, 0.5% sodium hydroxide, and PAX; potassium amyl xanthate), and OrePrep® F-549 Frother (a mixture of polyglycols). Prior to biooxidation experiments, the gold ore concentrate was washed with 1 M HNO3, deionized water, and ethanol.

Table 3.1 Elemental composition of the gold ore concentrate used in this study.

Element	Abundance (%)
Fe	19
As	9.8
S	19
Pb	3.7
Sb	4.3
Mn	0.18
Cu	0.06
Na	0.02
Zn	1.8
CaO	0.30
MgO	0.39
Al_2O_3	6.6
SiO_2	30
Size (P_{80})	20 μm
Au	23 g/t
Ag	364 g/t

Table 3.2 Mineral composition of the gold ore concentrate used in this study.

Mineral	Chemical formula	Abundance (%)
Arsenopyrite	FeAsS	24
Boulangerite	$Pb_5Sb_4S_{11}$	1.6
Stibnite	Sb_2S_3	2.3
Jamesonite	$Pb_4FeSb_6S_{14}$	5.2
Fuloppite	$Pb_3Sb_8S_{15}$	1.2
Andorite	$PbAgSb_3S_6$	0.3
Tetrahedrite	$(Cu,Ag)[Cu_4(Fe,Zn)_2]Sb_{14}S_{13}$	0.1
Pyrite	FeS_2	22
Sphalerite	((Zn,Fe)S)	3.5
Galena	PbS	0.5
Gangue		40

3.2.2 Biooxidation experiments

Pure or mixed cultures of moderate thermophiles were inoculated (final cell density; 1.0×10^7 cells/ml for each strain) in 500 ml Erlenmeyer flasks containing 200 ml of HBS medium (pH 1.5 with H_2SO_4) with 2% (w/v) mineral concentrate and 0.02% (w/v) yeast extract. Flasks were incubated at 45°C, shaken at 100 rpm. Well-mixed slurry samples were regularly withdrawn to monitor cell density, pH, Eh vs SHE, and concentrations of total Fe, total As, Fe(II) and As(III). For real-time PCR analysis of the microbial population structure, 10 ml of well-mixed slurry samples were taken from mixed cultures at day 14 and 30, followed by genomic DNA extraction using Soil DNA Isolation Kit (MO BIO). All experiments were done in duplicate.

3.2.3. Real-time PCR

To construct standard curves, genomic DNA was purified from pure culture of each strain using Ultra Clean Microbial DNA Isolation Kit (MO BIO). The genomic DNA was then used as template to amplify the partial 16S rRNA gene fragment (~ 270 bp) by Touchdown PCR using universal primer set (Buniv-F1 and Buniv-R1; Table 3.3). The PCR mixture (final volume 50 μl) included 25 μl Premix Taq (TaKaRa BIO), 15 pmol of each primer, and 2.5 μl DNA template. The final volume was adjusted with sterilized deionized water. Touchdown PCR was performed as follows: One cycle of 94°C for 2 min; before 7 cycles of 94°C for 20 sec, 58°C for 20 sec (decreasing by 0.5°C per cycle) and 72°C for 15 sec; which then links to 20 cycles of 94°C for 20 sec, 55°C for 20 sec and 72°C for 15 sec.

The resultant PCR products were extracted from agarose gel using QIAquick Gel Extraction Kit (Qiagen) and quantified. The 270-bp PCR product deriving from

each strain was diluted serially to give a final concentration of 1.0×10^3 to 1.0×10^8 copies/μl, to be used as template DNA for real-time PCR using species-specific primer set. The real-time PCR mixture (final volume 20 μl) contained 10 μl of SsoAdvanced SYBR Green Supermix (BioRad), 1 μl of template DNA, and 6 pmol of each primer (Table 3.3). The final volume was adjusted with sterilized deionized water. The real-time PCR was run as follows: One cycle of 95°C for 3 min, and then 40 cycles of 95°C for 10 sec and 70°C for 15 sec.

At the completion of each run, melting curves for the PCR products were measured by raising the temperature from 65 to 90°C, to examine the specificity of the PCR amplification. Linearity in the standard curve was obtained within the range of 1.0×10^3 to 1.0×10^9 copies/test for all three species. Next, a synthetic DNA mixture (composed of 1.0×10^7, 1.0×10^8, or 1.0×10^9 copies/test each from the three strains) was tested against each one of the three species-specific primer sets. All species-specific primer sets showed over 10^2-fold specificity against the target species, compared with nontarget species, ensuring the accuracy to display the results as percentages in whole numbers. Genomic DNAs purified from the actual biooxidation mixed cultures were then tested against the corresponding species-specific primer sets.

Table 3.3 PCR primers used in this study.

Primer set	Primer sequence (5'→ 3')	PCR product size	Target species
Buniv-F1 Buniv-R1	GTAGTCCACGCCSTAAACGWTG GAGCTGAC GACARC CATGCA	~270 bp	Universal (modified from "NR-F2" and "NR-R2 primers; Liu et al. 2006)
Acaldus-F1 Buniv-R1	TTGGCGCCTTAGGTGCTGAG -	240 bp	Species-specific; At. caldus (modified from "Acaldus-P1" primer; Liu et al. 2006)
Sbsib-F1 Buniv-R1	TAGGTGTCGCCCGGGTCCAC -	241 bp	Species-specific; *Sb. sibiricus* (this study)
Amferro-F1 Buniv-R1	TCATTCGACGGGCTCCGTG -	231 bp	Species-specific; *Am. ferrooxidans* (this study)

3.2.4. Other abiotic pretreatment options

Three following abiotic pre-treatments were conducted for the flotation concentrate: (1) pressure oxidation; flotation concentrate (P_{80} = 10 μm) was oxidized under vapor pressure 2.2 MPa at 120°C for 2 hours with addition of 45 g/l Fe(III) and 0.2 g/l lignin sulfonate, and 2 l/min O_2 aeration, (2) roasting; reducing roasting at 2 l/min N_2 supply were conducted at 600˚C for 1 hour, then oxidizing roasting 2 l/min aeration were conducted at 600˚C for 2 hours for flotation concentrate (P_{80} = 20 μm), (3) alkali dissolution; NaOH 497 kg/t was added to flotation concentrate (P_{80} = 20 μm) and reacted at 80°C for 20 hours with 0.8 l/min aeration.

3.2.5 Cyanide leaching for solid residues

Cyanide leaching was carried out for the solid residues obtained from each pretreatment procedure. Preaeration was conducted using 20% pulp density at 1 l/min O_2 for 8 h, followed by cyanidation at pH > 10.5 by maintaining the CN^-concentration at 1,000 ppm (added as NaCN), for 72 h.

3.3 Results and Discussion

3.3.1 Biooxidation of the gold ore concentrates by pure cultures

Biooxidation efficiencies of the gold ore concentrate by different pure cultures (without initial Fe(II) addition) were compared in Figures 3.1a–d. A heterotrophic iron-oxidizer, *Am. ferrooxidans* ICP was unable to grow even though the medium contained yeast extract as well as a small amount of soluble Fe(II); i.e., Fe(II) remained unoxidized (Figure 3.1b) and the amount of total Fe solubilized was similar to that in sterile control and non-iron-oxidizing *At. caldus* KU cultures (Figure 3.1a).

An iron- and sulfur-oxidizing mixotroph, *Sb. sibiricus* N1 was capable of

oxidizing the ore concentrate to some extent (45% of Fe solubilized by day 30; Table 3.4) by readily re-oxidizing Fe(II) to maintain high Eh values (Figure 3.1b). Its initial cell growth was also supported by metabolism of residual reduced inorganic sulfur compounds (RISCs) in the gold ore concentrate medium, as was also seen with a sulfur-oxidizing autotroph, *At. caldus* KU (Figure 3.1d). Figure 2c shows that As solubilized from the ore concentrate in the form of As(III) (Langhans et al., 1995), was partly oxidized to As(V) during biooxidation.

Addition of 10 mM Fe(II) greatly supported initial growth of *Am. ferrooxidans* ICP (data not shown), however, this bacterium still failed to oxidize Fe(II) and only 25% of Fe was solubilized by day 30 (Table 3.4). Initial addition of 10 mM Fe(II) also facilitated *Sb. sibiricus* N1 growth and Fe(II) was readily oxidized to Fe(III). However, the Eh value suddenly dropped at day 2 (data not shown), indicating the deposition of secondary precipitates. As a result, the extent of Fe solubilization was lowered from 45% to 31% (Table 3.4). This time, As(III) oxidation to As(V) was not noticeable in both *Sb. sibiricus* N1 and *Am. ferrooxidans* ICP pure cultures: This may be due to the deterioration of the pyrite surface as electron mediator for As(III) oxidation, through deposition of secondary precipitates (Barrett et al., 1993).

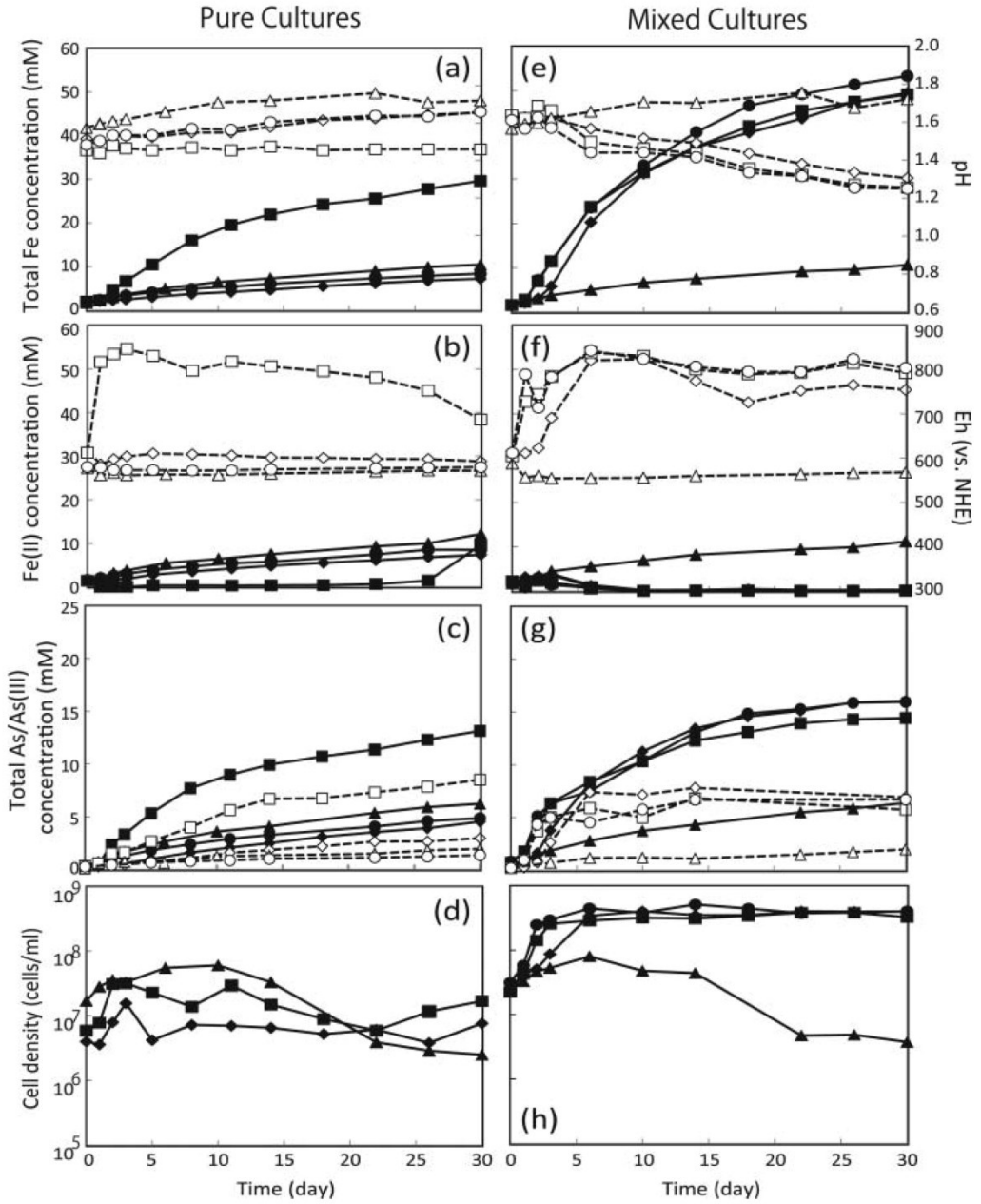

Figure 3.1 Biooxidation of the ore concentrate in pure (a-d) and mixed (e-h) cultures (without initial Fe(II) addition): (a, e) Total Fe concentrations (solid lines) and pH (broken lines); (b, f) Fe(II) concentrations (solid lines) and Eh (vs. NHE, broken lines); (c, g) Total As concentrations (solid lines) and As(III) concentrations (broken lines); (d, h) cell densities. Symbols in pure cultures: *Am. ferrooxidans* ICP (♦ ◊), *Sb. sibiricus* N1 (▪ □), *At. caldus* KU (▲△), sterile (• ○). Symbols in mixed cultures: *Am. ferrooxidans* ICP + *At. caldus* KU (♦ ◊), *Sb. sibiricus* N1 + *At. caldus* KU (▪ □), *Am. ferrooxidans* ICP + *Sb. sibiricus* N1 (▲△), *Am. ferrooxidans* ICP + *Sb. sibiricus* N1+ *At. caldus* KU (• ○).

3.3.2 Biooxidation of the gold ore concentrates by defined mixed cultures

Without initial addition of Fe(II), mixed culture of two iron-oxidizers (*Am. ferrooxidans* ICP and *Sb. sibiricus* N1) was ineffective at mineral dissolution and behaved similarly in all parameters to pure culture of *Am. ferrooxidans* ICP (Figures 3.1a–d; Table 3.4). Even though *Sb. sibiricus* N1 has advantages over *Am. ferrooxidans* ICP in metabolic capability of sulfur, the results indicate that the former was unable to compete with the latter for their substrates such as Fe(II) and organics. When *At. caldus* KU was mixed with one or both of the iron-oxidizers, mineral dissolution became significantly more effective; 74–80% of Fe and 55–61% of As were solubilized (Figure 3.1e, g; Table 3.4), and high cell densities as well as Eh values were maintained throughout the experiment (Figure 3.1f, h).

Culture pHs continued to decline down to approximately 1.3 (Figure 3.1e), due to its sulfur metabolism eventually producing sulfate. Interestingly, although *Am. ferrooxidans* ICP failed to oxidize Fe(II) in pure cultures (even though yeast extract was present), the presence of *At. caldus* KU in mixed culture indirectly enabled *Am. ferrooxidans* ICP to effectively exhibit its Fe(II) oxidation ability. Furthermore, oxidation of highly toxic As(III) to less toxic As(V) was especially noticeable in mixed cultures containing *At. caldus* KU: Concentrations of As(III) released from the ore concentrate reached their limits by day 3–5, whereas As(V) concentrations continuously increased thereafter (Figure 3.1g). This observation likely has resulted from the role of *At. caldus* KU in maintaining clean pyrite catalytic surfaces by avoiding precipitation of unwanted passivation layers (Barrett et al., 1993; Dopson and Lindström, 1999).

Initial addition of 10 mM Fe(II) generally did not affect positively on mineral dissolution by mixed cultures containing *At. caldus* KU (Table 3.4). Upon 10 mM

Fe(II) addition, a mixed culture of the two iron-oxidizers (*Am. ferrooxidans* ICP and *Sb. sibiricus* N1) behaved similarly to pure cultures of *Sb. sibiricus* N1, rather than those of *Am. ferrooxidans* ICP (Table 3.4): Since the trend was reverse without initial Fe(II) addition, the results here again suggest that *Sb. sibiricus* N1 fails to compete with *Am. ferrooxidans* ICP for Fe(II).

Table 4 shows that the dissolution of Fe was higher than those of As in mixed cultures containing *At. caldus* KU, whereas the trend was reverse in other pure and mixed cultures. This indicates that the presence of *At. caldus* KU prevented solubilized Fe ions from precipitating as secondary minerals, by lowering culture pHs.

Table 3.4 Amount of Fe and As solubilized in pure and mixed cultures after 30-days' biooxidation.

	No Fe(II) added		10 mM Fe(II) added	
Cultures	Fe solubilized (%)	As solubilized (%)	Fe solubilized (%)	As solubilized (%)
Am. ferrooxidans ICP	11	17	25	49
Sb. sibiricus N1	45	50	31	41
At. caldus KU	16	24	14	24
Am. ferrooxidans ICP + *Sb. sibiricus* N1	16	25	34	34
Am. ferrooxidans ICP + *At. caldus* KU	74	61	76	62
Sb. sibiricus N1 + *At. caldus* KU	74	55	73	57
Am. ferrooxidans ICP + *Sb. sibiricus* N1 + *At. caldus* KU	80	61	73	56
Sterile	13	19	16	21

Population structure analysis was conducted for effective mixed cultures containing *At. caldus* KU, using real-time PCR based on the amount of 16S rRNA genes of each strain. According to the known copy number of 16S rRNA genes per genome (i.e., 2 copes for *At. caldus* KU, Valdes et al., 2009; 2 copies for *Am. ferrooxidans* ICP, Clum et al., 2009; 3–5 copies for other *Sulfobacillus* spp., Anderson et al., 2012; Li et al., 2011; Travisany et al., 2012, the abundance of *Sb. sibiricus* N1 may be overestimated in this study. However, a general trend observed by real-time PCR was that *At. caldus* KU was the dominant species in all mixed cultures (Figure 3.2), due to more energy being available from oxidation of RISCs than that of Fe(II) (Okibe et al., 2003): The results suggest its major role in supporting the mineral dissolution.

The population ratios of iron-oxidizer(s) to *At. caldus*, however, somewhat increased at the later stage of biooxidation, owing to accumulation of dissolved organic carbon (deriving from *At. caldus* KU cell lysates and exudates) being utilized by heterotrophic/mixotrophic iron-oxidizers (Dopson and Lindström, 1999; Schnaitm and Lundgren, 1965). Although yeast extract was supplemented in this biooxidation experiment (expecting its possible effect in boosting microbial As(III) oxidation, as was observed with *Ac. brierleyi*; Okibe et al., 2014), it is generally not required by the heterotrophs/mixotrophs in mixed cultures with *At. caldus*, since the latter readily supports the growth of the former during biooxidation (e.g., Okibe and Johnson, 2004).

In biooxidation of ground rock pyrite (as a model mineral of high purity), a mixed culture comprising *Leptospirillum* MT6, *At. caldus* and *Ferroplasma* MT17 was the most efficient of all of those tested. Another mixed culture of *Am. ferrooxidans* and *At. caldus* also showed, however, almost comparative efficacy to the former (Okibe and Johnson, 2004). For biooxidation of the ore concentrate, rather than unprocessed

ores, residual flotation reagents may affect microbial activities: The fact that pure cultures of *Leptospirillum* MT6 were able to grow on unprocessed rock pyrite, but not on pyrite concentrate even after acid-washing (Okibe and Johnson, 2001) indeed indicates that toxicity effects of residual flotation reagents need to be taken into account in biooxidation.

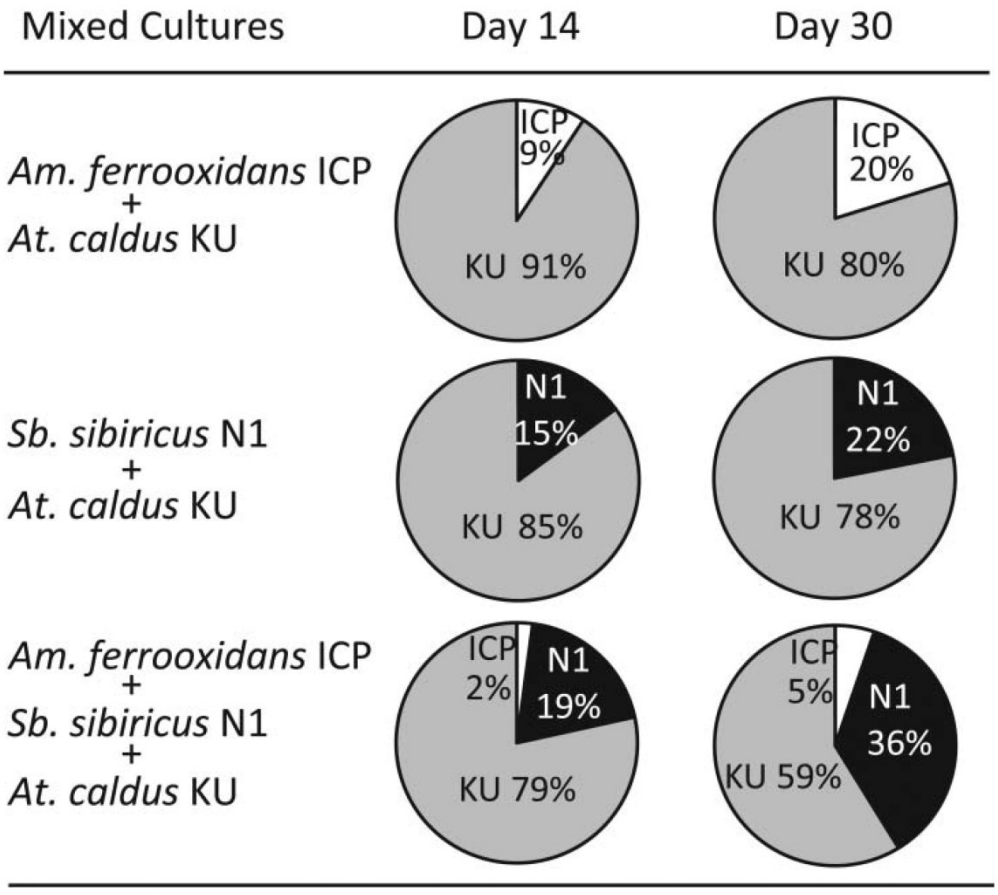

Figure 3.2 Population dynamics of mixed cultures of *Am. ferrooxidans* ICP + *At. caldus* KU, *Sb. sibiricus* N1 + *At. caldus* KU, and *Am. ferrooxidans* ICP + *Sb. sibiricus* N1 + *At. caldus* KU at day 14 and day 30 of biooxidation.

Okibe and Johnson (2002) reported that among the five mineral-oxidizing moderately thermophiles (*Leptospirillum* MT6, *Ferroplasma* MT17, *At. caldus* KU, *Sulfobacillus* NC, and *Am. ferrooxidans* ICP), *At. caldus* KU, *Sulfobacillus* NC, and *Am. ferrooxidans* ICP were shown to be robust to different flotation reagents, whereas the other two species were far more sensitive. In this study, dissolution of the highly refractory polymetallic gold ore concentrate (containing a mixture of potentially inhibitory metals and metalloids; e.g., Pb, Mn, Cu, Zn, Sb, As) was shown effective in mixed cultures of flotation reagent-tolerant moderately thermophilic species, even in a relatively simple mixed culture of two species, *Am. ferrooxidans* ICP and *At. caldus* KU. Such moderate thermophilic mixed cultures may become more advantageous than those comprising of flotation reagent-sensitive strains, depending on the ore concentrates used.

3.3.3 Evaluation of microbial As(III) oxidation ability

When each of the three moderate thermophiles was inoculated at 1.0×10^8 cell/ml in heterotrophic basal salts containing 6.5 mM As(III) without Fe(II) or tetrathionate, neither cell growth nor As(III) oxidation was observed (Figures 3.3c, d). This indicates that the strains are not capable of growth by oxidizing As(III) as the energy source. When their respective energy source was provided (10 mM Fe(II) for ICP/N1 pure cultures; 10 mM Fe(II) plus 5 mM sodium tetrathionate for KU pure cultures and all mixed cultures), the growth was readily observed (expect for *Am. ferrooxidans* ICP + *Sb. sibiricus* N1 mixed cultures; Figure 3.3b) and Fe(II) quickly oxidized by iron-oxidizers (data not shown). However, no noticeable As(III) oxidation was detected in any pure and mixed cultures (Figure 3.3a).

It can be concluded, therefore, that partial As(III) oxidation to As(V) seen in

biooxidation cultures (Figures 3.1c, g) include neither microbial As(III) oxidation reaction, nor chemical As(III) oxidation in bulk solution. As was observed by Barrett et al. (1993), there is a kinetic restriction of As(III) oxidation coupled with Fe(III) reduction and the reaction can be catalyzed only at the pyrite surface as an electron mediator. Possible indirect microbial roles (especially played by *At. caldus* KU in this study) involved in the As(III) oxidation process is to maintain clean pyrite catalytic surfaces by preventing formation of secondary passivation layers (e.g. elemental sulfur, jarosite, as was expected in biooxidation experiments); this would eventually support microbial growth and activity by lowering As(III) toxicity.

Although thermophilic, extremely acidophilic bioleaching archaea, *Acidianus brierleyi* and *Sulfolobus acidocaldarius* are known to oxidize As(III) (Okibe et al., 2013; Sehlin and Lindström, 1992), As(III) oxidizing abilities in moderately thermophilic, extremely acidophilic bacteria are yet largely unknown. In biooxidation experiments, arsenic was released from the concentrate in the form of highly toxic As(III), and partially oxidized to less toxic As(V): Because the three moderate thermophiles tested in this study were shown unable to oxidize As(III), this was shown simply due to chemical As(III) oxidation coupled with Fe(III) reduction, catalyzed on the pyrite surface. Search for those with effective As(III) oxidation ability would benefit further optimization of biooxidation process, in terms of minimizing its toxic effect on microbial activity, as well as remediation purpose of mining wastewaters.

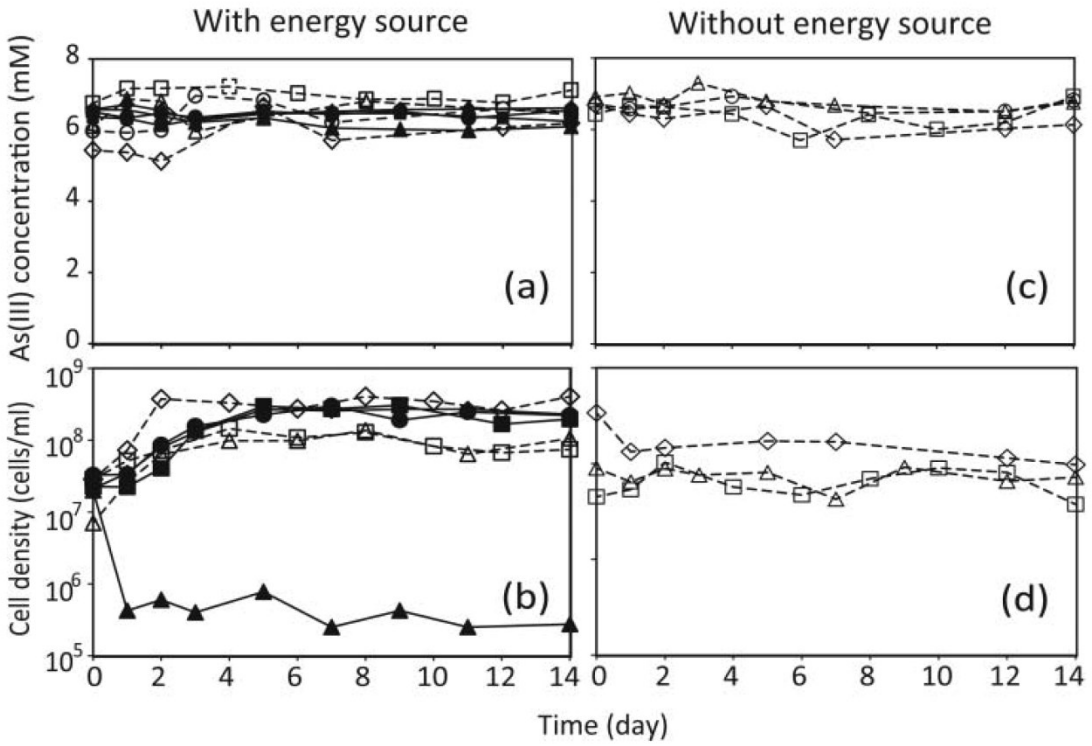

Figure 3.3 Evaluation of As(III) oxidation ability of the moderate thermophiles used for biooxidation, with (a, b) or without (c, d) respective energy source: (a, c) As(III) concentrations, (b, d) cell densities. Symbols: Broken lines indicate pure cultures of *Am. ferrooxidans* ICP (◊), *Sb. sibiricus* N1 (□), *At. caldus* KU (▲), and sterile culture (○). Solid lines indicate mixed cultures of *Am. ferrooxidans* ICP + *At. caldus* KU (♦), *Sb. sibiricus* N1 + *At. caldus* KU (□), *Am. ferrooxidans* ICP + *Sb. sibiricus* N1 (▲), and *Am. ferrooxidans* ICP + *Sb. sibiricus* N1 + *At. caldus* KU (•).

3.3.4 Residue analysis after biooxidation

After biooxidation, most of such sulfides peaks (e.g., arsenopyrite, pyrite, jamesonite) disappeared from XRD results (Figure 3.4a). Instead, peaks corresponding to insoluble anglesite ($PbSO_4$) appeared (Figure 3.4a), which were resulted from dissolution of Pb-containing sulfides (da Silva, 2004). Although mineralization of anglesite was readily noticeable by EPMA (e.g., particles P4 and P5 with the average elemental ratio of Pb:S:O = 1.0:1.0:4.1; Figure 3.4b), this secondary mineral tended to

precipitate independently, and its passivation on other mineral particles was not apparent. The formation of potassium jarosite ($KFe_3(SO_4)_2(OH)_6$) or scorodite ($FeAsO_4 \cdot 2H_2O$) were not observed after biooxidation (Figure 3.4a, b). A closer analysis of individual solid residues by EPMA revealed passivation layers locally formed on the surface of some particles (e.g., P1, P2, P3; Figure 3.4b). Beam spots from S1 through S6 exhibited similar elemental ratios and their average was calculated to be Fe:As:O:Sb:S = 0.9:0.8:6.0:0.5:0.6, indicating that passivation layers were composed mainly of scorodite. This was especially a characteristic feature observed with the remaining arsenopyrite grains after biooxidation, but not with pyrite grains. It is also interesting to note that Sb-enrichment was found accompanied with scorodite passivation, possibly by As replacement with Sb. Consequently, only a part of Sb, another valuable metal in the ore concentrate, was found soluble in the leachate. Although the amount of scorodite crystallization was limited based on the XRD result, microscopic observation with EPMA indicated that at least a part of As(III) solubilized from the ore concentrate was oxidized to As(V) and precipitated as scorodite during biooxidation. In contrast, no evidence of microscopic jarosite formation was found by EPMA. Overall, the formation of unwanted secondary mineral passivation was highly limited by the presence of *At. caldus* KU in mixed cultures, leading to a preferable effect to promote chemical As(III) oxidation by providing clean pyrite catalytic surface.

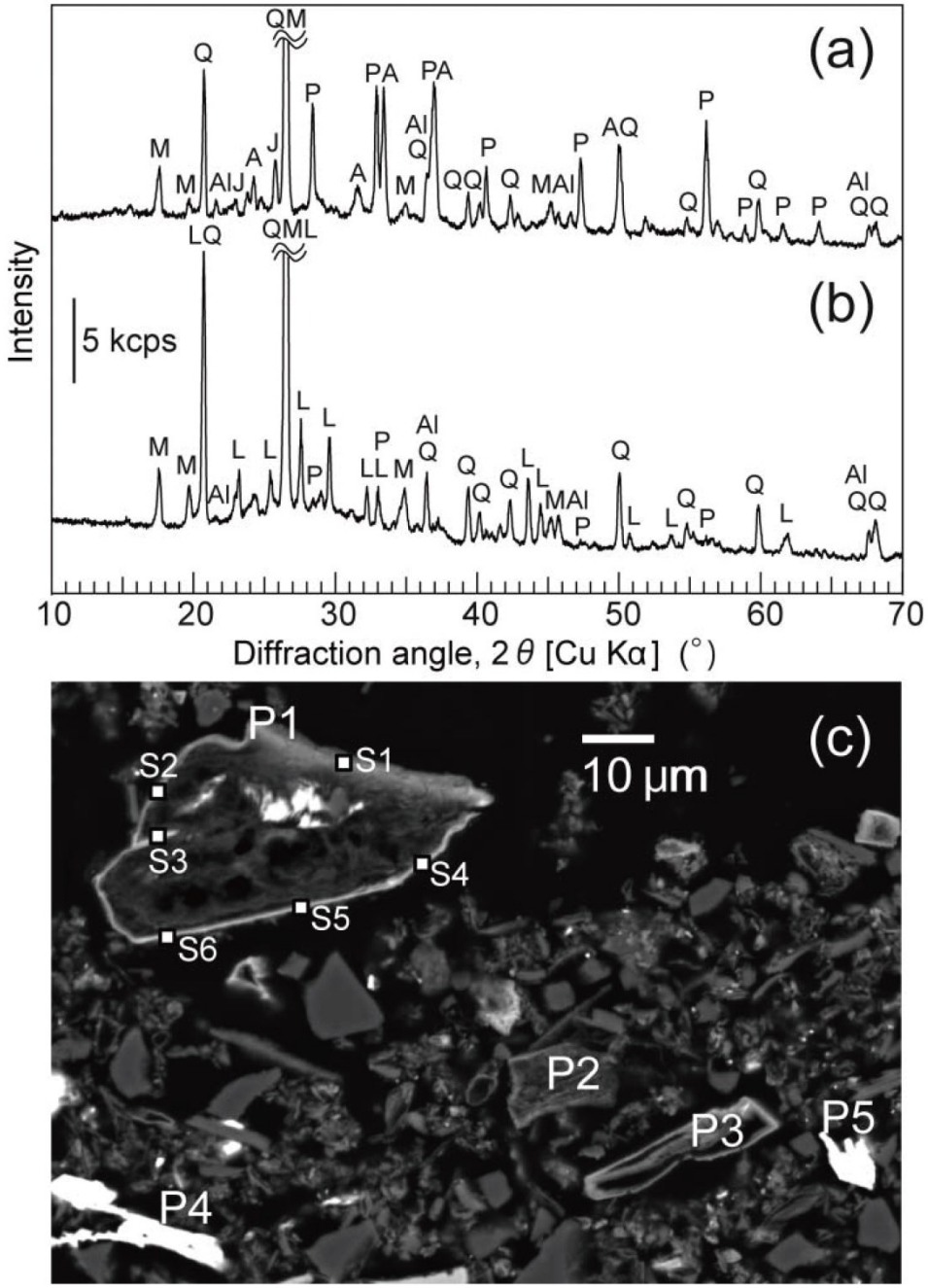

Figure 3.4 X-ray diffraction patterns of the ore concentrate before (a) and after (b) 30-days biooxidation. A; arsenopyrite (FeAsS; PDF No. 01-073-6021), P; pyrite (FeS_2; PDF No. 01-071-0053), J; Jamesonite ($Pb_4FeSb_6S_{14}$; PDF No. 00-042-1391), L; anglesite ($PbSO_4$; PDF No. 01-082-1855), Q; quartz (SiO_2; PDF No. 01-089-8936), Al; aluminium oxide (Al_2O_3; PDF No. 00-021-0010), M; potassium mica ($KAl_3Si_3O_{11}$; PDF No. 00-046-0741). (c) EPMA observation of the ore concentrate after biooxidation. P1-P5 and S1-S5 indicate the mineral particles and beam spot positions on the targets, respectively.

3.3.5 Recovery of gold and silver by cyanide leaching

A total of 200 g of the gold ore concentrate was bio-oxidized in the same flask set-ups, using the most effective mixed culture of all three moderate thermophiles (without initial addition of Fe(II)). After 30 days' incubation at 100 rpm, 45°C, the concentrations of Au, Ag, and Sb in the liquid phase were < 0.03 ppm, < 0.01 ppm, and 29.6 ppm, respectively. Solid residues were recovered after 30-days biooxidation, freeze-dried, and cyanide leached. The cyanide leaching and the recovery of Au and Ag obtained by biooxidation, were compared with those by other pretreatment options (Table 3.5). Other biooxidation studies on gold ore concentrates also reported an improvement in Au recovery (e.g., from 16.7% to 94.6%, Zaulochnyi et al., 2011; from 38% to 85%, Chandraprabha et al., 2002) and in Ag recovery (e.g., from 63% to 98%, Chandraprabha et al., 2002). Although the gold ore concentrate tested in this study was shown highly refractory (As; 1.1% and Ag; 3.2% without any pretreatment), the recovery of Au was still significantly improved by applying pretreatments such as biooxidation (86%), pressure oxidation (85%) and alkali dissolution (90%). It is worth noted that in the case of Ag, however, pressure oxidation turned out to be as ineffective as roasting, whereas biooxidation (87%) and alkali dissolution (87%) produced high total Ag recovery rates. Although the experiments were conducted in small-scales and further scaling-up will be needed to provide immediately implementable data, this study provides one of the very few available comparisons of the effectiveness of different pretreatment techniques for refractory gold ore concentrates. Overall, biooxidation using the described mixed cultures and alkali dissolution resulted to be the effective options for the highly refractory polymetallic gold ore concentrate in view of the Au and Ag recoveries.

Table 3.5 Total Au and Ag recovery and the amount of NaCN consumption using different pretreatment options.

Pretreatment option		None	Biooxidation	Pressure oxidation	Roasting	Alkali dissolution
Au	Flotation recovery (%)			95		
	Cyanide leaching recovery (%)[a]	1.2	91	90	59	95
	Total recovery (%)[b]	1.1	86	85	56	90
Ag	Flotation recovery (%)			97		
	Cyanide leaching recovery (%)[a]	3.3	89	23	21	90
	Total recovery (%)[b]	3.2	87	23	21	87
NaCN consumption		11	19	28	8.7	12

[a]Cyanide leaching recovery (%) = (1−(Au in residue) / (Au in feed)) × 100

[b]Total recovery (%) = Flotation recovery (%) × Cyanide leaching recovery (%) / 100

3.4 Conclusions

The findings of this study indicate the effectiveness of the defined mixed culture of moderately thermophilic, extremely acidophilic iron- and/or sulfur-oxidizing bacteria (*Am. ferrooxidans* ICP, *Sb. sibiricus* N1, *At. caldus* KU) for biooxidation of the gold-, silver, and antimony-bearing sulfide ore concentrate. Its usefulness can be stressed from the perspectives that; (i) the ore concentrate is highly refractory with complex mineralogy, containing a mixture of potentially inhibitory metals and metalloids, (ii) the three microbes used are flotation reagent-tolerant, and thus expected to show more robustness than other sensitive microbes to sulfide ore concentrates subjected to different flotation procedures, (iii) formation of unwanted passivation layers is highly limited in the mixed culture.

Roles of individual microbes and their synergistic interactions were elucidated, and the resultant biooxidation efficiencies were evaluated in detail, by comparing pure and mixed cultures of different permutations. Although none of the three moderate thermophiles exhibited direct As(III) oxidation activity, the involvement of indirect microbial effect in facilitating As(III) oxidation was noted. Finding and utilizing effective As(III)-oxidizing, moderately thermophilic extreme acidophiles may enable further optimization of the biooxidation process by minimizing As(III) toxicity.

Although an economically important rare metal, Sb, was solubilized during biooxidation, the evidence was found that Sb can be immobilized through formation of Sb-enriched scorodite. Applying the biooxidation pretreatment prior to cyanidation significantly improved the recoveries of both Au (from 1.1% to 86%) and Ag (from 3.2% to 87%), from highly refractory polymetallic gold ore concentrate. Compared with other abiotic pretreatment approaches (roasting, pressure oxidation, and alkali dissolution), biooxidation was shown to be one of the most effective options in terms

of the recovery of Au and Ag.

Data shown in this chapter were included in the paper accepted as:
Tanaka, M., Yamaji, Y., Fukano, Y., Shimada, K., Ishibashi, J.-I., Hirajima, T., Sasaki, K., Sawada, M. and Okibe, N., 2015. Biooxidation of gold-, silver, and antimony-bearing highly refractory polymetallic sulfide concentrates, and its comparison with abiotic pretreatment techniques. *Geomicrobiology Journal*, 32(6): 538-548.

Chapter 4

Optimal $[Fe(II)]_{ini}/[As(III)]_{ini}$ molar ratios and pH for bioscorodite crystallization efficiency from a range of dilute As(III) solutions

4.1 Introduction

Acidic wastewaters containing dilute As(III) (~8 mM) were produced after biooxidation of gold-ore concentrates in chapter 3. Partial As was immobilized as amorphous ferric arsenate, but not as crystalline scorodite at moderate temperature (45°C). For As-removal as the environmentally-stable forms, bioscorodite crystallization at 70°C from dilute As(III)-bearing acidic wastewaters was focused on.

Initial solution [Fe]/[As] molar ratio is one of the key factors affecting the efficiency of scorodite synthesis. General chemical synthesis methods commonly set to slightly higher $[Fe]_{ini}/[As]_{ini}$ molar ratios in the range of 1.0–1.5, even though the theoretical [Fe]/[As] molar ratio of scorodite is 1.0 ($FeAsO_4 \cdot 2H_2O$). In hydrothermal scorodite synthesis at 150°C, the rate of As precipitation decreased with increasing initial solution Fe(III)/As(V) molar ratios from 1.0 to 1.5–2.0 (Monhemius and Swash 1999). In previous research at $[As(III)]_{ini}$ = 6.5 mM, formed secondary minerals changes depending on the $[Fe(II)]_{ini}/[As(III)]_{ini}$ molar ratio (Okibe et al., 2013, 2014). Crystalline bioscorodite was precipitated by setting the molar ratio to 1.4, whilst higher molar ratio (2.8 and 5.5) resulted in formation of amorphous ferric arsenate. Whilst scorodite crystallization becomes further difficult at more dilute As concentrations under milder temperature condition, exploiting factors to enable such reaction is of great importance to broaden the applicability of scorodite method for a wide range of As(III)-contaminated waters. Hence, a range of As(III) solutions (3.3–26 mM) with varying $[Fe(II)]_{ini}/[As(III)]_{ini}$ molar ratios (0.8–6.0) was tested for bioscorodite crystallization to grasp the overall applicability of the bioscorodite method.

In addition, chemical scorodite syntheses are generally conducted at pH 1.0 or lower (Dutrizac and Jambor 1988; Gomez et al. 2011a; Fujita et al. 2008a, 2008b; Singhania et al. 2005). Fujita et al (2009b) chemically synthesized stable scorodite

particles at the pH range of 0.3–1.0, but higher pH levels (pH > 1.2) negatively affected scorodite stability. Still, microbial scorodite crystallization requires relatively higher pH than conventional chemical scorodite synthesis methodologies due to maintaining microbial activities such as cell growth, Fe(II) oxidation and As(III) oxidation (e.g., *Ac. brierleyi* at pH 1.5, Okibe et al., 2013, 2014, 2017; *Ac. sulfidivorans* at pH 1.0, Gonzalez-Contreras et al., 2010; mixed culture of *Sulfolobus* strains at pH 1.2, Gonzalez-Contreras et al., 2012a, 2012b). Therefore, the effect of lowing pH on bioscorodite crystallization was also tested here.

4.2 Materials and Methods

4.2.1 Bioscorodite crystallization experiment at dilute As(III) concentrations (3.3–26 mM) at pH 1.5

Pregrown *Ac. brierleyi* cells were inoculated (final cell density; 1.0 x 10^7 cells/ml) in 500 ml Erlenmeyer flasks containing 200 ml of HBS medium (pH 1.5 with H_2SO_4) with 4.5–36 mM Fe(II) (as $FeSO_4 \cdot 7H_2O$), 3.3–26 mM As(III) (as $NaAsO_2$) and 0.02% (w/v) yeast extract. $[Fe(II)]_{ini}/[As(III)]_{ini}$ molar ratio was set to 1.0–6.0. Bioscorodite were fed at 0.15% (w/v) as seed crystals where indicated. Flasks were incubated at 70°C, shaken at 100 rpm. Samples were regularly taken to monitor cell density, pH, Eh vs SHE, and concentrations of total Fe, total As, Fe(II) and As(III). Precipitates collected at the end of experiments were freeze-dried overnight for XRD (Ultima IV, Rigaku; Cu Kα 40 mA, 40 kV) and SEM (VE-9800, KEYENCE). Experiments were done in duplicate.

4.2.2 Bioscorodite crystallization experiment at pH 1.2

Ac. brierleyi cells were inoculated (final cell density; 1.0 x 10^7 cells/ml) in 500 ml Erlenmeyer flasks containing 200 ml of HBS medium (pH 1.2 with H_2SO_4) with 9.5 mM Fe(II) (as $FeSO_4 \cdot 7H_2O$), 4.7 mM As(III) (as $NaAsO_2$) and 0.02% (w/v) yeast extract. $[Fe(II)]_{ini}/[As(III)]_{ini}$ molar ratio was set to 2.0. Bioscorodite were fed at 0.15% (w/v) as seed crystals. Flasks were incubated at 70°C, shaken at 100 rpm. Samples were regularly taken to monitor cell density, pH, Eh vs SHE, and concentrations of total Fe, total As, Fe(II) and As(III). Precipitates collected at the end of experiments were freeze-dried overnight for XRD (Ultima IV, Rigaku; Cu Kα 40 mA, 40 kV) and SEM (VE-9800, KEYENCE). Experiments were done in duplicate.

4.3 Results and Discussion

4.3.1 Effect of $[Fe(II)]_{ini}/[As(III)]_{ini}$ molar ratio at pH 1.5

Bioscorodite crystallization test at $[As(III)]_{ini}$ = 4.7 mM (350 ppm) were showed in Figures 4.1 and 4.2. *Ac. brierleyi* were grown up to 1×10^8 cell/ml in all tested conditions by Fe(II) oxidation (Figures 4.1a and 4.2b). pH increased from 1.5 to 1.55–1.60 by Fe(II) oxidation and then decreased to 1.35 due to As(III) oxidation and precipitation (Figure 4.1b). Bioscorodite crystallization generally initiates with formation of brown-colored fine amorphous precipitates at the early stage (1st-stage As removal) which then turn pale-green in color (typical of scorodite) overnight at the middle stage (2nd-stage removal) (Okibe et al., 2017). In case of atmospheric scorodite synthesis at high As(V) concentration (100 mM) at 80°C, scorodite crystallization behavior was associated with the color change from brown to light-green (Le Berre et al., 2008). This reaction was also observed even at more dilute As(III) concentrations in this study.

Feeding (even at 0.15%) of bioscorodite seeds was found significantly effective especially when targeting more dilute $[As(III)]_{ini}$ of 3.3 mM (95% or 11% As removal with or without seeds at day 24, respectively at $[Fe(II)]_{ini}/[As(III)]_{ini}$ = 1.4; Table 4.1), and of 4.7 mM (94% or 15% As removal with or without seeds at day 21, respectively at $[Fe(II)]_{ini}/[As(III)]_{ini}$ = 1.4; Figure 4.3 and Table 4.1). Therefore, feeding bioscorodite seeds has favorable effects to improve bioscorodite formation from dilute As(III) solution (4.7 mM), a range of initial As(III) concentrations (3.3–20 mM) were tested to find their respective optimal $[Fe(II)]_{ini}/[As(III)]_{ini}$ molar ratio under these conditions.

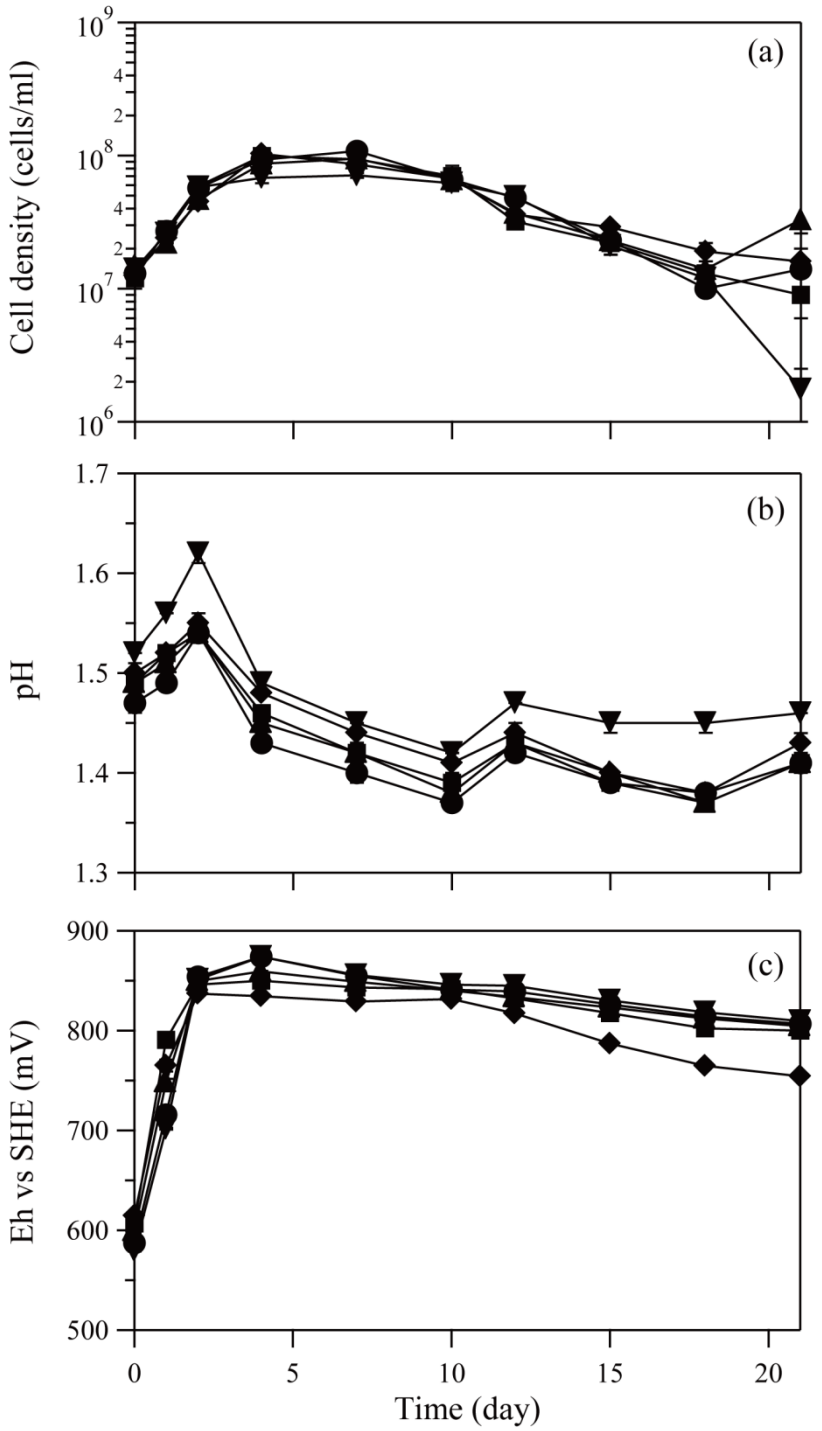

Figure 4.1 Changes in cell density (a), pH (b) and Eh vs SHE (c) in *Ac. brierleyi* cultures by changing $[Fe(II)]_{ini}/[As(III)]_{ini}$ molar ratio of 1.0 (◆), 1.4 (■), 2.0 (▲), 3.0 (●) and 4.0 (▼). Initial culture conditions were; $[As(III)]_{ini}$ = 4.7 mM, $[Fe(II)]_{ini}$ = 4.7, 6.5, 9.5, 14.0 and 19.0 mM, pH 1.5, fed with bioscorodite seeds at 0.15% (w/v).

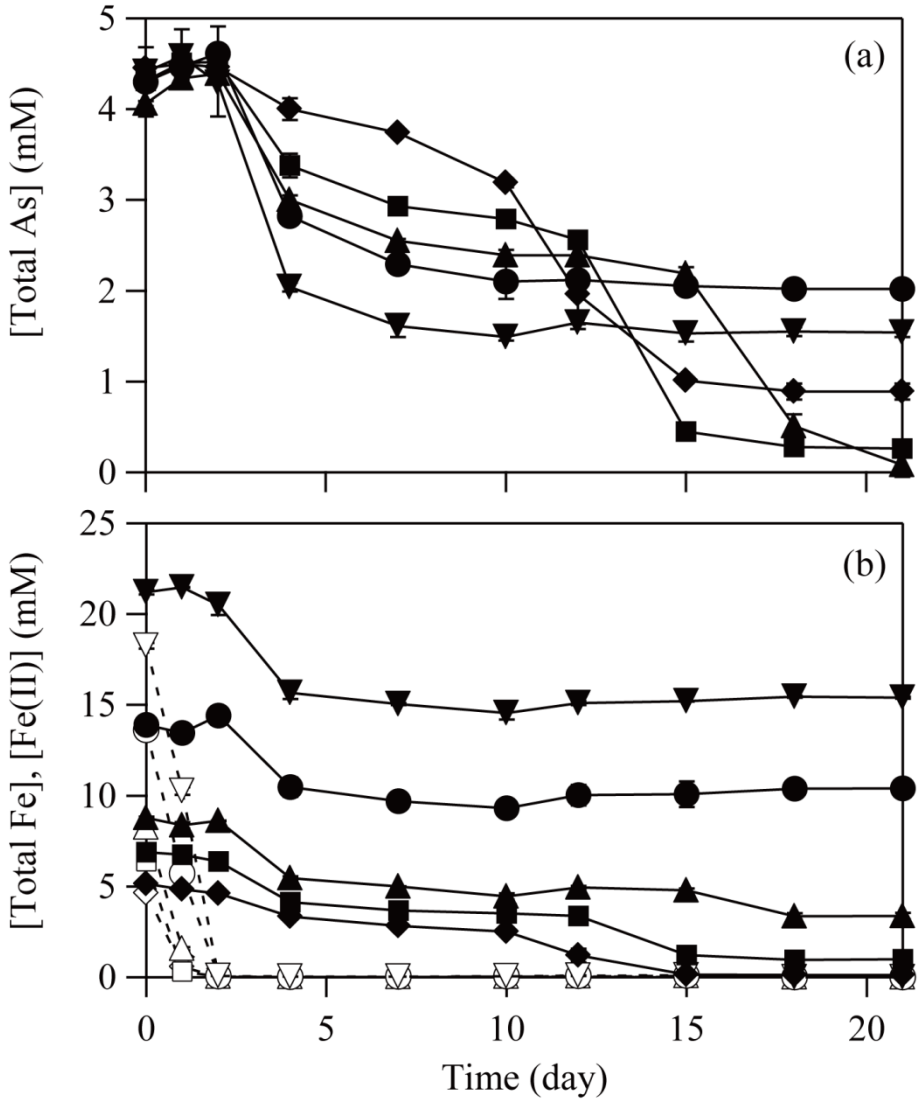

Figure 4.2 Changes in concentrations of total As (solid lines) (a), and total Fe (solid lines), Fe(II) (broken lines) (b) in *Ac. brierleyi* cultures by changing $[Fe(II)]_{ini}/[As(III)]_{ini}$ molar ratio of 1.0 (◆◇), 1.4 (■□), 2.0 (▲△), 3.0 (●○) and 4.0 (▼▽). Initial culture conditions were; $[As(III)]_{ini}$ = 4.7 mM, $[Fe(II)]_{ini}$ = 4.7, 6.5, 9.5, 14.0 and 19.0 mM, pH 1.5, fed with bioscorodite seeds at 0.15% (w/v).

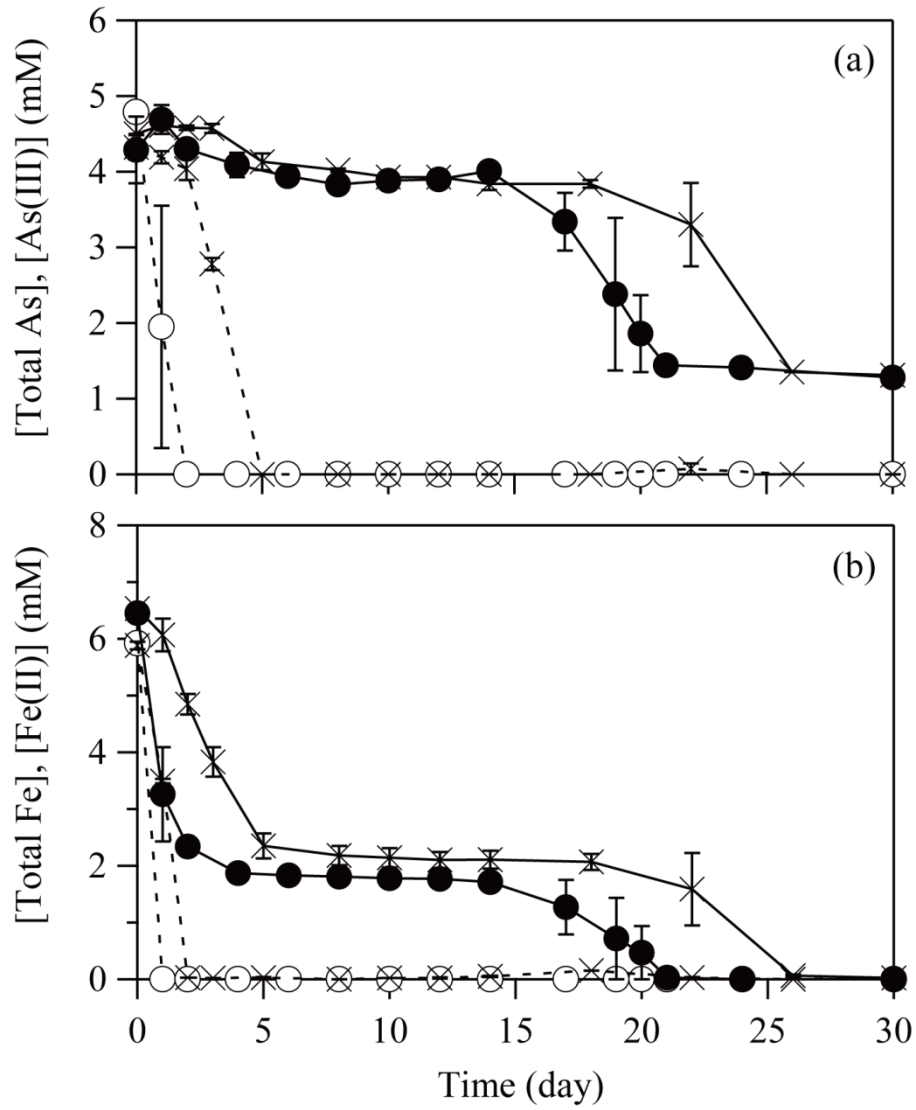

Figure 4.3 Changes in concentrations of total As (solid lines), As(III) (broken lines) (a), and total Fe (solid lines), Fe(II) (broken lines) (b) in *Ac. brierleyi* cultures fed with bioscorodite seeds at 0.15% (w/v) (●○) and without seed crystals (×). Initial culture conditions were; $[As(III)]_{ini}$ = 4.7 mM, $[Fe(II)]_{ini}$ = 6.5 mM, pH 1.5.

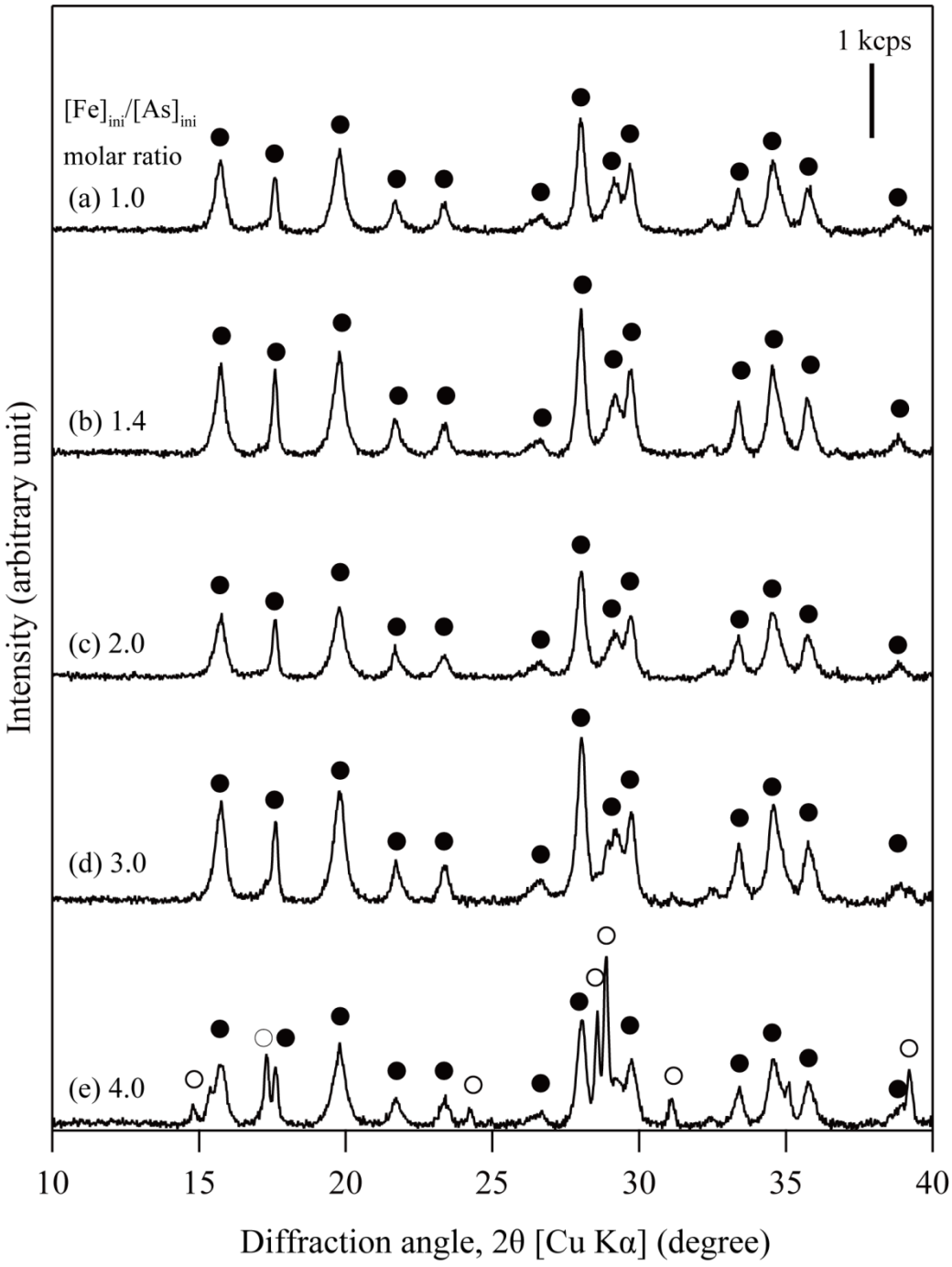

Figure 4.4 XRD patterns of the precipitates collected at day 30 formed in *Ac. brierleyi* cultures by changing $[Fe(II)]_{ini}/[As(III)]_{ini}$ molar ratio of 1.0 (a), 1.4 (b), 2.0 (c), 3.0 (d) and 4.0 (e). Initial culture conditions were; $[As(III)]_{ini}$ = 4.7 mM, $[Fe(II)]_{ini}$ = 4.7, 6.5, 9.5, 14.0 and 19.0 mM, pH 1.5, fed with bioscorodite seeds at 0.15% (w/v). The symbols are assigned to scorodite (●; JCPDS 37-0468) and potassium jarosite (○; JCPDS 01-078-4999).

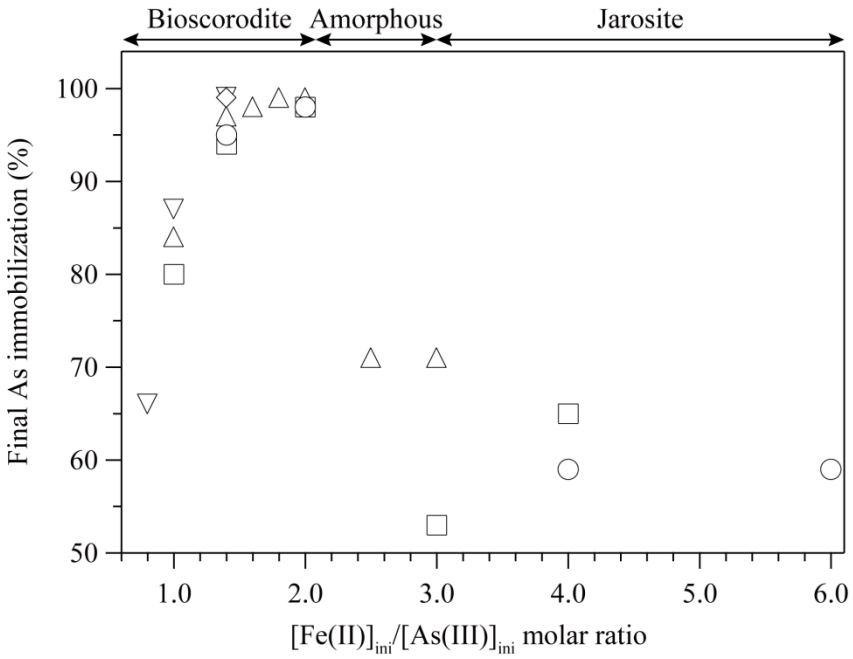

Figure 4.5 Effect of $[Fe(II)]_{ini}/[As(III)]_{ini}$ molar ratio on final As immobilization at $[As(III)]_{ini}$ = 3.3 (at day 24; ○), 4.7 (at day 21; □), 6.5 (at day 20; △), 13.0 (at day 14; ◇), 20.0 mM (at day 14; ▽).

The optimal $[Fe(II)]_{ini}/[As(III)]_{ini}$ ratio was generally 1.4–2.0 at all $[As(III)]_{ini}$ tested, enabling 94–99% of As removal as scorodite (although starting at lower $[As(III)]_{ini}$ required longer incubation time). Of which, providing an excess Fe(II) (closer to $[Fe(II)]_{ini}/[As(III)]_{ini}$ = 2.0) was found beneficial to improve the final As removal (up to 98–99%) especially from more dilute As(III) solutions (Figure 4.2, Table 4.1). Setting at $[Fe(II)]_{ini}/[As(III)]_{ini}$ = 1.0 (theoretical Fe/As molar ratio of scorodite) produced scorodite but with a decreased final As removal (80% at $[As(III)]_{ini}$ = 4.7 mM, 84% at 6.5 mM, 87% at 20 mM; Figure 4.2a, Table 4.1). Conversely, setting at $[Fe(II)]_{ini}/[As(III)]_{ini} \geq$ 2.5–6.0 lead to formation of unwanted amorphous precipitates or jarosite ($MFe_3(SO4)_2(OH)_6$; M = K^+, Na^+, NH_4^+) at all initial As(III) concentrations tested owing to the presence of monovalent cations in HBS medium (K^+ = 1 mM, Na^+ = 2 mM, NH_4^+ = 6.8 mM) (Figures 4.4 and 4.5). In abiotic hydrothermal and

atmospheric methods starting with high concentrations of oxidized species, the presence of excess Fe(III) (e.g., $[Fe(III)]_{ini}/[As(V)]_{ini} > 1.5$) generally negatively affected the precipitation kinetics of scorodite and thus the ratios of 1.0–1.5 are used (Gomez et al. 2011a; Monhemius and Swash 1999; Singhania et al. 2006). However, when treating this dilute, reduced species of As(III) and Fe(II) as starting materials microbiologically, it was found that Fe(III) should be added to an slight excess of $1.4 \leq [Fe(III)]_{ini}/[As(V)]_{ini} \leq 2.0$ for the best performance. Chemical composition of the resultant bioscorodite products ($[Fe]_{im}/[As]_{im}$ ratio) generally became closer to 1.0 (the theoretical ratio for scorodite) at higher initial As(III) concentrations (Table 4.1). Slightly higher $[Fe]_{im}/[As]_{im}$ ratios (1.2–1.5) observed at lower initial As(III) concentrations may be due to incorporation of SO_4^{2-}, as was reported in abiotic hydrothermal (Dutrizac and Jambor 2007; Gomez et al. 2011a, 2011b; Swash and Monhemius 1994) and atmospheric scorodite syntheses (Singhania et al. 2006).

Although $[Fe(II)]_{ini}/[As(III)]_{ini}$ molar ratio of 1.4 was the most effective for dilute As(III) concentration in the range of 6.5–20 mM, it was ineffective for $[As(III)]_{ini}$ = 26 mM (2000 ppm) due to low As immobilization (6%) and jarosite formation. This was caused by the inhibition of cell growth and microbial As(III) oxidation even though Fe(II) was completely oxidized. In case of chemical scorodite syntheses under atmospheric conditions, jarosite formation was prevented even for high Fe(II), Fe(III) and As(V) concentrations at around 70°C (e.g., As(V) 37–670 mM and Fe(II)/Fe(III) 43–1000 mM; Gonzalez-Contreras et al., 2012; Fujita et al., 2008b; Paktunc et al., 2010). These chemical synthesis targeted As(V) immobilization as a As valence and then Fe(III) was gradually supplied by Fe(II) oxidation, whilst the order of each ion supply was transposed in this study owing to fast Fe(II) oxidation by *Ac. brierleyi* before As(III) oxidation. For further improvement of biological scorodite

crystallization at high As(V) concentrations, elevating *Ac. brierleyi*'s As(III) tolerance and microbial Fe(II) oxidation control are considered to be effective approaches.

Table 4.1 Evaluation of initial As(III) concentration and $[Fe(II)]_{ini}/[As(III)]_{ini}$ molar ratio for As removal as bioscorodite (pH 1.5; with or without bioscorodite seed feeding).

Initial media condition				Final As removal		Solid analysis		
$[As(III)]_{ini}$ (mM)	$[Fe(II)]_{ini}$ (mM)	$[Fe(II)]_{ini}/[As(III)]_{ini}$ molar ratio	Seed feeding (bioscorodite; %)	(%)	(Days)	$[Fe]_{im}/[As]_{im}$ molar ratio	Secondary mineral identified	References
3.3	4.5	1.4	0	11	24	-	Amoprhous	This study
(250 ppm)			0.15	95		1.2	Scorodite	
	6.5	2.0		98		1.2	Scorodite	
	13.5	4.0		59		-	Jarosite	
	20.0	6.0		59		-	Jarosite	
4.7	6.3	1.4	0	15	21	-	Amoprhous	This study
(350 ppm)	4.7	1.0	0.15	80		-	Scorodite	
	6.5	1.4		94		1.5	Scorodite	
	9.5	2.0		98		1.4	Scorodite	
	14.0	3.0		53		-	Amoprhous	
	19.0	4.0		65		-	Jarosite	
6.5	6.5	1.0	0.15	84	20	1.1	Scorodite	This study
(500 ppm)	9.0	1.4		97		1.1	Scorodite	
	10.5	1.6		98		1.1	Scorodite	
	12.0	1.8		99		1.1	Scorodite	
	13.0	2.0		99		1.1	Scorodite	
	16.5	2.5		71		-	Amoprhous	
	19.5	3.0		71		-	Jarosite	
13.0	18.0	1.4	0	99	14	1.1	Scorodite	Okibe et al. 2014
(1000 ppm)								
20.0	16.0	0.8	0.15	66		1.1	Scorodite	This study
(1500 ppm)	20.0	1.0		87		1.1	Scorodite	
	28.0	1.4		99		1.1	Scorodite	
26.0	36.0	1.4	0	6	10	-	Jarosite	This study
(2000 ppm)								

4.3.2 Effect of lower pH 1.2 on As immobilization behavior

Bioscorodite crystallization test at pH 1.2 were shown in Figures 4.6, 4.7 and 4.8. Although As(III) and Fe(II) oxidation tendencies by *Ac. brierleyi* were not affected, lowering pH from 1.5 to 1.2 using bioscorodite seeds resulted in a different As removal behavior (Figure 4.6). A continuous formation of whitish bioscorodite particles were directly observed from the beginning at pH 1.2, instead of displaying 2-staged As removal as was shown at pH 1.5 (Figure 4.6a). Since general scorodite crystallization requires H^+, it is presumed that lowering initial pH resulted in faster reaction than pH 1.5. However, As removal remained relatively incomplete at pH 1.2 (91%), compared to at pH 1.5 (98%) (at day 30; Figure 4.6a). Overall lower supersaturation levels (log IAP continuously decreased from −22 to −23, Figure 4.7a) owing to lower As(V) ion activities (2.9×10^{-20} M) at pH 1.2 (Figure 4.7b) as well as continuous As precipitation likely promoted steady and continuous bioscorodite crystal growth, as was reported under abiotic atmospheric conditions (Caetano et al. 2009; Demopoulos et al. 1995; Filippou and Demopoulos 1997).

Increasing the $[Fe(II)]_{ini}/[As(III)]_{ini}$ molar ratio from 1.3 to 1.7 and 2.0 improved As immobilization efficiency from 70% to 87% and 91%, respectively (Figure 4.8). The reaction speed was almost same in all cultures regardless of $[Fe(II)]_{ini}/[As(III)]_{ini}$ higher molar ratios. As(V) ion activities in all tested molar ratios were approximately ten times lower ($\leq 3\times10^{-20}$ M; Figure 4.9b) than pH 1.5 (commonly 10^{-19} M in this study), whilst the value of Fe(III) ion activities at pH 1.2 increased as the $[Fe(II)]_{ini}/[As(III)]_{ini}$ molar ratios become larger (Figure 4.9c). This indicated that As(V) precipitation become difficult in case of lower As(V) ion activities, and hence higher Fe(III) ion activities are required to maintain the optimal supersaturation levels. The above has led to the conclusion that amorphous precursors

formation played an important role to achieve maximum As removal from dilute As(III) solutions.

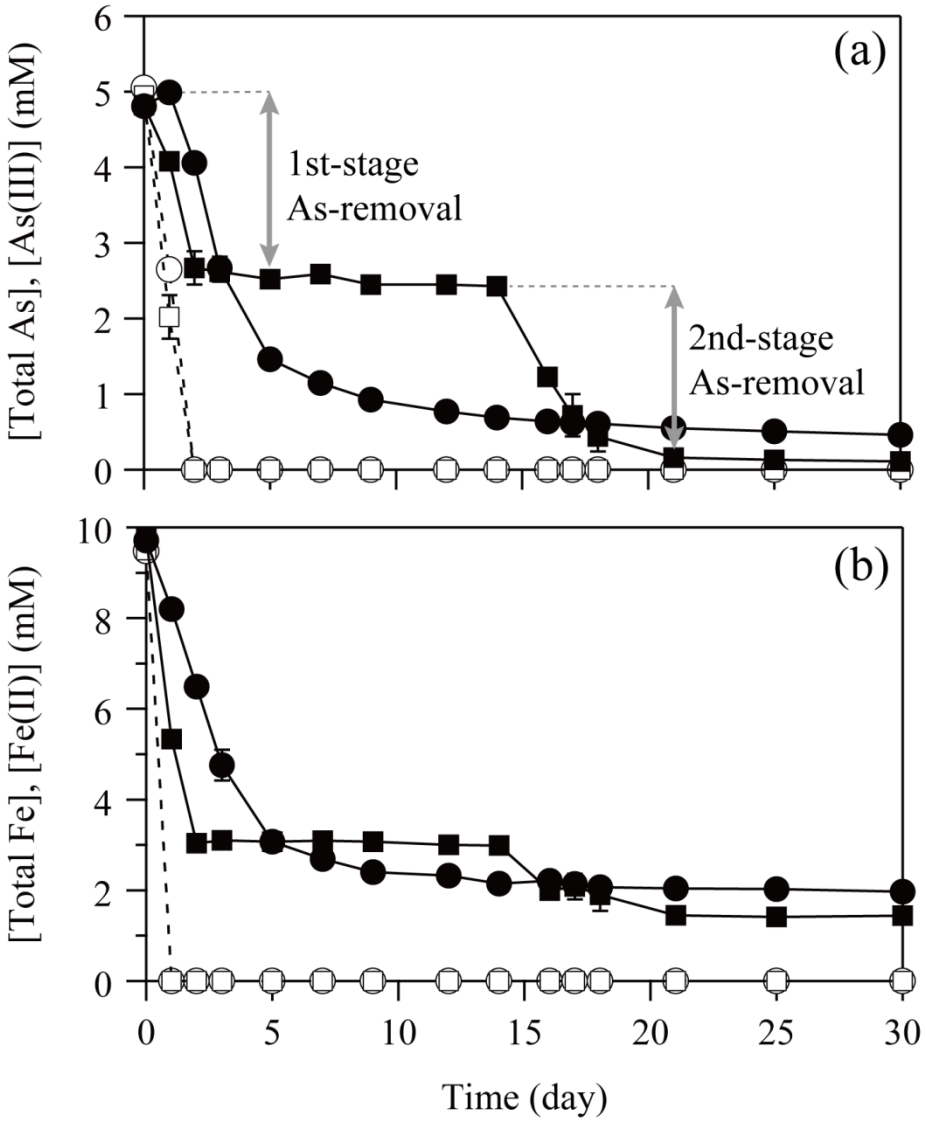

Figure 4.6 Changes in concentrations of total As (solid lines), As(III) (broken lines) (a), and total Fe (solid lines), Fe(II) (broken lines) (b) in *Ac. brierleyi* cultures at 1.2 (●○) and pH 1.5 (■□). Initial condition; $[As(III)]_{ini}$ = 4.7 mM, $[Fe(II)]_{ini}$ = 9.5 mM, fed with bioscorodite seeds at 0.15% (w/v).

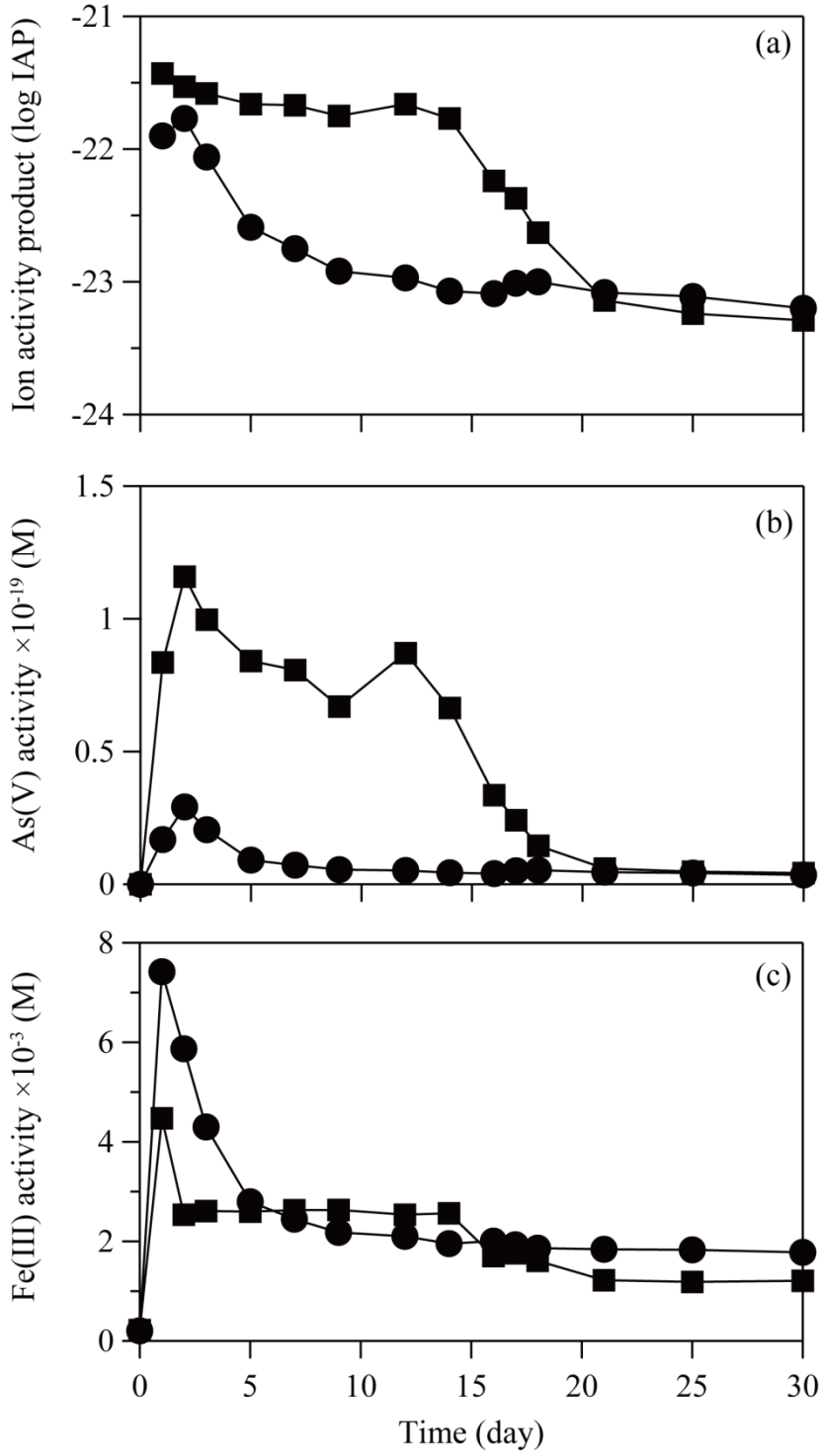

Figure 4.7 Ion activity products of bioscorodite (a), As(V) ion activity (b) and Fe(III) ion activity (c) in *Ac. brierleyi* cultures at 1.2 (●) and pH 1.5 (■). Initial condition; $[As(III)]_{ini}$ = 4.7 mM, $[Fe(II)]_{ini}$ = 9.5 mM, fed with bioscorodite seeds at 0.15% (w/v).

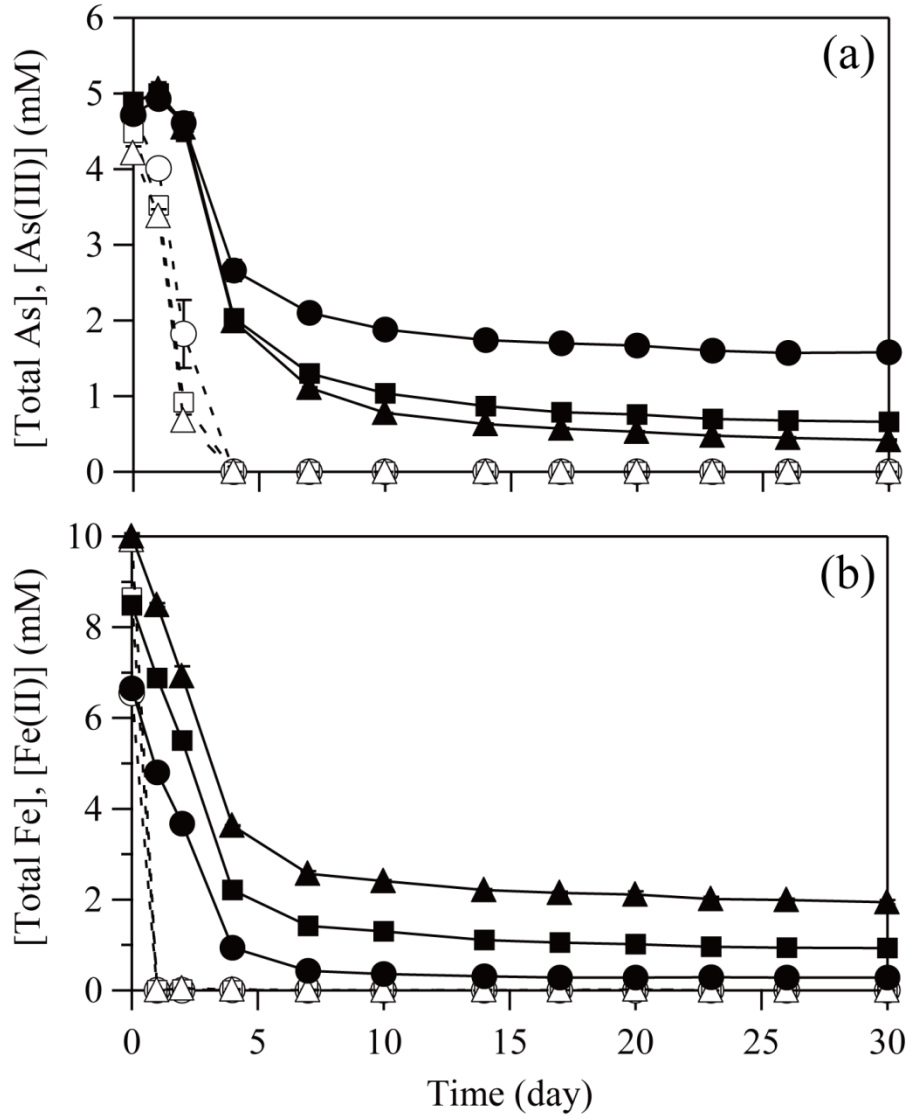

Figure 4.8 Changes in concentrations of total As (solid lines), As(III) (broken lines) (a), and total Fe (solid lines), Fe(II) (broken lines) (b) in *Ac. brierleyi* cultures at the $[Fe(II)]_{ini}/[As(III)]_{ini}$ molar ratio of 1.3 (●), 1.7 (■) and 2.0 (▲) at pH 1.2. Initial condition; $[As(III)]_{ini}$ = 4.7 mM, $[Fe(II)]_{ini}$ = 6.0, 8.0 and 9.5 mM, fed with bioscorodite seeds at 0.15% (w/v).

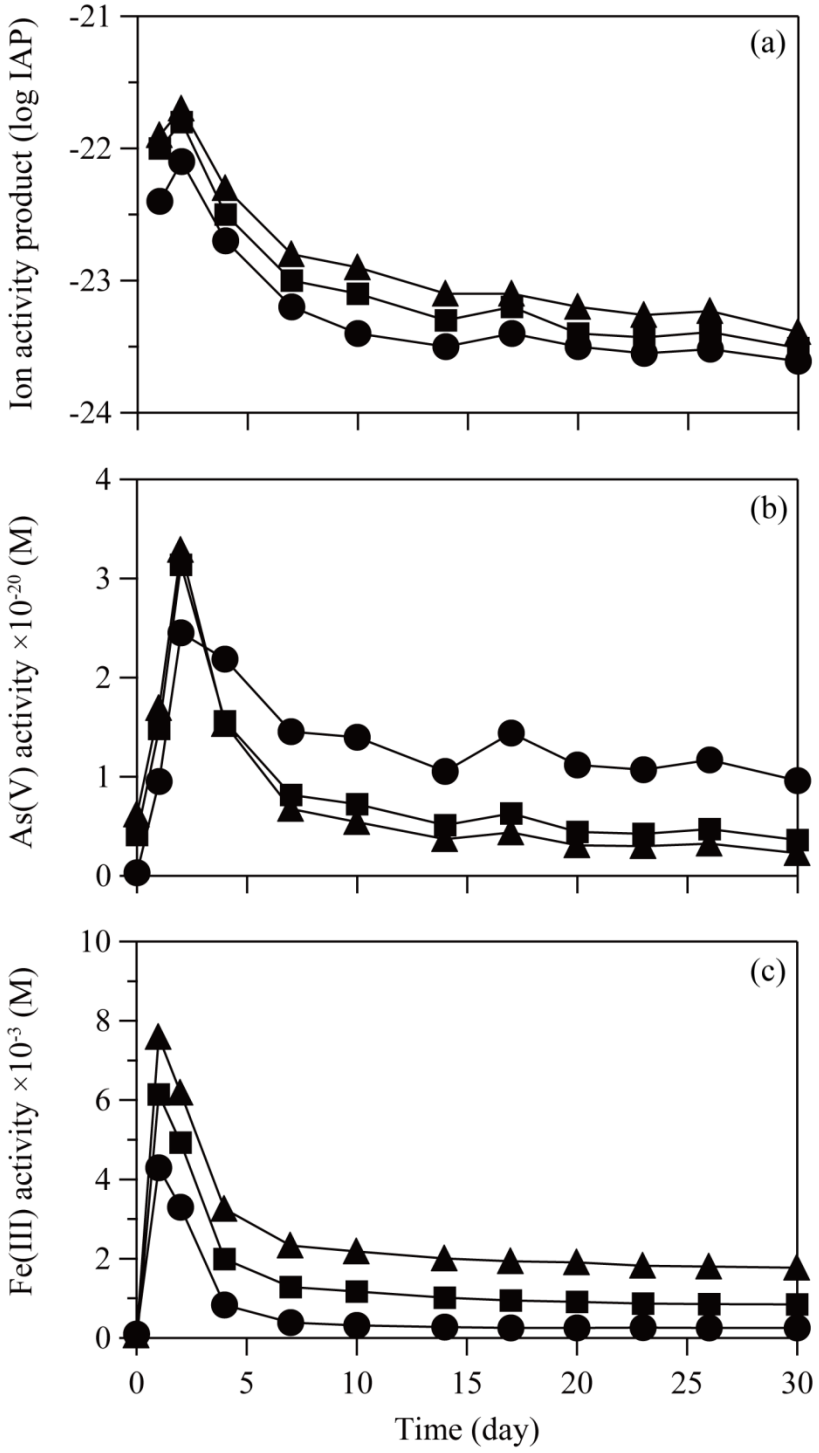

Figure 4.9 Ion activity products of bioscorodite (a), As(V) ion activity (b) and Fe(III) ion activity (c) in *Ac. brierleyi* cultures at the $[Fe(II)]_{ini}/[As(III)]_{ini}$ molar ratio of 1.3 (●), 1.7 (■) and 2.0 (▲) at pH 1.2. Initial condition; $[As(III)]_{ini}$ = 4.7 mM, $[Fe(II)]_{ini}$ = 6.0, 8.0 and 9.5 mM, fed with bioscorodite seeds at 0.15% (w/v).

4.4 Conclusions

From dilute As(III) solutions (3.3–20 mM), bioscorodite was crystallized in the $[Fe(II)]_{ini}/[As(III)]_{ini}$ molar ratio ranges of 0.8–2.0. Especially, 94–99% As was successfully removed as crystalline bioscorodite by setting an slight excess of $[Fe(II)]_{ini}/[As(III)]_{ini}$ molar ratio at 1.4–2.0. Higher molar ratio enable to increase As removal, but required longer reaction time. Molar ratio of over 2.5 resulted in the formation of amorphous ferric arsenate or jarosite.

Lowering the initial pH from 1.5 to 1.2 (using bioscorodite seeds) lead to a steady and continuous formation of bioscorodite particles (instead of two-stage As precipitation at pH 1.5). However, As removal remained relatively incomplete at pH 1.2 (91%), compared to at pH 1.5 (98%). Amorphous precursors formation at pH 1.5 played an important role to achieve maximum As removal from dilute As(III) solutions by inducing two-stage As and Fe precipitation.

Data shown in this chapter were partially included in the paper accepted as:
Tanaka, M. and Okibe, N., 2018. Factors to enable crystallization of environmentally-stable bioscorodite from dilute As(III)-contaminated waters. *Minerals*, 8(1): 23.

Chapter 5

Effect of seed crystals on bioscorodite crystallization

5.1 Introduction

From studies of conventional abiotic scorodite synthesis, seed feeding (scorodite or other heterogeneous crystals) was shown one of the influential factors to promote scorodite formation due to low supersaturation level control (Demopoulos et al., 1995; Filippou and Demopoulos, 1997; Caetano et al., 2009). Singhania et al. (2005) reported that utilization of fine particles such as hydrothermally synthesized scorodite, hematite and gypsum results in well-crystalline scorodite formation by providing high surface area. These researches were done at over 85°C and high initial arsenic concentrations (10 g/l~). Although scorodite crystallization becomes further difficult under milder temperature condition (70°C) and dilute As(III) solutions (4.7 mM), exploiting factors to enable such reaction is of great importance to broaden the applicability of scorodite method for a wide range of As(III)-contaminated wastewaters. Based on that, bioscorodite and chemical scorodite particles were produced to compare for their characteristics, and their effectiveness as seed crystals was evaluated for bioscorodite crystallization reaction from dilute 4.7 mM As(III) solution. Additionally, stability of the resultant bioscorodite products was evaluated by TCLP test.

Incidentally, Shibata et al. (2015) reported the effect of hematite feeding on scorodite synthesis at high As(V) concentrations (50 g/l) and high temperature (95°C) This report mentioned that hematite worked as an iron source, and coarse scorodite particles were crystallized. For further dilute As(III) solutions, the effectiveness of feeding hematite particles should be examined. Therefore, three different substances (hematite, bioscorodite, and perlite (porous SiO_2, Al_2O_3)) were evaluated as seed crystals.

5.2 Materials and Methods

5.2.1 Preparation of bioscorodite and chemical scorodite as seed crystals

Bioscorodite seeds: *Ac. brierleyi* was grown as described in "*2.2.1 Acidianus brierleyi*^{T} *(DSM 1611)*" for 14 days to collect bioscorodite particles. Chemical scorodite seeds: Five-hundred milliliter Erlenmeyer flasks containing 200 ml deionized water (pH 1.5 with H_2SO_4) with 358 mM Fe(II) (20 g/l; as $FeSO_4 \cdot 7H_2O$) and 267 mM As(V) (20 g/l; as $Na_2HAsO_4 \cdot 7H_2O$) were incubated at 70°C, shaken at 100 rpm for 7 days. The resultant chemical scorodite particles were collected respectively and freeze-dried overnight. Production of seed crystals did not involve seed feeding. Bioscorodite/chemical scorodite seeds were characterized by XRD (Ultima IV, Rigaku; Cu Kα 40 mA, 40 kV), FT-IR (FT/IR-670Plus, Jasco; KBr pellet method) and TG-DTA (TG-DTA2000SA, Bruker; heated from room temperature to 1200°C at 10°C/min with N2 gas 100 ml/min) analysis.

5.2.2 Bioscorodite crystallization experiment fed with seed crystals

Ac. brierleyi cells were inoculated (final cell density; 1.0 x 10^7 cells/ml) in 500 ml Erlenmeyer flasks containing 200 ml of heterotrophic basal salts medium (pH 1.5 with H_2SO_4) with 9.5 mM Fe(II) (as $FeSO_4 \cdot 7H_2O$), 4.7 mM As(III) (as $NaAsO_2$) and 0.02% (w/v) yeast extract. $[Fe(II)]_{ini}/[As(III)]_{ini}$ molar ratio was set to 2.0. Bioscorodite or chemical scorodite were fed at 0.15% (w/v) as seed crystals. Flasks were incubated at 70°C, shaken at 100 rpm. Samples were regularly taken to monitor cell density, pH, Eh vs SHE, and concentrations of total Fe, total As, Fe(II) and As(III). Precipitates were regularly taken and washed once by pure water. After freeze-drying, precipitates were embedded in resin and polished to observe SEM cross-section views (ULTRA55, ZEISS).

5.2.3 Zeta-potential measurement

Zeta-potentials of *Ac. brierleyi* cells (5.0×10^7 cells/ml) and resultant precursors and bioscorodite particles (0.2% (w/v); recovered at day 3, 8, 9, 14) were measured in 10^{-3} M KCl solution using Zetasizer Nano ZS (Malvern) at pH values ranging from 2.0 to 5.0 (adjusted with HCl and KOH). Zeta-potential of the mixture of the two was measured as follows: *Ac. brierleyi* cells (5.0×10^7 cells/ml) were mixed with resultant particles (0.2% (w/v)) in 20 ml of 10^{-3} M KCl (in 100 ml flasks) at pH values ranging from 2.0 to 5.0. Prior to the zeta-potential measurement, the flasks were incubated shaken at 70°C, 150 rpm for 1 hour. Measurements were conducted at least in triplicate.

5.3 Results and Discussion

5.3.1 Characterization of scorodite seeds (bioscorodite vs chemical scorodite)

Scorodite seed crystals were prepared by either biological or chemical methods and identified by XRD (Figure 5.1a). According to TG-DTA analysis, weight losses (at 125-250°C, accompanied with DTA curve changes) of bioscorodite and chemical scorodite seeds were 15.0% and 12.5%, respectively (Figure 5.1c), suggesting that their structural water contents were $FeAsO_4 \cdot 1.91H_2O$ and $FeAsO_4 \cdot 1.55H_2O$, respectively (cf. the theoretical structural water content is 15.6% for scorodite ($FeAsO_4 \cdot 2H_2O$)). A gradual and continuous weight loss observed with bioscorodite (but not with chemical scorodite) was likely resulted from decomposition of organic matters deriving from cells, as was faintly detected by FT-IR (Figure 5.1b). Different XRD peak sharpness between bioscorodite and chemical scorodite seeds (Figure 5.1a) may therefore reflect difference in their crystallinity due to encrustation of cells within bioscorodite particles (Figure 5.1b) as well as in their structural water

content (Figure 5.1c).

The specific surface areas and mesopore diameter were calculated based on N_2 adsorption/desorption isotherms (Figure 5.2a, b). The curves of N_2 adsorption/ desorption isotherms were classified as type III defined by IUPAC (International Union of Pure and Applied Chemistry), which indicates non-porous or macro-porous features (Sing et al., 1985). The pore diameter of bioscorodite seeds widely distributed from 1 nm to 100 nm and the peak top located in the region of 2–5 nm (Figure 5.2c), while the chemical scorodite seeds have the larger pores (10–50 nm) as well as micro or mesopore (2–5 nm) (Figure 5.2d).

Morphological differences were clearly seen by SEM observation: Chemical scorodite seeds were aggregates of orthorhombic crystals (Figure 5.3b_1, b_2), with the average particle size and specific surface area of 98 μm and 0.7 m^2/g, respectively (Table 5.1). Meanwhile, bioscorodite seeds were found as spherical aggregates (Figure 5.3a_1, a_2) with the average particle size and specific surface area of 36 μm and 2.0 m^2/g, respectively (Table 5.1). There was a significant difference in crystal surface roughness and small almond shaped grains covered the bioscorodite surface (Figure 5.3a_2). SEM cross-section views found hollow bioscorodite particles (Figure 5.3a_3) whereas chemical scorodite particles were completely filled (Figure 5.3b_3). Other than the presence/absence of cells, this morphology difference may be partly attributed to Fe and As ionic species available during the scorodite crystallization process: In the chemical process, As(V) is initially fed where Fe(III) is gradually provided from Fe(II) oxidation by dissolved oxygen. In the biological process, on the other hand, microbial Fe(II) oxidation to Fe(III) is rapidly completed, after which As(V) is gradually provided by microbial As(III) oxidation.

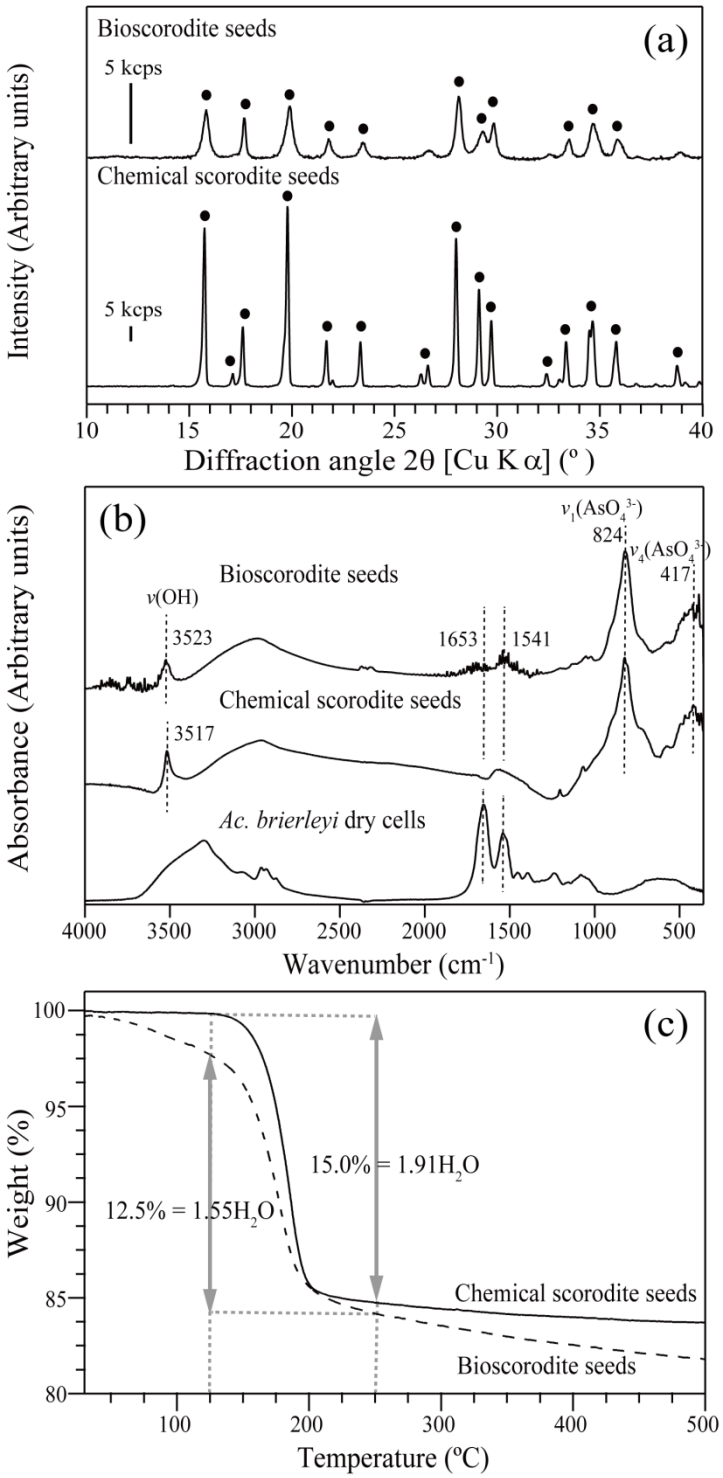

Figure 5.1 Characterization of bioscorodite and chemical scorodite by XRD (a), FT-IR (b), and TG-DTA (c) analyses. (a) The symbol ● is assigned to scorodite (JCPDS 37-0468). (b) Dotted lines at 417 and 824 cm^{-1} can be assigned to AsO_4^{3-} stretching vibration (436 and 825 cm^{-1}; Ondrus et al. 1999) and those at 3523 and 3517 cm^{-1} to OH stretching vibration (3511 cm^{-1}; Baghurst et al. 1996). Two peaks at 1541 and

1653 cm^{-1} are attributed to cell proteins (1545 and 1654 cm^{-1}; Legal et al. 1991). (c) The structural water content was calculated based on the weight loss at 125–250°C of bioscorodite (broken line) and chemical scorodite (solid line).

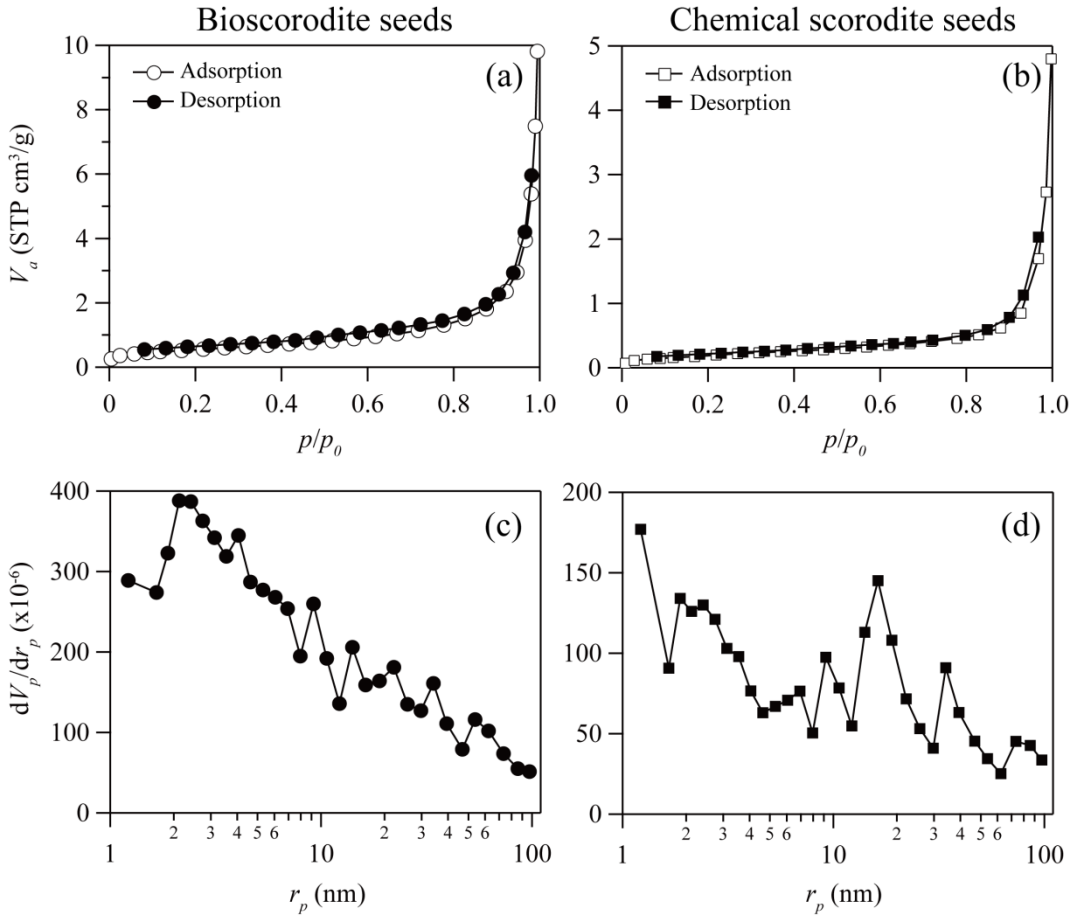

Figure 5.2 N_2 adsorption/desorption isotherms (a,b) and mesopore size distribution (BJH plot) (c,d) of bioscorodite seeds (a,c) and chemical scorodite seeds (b,d).

Table 5.1 Particle size and specific surface area of bioscorodite and chemical scorodite seed crystals.

	Particle size (μm)			Specific surface area (m^2/g)
	Average	Median	Mode	
Bioscorodite seeds	36	35	36	2.0
Chemical scorodite seeds	98	91	90	0.7

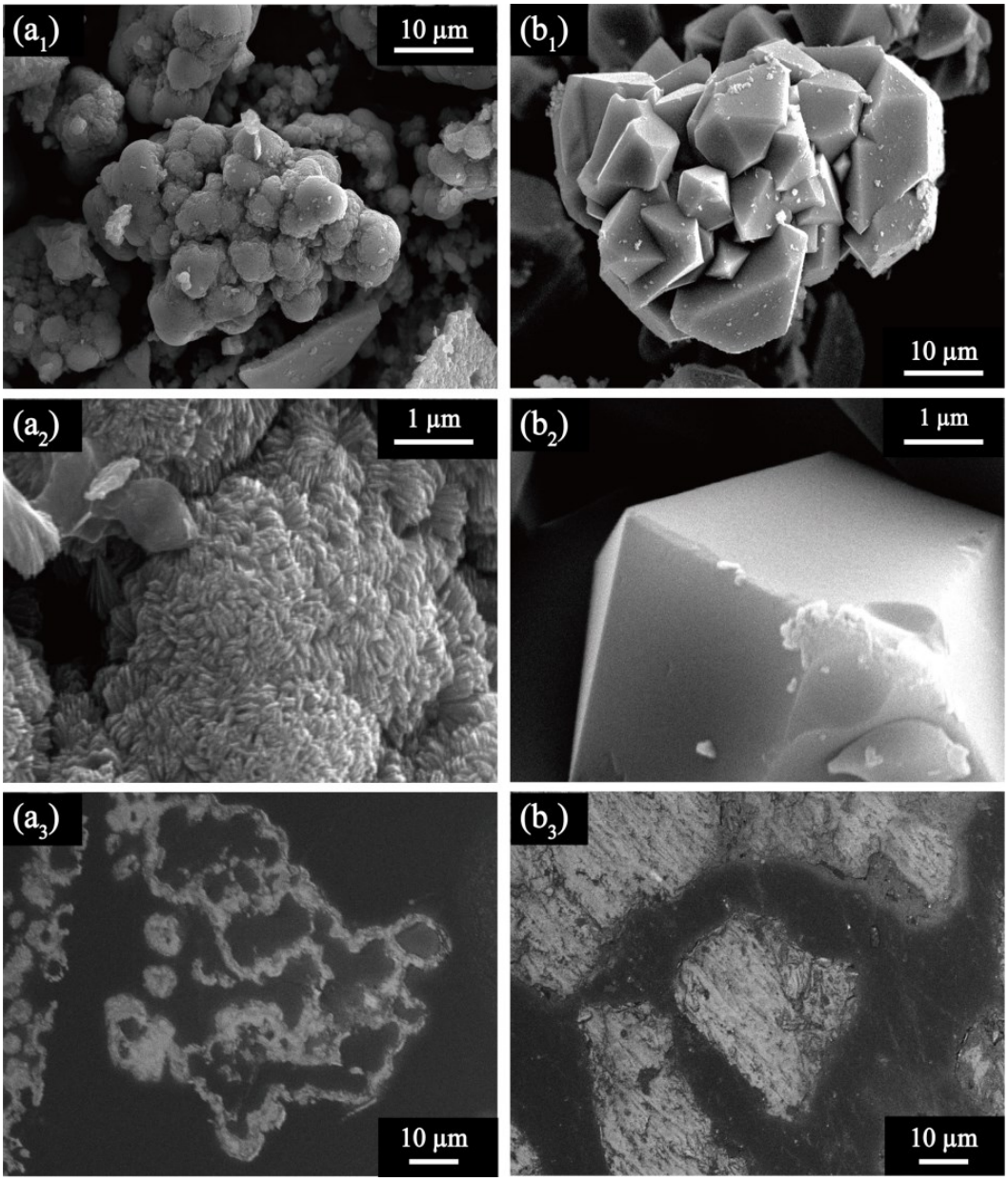

Figure 5.3 SEM images of (a) bioscorodite and (b) chemical scorodite seed crystals at 2,000× (a_1; b_1) or 20,000× (a_2; b_2) magnification. Cross-section views are shown at 3,000× magnification (a_3; b_3).

5.3.2 Effect of seed crystals morphology

Although microbial oxidation speed of As(III) and Fe(II) was not affected in all cases, a clear difference in As and Fe precipitation behaviors was found at pH 1.5 (Figure 5.4). The 1st-stage As removal observed at day 0-2 (brown-colored amorphous precursor formation; Okibe et al. 2017) was an almost common phenomenon, but the 2nd-stage As removal observed at day 14-21 (whitish green-colored scorodite formation; Okibe et al. 2017) was promoted on bioscorodite seeds, resulting in 98% As removal at day 21 (Figure 5.4). However, the reaction speed became slower by feeding with chemical scorodite seeds. Clear color change of precipitates into whitish green was observed at day 30~ (Figure 5.4).

The supersaturation of scorodite was evaluated based on the IAP (Figure 5.4a) calculated from Fe(III) and As(V) ion activities (Figure 5.5b, c). The log K_{sp} for scorodite was reported to be −25.8 (Langmuir et al. 2006). Microbiological crystallization can keep the metastable oversaturation for crystal growth (Weijma et al., 2017), and metastable range was also kept in this study (saturation index was bioscorodite seeds: 4.8 and chemical scorodite seeds: 4.5) (Figure 5.5). The greater 1st-stage As-removal on bioscorodite seeds (than on chemical scorodite seeds; Figure 5.4a) lead to the lower and stable supersaturation level during day 2-14 (Figure 5.5a), before a sudden 2nd-stage As removal was triggered to produce crystalline scorodite.

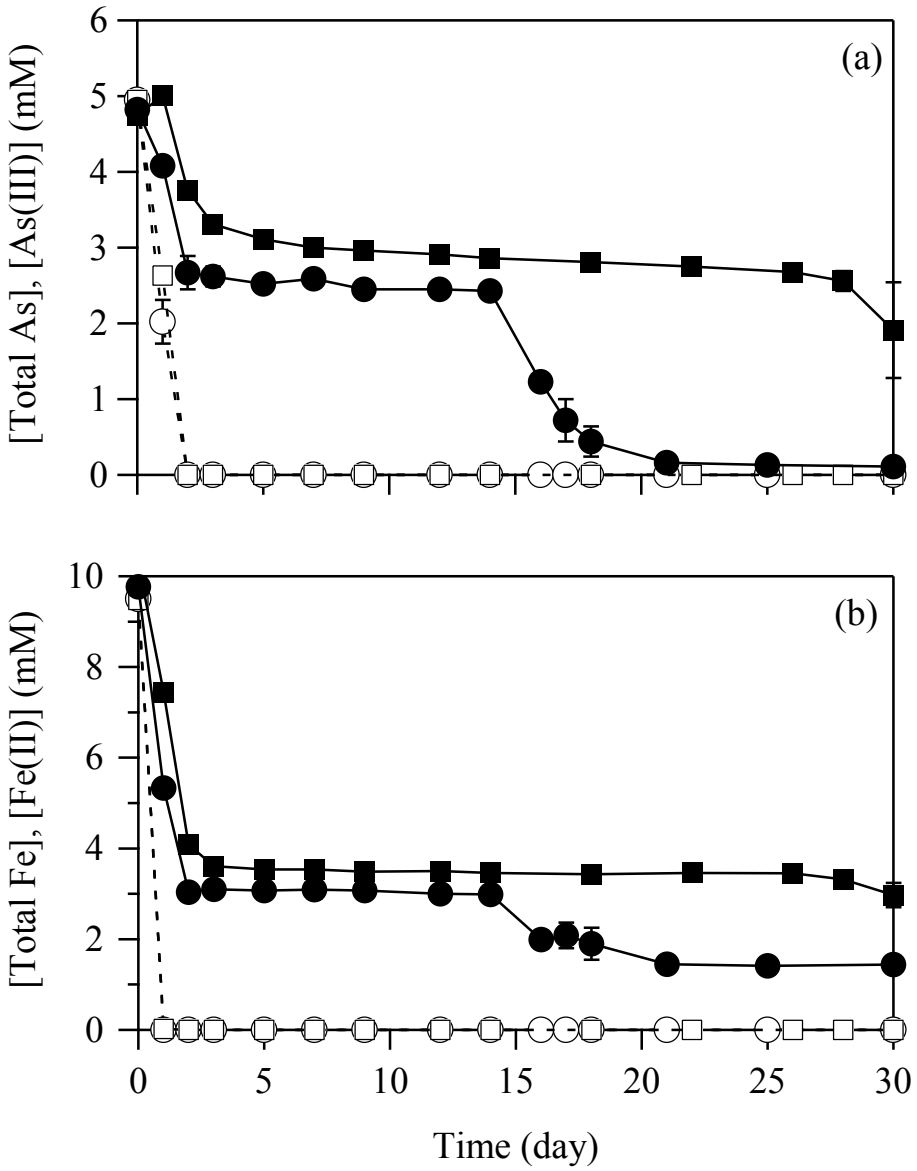

Figure 5.4 Changes in concentrations of total As (solid lines), As(III) (broken lines) (a), and total Fe (solid lines), Fe(II) (broken lines) (b) in *Ac. brierleyi* cultures fed with bioscorodite seeds (●○) or chemical scorodite (■□) seeds at 0.15% (w/v). Initial condition; $[As(III)]_{ini}$ = 4.7 mM, $[Fe(II)]_{ini}$ = 9.5 mM, pH 1.5.

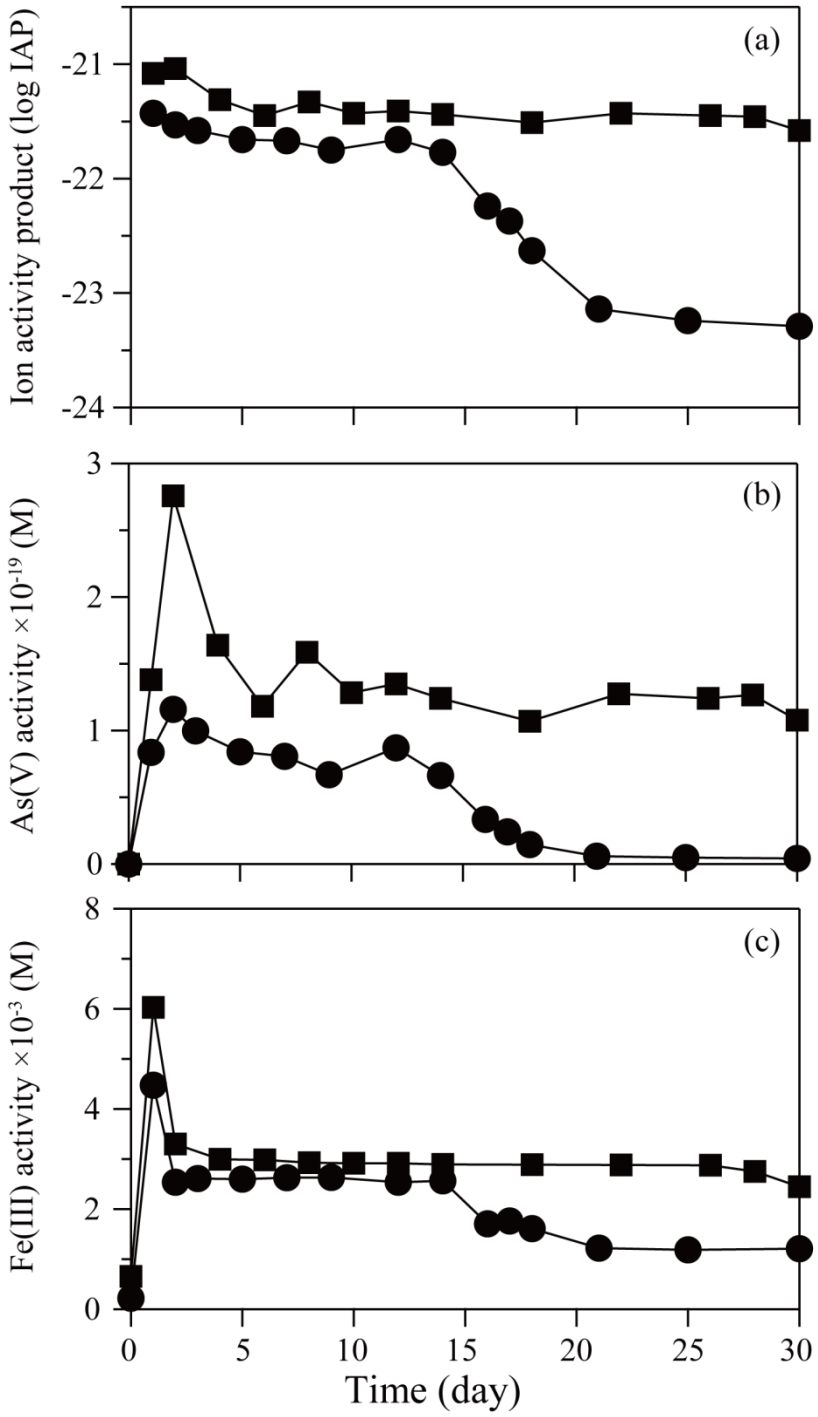

Figure 5.5 Ion activity products of bioscorodite (a), As(V) ion activity (b) and Fe(III) ion activity (c) in *Ac. brierleyi* cultures fed with bioscorodite seeds (●) or chemical scorodite (■) seeds at 0.15% (w/v). Initial condition; $[As(III)]_{ini}$ = 4.7 mM, $[Fe(II)]_{ini}$ = 9.5 mM, pH 1.5.

SEM cross section views revealed contrasting bioscorodite crystallization patterns on bioscorodite seeds (Figure 5.6a) and on chemical scorodite seeds (Figure 5.6b): Hollow bioscorodite seed particles were found increasingly filled with newly formed scorodite (Figure 5.6a_1–a_6), whilst solid chemical seeds induced their surface to be thoroughly coated with new scorodite precipitates (Figure 5.6b_1–b_6).

Other abiotic, atmospheric studies using As(V) and Fe(III) as starting species have also reported a positive effect of seeds with high specific surface area (SSA): e.g., the better scorodite precipitation kinetics were observed by using finer seeds such as hematite and hydrothermal scorodite (Singhania et al. 2005). Caetano et al. (2009) reported that a SSA higher than 270 m^2/g was required to achieve 85% As removal. The fact that the SSA of bioscorodite (2.0 m^2/g; Table 5.1) was nearly three times greater than that of chemical scorodite (0.7 m^2/g; Table 5.1) likely allowed the former to show better seeding effect.

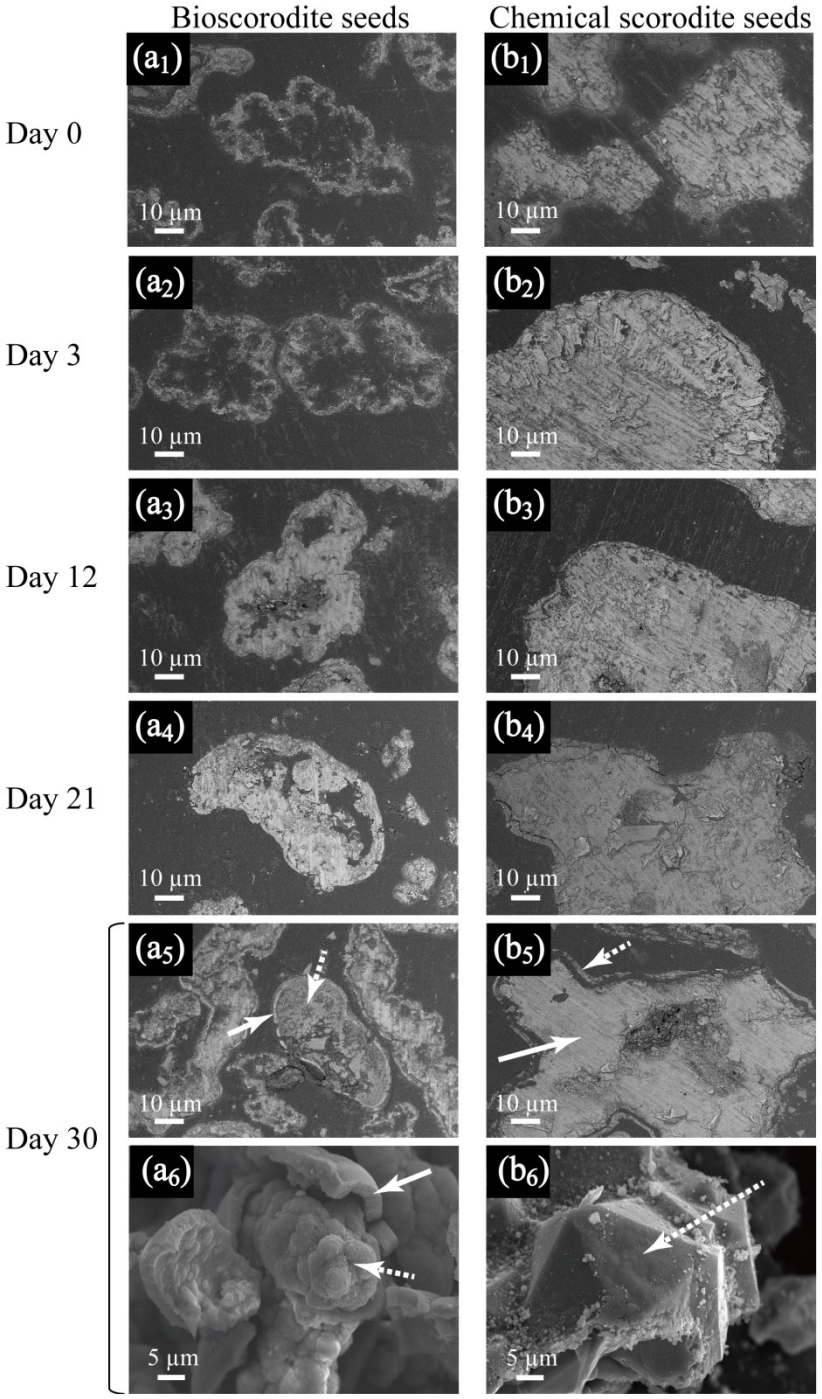

Figure 5.6 SEM cross-section images depicting bioscorodite crystallization process (from day 0 to day 30) on bioscorodite seeds (from a_1 to a_5) or chemical scorodite seeds (from b_1 to b_5), respectively. SEM whole view images of the resultant particles (day30) on bioscorodite seeds (a_6) or chemical scorodite seeds (b_6) are also shown. Solid and dotted arrows (a_5, a_6, b_5, b_6) indicate locations of seed crystals and fresh scorodite precipitates, respectively.

5.3.3 Other seed substances

As other seed substances, the effect of hematite (Fe_2O_3) and perlite (major contains: SiO_2 and Al_2O_3) were investigated on bioscorodite crystallization. Feeding hematite seeds led to a rapid and linear decrement of total As and Fe concentrations without induction period which is characteristic phenomenon in bioscorodite crystallization, and 95% of As was immobilized by day 6, while second As removal was observed in the cultures fed with bioscorodite or perlite seeds and 98% of As removal was achieved by day 10 (Figure 5.7). Positive effect of hematite seeds on the efficiency of atmospheric scorodite synthesis were investigated in chemically synthesis method for high As(V) concentrations (10 g/l; Singhania et al., 2005) due to finer property of hematite particles (1–10 μm). Although hematite was also proposed to act not only as seed crystals but also as the source of Fe(III) in chemical scorodite synthesis (from 50 g/l As(V); Shibata et al., 2015), its detailed mechanism is still unclear.

In contrast, perlite was expected to have high surface area due to porous surface (Figure 5.8c_1). However, the reaction speed was as same as fed with bioscorodite seeds (Figure 5.7). Fine bioscorodite particles were crystallized in bulk solution rather than on the surface of perlite seeds (Figure 5.8c), whereas hematite and bioscorodite seeds were covered with newly formed bioscorodite (Figure 5.8a, b). This indicated that perlite surface did not act as a support of bioscorodite crystal growth.

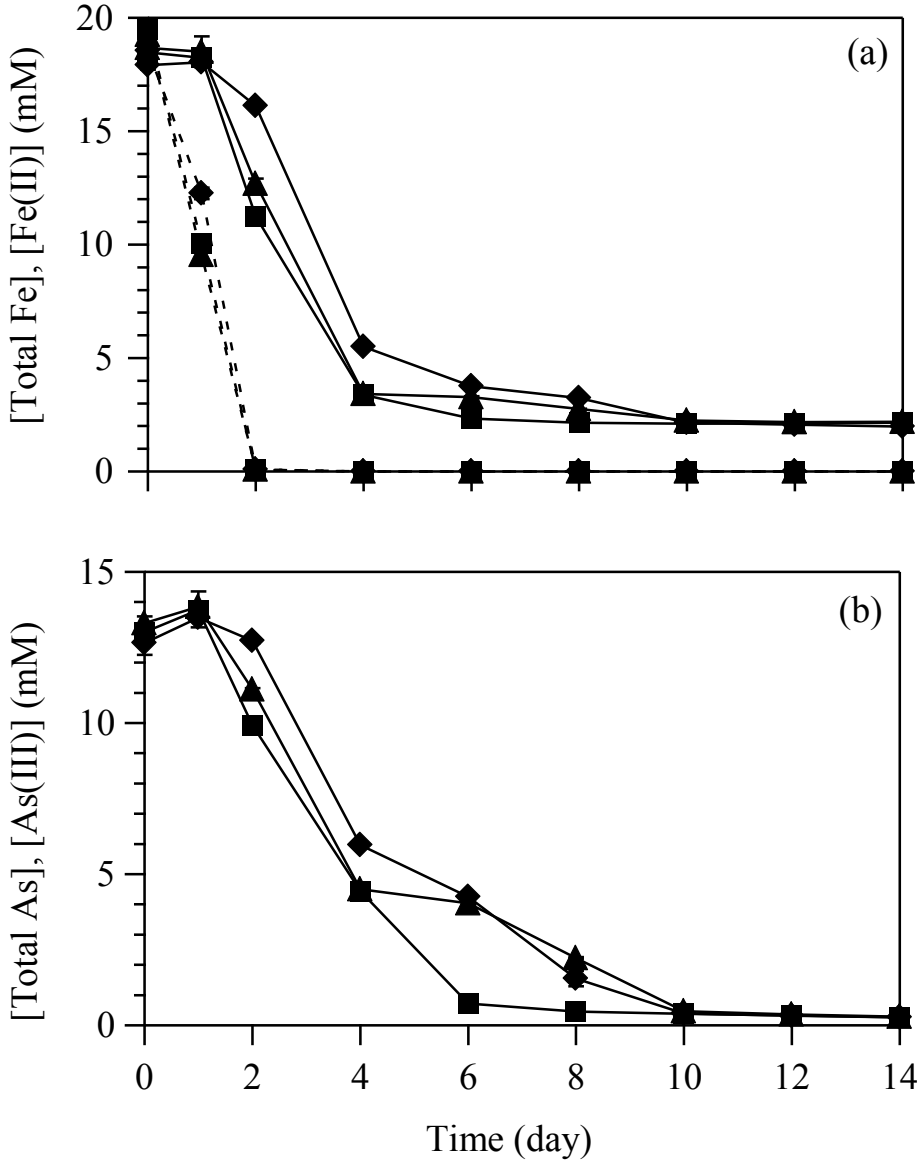

Figure 5.7 Changes in concentrations of total soluble Fe (solid lines), Fe(II) (broken lines) (a), and total soluble As (solid lines), As(III) (broken lines) (b) in *Ac. brierleyi* cultures by feeding different seed crystals. Bioscorodite (◆), hematite (■) and perlite (▲) were fed at 0.5% (w/v). Initial condition was $[As(III)]_{ini}$ = 13 mM, $[Fe(II)]_{ini}$ = 18 mM.

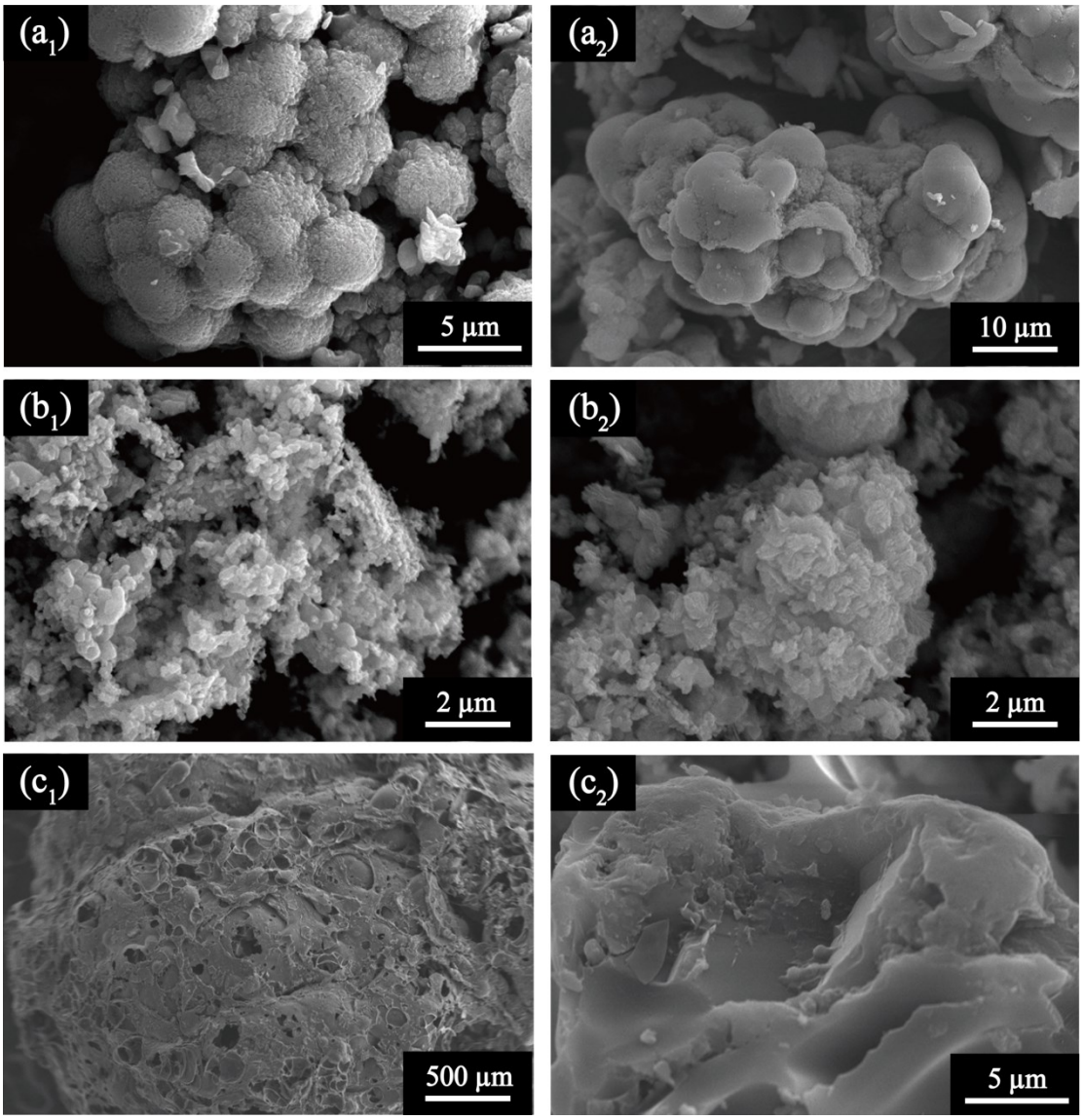

Figure 5.8 SEM images of seed crystals at day 0 (a_1–c_1) and final products at day 14 (a_2–c_2). Bioscorodite (a), hematite (b) and perlite (c) were fed at 0.5% (w/v). Initial condition; $[As(III)]_{ini}$ = 13 mM, $[Fe(II)]_{ini}$ = 18 mM, pH 1.5.

5.3.4 Effect of surface charge of seed crystals

As an effect of feeding seed crystals, microbial cells attachment on the seed surface can be expected for cell growth and bioscorodite crystallization. To elucidate the role of seed crystals, zeta-potentials of *Ac. brierleyi* cells, precursors (day3, 8, 9), bioscorodite (day 14), hematite and perlite were measured in 10^{-3} M KCl solution. Zeta-potentials of scorodite precursors gradually increased from +25 mV (day 3, 8) to +34 mV (day 9) and finally +50 mV (day 14; Figure 5.9d_1), when the amorphous precursors transformed into crystalline bioscorodite. Since *Ac. brierleyi* cells were charged slightly positive at high acidic pH (+ 5 mV at pH 2.0) (Figure 5.9), the large difference of electrostatic potential between cells and bioscorodite seeds caused cells to readily attach on the bioscorodite surface. This attachment was demonstrated as emergence of a new peak at +30 mV in zeta-potential distribution of the mixture of cells and bioscorodite seeds (Figure 5.9d_2). On the other hand, since the surface of precursors at day 3 and 8 charged less positive, cells did not attached on the precursors, which were also displayed in zeta-potential distribution of the mixture of the two (Figure 5.9a_2, b_2). These results elucidated that bioscorodite crystallization without seed crystals become less effective because precursors was impossible to work as seed crystals. Overall, feeding bioscorodite seeds attributed the cell attachment on the seed surface, and played roles of cell growth and providing the reaction area of bioscorodite crystallization.

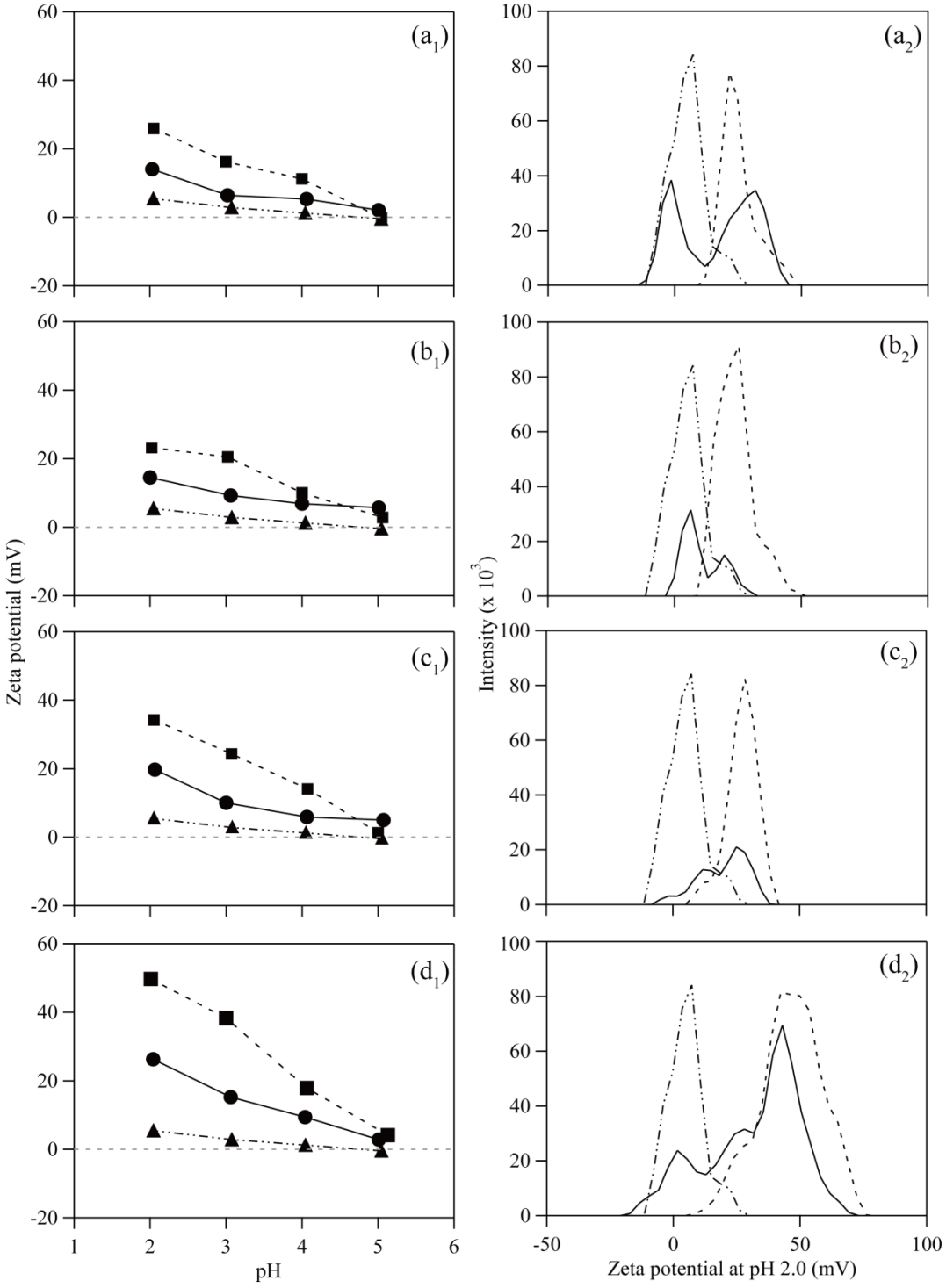

Figure 5.9 Zeta-potentials as a function of pH (a_1–d_1) and zeta-potential distribution at pH 2.0 (a_2–d_2) of *Ac. brierleyi* cells (▲, dash-dotted lines), precursors (day 3 (a), 8 (b), 9 (c))/bioscorodite (day 14, d) particles (■, dotted lines), and the mixture of the two (●, solid lines) (Okibe at al., 2017).

In case of other substances, hematite was charged most highly positive (+60 mV at pH 2) under high acidic conditions due to the protonation of hydroxyl group on the surface (Giménez et al., 2007; Mamindy-Pajany et al., 2009), while perlite surface was negatively charged (−41 mV at pH 2.0) (Figure 5.10). Anionic As(V) ($H_2AsO_4^-$) adsorption on hematite surface was reported by Mamindy-Pajany et al., 2009. Since hematite seeds attracted the anionic As(V) ions near the surface, precipitation with Fe(III) as scorodite may readily occur. That is, highly positive charged particles such as hematite and bioscorodite possibly utilized as seed crystals.

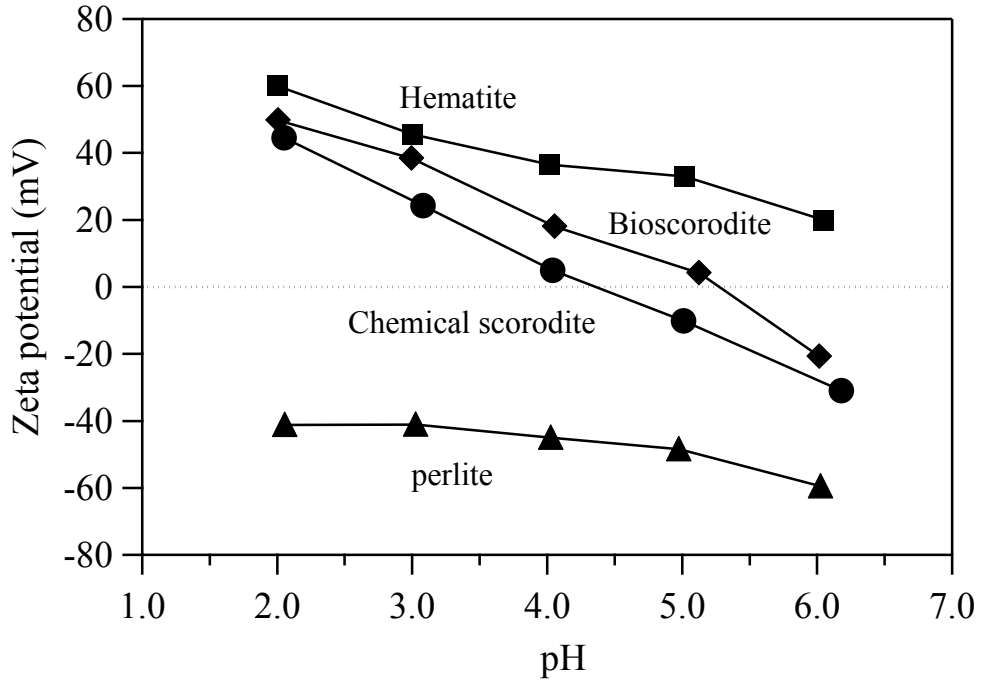

Figure 5.10 Zeta-potential of seed crystals in 10^{-3} M KCl solutions. Bioscorodite (◆), chemical scorodite (●), hematite (■) and perlite (▲).

5.3.5 Stability of final bioscorodite products

TCLP tests were conducted for original scorodite seeds as well as for the resultant bioscorodite products (Table 5.2).

Original seed crystals: Despite of their smaller particle size and larger specific surface area (Table 5.1), bioscorodite seeds showed greater stability (As; 0.33 ± 0.08 mg/l; Table 5.2) compared to chemical scorodite seeds (As; 5.49 ± 0.03 mg/l; Table 5.2) by the TCLP test. Both TCLP and JLT46 tests demonstrated the leached As concentrations of bioscorodite seeds were below the regulatory limit for landfill (5 mg/l for TCLP and 0.3 mg/l for JLT46; Table 5.2). Although Fe/As molar ratio of all scorodite seeds and products were 1.0-1.1 and 1.3-1.4, respectively, the amount of Fe leached generally remained only below one-tenth of that of As (Table 5.2), due to selective re-precipitation of Fe(III) at pH 4.9. Other chemical scorodite studies reported TCLP leachabilities ranging 0.1-13.6 As-mg/l (Singhania et al. 2006; Fujita et al. 2009a; Caetano et al. 2009; Table 5.3), generally often higher than those of bioscorodite (this study and Gonzalez-Contreras et al., 2012a, b). Such stability difference between bioscorodite seeds and chemical seeds may be attributed to factors such as involvement of cell encrustation, structural water content and morphological difference, and crystal maturity (speed of crystallization), but exact reasons remains to be unclear.

Final bioscorodite products: Stability of final bioscorodite products was improved (As; from 5.49 ± 0.03 to 1.86 ± 0.05 mg/l; Table 5.2) when chemical seed surface became coated with fresh bioscorodite precipitates, whilst As leachability remained at a low level both before (As; 0.33 ± 0.08 mg/l) and after (As; 0.59 ± 0.08 mg/l) the bioscorodite crystallization reaction when biological seeds were used (Table 5.2). Use of lower pH of 1.2 for bioscorodite crystallization reaction on bioscorodite

seeds slightly improved the product stability (As; 0.20 ± 0.01 mg/l), compared to that of pH1.5 (As; 0.59 ± 0.20 mg/l; Table 5.2), although the final As removal was lower at pH 1.2 (Figure 4.5a in chapter 4).

Table 5.2 TCLP test results for seed scorodite crystals and final bioscorodite products.

Conditions used for bioscorodite crystallization reaction:		Original seed crystals[a]						
		TCLP leachability:		JLT46 leachability:		Chemical composition (weight in 50 mg sample; mg):		
Seed crystals fed:	Initial pH	[As] (mg/l)	[Fe] (mg/l)	[As] (mg/l)	[Fe] (mg/l)	Fe	As	Fe/As molar ratio
Bioscorodite	1.5	0.33 ± 0.08	<0.004	0.28 ± 0.01	3.23 ± 0.02	11.7 (0.21 mmol)	14.1 (0.19 mmol)	1.1
	1.2							
Chemical scorodite	1.5	5.49 ± 0.03	0.11 ± 0.01	20.8 ± 0.38	45.4 ± 0.54	9.12 (0.16 mmol)	12.2 (0.16 mmol)	1.0

Conditions used for bioscorodite crystallization reaction:		Final bioscorodite products[b]						
		TCLP leachability:		JLT46 leachability:		Chemical composition (weight in 50 mg sample; mg):		
Seed crystals fed:	Initial pH	[As] (mg/l)	[Fe] (mg/l)	[As] (mg/l)	[Fe] (mg/l)	Fe	As	Fe/As molar ratio
Bioscorodite	1.5	0.59 ± 0.20	< 0.004	–	–	12.1 (0.22 mmol)	12.0 (0.16 mmol)	1.4
	1.2	0.20 ± 0.01	0.11 ± 0.03	–	–	11.5 (0.21 mmol)	11.8 (0.16 mmol)	1.3
Chemical scorodite	1.5	1.86 ± 0.05	0.005	–	–	10.5 (0.19 mmol)	11.2 (0.15 mmol)	1.3

[a] Bioscorodite seeds were produced at $[As(III)]_{ini}$ = 13 mM and $[Fe(II)]_{ini}$ = 18 mM (Fe(II)/As(III) = 1.4), whereas chemical scorodite seeds at $[As(V)]_{ini}$ = 267 mM and $[Fe(II)]_{ini}$ = 358 mM (Fe(II)/As(V) = 1.3).

[b] Final bioscorodite products were produced at $[As(III)]_{ini}$ = 4.7 mM and $[Fe(II)]_{ini}$ = 9.5 mM (Fe(II)/As(III) = 2.0) using either bio- or chemical scorodite seeds.

Table 5.3 Review of TCLP test results (revised from Gonzalez-Contreras et al. 2012b)

Nature of crystals	Crystal Size	Arsenic leaching TCLP test, pH 5	Other test conditions
Mineral			
Scorodite (Krause and Ettel 1988)	-	-	0.32 mg/L pH 2.43, 14 d (H_2SO_4)
	-	-	1.49 mg/L pH 2.05, 14 d (H_2SO_4)
Biogenic crystals			
Bioscorodite 72°C	<1cm	0.1 mg/L, 1 d	-
(Gonzalez-Contreras et al. 2012a)		0.5 mg/L, 100 d	
(Gonzalez-Contreras et al. 2012b)	175 µm	1.9 mg/L, 60 d	-
Chemical synthesized crystals (70-95°C)			
Nanocrystalline scorodite 70°C	50 nm	0.58 mg/L, 13 d	20.8 mg/L pH 1, 13 d
(Paktunc and Bruggeman 2010)			0.56 mg/L pH 2, 13 d
			5.38 mg/L pH 7, 13 d
Amorphous ferric arsenate 70°C	50-100 nm	60 mg/L, 13 d	90 mg/L pH 2, 13 d
(Paktunc and Bruggeman 2010)			30 mg/L pH 3, 13 d
			50 mg/L pH 4, 13 d
Scorodite 70°C (Fujita et al. 2012)	0.77 µm	5.13 mg/L, 7 h	2.69 mg/L pH 3.00, 7 h
			1.01 mg/L pH 5.74, 7 h
Scorodite 95°C (Caetano et al. 2009)	1.6 µm	13.6 mg/L, 18 h	-
	5.3 µm	0.1 mg/L, 18 h	
Scorodite 95°C (Fujita et al. 2009a)	16 µm	0.37 mg/L, 6 h	-
Scorodite 95°C (Fujita et al. 2009b)	17 µm	0.18 mg/L, 35 d	0.4 mg/L pH 3, 35 d
			3.1 mg/L pH 7, 35 d
			351 mg/L pH 9, 35 d
Scorodite 95°C (Harvey et al. 2006)	-	0.3 mg/L, 4 h	0.45 mg/L pH 6, 4 h
Scorodite 95°C (Singhania et al. 2005)[a]	10 µm	4.8 mg/L, 20 h	-
Chemical synthesized crystals (150-175°C)			
Scorodite 150°C (Caetano et al. 2009)	1.5 µm	13 mg/L, 8 h	-
	2.5 µm	5 mg/L, 8 h	
Scorodite 160°C	-	0.35 mg/L, 460 d	0.61 mg/L pH 6, 460 d
(Bluteau and Demopoulos 2007)			5.89 mg/L pH 7, 460 d
Scorodite 160°C (Bluteau et al. 2009)	0.3 µm	0.35 mg/L, 460 d	5.89 mg/L pH7, 460 d
			386 mg/L pH 9, 460 d
Scorodite 160°C (Singhania et al. 2005)[a]	5 µm	0.8 mg/L, 20 h	-
Scorodite 160°C (Krause and Ettel 1988)	2.5 µm	-	0.2 mg/L pH 5.57, 14 d (H_2SO_4)
			0.19 mg/L pH 3.45, 14 d (H_2SO_4)
			0.33 mg/L pH 2.85, 14 d (H_2SO_4)
Scorodite 175°C (Gomez et al. 2008)	-	0.1 mg/L, 20 h	-

[a] amended from the original Table by Gonzalez-Contreras et al. (2012b)

5.4 Conclusions

Morphological and structural characteristics of bioscorodite and chemical scorodite seed crystals were compared; bioscorodite ($FeAsO_4 \cdot 1.55H_2O$; spherical aggregates; 36 μm; 2.0 m^2/g), chemical scorodite ($FeAsO_4 \cdot 1.91H_2O$; orthorhombic crystals; 98 μm; 0.7 m^2/g). Bioscorodite seeds showed greater stability than the latter by TCLP test. Feeding bioscorodite seeds enabled effective As removal from dilute As(III) solution (98% final As removal at day 21). Contrasting bioscorodite crystallization process on bioscorodite and chemical scorodite seeds were found: Hollow bioscorodite seed particles became increasingly filled with newly formed scorodite, whilst solid chemical seeds induced their surface to be thoroughly coated with new scorodite precipitates. TCLP leachabilities of final bioscorodite products formed on bioscorodite and chemical scorodite seeds were 0.59 ± 0.08 mg/l and 1.86 ± 0.05 mg/l, respectively, which were lower than the regulatory limit of As by TCLP test.

Utilization of hematite seed crystals displayed fastest As immobilization due to not only fine particles (large surface area) but also electrostatic features. Since hematite and scorodite (bio/chem) surface was charged highly positive, they performed as absorbent of As(V) and *Ac. brierleyi* cells. As a result, bioscorodite crystallization readily progressed.

Data shown in this chapter were partially included in the paper accepted as:
Tanaka, M. and Okibe, N., 2018. Factors to enable crystallization of environmentally-stable bioscorodite from dilute As(III)-contaminated waters. *Minerals*, 8(1): 23.

Chapter 6

Effect of SO_4^{2-} ions on amorphous precursor formation and transformation into crystalline scorodite

6.1 Introduction

Metal refinery wastewater generally contains high concentrations of sulfate (SO_4^{2-}) ions due to extremely low pH and dissolution of sulfide minerals. The effects of SO_4^{2-} ions on chemical scorodite syntheses have been reported: e.g., Demopoulos et al. (1995) reported an inhibitory effect of SO_4^{2-} ions (100 mM) in scorodite yield in 2 g/l (27 mM) As(V)-Fe^{3+}-HCl solution. Substitution of SO_4^{2-} with AsO_4^{3-} in scorodite was observed using 25 g/L (334 mM) As(V)- Fe^{3+}-HNO_3 medium by addition of ~2 M Li_2SO_4 in hydrothermal synthesis (Dutrizac and Jambor, 1988). Incorporation of SO_4^{2-} in scorodite was also suggested by excess addition of SO_4^{2-} (1-2 M) in 10 g/L (133 mM) As(V)-Fe^{3+}-H_2SO_4 solution in atmospheric synthesis (Singhania et al., 2006). Gomez et al., (2011a) displayed the higher initial Fe(III)/As(V) molar ratio resulted in formation of basic ferric arsenate sulfate (BFAS; $Fe(AsO_4)_{1-x}(SO_4)_x(OH)_x \cdot (1-x)H_2O$) rather than scorodite (in this case, trace SO_4^{2-} ions were substituted in scorodite structure) under hydrothermal method. That study utilized ferric sulfate ($Fe_2(SO_4)_3 \cdot xH_2O$) as iron sources, that is, high Fe(III)/As(V) molar ratio condition contains high concentrations of SO_4^{2-} ions. In our experiments, much higher concentrations of SO_4^{2-} ions (65 mM at pH 1.5) exist in microbial media compared to As(III) (13 mM) and Fe(II) (18 mM) for microbial growth. It may affect the bioscorodite crystallization even at low As(III) concentrations.

Incidentally, bioscorodite crystallization progresses through second As concentration decrease (1st-stage As-removal at ~ day 4; 2nd-stage As-removal at day 10~) as shown in chapter 4. At the 1st-stage As-removal, brown-colored amorphous precipitates (precursors) formed, and then it was transformed into scorodite at 2nd-stage As-removal. However, this transformation mechanism is still unclear.. Therefore, this chapter focused on the effect of SO_4^{2-} ions on bioscorodite

crystallization process. Characterization of amorphous precursors and final bioscorodite were conducted from chemical compositions of Fe(III), As(V) and SO_4^{2-}, FT-IR spectra, TG-DTA analysis and XAFS measurement. In this chapter, precursor formation was conducted at $[As(III)]_{ini}$ = 13 mM and $[Fe(II)]_{ini}/[As(III)]_{ini}$ molar ratio of 1.4.

6.2 Materials and Methods

6.2.1 Precursors and bioscorodite crystallization experiment

Ac. brierleyi cells were inoculated (final cell density; 1.0 x 10^7 cells/ml) in 500 ml Erlenmeyer flasks containing 200 ml of HBS medium (pH 1.5 with H_2SO_4) with 18 mM Fe(II) (as $FeSO_4 \cdot 7H_2O$), 13 mM As(III) (as $NaAsO_2$) and 0.02% (w/v) yeast extract. $[Fe(II)]_{ini}/[As(III)]_{ini}$ molar ratio was set to 1.4. Flasks were incubated at 70°C, shaken at 100 rpm. Precipitates were regularly taken and washed once by pure water. After freeze-drying, 50 mg of samples were digested in 35% HCl to determine the chemical composition by measuring total Fe, As and S concentrations. Precipitates were analyzed by FT-IR, TG-DTA and XAFS. The Fe^{3+} (20 mM $FeCl_3 \cdot 6H_2O$; pH 1.5 with HCl), SO_4^{2-} (20 mM Na_2SO_4; pH 1.5 with HCl) and AsO_4^{3-} (1 M $Na_2HAsO_4 \cdot 7H_2O$; pH 6.0 with HCl) were examined using the attenuated total reflection Fourier Transform infrared spectroscopy (ATR-FTIR) using ZnSe crystal. Overlapped peaks were determined by the curve-fitting program PeakFit ver. 4.12 (Systat Software) with the mixed Gaussian and Lorentzian function (Maddams, 1980). Particles size distribution of precipitates at each day point was measured by LA-950 (Horiba).

6.2.2 Chemically scorodite crystallization test with/without sulfuric acid

Scorodite crystallization with or without H_2SO_4 were conducted by chemical

method in order to confirm the uptake of SO_4^{2-} ions. Five hundred milliliter Erlenmeyer flasks containing 18 mM Fe(III) and 13 mM As(V) (as $Na_2HAsO_4 \cdot 7H_2O$) in 200 ml of ultrapure water were incubated shaken at 70°C and 150 rpm. Ferric sulfate ($Fe_2(SO_4)_3 \cdot nH_2O$), ferric chloride ($FeCl_3 \cdot 6H_2O$) and ferric nitrate ($Fe(NO_3)_3 \cdot 9H_2O$) were utilized as Fe(III) reagents in response to acid conditions. Initial pH was adjusted to 1.5 using 1M H_2SO_4, HCl and HNO_3, respectively.

6.2.3 Bioscorodite crystallization experiment at high sulfate concentrations

Ac. brierleyi cells were inoculated (final cell density; 1.0 x 10^7 cells/ml) in 500 ml Erlenmeyer flasks containing 200 ml of HBS medium (pH 1.5 with H_2SO_4) with 18 mM Fe(II) (as $FeSO_4 \cdot 7H_2O$), 13 mM As(III) (as $NaAsO_2$) and 0.02% (w/v) yeast extract. $[Fe(II)]_{ini}/[As(III)]_{ini}$ molar ratio was set to 1.4. Initial SO_4^{2-} concentrations were set to 60 (original concentration), 100, 150 and 200 mM by adding H_2SO_4 and pH was adjusted to 1.5 using granular NaOH. Flasks were incubated at 70°C, shaken at 100 rpm.

6.2.4 Zeta-potential measurement of bioscorodite particles in arsenate and sulfate solutions

In order to evaluate the adsorption of arsenate and sulfate on bioscorodite seed crystals, zeta-potentials of bioscorodite particles at pH values ranging from 2.0 to 5.0 (adjusted with HCl and NaOH) were measured. Bioscorodite particles (0.2% (w/v); recovered at day 14) were suspended into 100 ml Erlenmeyer flasks containing 20 ml of 10^{-2} M NaCl solution with 0.2 mM As(V) (as KH_2AsO_4) or 0.2 mM SO_4^{2-} (as Na_2SO_4). Flasks were incubated at 70°C, shaken at 150 rpm for 1 hour, followed by zeta-potential measurement using Zetasizer Nano ZS (Malvern). Measurements were

conducted at least in triplicate.

6.3 Results and Discussion

6.3.1 Precursor formation in the presence of sulfate ions

In order to observe the roles of SO_4^{2-} ions on bioscorodite crystallization, brown amorphous precursors formed at each day point were collected. From liquid analysis, soluble SO_4^{2-} concentrations decreased from 67.0 mM to 64.5 mM (Figure 6.1c), together with the decrease of total Fe and As concentrations (Figure 6.1ab), followed by the formation of brown amorphous precursors. To observe the behavior of Fe^{3+}, AsO_4^{3-} and SO_4^{2-} ions in solid, amorphous precipitates were digested in 35% HCl (Figure 6.2). The results showed that SO_4^{2-} ion was one of the constituents of precursors. The measured $[AsO_4]_{im}/[Fe]_{im}$ molar ratio at day 5 was smaller (0.78) than the theoretical value of scorodite (1.0), while $[AsO_4+SO_4]_{im}/[Fe]_{im}$ was 0.94. At the end of reaction, $[SO_4]_{im}/[Fe]_{im}$ decreased from 0.16 to 0.08 as $[AsO_4]_{im}/[Fe]_{im}$ increased to 0.94 (Figure 6.2). This indicates that excess Fe was precipitated due to incorporation of SO_4^{2-} ions instead of AsO_4^{3-} ions. In order to confirm the uptake of SO_4^{2-} ions, chemical scorodite synthesis was attempted with or without use of H_2SO_4. When other acids such as HCl and HNO_3 were used instead of H_2SO_4, no precipitates were obtained in 1 week (Figure 6.3 and 6.4b, c). In contrast, yellowish precipitates readily formed within 1 hour when H_2SO_4 was used (Figure 6.4a_1), and were transformed into scorodite at day 7 (Figures 6.3 and 6.4a_2). Although inhibitory effects of SO_4^{2-} ions on chemical scorodite synthesis have been reported for As(V) solutions (Demopoulos et al., 1995), uptake of SO_4^{2-} ion was shown to be the key for precursor formation for dilute As(III) solutions (e.g., ~13 mM).

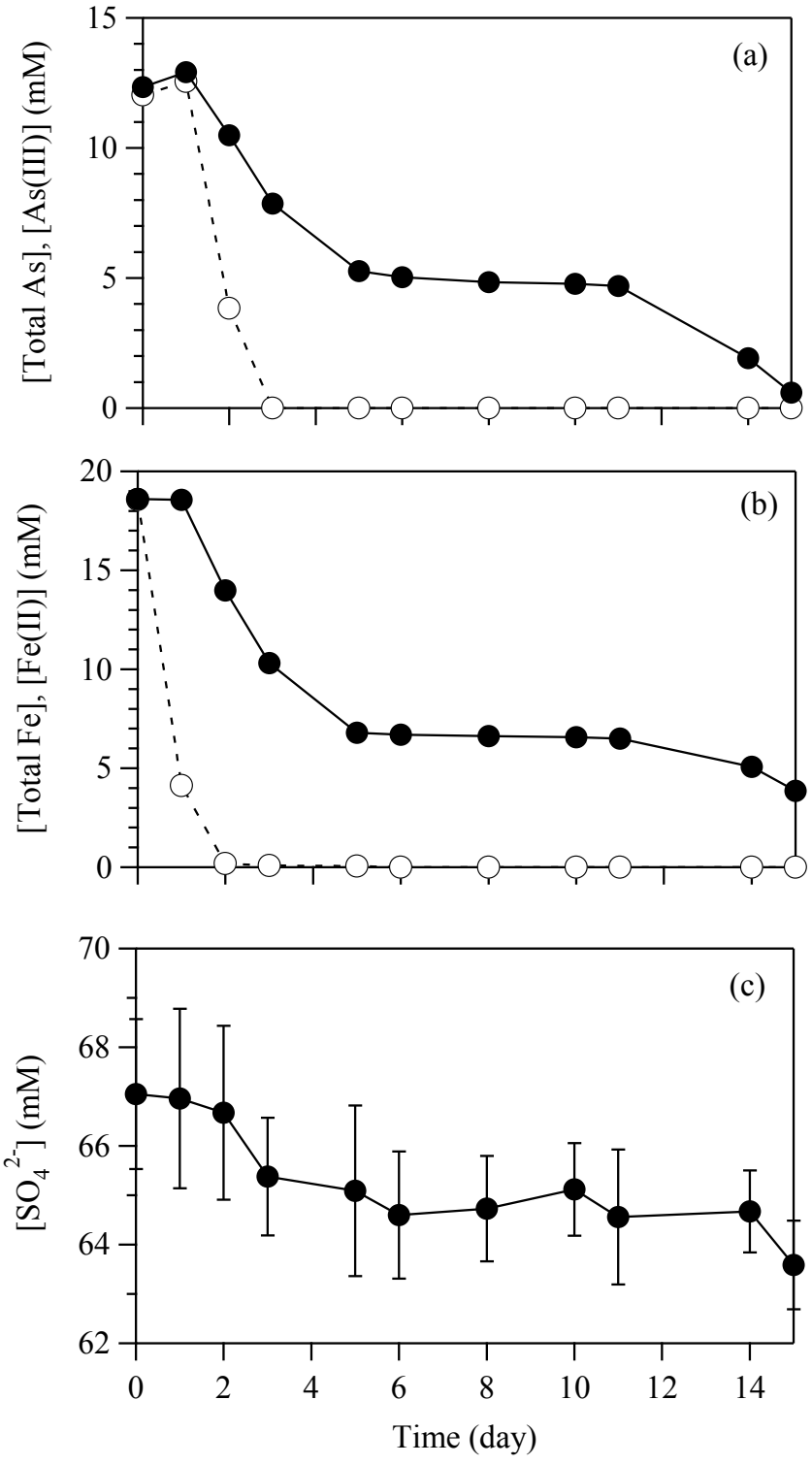

Figure 6.1 Changes in concentrations of total soluble As (solid line), As(III) (broken line) (a), total soluble Fe (solid line), Fe(II) (broken line) (b), and soluble SO_4^{2-} (c) in *Ac. brierleyi* cultures. Initial conditions; $[As(III)]_{ini}$ = 13 mM, $[Fe(II)]_{ini}$ = 18 mM, pH 1.5 with H_2SO_4.

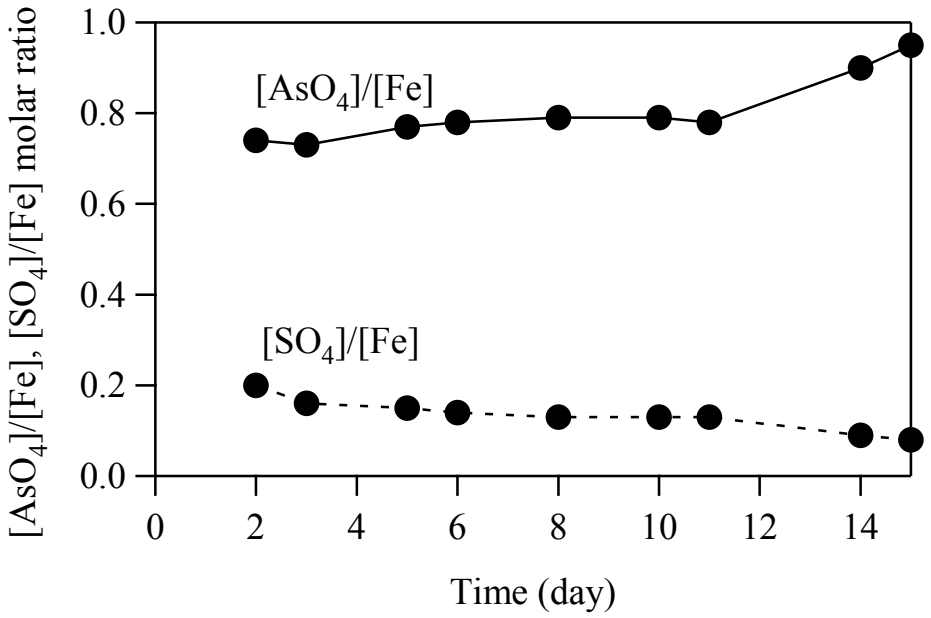

Figure 6.2 Changes in $[AsO_4]_{im}/[Fe]_{im}$ and $[SO_4]_{im}/[Fe]_{im}$ molar ratio in precipitates formed in *Ac. brierleyi* cultures described in Figure 5.1.

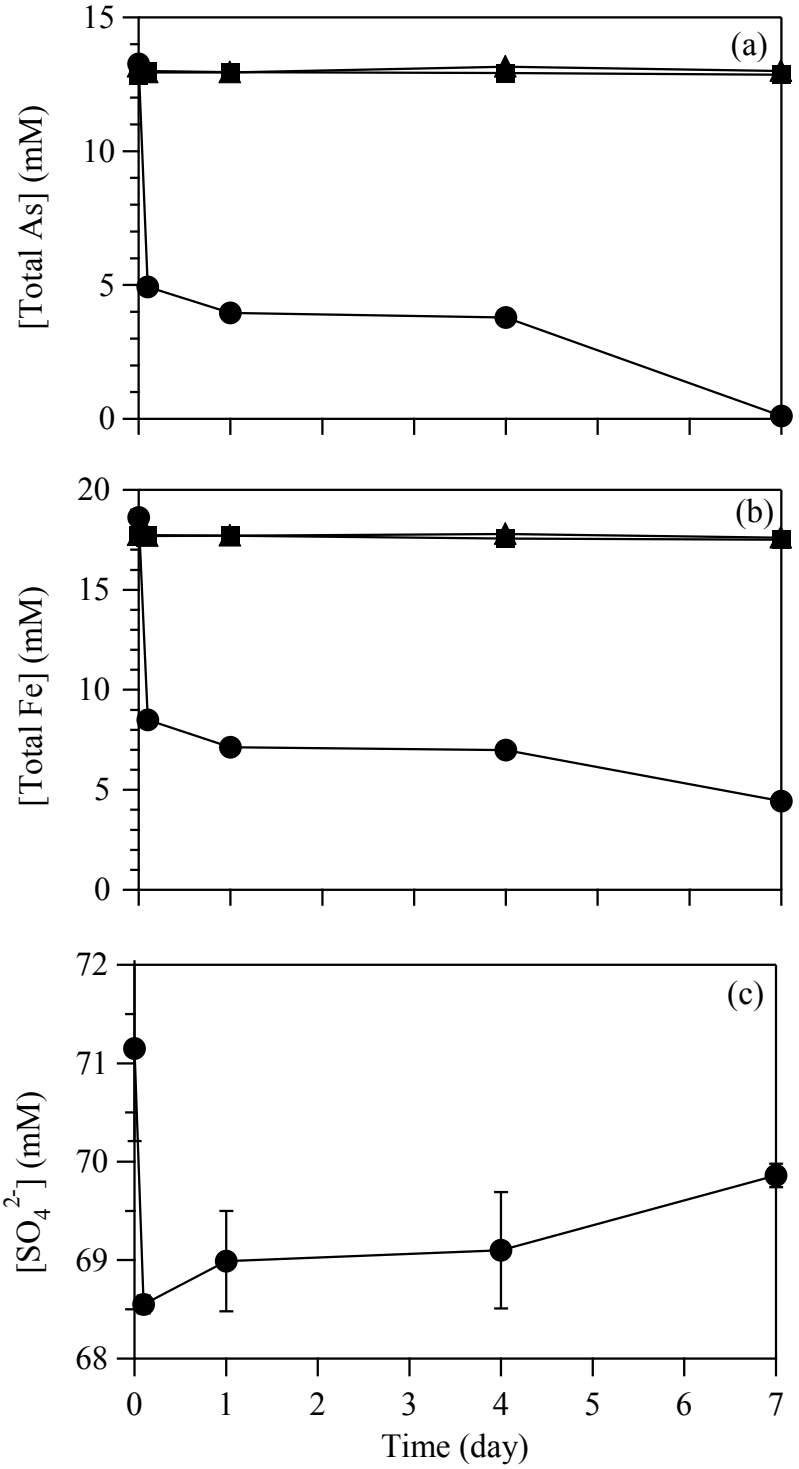

Figure 6.3 Changes in concentrations of total soluble As (a), total soluble Fe (b) and SO_4^{2-} ions (c) in chemical scorodite crystallization under H_2SO_4 (●), HCl (■) and HNO_3 (▲) conditions. Initial condition; $[As(V)]_{ini}$ = 13 mM, $[Fe(III)]_{ini}$ = 18 mM.

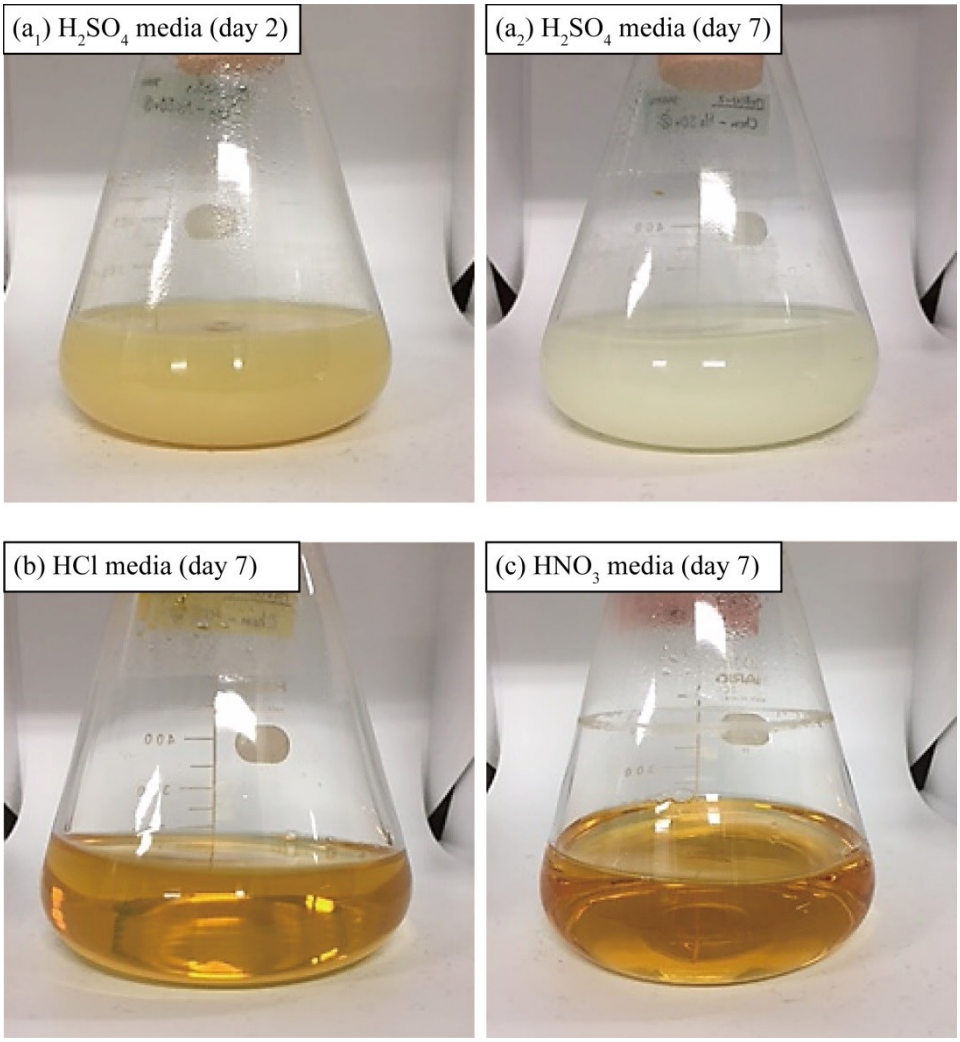

Figure 6.4 Solution color changes in chemical scorodite crystallization experiment in H_2SO_4 media (a) (day 2; a_1 and day7; a_2), HCl media at day 7 (b) and HNO_3 media at day 7 (c).

6.3.2 Behavior of sulfate ions in precipitates

Figure 6.5 showed the changes in FT-IR spectra of precipitates during bioscorodite crystallization. Distinct SO_4^{2-} peaks (1060 and 1121 cm^{-1}) originally present in precursors disappeared after day 9, corresponding to the clear color change to pale-green. This was accompanied by the emergence of OH peaks deriving from water molecules (sharp 3525 cm^{-1}, broad 2976 cm^{-1}) (Figure 6.5), which indicates occurrence of H-bond cleavage (Gomez et al., 2010). In the region of 700–1000 cm^{-1}, the shape of stretching AsO_4 peaks (day 3–8) transformed to sharp (day 10~), indicating the cleavage of Fe-OH (Ruan et al., 2002). SO_4^{2-} ions were once incorporated in the precursor structure by weak H-bonding, and then released to form final scorodite products. The shape of broad OH stretching peaks in the region of 2500–3600 cm^{-1} gradually changed from day 3–8 to 14, which became similar to the typical FT-IR spectra of scorodite (Figures 6.5).

For further understandings, the above mentioned broad bands (2500–3650 cm^{-1}) from samples (day 5, 9 and 14) and standards ($FeAsO_4 \cdot 2H_2O$ and $Fe_2(SO_4)_3 \cdot nH_2O$) were subjected to peak separation (Figure 6.6). The peaks at 3182, 3337 and 3465 cm^{-1} (day 5; Figure 6.6a), representing H_2O coordinated with Fe^{3+}-SO_4^{2-} compounds, progressively disappeared towards the completion of crystallization. Instead, a clear peak at 3523 cm^{-1} (day 14; Figure 6.6c) (corresponding to the Fe^{3+}-H_2O band in crystalline scorodite) became visible by day 14. At the same time, the peak at 2984 cm^{-1} (deriving from H_2O coordinated with crystalline scorodite) emerged to represent the top of the broad peak (day 14; Figure 6.6c).

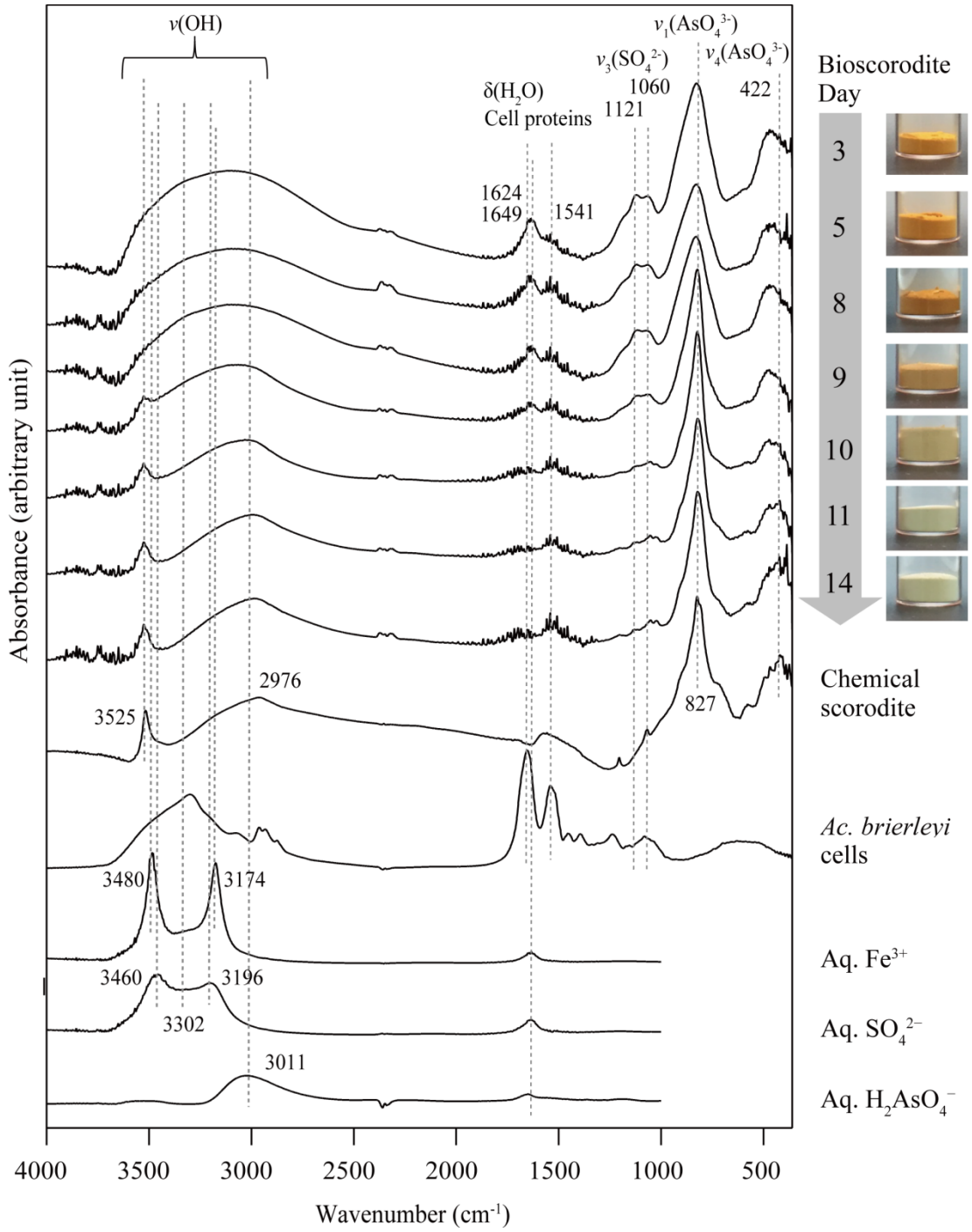

Figure 6.5 Changes in FT-IR spectra and color of precipitates recovered at day 3, 5, 8, 9, 10, 11 and 14 and related compounds (chemical scorodite, ferric sulfate, dried *Ac. brierleyi* cells, aqueous Fe^{3+} and SO_4^{2-}).. The spectra of solid samples were obtained by KBr pellet method, and liquid samples were obtained using ATR-FTIR.

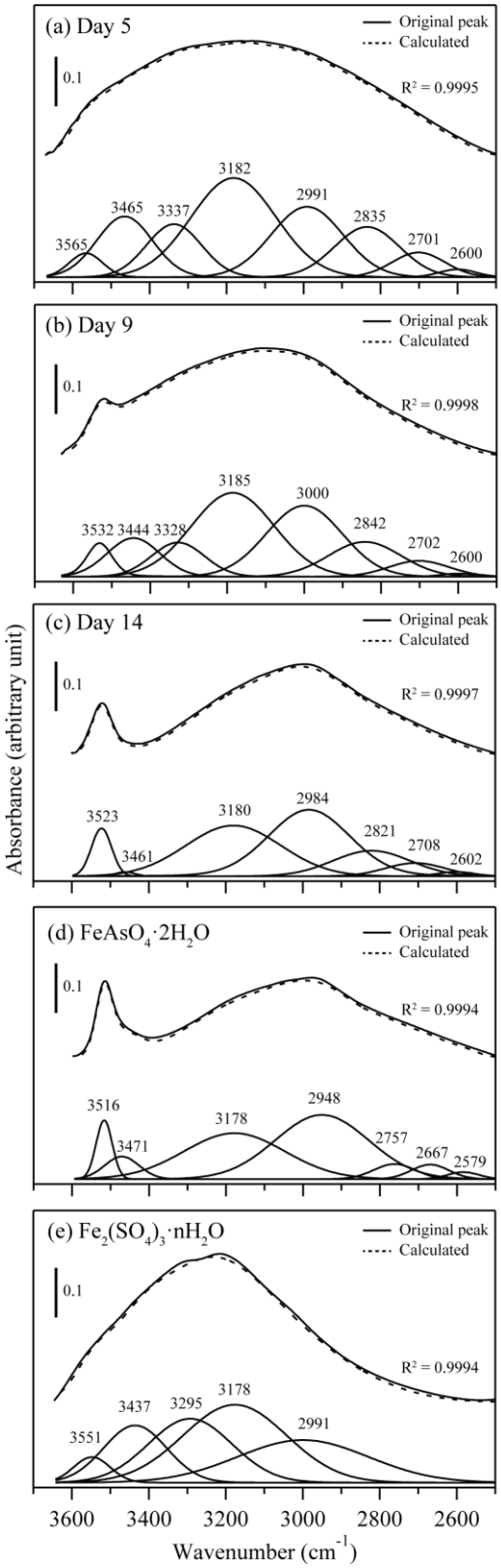

Figure 6.6 Curve fitted FT-IR spectra of 2500–3700 cm^{-1} region for As precipitates (a, day 5; b, day 9; c, day 14) and the standards (d, $FeAsO_4 \cdot 2H_2O$; e, $Fe_2(SO_4)_3 \cdot nH_2O$).

In order to elucidate the detailed mechanism of precursor formation, XANES spectra analysis was conducted. First, it was found that precursors were formed as Fe(III)-As(V) complex (Figure 6.7). From k^3-weighted As and Fe K-edge EXAFS data, although the peaks of amorphous precursors at day 3–8 transformed into that of typical scorodite at day 10–14 (Figure 6.8a_1, b_1) as well as the FT-IR spectra, it displayed the differences compared to pure scorodite in the regions of 8.0–9.2 $Å^{-1}$, 10.0–11.4 $Å^{-1}$ (As; Figure 6.8a_2, a_3) and 5.0–5.8 $Å^{-1}$, 6.8–8.0 $Å^{-1}$ (Fe; Figure 6.8b_2, b_3). That indicated that bioscorodite contains impurities in crystal structure, which are considered as SO_4^{2-} ions and organic substances derived from *Ac. brierleyi* cells. Fourier transforms of As K-edge EXAFS spectra displayed the first coordination shell about As was oxygen at a distance of 1.29 Å (AsO_4 tetrahedra) (Figure 6.9a_1) (Kitahama et al., 1975; Hawthorne, 1976; Sherman and Randall, 2003). While the As-O bond were observed in all samples, the peak at 2.91 Å were gradually emerged from the precipitates recovered at day 9 to day 14 (Figure 6.9a_2). These peaks were identified as As-Fe distance and indicated single corner linkages between AsO_4 tetrahedra and FeO_6 octahedra (Sherman and Randall, 2003). No peaks describing As-Fe distance at day 3–8 came from amorphous structure. These results proved that the crystal structure of amorphous ferric arsenate transformed into crystalline phase. In contrast, broad peaks were observed in the range of 2.5–3.4 Å from Fourier transforms of Fe K-edge EXAFS spectra results (Figure 6.9b_2). Precursors at day 3–8 displayed two peaks, and then the magnitude gradually increased through the crystallization as well as As. These two peaks showed the Fe-S bond and Fe-As bond, respectively (Chen et al., 2009, Kato and Miura 1977, Paktunc and Dutrizac 2003, Savage et al., 2005 as jarosite). Since As-S bond was not observed in As K-edge EXAFS spectra, AsO_4^{3-} and SO_4^{2-} ions were independently precipitated with Fe^{3+}, rather than Fe–

AsO_4–SO_4 compounds.

Overall, transformation process of amorphous precursors to crystalline bioscorodite involved the disappearance of SO_4^{2-} and Fe-OH bands while retaining AsO_4^{3-} bands. Therefore, it can be considered that the amorphous precursors formed during the first As-removal stage consist of at least two types of precipitates (Fe–SO_4 compounds and Fe–AsO_4 compounds), most likely in this case, basic ferric sulfate ($MFe_x(SO_4)_y(OH)_z$; M^+ = K^+, Na^+, NH_4^+) and amorphous ferric arsenate ($FeAsO_4 \cdot (2+n)H_2O$; Le Berre et al., 2008). Microbial jarosite formation during Fe(II) oxidation has been reported (e.g., *Thiobacillus ferrooxidans*, Ivarson, 1973; Sasaki and Konn, 2000; *Acidithiobacillus ferrooxidans*, Daoud and Karamanev, 2006; mixed culture of *Sulfolobales* species, Gonzalez-Contreras et al., 2012a) In biological scorodite crystallization, Weijma et al., 2017 reported the formation of jarosite nano-precipitates on the cell surface together with scorodite at 72°C, pH 1.2. In chemical scorodite synthesis under nitrate or chloride medium conditions, the initial formation of brownish amorphous precursor phase partly containing scorodite was reported, which was made up of poorly crystalline ferric arsenate ($FeAsO_4 \cdot (2+x)H_2O$; 80%) and ferrihydrite (20%) (nitrate solution: 80ºC, $[As(V)]_{ini}$ = 100 mM; Le Berre et al., 2008), β-goethite (chloride solution: 95ºC, $[As(V)]_{ini}$ = 26.7 mM; Demopoulos et al., 1995). In the presence of SO_4^{2-} ions and monovalent cations (e.g., Na^+, K^+, NH_4^+) in basal salts medium, the precipitation of ferrihydrite and goethite is possibly substituted for basic ferric sulfate formation. Therefore, brown-colored amorphous precursors are considered as the mixture of amorphous ferric arsenate and basic ferric sulfate.

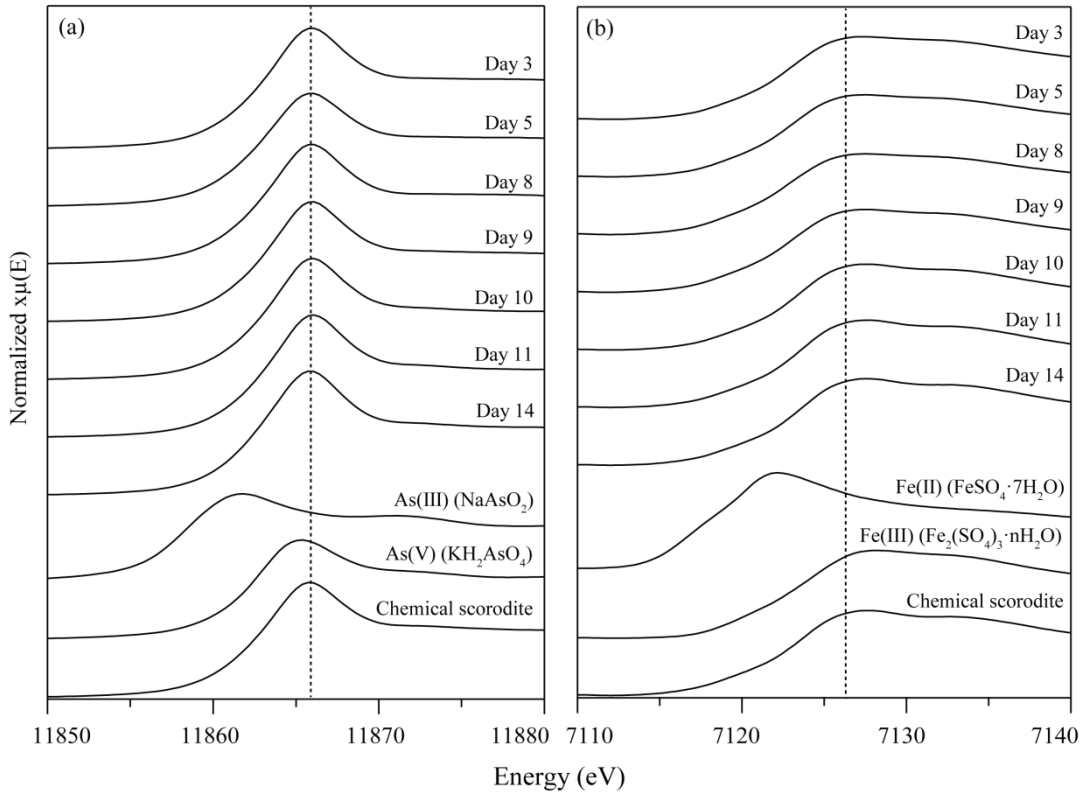

Figure 6.7 Normalized XANES spectra at the As (a) and Fe K-edge (b) of precipitates recovered at day 3, 5, 8, 9, 10, 11 and 14.

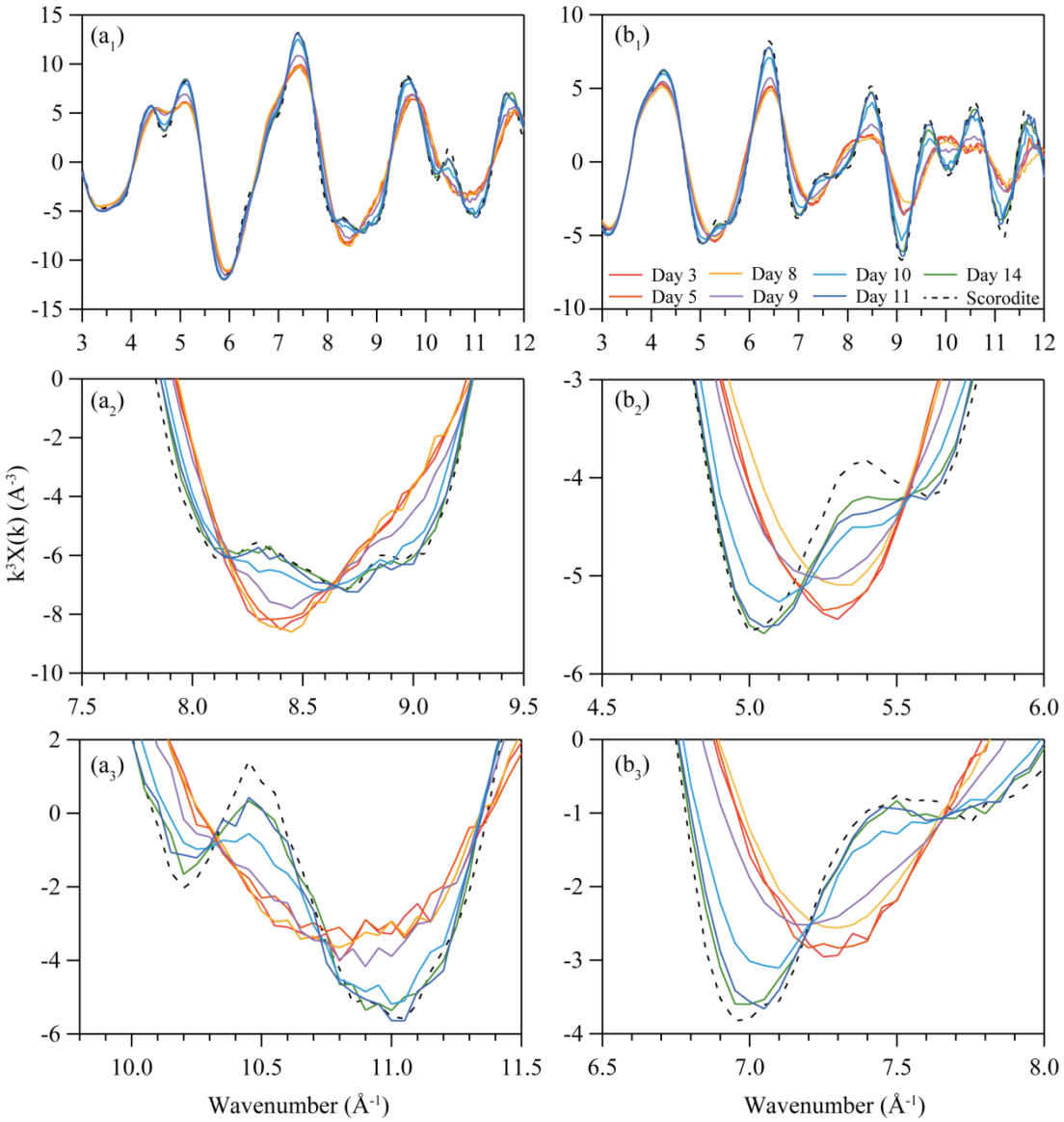

Figure 6.8 k^3-weighted As (a) and Fe (b) K-edge EXAFS spectra of precipitates recovered at day 3, 5, 8, 9, 11 and 14. Solid lines indicate the precipitates formed in *Ac. brierleyi* cultures, and broken line indicates pure scorodite.

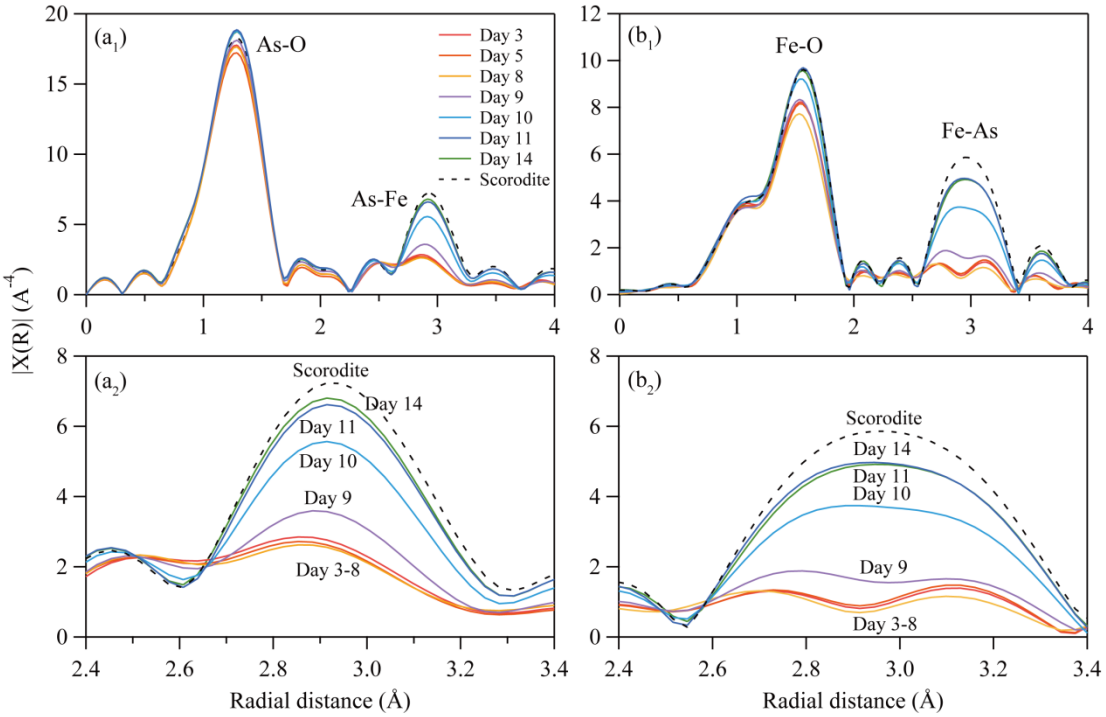

Figure 6.9 Fourier transforms of k^3-weighted EXAFS spectra of precipitates recovered at day 3, 5, 8, 9, 10, 11 and 14, yielding radial distribution from As (a) and Fe (b) atoms in the range of 0–4 Å (a_1, b_1) and 2.4–3.4 Å (a_2, b_2).

6.3.3 Transformation of amorphous precursors into crystalline bioscorodite

From TG curves of precursors at day 1 and 5, the continuous weight loss was observed from 100 to 700°C which was attributed to water vaporization of OH groups (solid lines; Figure 6.10a, b). Since the gentle TG curve was similar to previously reported basic ferric arsenate sulfate (BFAS; $Fe(AsO_4)_{1-x}(SO_4)_x(OH)_x \cdot wH_2O$) (hydrothermally synthesized at 225°C, $[As(V)]_{ini}$ = 160 mM; Gomez et al., 2011) and poorly-crystalline ferric arsenate ($Fe_{1.07}AsO_4 \cdot 3.06H_2O$) (atmospheric synthesis at room temperature, $[As(V)]_{ini}$ = 100 mM; Le Berre et al., 2007) it was possibly caused by the contamination of SO_4^{2-} ions and hydration in precipitates. DTA curve at day 1 (early stage in precipitation of Fe^{3+}) displayed two endothermic peaks at 590 and 680°C (broken line; Figure 6.10a), which showed the two types of water in different bonding state exist in precipitates. Interestingly, weight loss of precursors gradually decreased from day 5 to day 8 at 550°C (21.4%, day 5; 20.3%, day 6; 19.7%, day 7; 18.9%, day8) (Figure 6.11). These results indicated that dehydration of precursors derived from the changes of binding energy distribution continuously proceeded during induction period. From day 9, weight loss derived from crystalline water was observed at 125–200°C and transformed into the typical scorodite TG curve at day 14 (Figure 6.11).

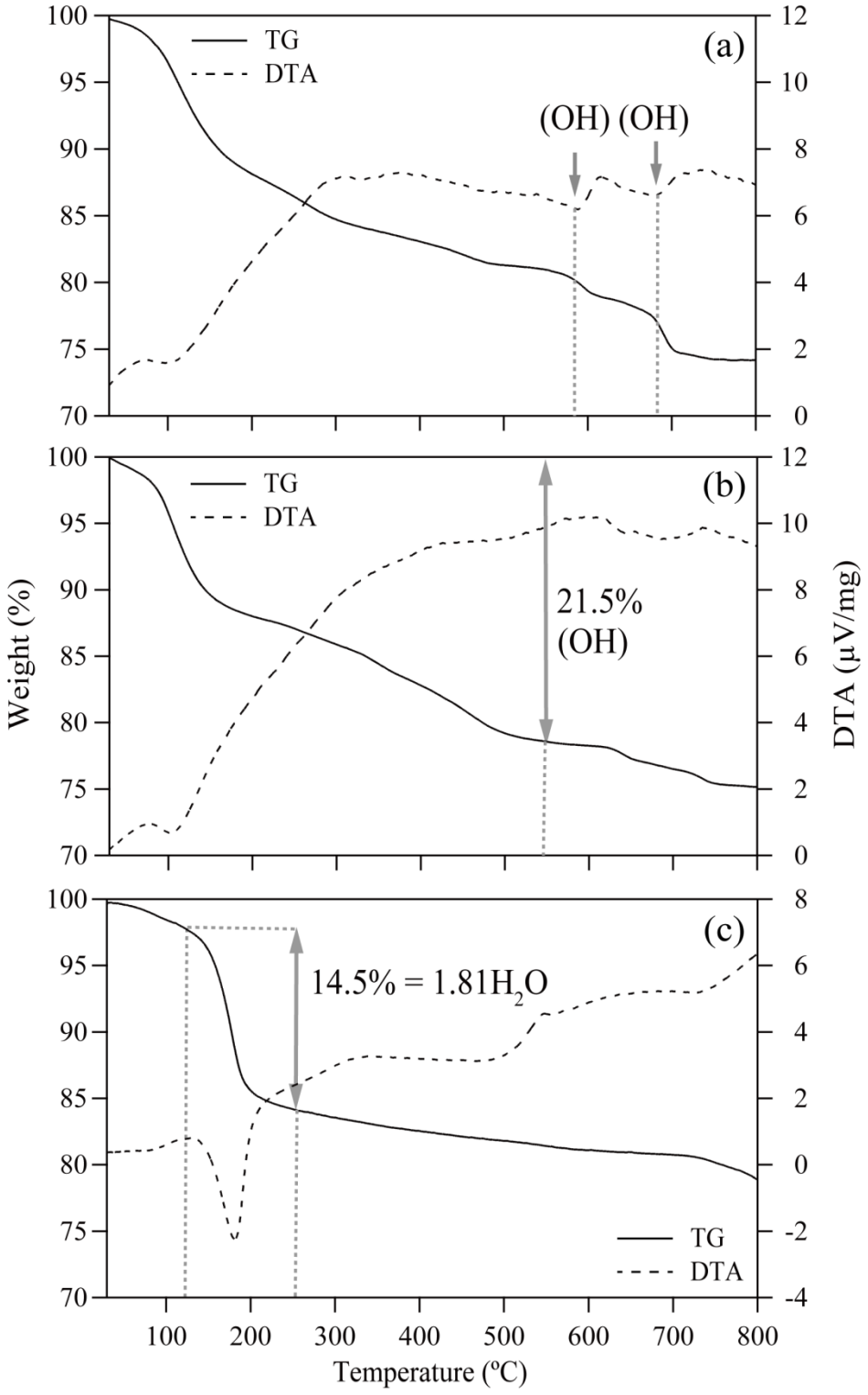

Figure 6.10 TG-DTA analyses of precursor at day 1 (a), day 5 (b) and bioscorodite at day 14 (c). The structural water contents were calculated based on the weight loss at 550°C (precursor) and 125–250°C (bioscorodite). Solid lines indicate TG curves and broken lines indicate DTA curves, respectively.

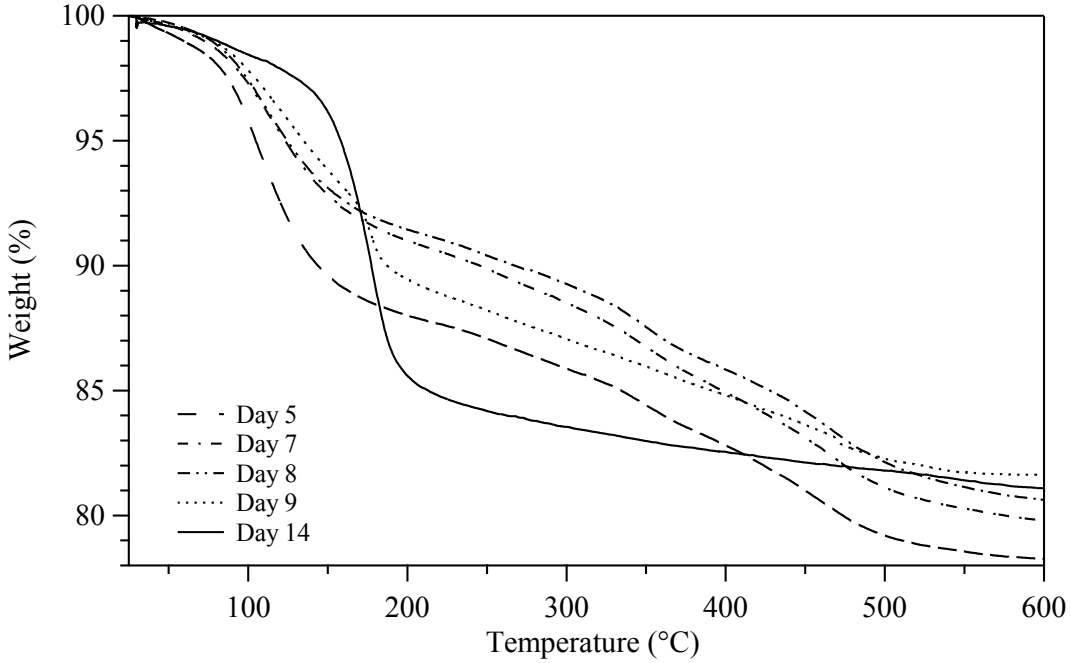

Figure 6.11 Changes in TG curves of amorphous precursors at day 5 (dashed line), day 7 (dashed dotted line), day 8 (dashed double-dotted line), day 9 (dotted line) and bioscorodite at day 14 (solid line). The structural water contents were calculated based on the weight loss at 550°C (precursors) and 125–250°C (bioscorodite).

SEM images displayed that fine rhombohedral particles (0.5–1 μm; jarosite-like particles) formed and aggregated at day 1, and then each particle grew in round shape (2–5 μm) at day 2–5 (Figure 6.12). Particle size of amorphous precursor at day 3 and 7 widely distributed from 4 to 200 μm (aggregated due to low zeta-potentials of 25 mV; chapter 5), and then it changed in narrow range at day 10 and 14 (Figure 6.14) via second-time precipitation on the surface of precipitates (Figure 6.12, day 8–11). The dense particles of amorphous precursors began to dissolve from day 8 and crystalline scorodite formed as passivation layer (Figure 6.13). Finally bioscorodite particles displayed the hollow structure (Figure 6.13). At 2nd-stage As-removal generally observed in bioscorodite crystallization process (chapter 4), excess As is removed (Fe/As = 0.4–0.6) compared to theoretical scorodite (Fe/As = 1) (e.g., the decrement of total Fe concentration is 2 mM, while 5 mM of As is removed at $[As(III)]_{ini}$ = 13 mM). This behavior indicated that dissolved ferric compounds were consumed as Fe source for the 2nd-stage As-removal.

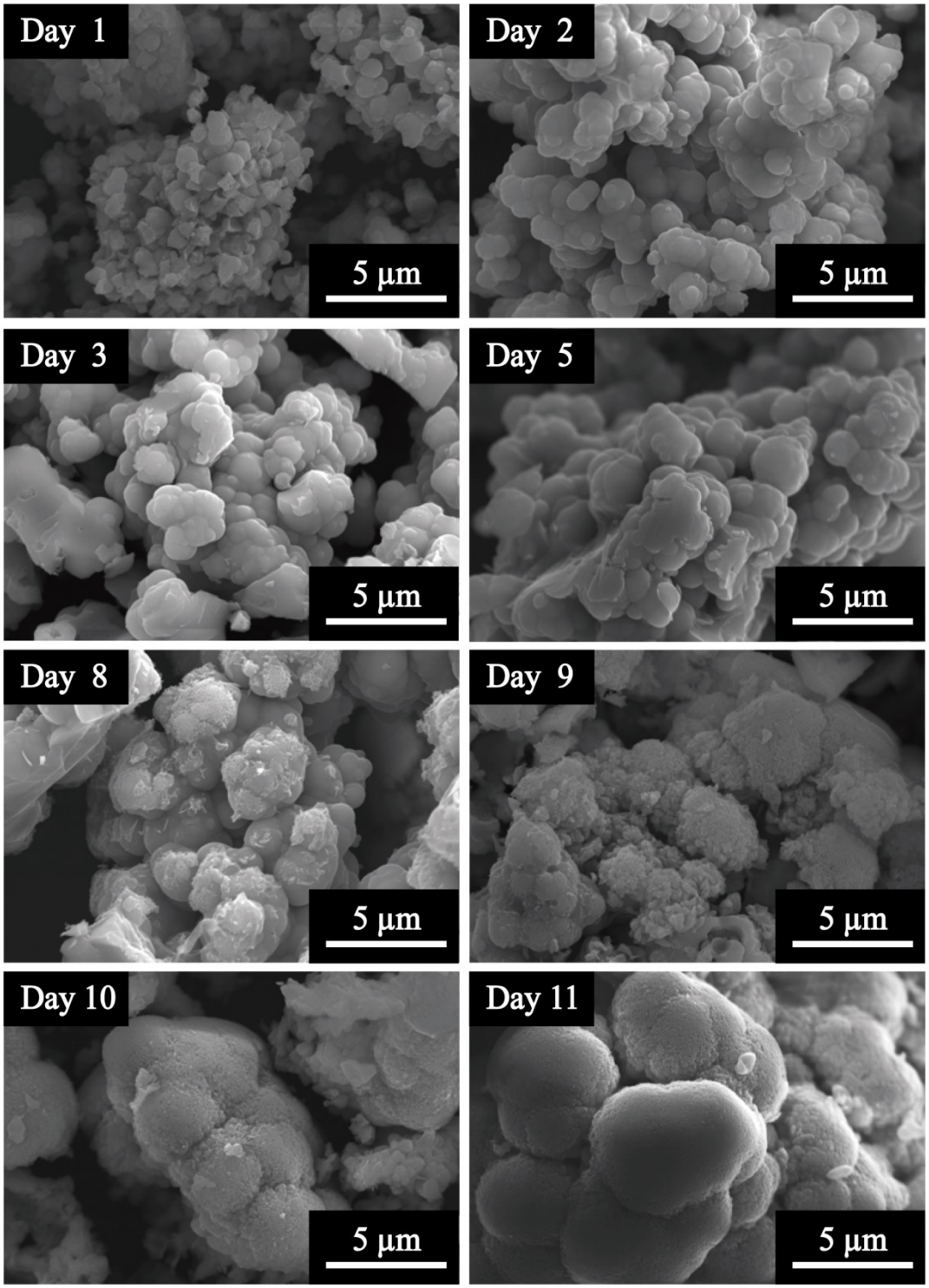

Figure 6.12 SEM observation of precipitates recovered at day 1, 2, 3, 5, 8, 9, 10 and 11.

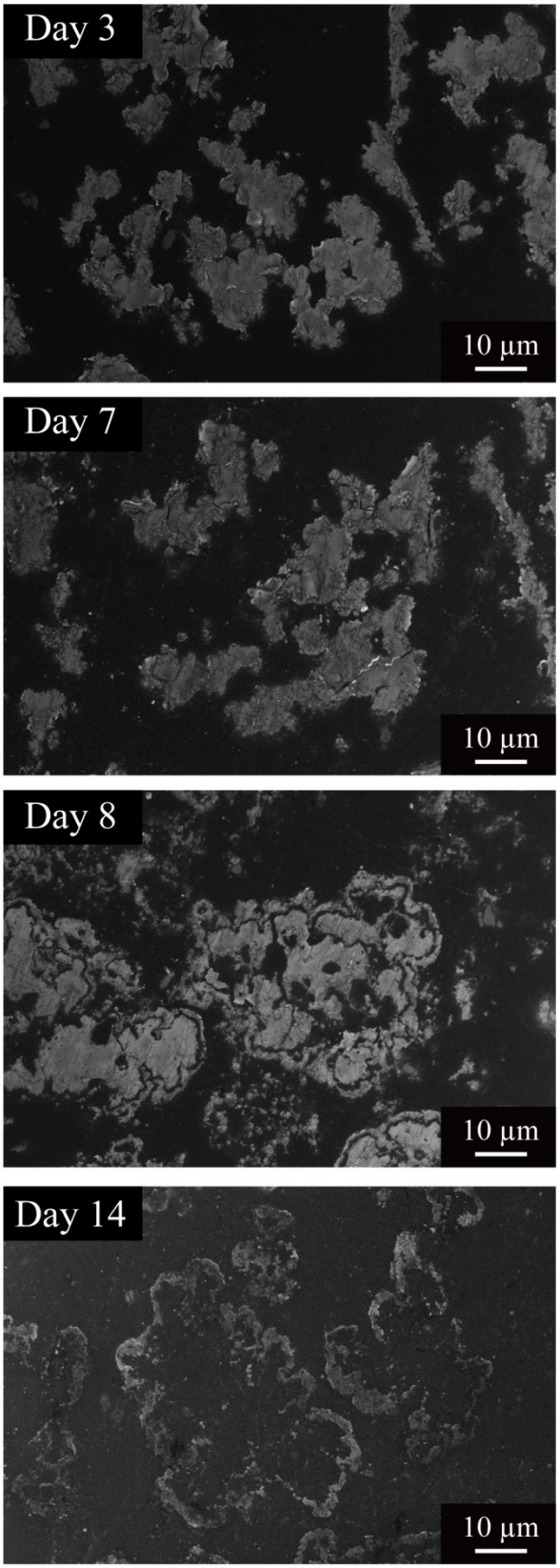

Figure 6.13 SEM cross-section views of precipitates recovered at day 3, 7, 8 and 14.

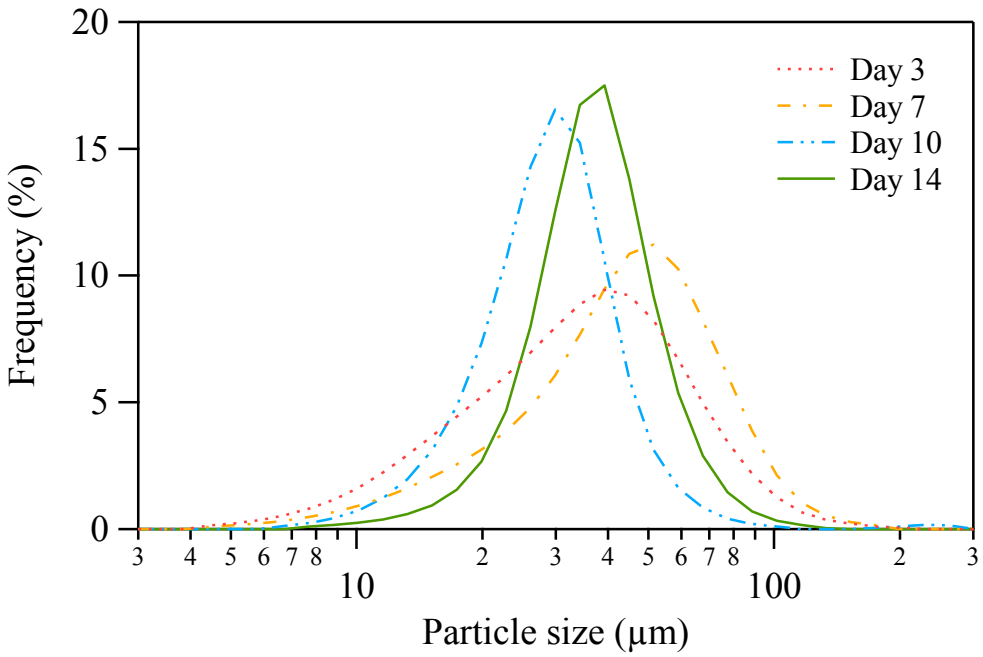

Figure 6.14 Particle size distribution of precursors (day 3 and 7), mixture of precursor and bioscorodite (day 10) and bioscorodite (day 14) formed in *Ac. brierleyi* cultures. Initial conditions; $[As(III)]_{ini}$ = 13 mM, $[Fe(II)]_{ini}$ = 18 mM, 0.02% (w/v) yeast extract, pH 1.5.

Solution pH was maintained low (pH 1.35) during induction period at day 3–8 (Figure 6.15a). Since jarosite is more likely to dissolve at extremely acidic pH (Baron and Palmer, 1995; Smith et al., 2006; Welch et al., 2008), amorphous ferric arsenate and basic ferric sulfate was gradually dissolved. This was also supposed that log IAP values increased to −20.5 and maintained −21.3 throughout 1st-stage As-removal and induction period (day 5–8) (Figure 6.15b), which is over the range of solubility products (log K_{sp}) value of amorphous ferric arsenate (−23.0; Langmuir et al., 2006). Dissolution of amorphous ferric arsenate and transformation into crystalline scorodite proceeded which accompanied with the decrease of log IAP value to −22.6 during the 2nd-stage As-removal process (Figure 6.15b). In crystallization process, a phase with higher solubility precipitates initially according to Stranski's rule. The order of initial precipitation rates $R_A > R_B > R_C$ follow the order of solubilities S(A)>S(B)>S(C), and these are dissolved depending on the soluble metal concentrations (Blesa and Matijevic, 1989; Demopoulos, 2009). The log K_{sp} values of amorphous ferric arsenate (−23.0) and basic ferric sulfate (e.g., jarosite, −11.0; Baron and Palmer, 1996) are higher than crystalline scorodite (−25.8; Langmuir et al., 2006). The long dissolution-recrystallization kinetic was caused by the milder conditions (low As concentrations, 70°C, pH 1.5) than other chemical methodologies (95–120°C, pH~1). Hence, about one fifth of the AsO_4^{3-} locus was occupied by SO_4^{2-} ions at the early stage, which were then released from precursors to form final product ($Fe(AsO_4)_{0.94}(SO_4)_{0.08}\cdot 1.81H_2O$; calculated from TG curve; Figure 6.10c) with a chemical formula close to theoretical scorodite ($FeAsO_4\cdot 2H_2O$).

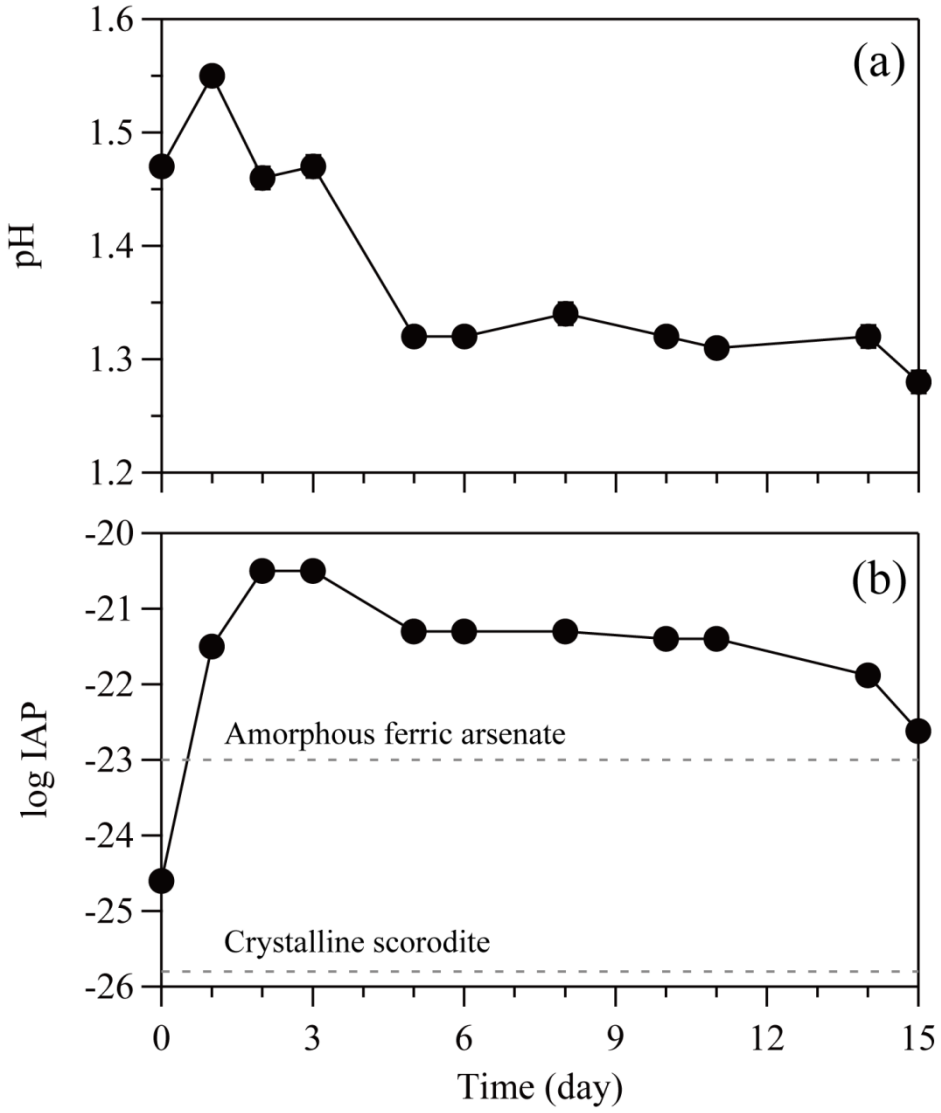

Figure 6.15 Changes in solution pH (a) and ion activity products (b) in Ac. brierleyi culture. Solubility products of amorphous ferric arsenate ($10^{-23.0}$) and crystalline scorodite ($10^{-25.8}$) was referred from Langmuir et al., 2006.

6.3.4 Proposed mechanism of precursor formation and transformation into crystalline bioscorodite via sulfate ion release

Proposed mechanism of precursor formation and transformation into crystalline bioscorodite was described in Figure 6.16a. First, microbial Fe(II) and As(III) oxidation proceeds by *Ac. brierleyi* described as Eqs. 6.1 and 6.2.

$$4Fe^{2+} + O_2 + 4H^+ = Fe^{3+} + 2H_2O \quad \text{(biological)} \qquad \text{(Eq. 6.1)}$$

$$2H_3As^{III}O_3 + O_2 = 2H_2As^{V}O_4^- + 2H^+ \quad \text{(biological)} \qquad \text{(Eq. 6.2)}$$

As a result, amorphous basic ferric sulfate (Eq. 6.3) and ferric arsenate (Eq. 6.4) are precipitated as precursors in SO_4^{2-}-bearing solutions (1st-stage As-removal).

$$M^+ + xFe^{3+} + yHSO_4^- + zH_2O = MFe_x(SO_4)_y(OH)_{z\,(amorphous)} + (y+z)H^+ \qquad \text{(Eq. 6.3)}$$

$(M^+ = K^+, Na^+, NH_4^+)$

$$Fe^{3+} + H_2AsO_4^- + (2+n)H_2O = FeAsO_4 \cdot (2+n)H_2O_{(amorphous)} + 2H^+ \qquad \text{(Eq. 6.4)}$$

Under steady-state condition, dehydration, dissolution and recrystallization of amorphous precursors with higher solubility proceeded (induction period). When the surface energy per mass unit becomes lower energy state, amorphous ferric arsenate and hydroxysulfate were readily dissolved. Released Fe(III) and dissolved As(V) in medium were precipitated for the coarsening of ferric arsenate particles, followed by scorodite crystallization (Eq. 6.5 and 6.6) (2nd-stage As-removal).

$$FeAsO_4 \cdot (2+n)H_2O_{(amorphous)} = FeAsO_4 \cdot 2H_2O_{(crystalline)} + nH_2O \qquad \text{(Eq. 6.5)}$$

$$Fe^{3+} + H_2AsO_4^- + 2H_2O = FeAsO_4 \cdot 2H_2O_{(crystalline)} + 2H^+ \qquad \text{(Eq. 6.6)}$$

Incidentally, high $[Fe(II)]_{ini}/[As(III)]_{ini}$ molar ratio (>2.0) (i.e. high initial Fe(III) and SO_4^{2-} concentrations) resulted in formation of jarosite as described in chapter 4. To search the effect of high SO_4^{2-} concentrations, bioscorodite crystallization test at higher SO_4^{2-} concentrations (100, 150 and 200 mM) was conducted. Although high initial SO_4^{2-} concentration did not affect the final As removal, the amount of As-removal in 1st–stage decreased (Figure 6.17a). That indicates the formation of basic ferric sulfate and ferric arsenate competed for Fe(III) ions. Hence, it was proved that SO_4^{2-} ions was the key for precursor (basic ferric sulfate) formation and high $[Fe(II)]_{ini}/[As(III)]_{ini}$ molar ratio (>2.0) resulted in formation of jarosite due to higher concentrations of Fe(III) and SO_4^{2-}. (Figure 6.16b)

6.3.5 Proposed mechanism of bioscorodite crystallization at lower pH 1.2

Direct bioscorodite crystallization without formation of precursors was observed at pH 1.2 as shown in chapter 4. At extremely acidic pH, jarosite is more likely to dissolve (Baron and Palmer, 1995; Smith et al., 2006; Welch et al., 2008). Indeed, we have observed the dissolution of jarosite in pure water at pH 1.2, 70°C (data not shown). Since low pH enabled to dissolve faster even in case of jarosite-like basic ferric sulfate, the reaction time for bioscorodite crystallization became shorter than pH 1.5, rather than the formation of precursors (Figure 6.16c). Although the formation of basic ferric sulfate triggered the amorphous ferric arsenate, basic ferric sulfate is dissolved faster at pH 1.2. Therefore, lower initial pH resulted in the decrement of final As removal.

6.3.6 Proposed mechanism of faster crystallization fed with seed crystals

As an effect of seed feeding, SO_4^{2-} ions adsorption on the surface of hematite hydroxyl groups has been reported (Watanabe et al., 1994) as well as As(V) ($H_2AsO_4^-$) adsorption (Mamindy-Pajany et al., 2009). The same is equally true of bioscorodite particles. Zeta-potential values of bioscorodite decreased from +43 mV (raw bioscorodite) to +28 mV (in As(V) solution) and +35 mV (in SO_4^{2-} solution) caused by adsorption of $H_2AsO_4^-$ and SO_4^{2-} on bioscorodite surface (Figure 6.18). That indicated that As(V) and SO_4^{2-} ions were locally concentrated in the vicinity of the bioscorodite surface. Hence, the amorphous ferric arsenate sulfate tended to precipitate rather than in absence of bioscorodite seeds. Simultaneously, concentration gradient of SO_4^{2-} ions possibly occurred due to adsorption on seed crystals, followed by faster transformation of precursor into scorodite (Figure 6.16d). Indeed, when bioscorodite crystallization readily proceeded (in the cultures at pH 1.2 in chapter 4 and fed with hematite seeds in chapter 5), [SO_4]/[Fe] molar ratio in precipitates displayed lower value (0.01–0.13) (Table 6.1) than that in conventional precursors (0.16–0.20). Overall, highly positive charged particles such as hematite and bioscorodite possibly utilized as seed crystals on bioscorodite crystallization at dilute As(III) concentrations.

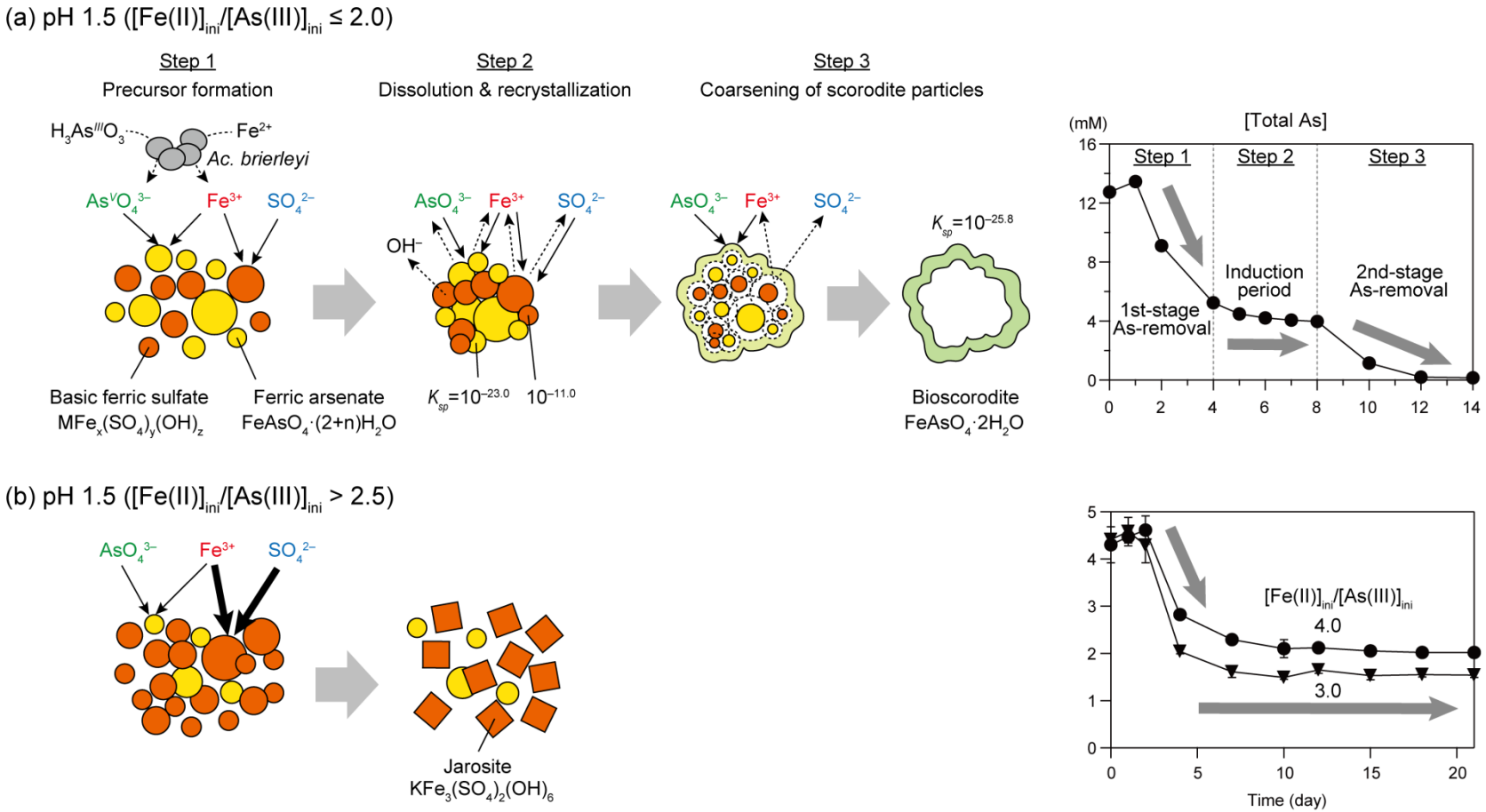

Figure 6.16 Schematic illustration of amorphous precursor formation and transformation into crystalline scorodite using *Ac. brierleyi* from dilute As(III) solutions at pH 1.5 (a), under the conditions of high $[Fe(II)]_{ini}/[As(III)]_{ini}$ molar ratio at pH 1.5 (b), pH 1.2 (c) and fed with seed crystals at pH 1.5 (d).

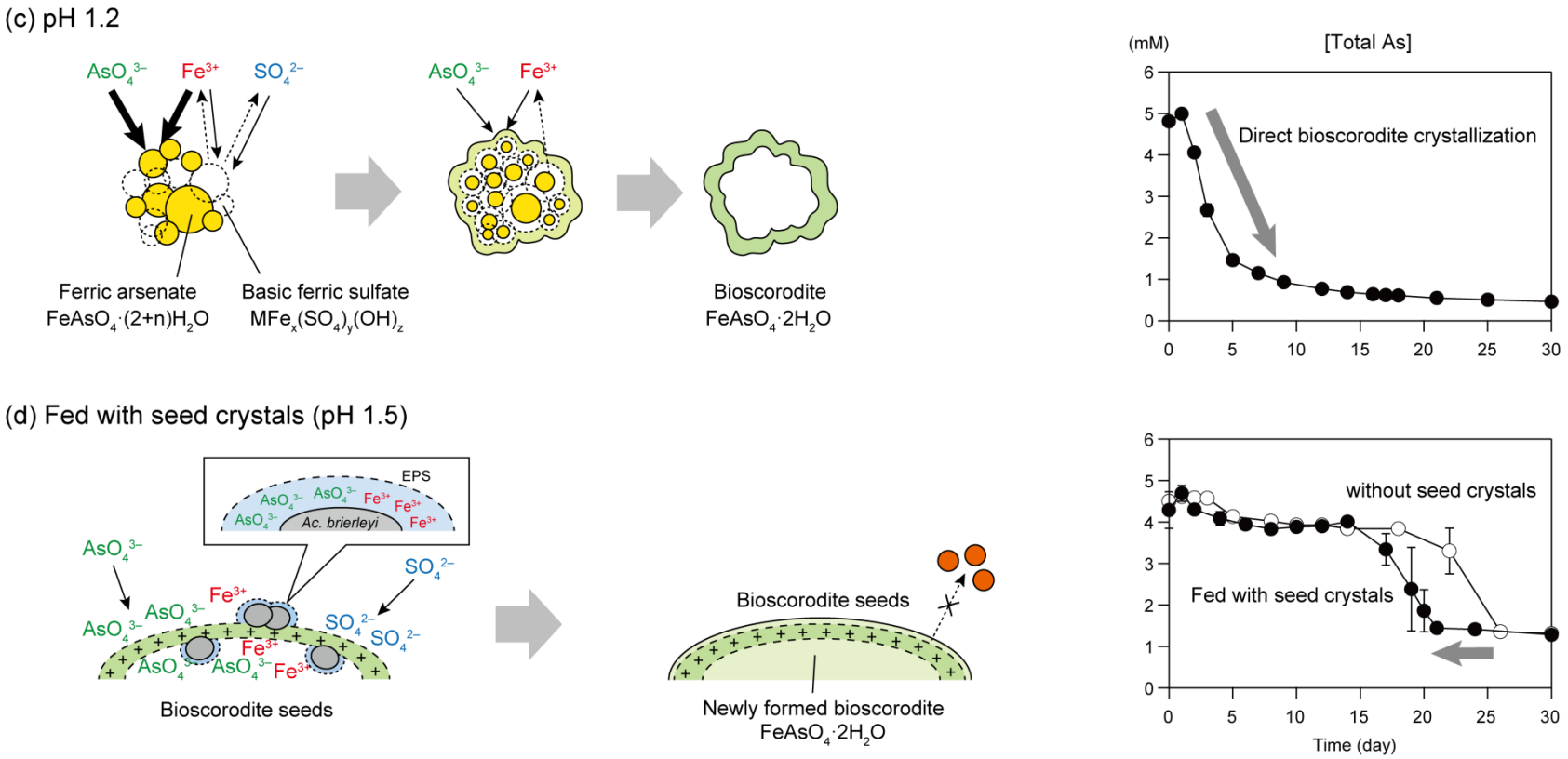

Figure 6.16 (*continued*).

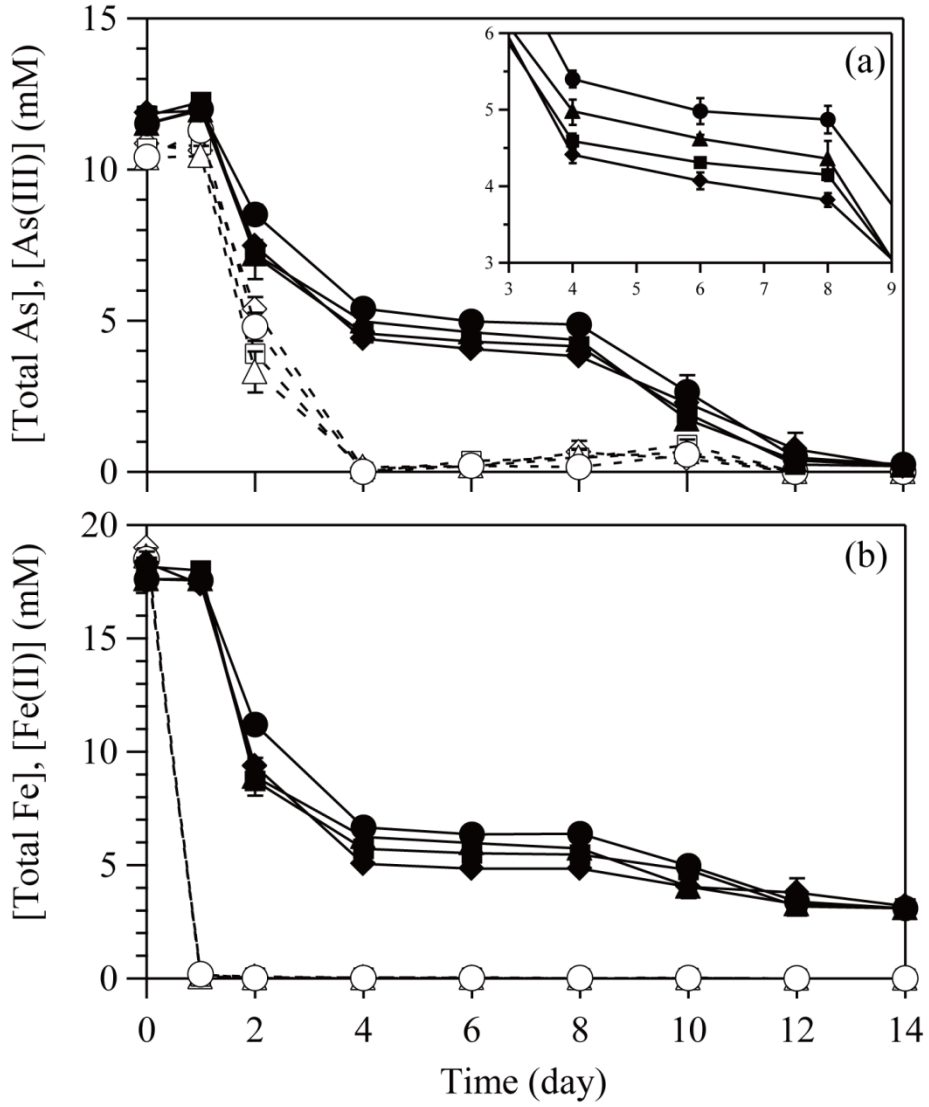

Figure 6.17 Changes in concentrations of total soluble As (solid line), As(III) (broken line) (a), and total soluble Fe (solid line), Fe(II) (broken line) (b) in *Ac. brierleyi* cultures containing initial SO_4^{2-} concentrations of 60 (◆◇), 100 (■□), 150 (▲△), and 200 mM (●○). Initial conditions; $[As(III)]_{ini}$ = 13 mM, $[Fe(II)]_{ini}$ = 18 mM, pH 1.5 with H_2SO_4.

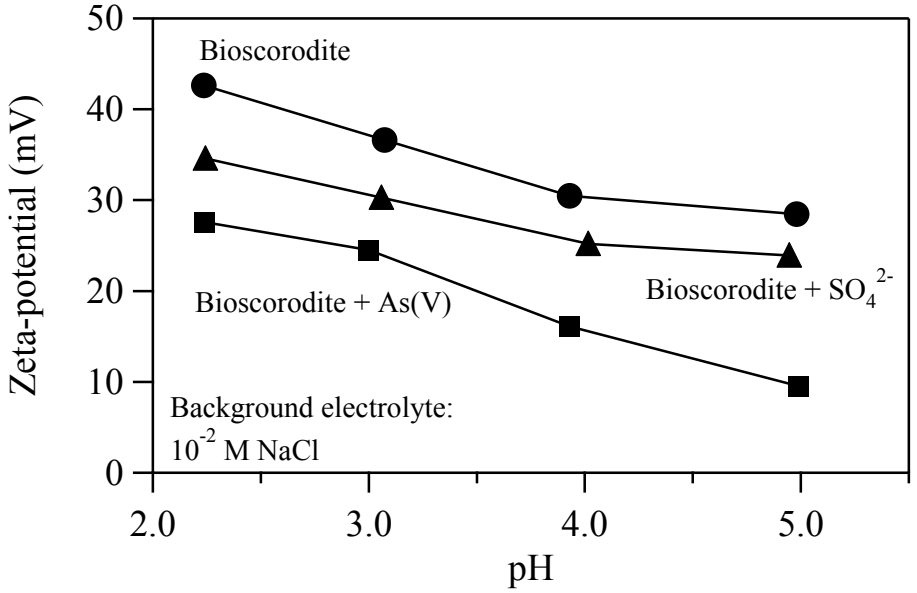

Figure 6.18 Zeta-potentials of raw bioscorodite (●), bioscorodite incubated with 0.2 mM As(V) (■) and bioscorodite incubated with 0.2 mM SO_4^{2-} (▲) in 10^{-2} M NaCl solutions.

Table 6.1 Chemical compositions of precipitates fed with hematite seeds 0.15% (w/v) at pH 1.5 (in chapter 5) and bioscorodite seeds 0.15% (w/v) at pH 1.2 (in chapter 4).

Seed crystals fed:		Ion contents in solid (mmol/g)			Molar ratio	
		[Fe]	[As]	[S]	[As]/[Fe]	[S]/[Fe]
Hematite	Day 2	0.04	0.05	0.01	1.15	0.28
(pH 1.5)	Day 4	0.07	0.05	0.01	0.76	0.13
	Day 6	0.07	0.05	0.01	0.73	0.10
	Day 8	0.06	0.05	0.01	0.83	0.09
	Day 11	0.07	0.06	0.01	0.88	0.10
	Day 14	0.06	0.04	0.005	0.64	0.08
Bioscorodite	Day 3	1.90	1.00	0.23	0.52	0.12
(pH 1.2)	Day 7	2.32	1.43	0.21	0.62	0.09
	Day 30	2.27	1.28	0.02	0.56	0.01

6.4 Conclusions

Bioscorodite crystallization progresses through second As concentration decrease (1st-stage As-removal at ~ day 4; 2nd-stage As-removal at day 10~). At the 1st-stage As-removal, brown-colored amorphous precursors formed by precipitation of basic ferric sulfate ($MFe_x(SO_4)_y(OH)_z$) and ferric arsenate ($FeAsO_4 \cdot (2+n)H_2O$). These precipitates have high solubility and they were gradually dissolved under extremely acidic conditions (1.35). Under steady-state condition, dehydration, dissolution and recrystallization of precursors and incrementally finer particles are consumed (induction period). When the surface energy per mass unit becomes lower energy state, amorphous ferric arsenate and hydroxysulfate were readily dissolved. Released Fe(III) and dissolved As(V) in medium were precipitated as a passivation layer on the surface of precursor particles, followed by bioscorodite crystallization (2nd-stage As-removal). Since the formation of ferric arsenate and scorodite were occurred only in the presence of SO_4^{2-} ions at dilute As concentrations, effective As removal was triggered by the formation of basic ferric sulfate. Although the uptake of SO_4^{2-} ions displayed the inhibitory effect on chemical scorodite synthesis at high temperature and high As(V) concentrations, it was shown to be the key for precursor formation and effective bioscorodite crystallization for dilute As(III) solutions (e.g., ~13 mM).

Taking the above into account, the effects of high $[Fe(II)]_{ini}/[As(III)]_{ini}$ molar ratio, low initial pH, and seed-feeding are accountable for the formation of basic ferric sulfate. High $[Fe(II)]_{ini}/[As(III)]_{ini}$ molar ratio (>2.0) resulted in formation of jarosite rather than the formation of basic ferric sulfate due to high concentrations of Fe(III) and SO_4^{2-}. Since low pH enabled to dissolve basic ferric sulfate readily, the reaction time for bioscorodite crystallization became shorter than pH 1.5, but resulted in the decrement of final As removal owing to the lack of basic ferric sulfate which triggered

the amorphous ferric arsenate precipitation.

Additionally, highly positive charged seed crystals (hematite and bioscorodite) played an important role to shorten the reaction time. Anionic As(V) and SO_4^{2-} ions were locally concentrated in the vicinity of the positively charged bioscorodite surface. Hence, ferric arsenate and bioscorodite tended to precipitate rather than in absence of bioscorodite seeds. Simultaneously, since Fe(III) was readily consumed for the ferric arsenate, the formation of basic ferric sulfate was partly prevented, followed by faster transformation of precursor into scorodite.

Chapter 7

As(III) oxidation and bioscorodite crystallization by thermo-acidophilic, iron- and sulfur-oxidizing archaeon, *Metallosphaera sedula* strain TH2

7.1 Introduction

Bioscorodite crystallization using *Ac. brierleyi* was performed in the solution containing 3–20 mM As(III) at pH 1.2–1.5 described in chapter 3–5. To enhance the applicable range of As(III)-bearing metal refinery wastewaters such as low pH, high As(III) concentration and containing some inhibitory metals, utilization of other microorganisms will be required. However, archaea strains which possess high As(III)-resistance and oxidation ability as well as *Ac. brierleyi* has not been found yet. Just for trace As concentrations, As(III) oxidation ability of *S. acidocaldarius* strain BC (renamed *S. metallicus*) was reported (~1 mM As(III); Sehlin and Lindström, 1992). Additionally, *S. tokodaii* possesses homologs of arsenite oxidase (molybdopterin subunit and Rieske subunit; Lebrun et al., 2003). In our group study, it is suggested that *Metallosphaera sedula* strain TH2 possesses As(III) oxidation ability (Morishita, 2015). Therefore, four kinds of thermophilic acidophilic archaea strains were tested, Fe(II)-oxidizers: *Sulfolobus tokodaii* strain 7, *Sulfolobus acidocaldarius* strain 98-3, *Sulfolobus metallicus* strain Kra23, and sulfur- and Fe(II)-oxidizer *Metallosphaera sedula* strain TH2. Since these archaea strains are close relative to *Ac. brierleyi*, As(III) oxidation can be expected (Figure 7.1).

First, As(III)-resistance of these four archaea strains were enhanced by regular addition of low concentration of As(III) (0.65 mM; 50 ppm). Next, the strain which displayed As(III) oxidation potential were utilized in bioscorodite crystallization experiment at $[As(III)]_{ini}$ = 6.5 mM, $[Fe(II)]_{ini}$ = 9 mM, 0.1% (w/v) elemental sulfur and 0.02% (w/v) yeast extract at pH 1.5. Finally, As(III) oxidation mechanism in microbial culture was elucidated in the presence/absence of yeast extract, elemental sulfur and Fe(II).

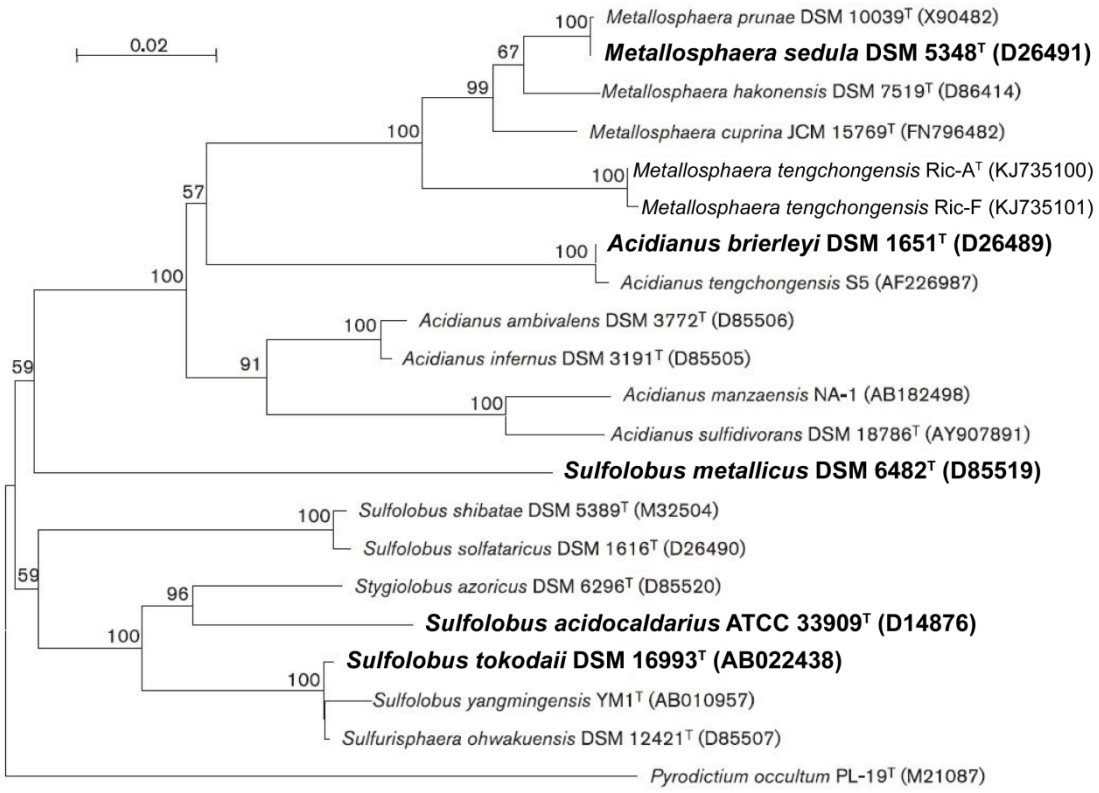

Figure 7.1 Phylogenetic trees reconstructed with the neighbor-joining method based on 16S rRNA gene sequences (modified from Peng et al., 2015).

7.2 Materials and Methods

7.2.1 Enhancing As(III)- resistance of four thermophiles

Four thermophiles; *S. metallicus* strain Kra23, *S. tokodaii* strain 7, *S. acidocaldarius* strain 98-3 and *M. sedula* strain TH2 were maintained in 500 ml Erlenmeyer flask containing 200 ml of heterotrophic basal salts medium (pH 1.5 with H_2SO_4) with 18 mM Fe(II), 0.1% (w/v) elemental sulfur and 0.02% (w/v) yeast extract. As(III) was regularly added at 0.65 mM. Flasks were incubated at 70°C, shaken at 100 rpm. Samples were taken at day 30 to measure As(III) concentrations. Precipitates formed in microbial cultures were identified by XRD patterns.

7.2.2 Bioscorodite crystallization experiment using *M. sedula* TH2

Pregrown *M. sedula* TH2 cells were inoculated (final cell density; 1.0 x 10^7 cells/ml) in 500 ml Erlenmeyer flasks containing 200 ml of heterotrophic basal salts medium (pH 1.5 with H_2SO_4) with 9 mM Fe(II) (as $FeSO_4 \cdot 7H_2O$), 6.5 mM As(III) (as $NaAsO_2$), 0.1% (w/v) elemental sulfur and 0.02% (w/v) yeast extract. $[Fe(II)]_{ini}/[As(III)]_{ini}$ molar ratio was set to 1.4. Flasks were incubated at 70°C, shaken at 100 rpm. Samples were regularly withdrawn to monitor pH, Eh, cell density, and concentrations of total soluble Fe, As, Fe(II) and As(III). Precipitation was filtrated and freeze-dried at the end of the experiment. For analyzing the chemical composition of the resultant bioscorodite, a 50 mg bioscorodite was dissolved in 10 ml of 35% HCl. The leachate was then analyzed by ICP-OES.

7.2.3 As(III) oxidation experiment

Pregrown *M. sedula* TH2 cells were recovered by centrifugation and washed by pure water (pH 1.5 with H_2SO_4) to be inoculated (final cell density; 1.0 x 10^7 cells/ml) in 500 ml Erlenmeyer flasks containing 200 ml of heterotrophic basal salts medium (pH 1.5 with H_2SO_4) with 0.65 or 6.5 mM As(III) (as $NaAsO_2$). Where indicated, 0.1% (w/v) elemental sulfur and 0.02% (w/v) yeast extract were added into the media. Flasks were incubated at 70°C, shaken at 100 rpm. Samples were regularly taken to monitor cell density, pH, Eh vs SHE, and As(III) concentrations. All experiments were carried out in duplicate.

7.3 Results and Discussion

7.3.1 As(III) oxidation during enhancing As(III)-resistance

As-resistance of all tested thermophiles enhanced up to 6.5 mM (500 ppm) by continuous addition of 0.65 mM (50 ppm) As(III) during cultivation. As(III) concentrations were measured when total added-As(III) concentration reached 500 ppm. As(III) oxidation results were shown in Table 7.1 As(III) oxidation ability of *S. acidocaldarius* strain BC (renamed *S. metallicus*) was reported (~1 mM As(III); Sehlin and Lindström et al., 1992), and *S. tokodaii* possesses homologs of arsenite oxidase (molybdopterin subunit and Rieske subunit; Lebrun et al., 2003). However, As(III) oxidation was not observed in the cultures of three *Sulfolobus* strains (Table 7.1), whilst cell growth were observed by ready Fe(II) oxidation. In contrast, As(III) concentration decreased from 500 ppm to 258 ppm, that is, 48% of As(III) was oxidized during incubation in *M. sedula* TH2 culture as well as 500 ppm Fe(II) oxidation (Table 7.1). Color change of brown precipitates into white was observed in *M. sedula* TH2 culture and it was detected as scorodite from XRD (data not shown). From the phylogenetic tree as shown in Figure 7.1, *M. sedula* TH2 located relatively closer to *Ac. brierleyi* compared to other *Sulfolobus* strains used in this study. Although As(III) oxidation by *M. sedula* has not been reported, this implied that *M. sedula* TH2 possesses As(III) oxidation ability.

Table 7.1 As(III) oxidation ability of four thermophiles during As(III) resistance enhancement cultivation.

Strains	Totally added As(III) concentrations (ppm)	As(III) concentrations at day 30 (ppm)	As(V) concentrations at day 30 (ppm)
S. metallicus^T Kra23	500	512	0 (0%)
S. tokodaii^T 7		536	0 (0%)
S. acidocaldarius^T 98-3		500	0 (0%)
M. sedula^T TH2		258	242 (48%)

7.3.2 Bioscorodite crystallization using *M. sedula* TH2 at $[As(III)]_{ini}$ = 6.5 mM fed with elemental sulfur

During cultivation in As(III)-bearing growth media, bioscorodite was crystallized only in *M. sedula* culture. In order to confirm the effective conditions, bioscorodite crystallization test were conducted at $[As(III)]_{ini}$ = 6.5 mM ($[Fe(II)]_{ini}/[As(III)]_{ini}$ molar ratio of 1.4) fed with 0.1% (w/v) elemental sulfur. The results were described in Figures 7.2, 7.3 and 7.4. Although *M. sedula* TH2 cells usually grow up to 1×10^8 cells/ml within 7 days in the absence of As(III), the cell density did not increase (Figure 7.2a) due to possible two reasons; cells growth were inhibited by 6.5 mM As(III), or cells were adsorbed on the surface of elemental sulfur. Nevertheless, Fe(II) was readily oxidized within 2 days (Figure 7.3b). Slower As(III) oxidation than in *Ac. brierleyi* cultures (~day 4) was observed in *M. sedula* culture and it was completely oxidized by day 18 (Figure 7.3a). During the As(III) oxidation, total soluble As continuously decreased without typical 1st-stage As-removal, whereas second As removal was observed in *Ac. brierleyi* cultures. This behavior was possibly derived from the continuous pH decrement up to 1.2 via sulfur oxidation and formation of brownish amorphous precipitates (Figure 7.3b). The color of precipitates turned into

pale-green from day 18 as well as *Ac. brierleyi* cultures, and eventually resulted in 93% of As removal within day 23. Precipitates were identified as scorodite from XRD results (Figure 7.5). Elemental sulfur was not detected in XRD patterns and SEM observation (Figures 7.5 and 7.6b$_2$), which indicated that *M. sedula* TH2 completely consumed as an energy source. Table 7.2 showed the chemical composition of final bioscorodite products. $[Fe]_{im}/[As]_{im}$ molar ratio formed in *M. sedula* culture resulted in 1.0 as well as theoretical scorodite molar ratio. Since lower and stable supersaturation level was maintained during day 1–14 (as shown in log IAP value of over −21.5; Figure 7.4a), slower reaction allowed the formation of matured bioscorodite. Eventually, bioscorodite crystallization proceeded in *M. sedula* TH2 culture. Oxidation of elemental sulfur lowered the pH, and resulted in the crystallization of pure bioscorodite.

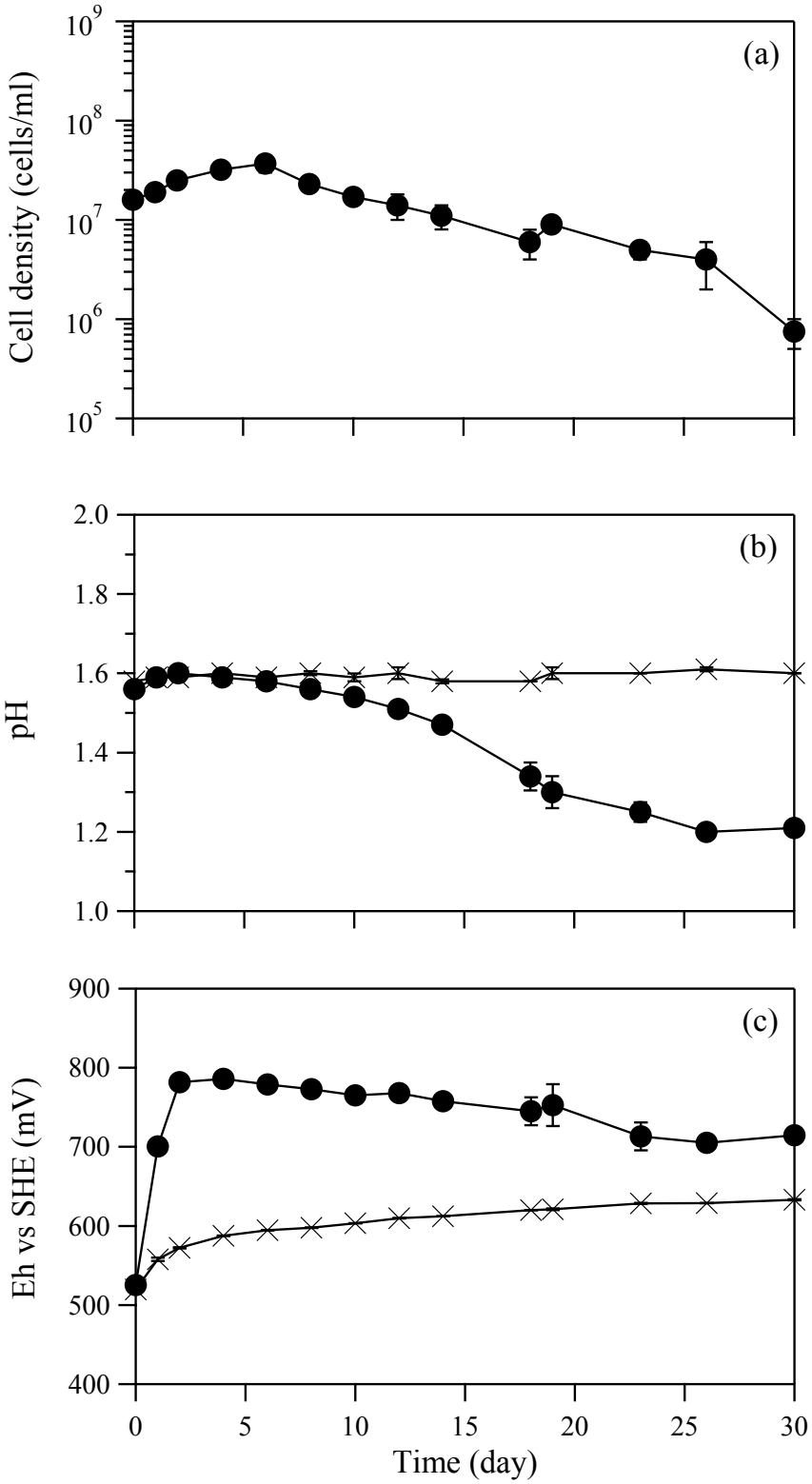

Figure 7.2 Changes in cell density (a), pH (b), and Eh vs SHE (c) in *M. sedula* TH2 cultures (●) and sterile control cultures (×).

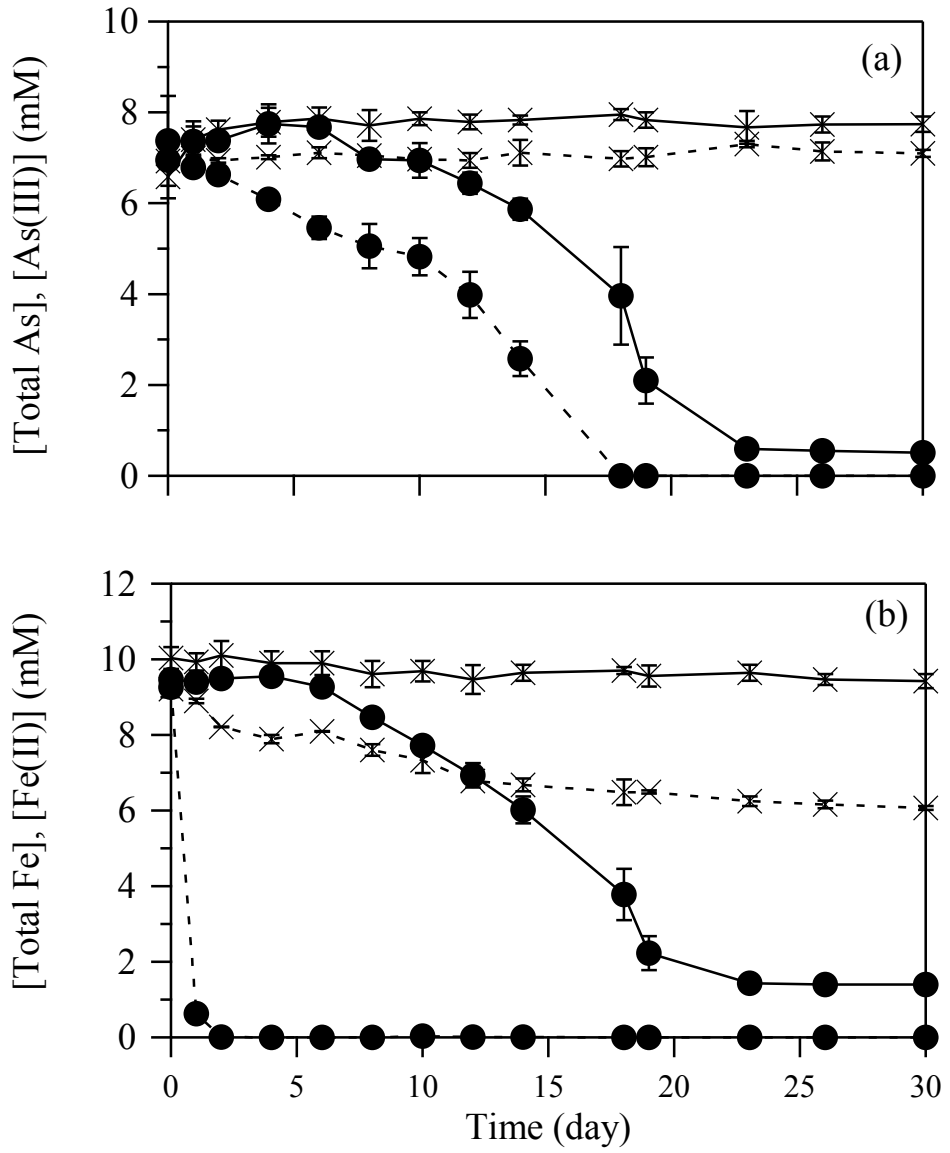

Figure 7.3 Changes in concentrations of total soluble As (solid lines), As(III) (broken lines) (a), and total soluble Fe (solid lines), Fe(II) (broken lines) (b) in *M. sedula* TH2 cultures (●) and sterile control cultures (×). Initial condition; $[As(III)]_{ini}$ = 6.5 mM, $[Fe(II)]_{ini}$ = 9 mM, 0.1% (w/v) elemental sulfur.

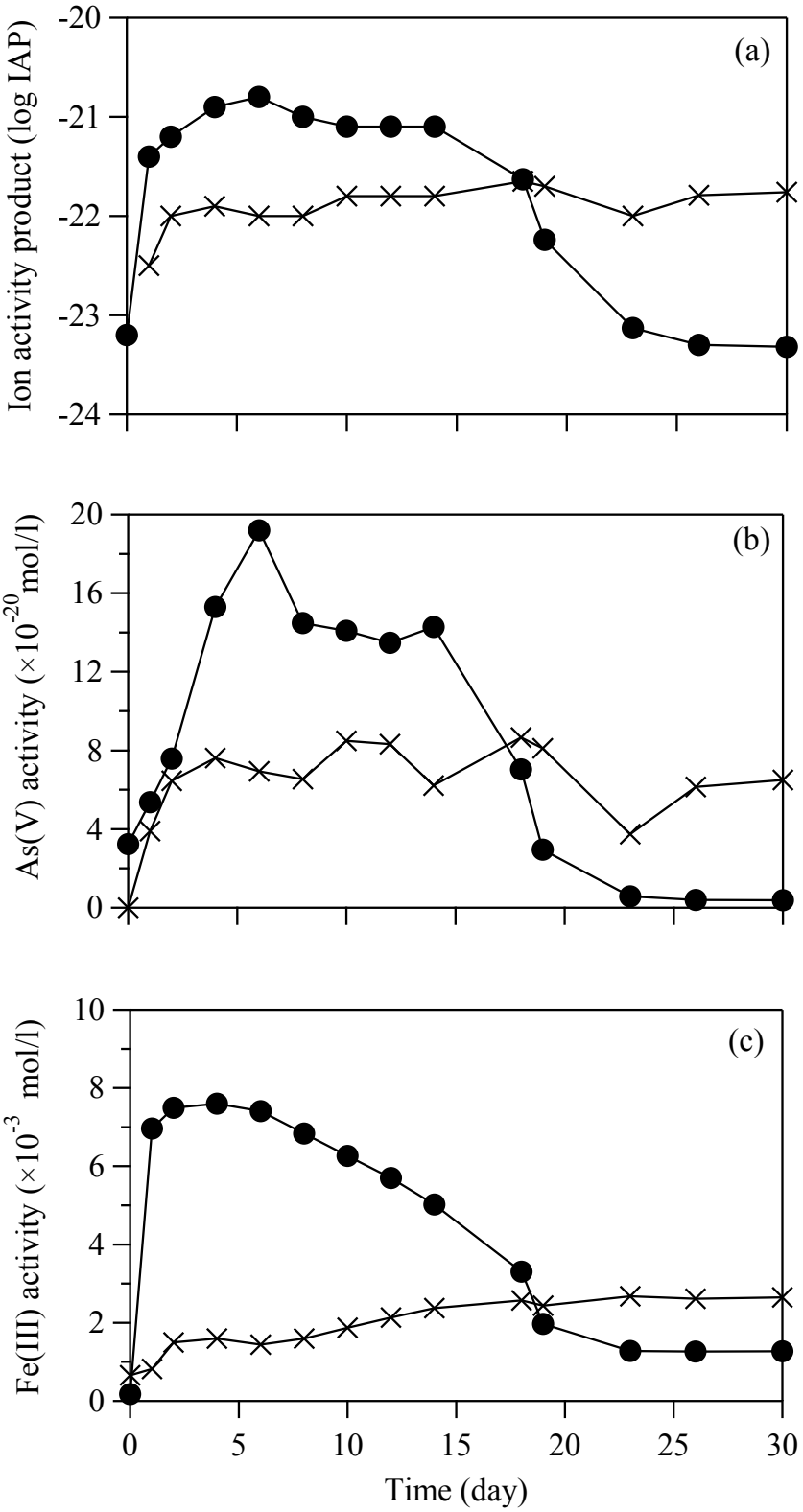

Figure 7.4 Ion activity product (a), As(V) ion activity (b) and Fe(III) ion activity of bioscorodite in *M. sedula* TH2 cultures (●) and sterile control cultures (×).

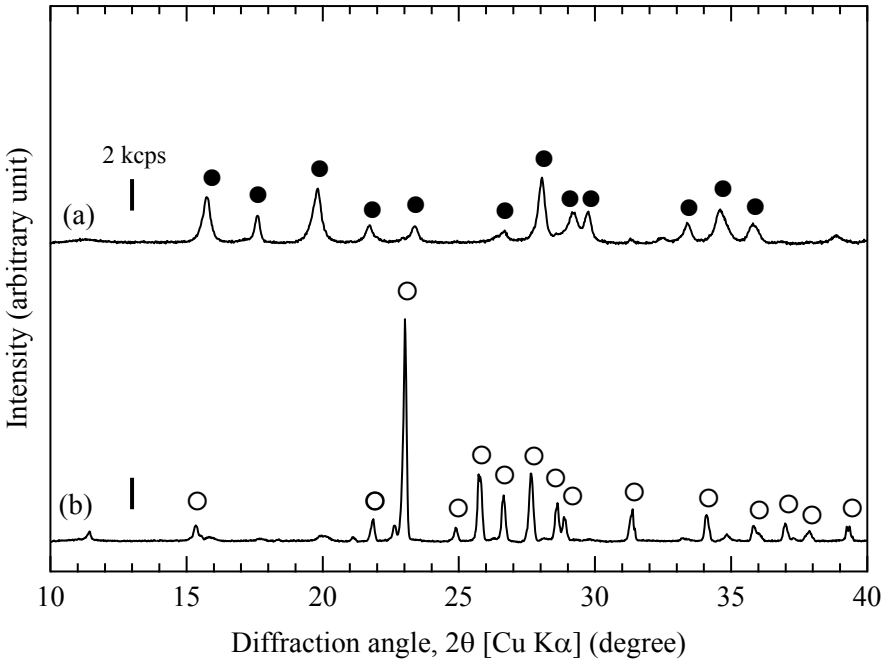

Figure 7.5 XRD patterns of precipitates formed in *M. sedula* TH2 cultures (a), and sterile control cultures (b). The symbols are assigned to scorodite (●; JCPDS 37-0468) and elemental sulfur (○; JCPDS 01-0478).

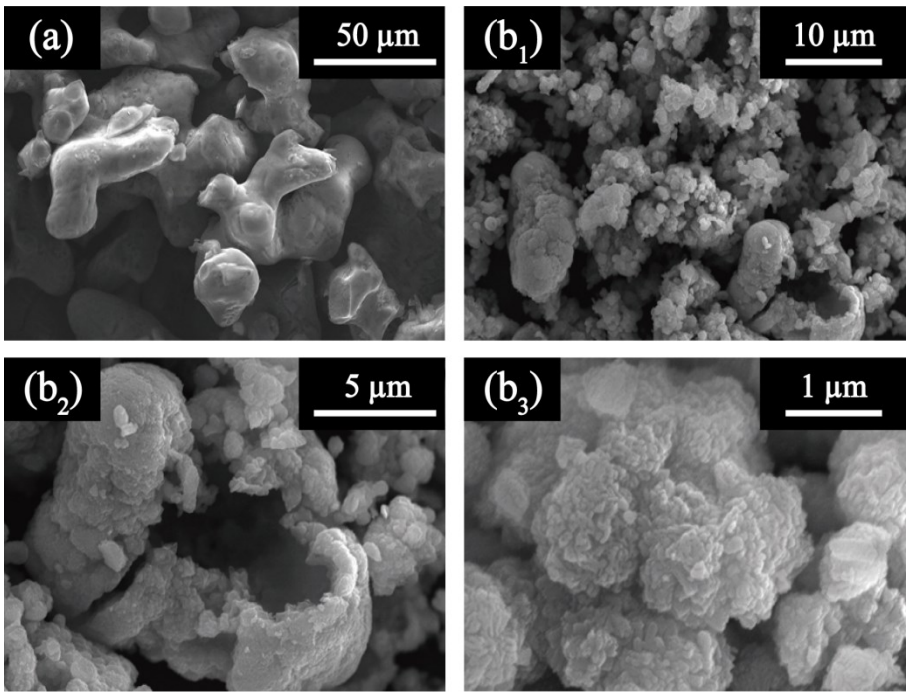

Figure 7.6 SEM images of elemental sulfur (a) and resultant bioscorodite formed in *M. sedula* TH2 cultures (b).

Table 7.2 Chemical composition of the resultant bioscorodite formed in *M. sedula* TH2 cultures.

Sample	Weight in 50 mg bioscorodite sample (mg)		Fe/As molar ratio
	Fe	As	
Bioscorodite formed in *M. sedula* TH2 cultures	10.0 (0.18 mmol)	13.4 (0.18 mmol)	1.00

7.3.3 As(III) oxidation mechanism

7.3.3.1 As(III) oxidation with/without yeast extract

Utilization of *M. sedula* TH2 enable to crystallize bioscorodite from As(III)-bearing solutions through the Fe(II) and As(III) oxidation. Although microbial As(III) oxidation by *Ac. brierleyi* was previously reported that As(III) oxidation was induced in the presence of yeast extract and high initial As(III) concentrations (Okibe et al., 2014), microbial As(III) oxidation features by *M. sedula* is still unclear. Since Dinkla et al. (2013) reported As(III) oxidation in mixed culture of thermopacidophiles including *Acidianus* sp. in the presence of yeast extract, addition of yeast extract possibly affect the microbial As(III) oxidation ability of thermoacidophiles. In order to elucidate the mechanism of As(III) oxidation in *M. sedula* TH2 culture, As(III) oxidation test were performed at different initial As(III) concentrations with or without yeast extract in the absence of Fe(II) and elemental sulfur. As shown in Figure 7.7a, cell density did not increased without yeast extract at $[As(III)]_{ini}$ = 0.65 and 6.5 mM owing to lack of energy source. In the presence of yeast extract, cell growth was observed at $[As(III)]_{ini}$ = 0.65 mM, except at 6.5 mM (Figure 7.7a), which indicated *M. sedula* TH2 activity was inhibited at high As(III) concentrations. However, As(III) oxidation did not proceeded under the all tested conditions (Figure 7.8). From this result, it was revealed that As(III) did not support the growth of *M. sedula* TH2 cells as

well as *Ac. brierleyi* which oxidize As(III) for detoxification (Okibe et al., 2014).

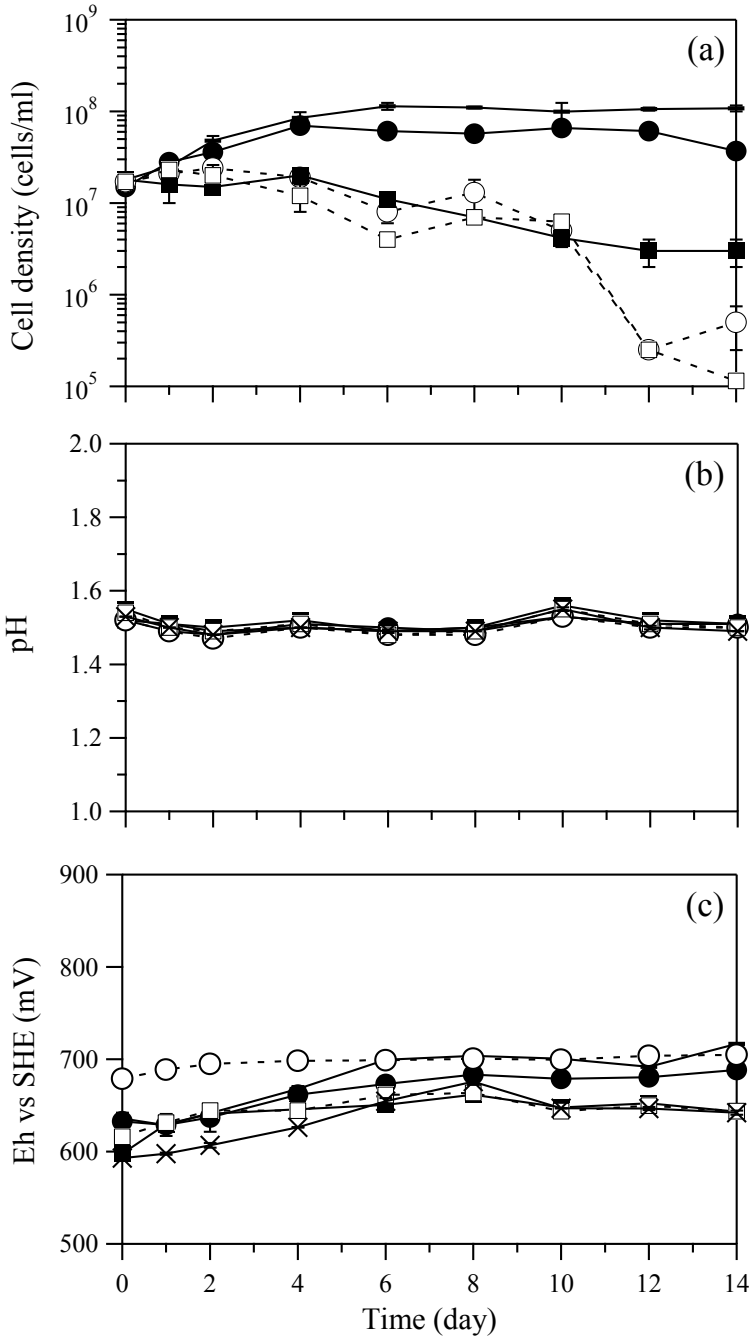

Figure 7.7 Changes in cell density (a), pH (b), and Eh vs SHE (c) in *M. sedula* TH2 cultures with (solid lines) or without (broken lines) 0.02% (w/v) yeast extract, in the absence of Fe(II) and elemental sulfur. Initial As(III) concentrations were; 0 mM (–), 0.65 mM (●○) and 6.5 mM (■□). Sterile control cultures (×) were conducted at As(III) concentrations of 0.65 mM with 0.02% (w/v) yeast extract.

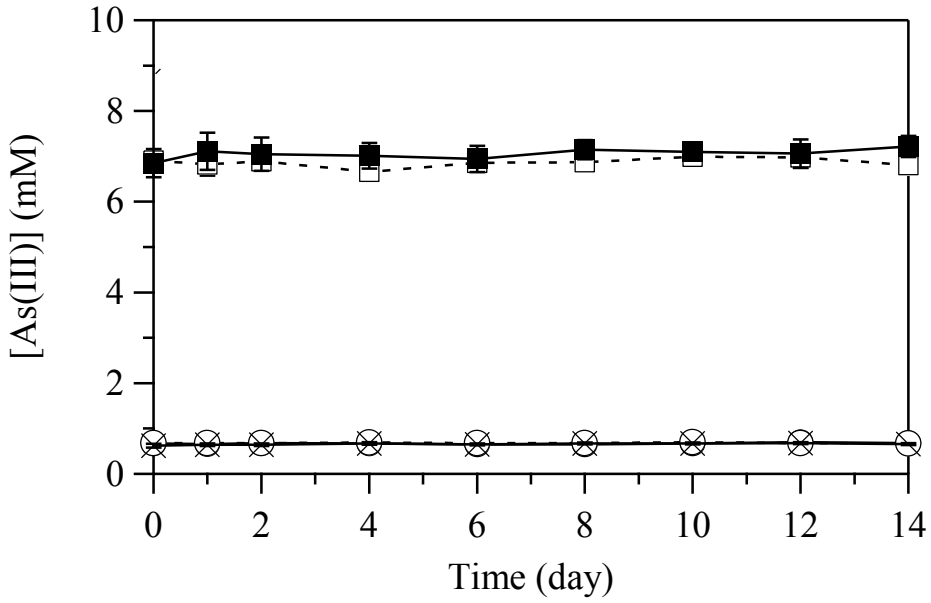

Figure 7.8 Changes in As(III) concentrations in *M. sedula* TH2 cultures with (solid lines) or without (broken lines) 0.02% (w/v) yeast extract, in the absence of Fe(II) and elemental sulfur. Initial As(III) concentrations were; 0.65 mM (●○) and 6.5 mM (■□). Sterile control cultures (×) were conducted at As(III) concentrations of 0.65 mM with 0.02% (w/v) yeast extract.

7.3.3.2 As(III) oxidation fed with elemental sulfur

M. sedula TH2 oxidizes elemental sulfur and reduced inorganic sulfur compounds as energy source. In bioscorodite crystallization experiment, sulfur oxidation was observed with the description of pH decrease. This implies that As(III) oxidation by *M. sedula* TH2 possibly progresses when energy is obtained via sulfur oxidation. Due to this expectation, As(III) oxidation test fed with elemental sulfur were performed at different initial As(III) concentrations with or without yeast extract in the absence of Fe(II). The results described in Figures 7.9 and 7.10 showed that *M. sedula* TH2 unable to utilize elemental sulfur at $[As(III)]_{ini}$ = 6.5 mM no matter whether yeast extract was fed or not. That was described as no cell growth and no pH value change (Figure 7.9a, b). Sulfur oxidizing ability of *M. sedula* TH2 was completely inhibited by

high As(III) concentrations. Taking the above into account, it was suggested that As(III) oxidation in *M. sedula* TH2 culture enable to proceed only in the presence of Fe(II). Possible mechanisms include coupling reaction between As(III) oxidation to As(V) and Fe(III) reduction to Fe(II). These reactions were described as follows;

$$2Fe^{3+} + H_3As^{III}O_3 + H_2O \rightarrow 2Fe^{2+} + H_3As^{V}O_4 + 2H^+ \quad \text{(Eq. 7.1)}$$

$$Fe^{3+} + e^- \rightarrow Fe^{2+} \quad (E_{0'} = 771\ mV) \quad \text{(Eq. 7.2)}$$

$$H_3As^{V}O_4 + 2H^+ + 2e^- \rightarrow H_3As^{III}O_3 + H_2O \quad (E_{0'} = 560\ mV) \quad \text{(Eq. 7.3)}$$

This coupling reaction is reported to occur in the presence of electron mediator such as pyrite in metallurgical operations (Barrett et al., 1993; Wiertz et al., 2006). We have also observed it during biooxidation of arsenopyrite concentrates containing pyrite (Tanaka et al., 2015). In the absence of particles, this reaction is proposed to progress within EPS (Extracellular Polymeric Substances) of microorganisms (Okibe et al., 2013, 2014). It was reported that *S. tokodaii* and *S. acidocaldarius* form biofilm (Koerdt et al., 2010). However, As(III) oxidation was not observed in *S. tokodaii* 7 and *S. acidocaldarius* 98-3 cultures during enhancing As(III)-resistance test (in section 7.3.1) even though Fe(II) was microbially oxidized. This implied that the reaction did not occur even in *M. sedula* TH2 cultures as the coupling reaction kinetics is very slow. Hence, As(III) might be oxidized microbially by *M. sedula* TH2 induced by the presence of Fe(II) or Fe(II) oxidation.

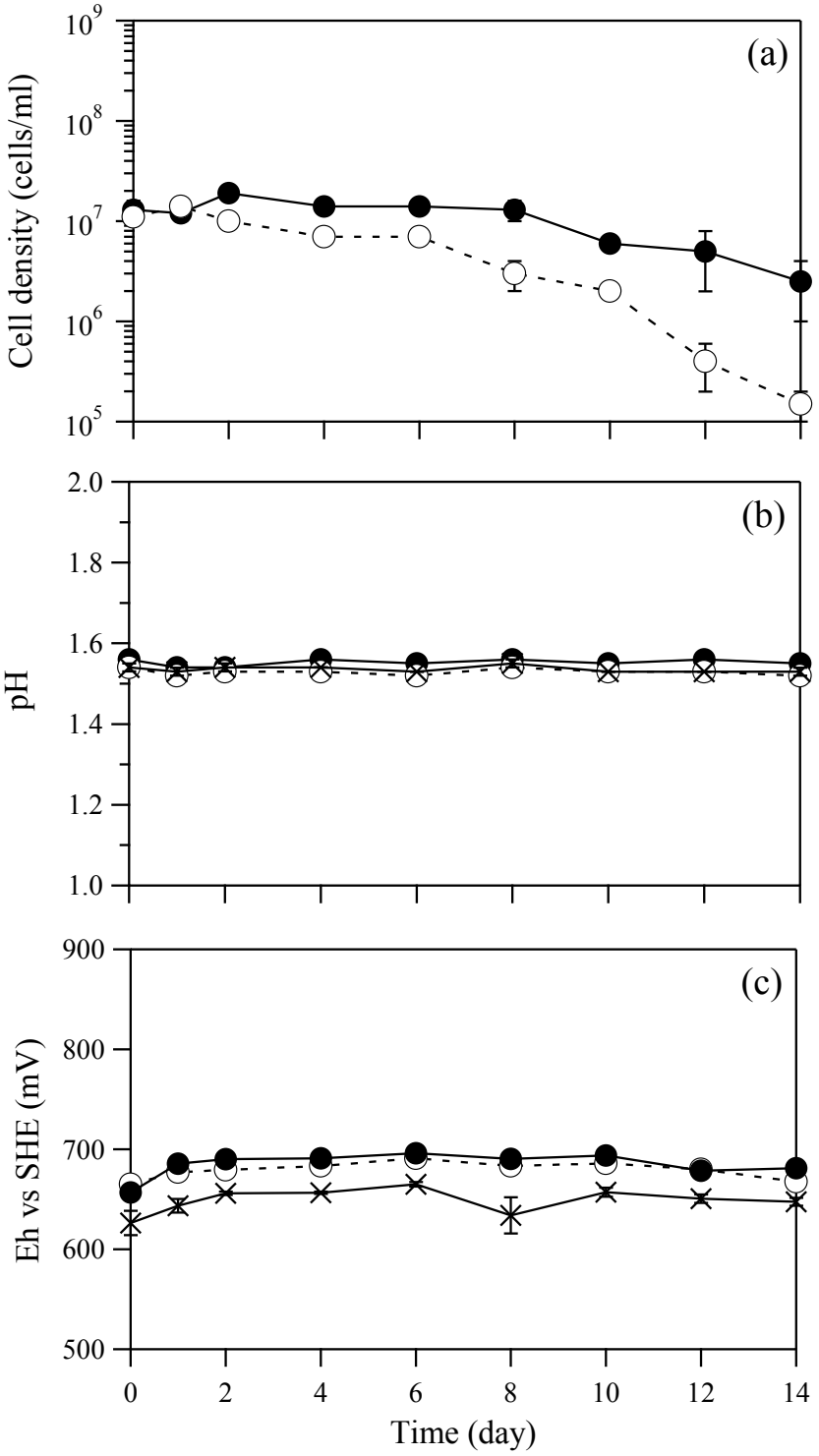

Figure 7.9 Changes in cell density (a), pH (b), and Eh vs SHE (c) in *M. sedula* TH2 cultures (●○) and sterile control cultures (×) with (solid lines) or without (broken lines) 0.02% (w/v) yeast extract fed with 0.1% (w/v) elemental sulfur, in the absence of Fe(II). Initial As(III) concentrations were 6.5 mM.

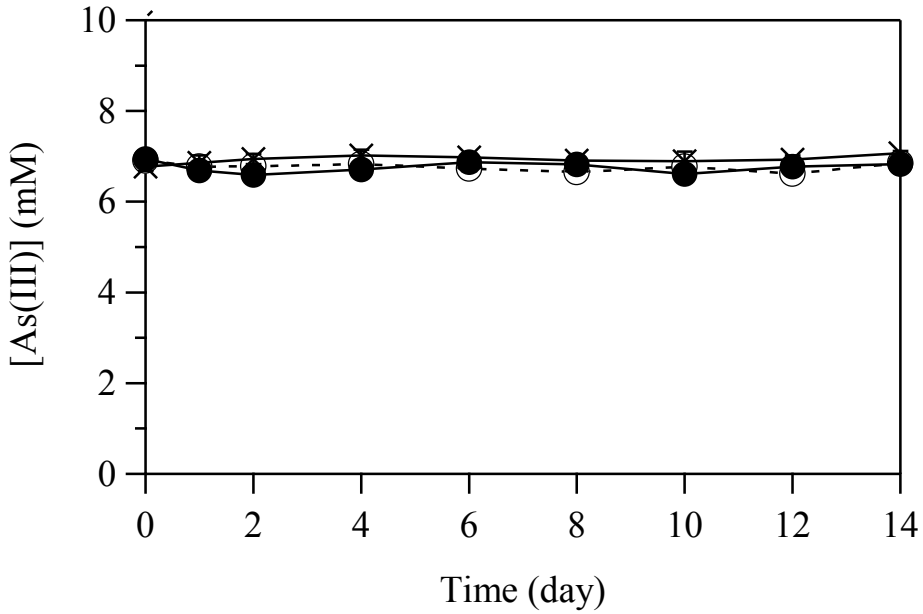

Figure 7.10 Changes in As(III) concentrations in *M. sedula* TH2 cultures (●○) and sterile control cultures (×) with (solid lines) or without (broken lines) 0.02% (w/v) yeast extract fed with 0.1% (w/v) elemental sulfur, in the absence of Fe(II). Initial As(III) concentrations were 6.5 mM.

7.4 Conclusions

This chapter investigated the alternative archaea for bioscorodite crystallization. From the screening of four thermo acidophilic Fe(II)- and sulfur-oxidizing archaea, partial As(III) oxidation was observed in *M. sedula* TH2 culture in the presence of Fe(II) and elemental sulfur. Bioscorodite was successfully crystallized in *M. sedula* culture containing 6.5 mM As(III), 9 mM Fe(II) and 0.1% (w/v) elemental sulfur at pH 1.5. Although the reaction speed was slower (23 days) than in *Ac. brierleyi* cultures (10–11 days), pure bioscorodite was crystallized ($[Fe]_{im}/[As]_{im}$ molar ratio of 1.0 as well as theoretical scorodite molar ratio). In absence of Fe(II), microbial As(III) oxidation was not observed regardless of presence/absence of elemental sulfur and yeast extract. This result implied that the presence of Fe(II) induced microbial As(III) oxidation ability of *M. sedula* TH2.

Chapter 8

Conclusions

Arsenic contamination is a growing problem in metallurgical operations due to the increasing metal demand that necessitates processing of even As-bearing low-grade copper sulfide ores. As one of the approaches to immobilize soluble As species from wastewaters, scorodite ($Fe^{III}As^{V}O_4 \cdot 2H_2O$) synthesis has been researched under hydrothermal and atmospheric conditions. There are also cases that dilute As(III) solutions are produced in metallurgical operations, wherein chemical scorodite synthesis turns ineffective. In order to realize effective scorodite formation even from dilute As solutions, our studies enabled simultaneous microbial As(III) and Fe(II) oxidation using the thermophilic archaeon *Acidianus brieleyi* (70°C), which for the first time realized one-step bioscorodite crystallization from original wastewater solutes of As(III) and Fe(II), without necessitating any As(III) oxidation pretreatments or chemical oxidants. Whilst scorodite crystallization becomes further difficult at more dilute As concentrations under milder temperature condition, exploiting factors to enable such reaction is of great importance to broaden the applicability of scorodite method for a wide range of As(III)-contaminated waters. Hence, this thesis investigated the factors that enable effective bioscorodite crystallization from dilute As(III)-bearing acidic solutions (3.3-20 mM); (i) $[Fe(II)]_{ini}/[As(III)]_{ini}$ molar ratios, (ii) initial pH, (iii) seed-feeding, (iv) SO_4^{2-} ions. Moreover, in order to enhance the applicable range of As(III)-bearing metal refinery wastewaters, utilization of other thermo-acidophilic Fe(II)- and sulfur-oxidizing archaea strains were tested for bioscorodite crystallization.

In **chapter 3**, the effectiveness of different pure and mixed cultures of three moderately thermophilic bacterial strains were investigated for biooxidation of As-bearing highly refractory polymetallic Au-ore concentrates. Despite of the complex mineralogy and the presence of a mixture of potentially inhibitory metals and metalloids, the concentrates were readily dissolved in defined mixed cultures including

both Fe(II)- and S-oxidizers, releasing as much as 80% of soluble Fe and 61% of soluble As at 45°C. Partial As was immobilized as amorphous ferric arsenate, but not as crystalline scorodite. Applying the biooxidation pretreatment improved the recovery of both Au (from 1.1% to 86%) and Ag (from 3.2% to 87%), which was shown to be one of the most effective options compared with other abiotic pretreatment approaches.

In **chapter 4**, a range of As(III) solutions (3.3–26 mM) with varying $[Fe(II)]_{ini}/[As(III)]_{ini}$ molar ratios was tested to grasp the overall applicability of the bioscorodite method. Bioscorodite was crystallized in the $[Fe(II)]_{ini}/[As(III)]_{ini}$ molar ratio range of 0.8–2.0 from dilute As(III) solutions. Especially, 94–99% As was successfully removed as crystalline bioscorodite by setting an slight excess of $[Fe(II)]_{ini}/[As(III)]_{ini}$ molar ratio at 1.4–2.0. Higher molar ratio enable to increase As removal, but required longer reaction time. Molar ratio of over 2.5 resulted in the formation of amorphous ferric arsenate or jarosite. Lowering the initial pH from 1.5 to 1.2 using bioscorodite seeds lead to a steady and continuous formation of bioscorodite particles, but As removal remained relatively incomplete at pH 1.2 (91%), compared to at pH 1.5 (98%). Amorphous precursors formation at pH 1.5 played an important role to achieve maximum As removal from dilute As(III) solutions by inducing two-stage As and Fe precipitation.

In **chapter 5**, the effect of seed-feeding on bioscorodite crystallization from dilute 4.7 mM As(III) solution were investigated such as morphological and structural characteristics of bioscorodite (low-density, fine particles) and chemical scorodite (high-density, coarse particles) seed crystals. Feeding bioscorodite seeds enabled effective As removal from dilute As(III) solution (98% final As removal at day 21). As the differences of bioscorodite crystallization process, hollow bioscorodite seed particles became increasingly filled with newly formed scorodite, whilst solid chemical

seeds induced their surface to be thoroughly coated with new scorodite precipitates. TCLP leachabilities of final bioscorodite products formed on bioscorodite and chemical scorodite seeds were 0.59 ± 0.08 mg/l and 1.86 ± 0.05 mg/l, respectively, which were lower than the regulatory limit of As by TCLP test. Utilization of highly positive such as hematite (+ 60 mV) and bioscorodite (+ 50 mV) displayed immediate bioscorodite crystallization due to the characteristic as absorbent of anionic As(V) ($H_2AsO_4^-$) and *Ac. brierleyi* cells (+ 5 mV).

In **chapter 6**, behavior of SO_4^{2-} during bioscorodite formation was investigated by liquid/solid characterization analyses, and the mechanism of bioscorodite crystallization process (precursor formation and transformation into crystalline scorodite) was elucidated. At the 1st-stage As-removal, brown-colored amorphous precursors formed by precipitation of the mixture of basic ferric sulfate ($MFe_x(SO_4)_y(OH)_z$) and ferric arsenate ($FeAsO_4 \cdot (2+n)H_2O$), which have high solubility. Under steady-state condition, dehydration, dissolution and recrystallization of precursors and incrementally finer particles are consumed (induction period). When the surface energy per mass unit becomes lower energy state, amorphous ferric arsenate and hydroxysulfate were readily dissolved. Released Fe(III) and dissolved As(V) in medium were precipitated for the coarsening of ferric arsenate particles, followed by scorodite crystallization (2nd-stage As-removal). Since the formation of ferric arsenate and scorodite were occurred only in the presence of SO_4^{2-} ions at dilute As concentrations, effective As removal was triggered by the formation of basic ferric sulfate. Therefore, the uptake of SO_4^{2-} was shown to be the key for precursor formation and effective bioscorodite crystallization for dilute As(III) solutions. The effects of high $[Fe(II)]_{ini}/[As(III)]_{ini}$ molar ratio, low initial pH (**chapter 4**), and seed-feeding (**chapter 5**) are also accountable for the formation of basic ferric sulfate.

High $[Fe(II)]_{ini}/[As(III)]_{ini}$ molar ratio (>2.0) resulted in formation of jarosite rather than the formation of basic ferric sulfate due to high concentrations of Fe(III) and SO_4^{2-}. Since low pH enabled to dissolve basic ferric sulfate and ferric arsenate readily, the reaction time for bioscorodite crystallization became shorter than pH 1.5, but resulted in the decrement of final As removal owing to the lack of basic ferric sulfate which triggered the amorphous ferric arsenate precipitation (described in **chapter 4**). Highly positive charged seed crystals acts as adsorbent of anionic As(V) and SO_4^{2-} ions, which were locally concentrated in the vicinity of the seed surface. Hence, ferric arsenate and bioscorodite tended to precipitate rather than the formation of basic ferric sulfate (described in **chapter 5**).

In **chapter 7**, the alternative archaea for bioscorodite crystallization were investigated for enhancing the applicable range of As(III)-bearing metal refinery wastewaters; *S. metallicus* Kra23, *S. tokodaii* 7, *S. acidocaldarius* 98-3 and *M. sedula* TH2. Partial As(III) oxidation was observed only in *M. sedula* TH2 culture in the presence of Fe(II) and elemental sulfur. Bioscorodite was successfully crystallized in *M. sedula* culture containing 6.5 mM As(III), 9 mM Fe(II) and 0.1% (w/v) elemental sulfur at pH 1.5 at 23 days. In absence of Fe(II), microbial As(III) oxidation was not observed regardless of presence/absence of elemental sulfur and yeast extract. This result implied that the presence of Fe(II) induced microbial As(III) oxidation ability of *M. sedula* TH2.

From the findings obtained in the batch tests of bioscorodite crystallization, proposed practical application using the continuous processes was described in Figure 8.1. It is supposedly composed of an aeration tank followed by a settling tank. Microbiologically active bioscorodite sludge separated in a settling tank are recycled in an aeration tank, and they could maintain both high cell density and seed pulp density

to support steady As(III) and Fe(II) oxidation and the resultant scorodite crystallization (Figure 8.1).

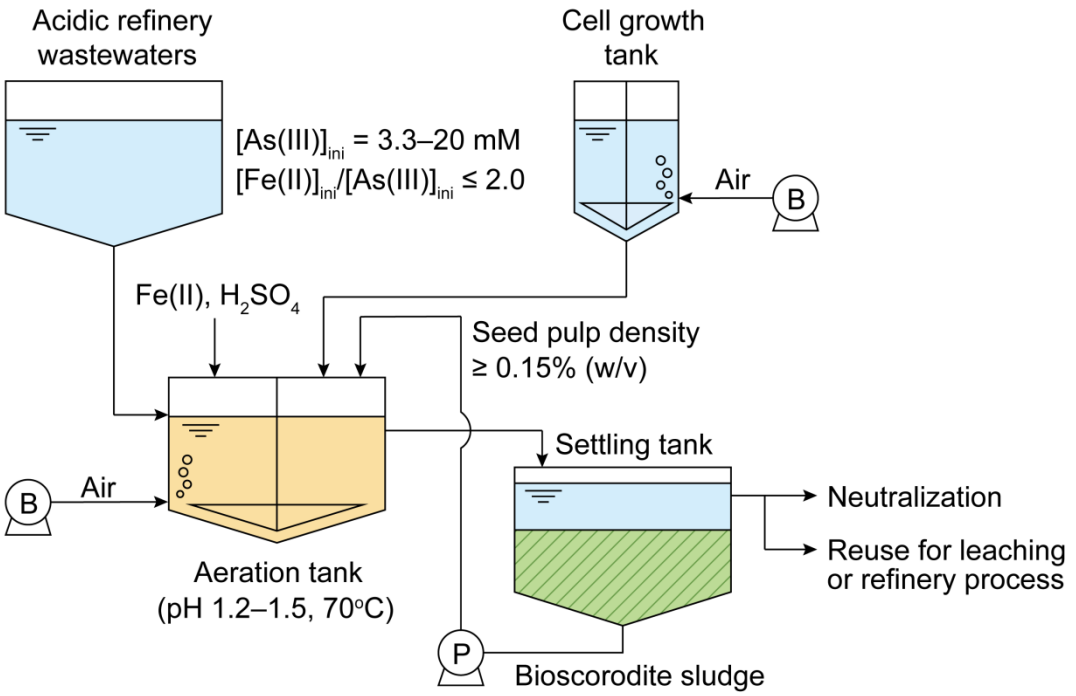

Figure 8.1 Proposed flowsheet of continuous process for As(III)-removal as bioscorodite from acidic metal refinery wastewaters.

Overall, this study demonstrated the bioscorodite crystallization at low As(III) concentrations by arranging the conditions such as initial $[Fe(II)]_{ini}/[As(III)]_{ini}$ molar ratio, initial pH and addition of seed crystals. Moreover, the mechanism of bioscorodite crystallization was revealed and the formation of basic ferric sulfate and its dissolution was the key for maximize the As immobilization efficiency and reaction speed for dilute As(III)-bearing solutions. This study will enable to further develop the biological As immobilization techniques for not only hydrometallurgical operations but also environmental remediation such as much lower As(III) concentrations and milder temperature.

References

Acevedo, F., 2002. Present and future of bioleaching in developing countries. *Electronic Journal of Biotechnology*, 5(2): 18-19.

Anderson, I., Chertkov, O., Chen, A., Saunders, E., Lapidus, A., Nolan, M., Lucas, S., Hammon, N., Deshpande, S., Cheng, J.-F., Han, C., Tapia, R., Goodwin, L.A., Pitluck, S., Liolios, K., Pagani, I., Ivanova, N., Mikhailova, N., Pati, A., Palaniappan, K., Land, M., Pan, C., Rohde, M., Pukall, R., Göker, M., Detter, J.C., Woyke, T., Bristow, J., Eisen, J.A., Markowitz, V., Hugenholtz, P., Kyrpides, N.C., Klenk, H.-P. and Mavromatis, K., 2012. Complete genome sequence of the moderately thermophilic mineral-sulfide-oxidizing firmicute *Sulfobacillus acidophilus* type strain (NALT). *Standards in Genomic Sciences*, 6(3): 293-303.

Asta, M.P., Cama, J., Martínez, M. and Giménez, J., 2009. Arsenic removal by goethite and jarosite in acidic conditions and its environmental implications. *Journal of Hazardous Materials*, 171(1–3): 965-972.

Aylmore, M. and Jaffer, A., 2012. Evaluating process options for treating some refractory ores. Technical papers available from the Xstrata ALBION PROCESSTM Available at http://www.albionprocess.com/EN/downloads/Pages/TechnicalPapers.
aspx.

Baghurst, D.R., Barret, J., Coleyshaw, E.E., Griffith, W.P. and Mingos, D.M.P., 1996. Microwave techniques for the synthesis and deuteration of minerals, with particular reference to scorodite, $FeAsO_4 \cdot 2H_2O$, *Mineralogical Magazine*, 821.

Baron, D. and Palmer, C.D., 1996. Solubility of jarosite at 4–35 °C. *Geochimica et Cosmochimica Acta*, 60(2): 185-195.

Barrett, J., Ewart, D.K., Hughes, M.N. and Poole, R.K., 1993. Chemical and biological pathways in the bacterial oxidation of arsenopyrite. *FEMS Microbiology Reviews*, 11(1): 57-62.

Bissen, M. and Frimmel, F.H., 2003. Arsenic — a review. Part II: Oxidation of arsenic and its removal in water treatment. *Acta hydrochimica et hydrobiologica*, 31(2): 97-107.

Blesa, M.A. and Matijević, E., 1989. Phase transformations of iron oxides, oxohydroxides, and hydrous oxides in aqueous media. *Advances in Colloid and Interface Science*, 29(3): 173-221.

Bluteau, M.-C., Becze, L. and Demopoulos, G.P., 2009. The dissolution of scorodite in gypsum-saturated waters: Evidence of Ca–Fe–AsO_4 mineral formation and its impact on arsenic retention. *Hydrometallurgy*, 97(3): 221-227.

Bluteau, M.-C. and Demopoulos, G.P., 2007. The incongruent dissolution of scorodite — Solubility, kinetics and mechanism. *Hydrometallurgy*, 87(3–4): 163-177.

Bothe, J.V. and Brown, P.W., 1999. Arsenic immobilization by calcium arsenate formation. *Environmental Science & Technology*, 33(21): 3806-3811.

Bowell, R.J., 1994. Sorption of arsenic by iron oxides and oxyhydroxides in soils. *Applied Geochemistry*, 9(3): 279-286.

Boyle, R.W. and Jonasson, I.R., 1973. The geochemistry of arsenic and its use as an indicator element in geochemical prospecting. *Journal of Geochemical Exploration*, 2(3): 251-296.

Brandhuber, P. and Amy, G., 2001. Arsenic removal by a charged ultrafiltration membrane — influences of membrane operating conditions and water quality on arsenic rejection. *Desalination*, 140(1): 1-14.

Breed, A.W., Glatz, A., Hansford, G.S. and Harrison, S.T.L., 1996. The effect of As(III) and As(V) on the batch bioleaching of a pyrite-arsenopyrite concentrate. *Minerals Engineering*, 9(12): 1235-1252.

Brierley, J.A. and Brierley, C.L., 2001. Present and future commercial applications of biohydrometallurgy. *Hydrometallurgy*, 59(2): 233-239.

Brock, T.D., Brock, K.M., Belly, R.T. and Weiss, R.L., 1972. *Sulfolobus*: A new genus of sulfur-oxidizing bacteria living at low pH and high temperature. *Archiv für Mikrobiologie*, 84(1): 54-68.

Caetano, M.L., Ciminelli, V.S.T., Rocha, S.D.F., Spitale, M.C. and Caldeira, C.L., 2009. Batch and continuous precipitation of scorodite from dilute industrial solutions. *Hydrometallurgy*, 95(1): 44-52.

Chandraprabha, M.N., Modak, J.M., Natarajan, K.A. and Raichur, A.M., 2002. Strategies for efficient start-up of continuous biooxidation process for refractory gold ores. *Minerals Engineering*, 15(10): 751-753.

Chen, N., Jiang, D.T., Cutler, J., Kotzer, T., Jia, Y.F., Demopoulos, G.P. and Rowson, J.W., 2009. Structural characterization of poorly-crystalline scorodite, iron(III)–arsenate co-precipitates and uranium mill neutralized raffinate solids using X-ray absorption fine structure spectroscopy. *Geochimica et Cosmochimica Acta*, 73(11): 3260-3276.

Clark, D.A. and Norris, P.R., 1996. *Acidimicrobium ferrooxidans* gen. nov., sp. nov.: mixed-culture ferrous iron oxidation with *Sulfobacillus* species. *Microbiology*, 142(4): 785-790.

Clum, A., Nolan, M., Lang, E., Del Rio, T.G., Tice, H., Copeland, A., Cheng, J.-F., Lucas, S., Chen, F., Bruce, D., Goodwin, L., Pitluck, S., Ivanova, N., Mavromatis, K., Mikhailova, N., Pati, A., Chen, A., Palaniappan, K., Göker, M., Spring, S., Land, M., Hauser, L., Chang, Y.-J., Jeffries, C.C., Chain, P., Bristow, J., Eisen, J.A., Markowitz, V., Hugenholtz, P., Kyrpides, N.C., Klenk, H.-P. and Lapidus, A., 2009. Complete genome sequence of *Acidimicrobium ferrooxidans* type strain (ICPT). *Standards in Genomic Sciences*, 1(1): 38-45.

Corkhill, C.L., Wincott, P.L., Lloyd, J.R. and Vaughan, D.J., 2008. The oxidative dissolution of arsenopyrite (FeAsS) and enargite (Cu_3AsS_4) by *Leptospirillum ferrooxidans*. *Geochimica et Cosmochimica Acta*, 72(23): 5616-5633.

Cullen, W.R. and Reimer, K.J., 1989. Arsenic speciation in the environment. *Chemical Reviews*, 89(4): 713-764.

Dabekaussen, R., Droppert, D. and Demopoulos, G., 2001. Ambient pressure hydrometallurgical conversion of arsenic trioxide to crystalline scorodite. *CIM Bulletin*, 94: 116-122.

Daoud, J. and Karamanev, D., 2006. Formation of jarosite during Fe^{2+} oxidation by *Acidithiobacillus ferrooxidans*. *Minerals Engineering*, 19(9): 960-967.

da Silva, G., 2004. Kinetics and mechanism of the bacterial and ferric sulphate oxidation of galena. *Hydrometallurgy*, 75(1): 99-110.

Demopoulos, G.P., 2009. Aqueous precipitation and crystallization for the production of particulate solids with desired properties. *Hydrometallurgy*, 96(3): 199-214.

Demopoulos, G.P., Droppert, D.J. and Van Weert, G., 1995. Precipitation of crystalline scorodite ($FeAsO_4 \cdot 2H_2O$) from chloride solutions. *Hydrometallurgy*, 38(3): 245-261.

d'Hugues, P., Norris, P.R., Johnson, B., Grotowski, A., Chmielewski, T., Łuszczkiewic, A., Sadowski, Z., Sklodowska, A. and Farbiszewska, T., 2007. Presentation of the FP6 European Project Bioshale. Exploitation of black shale ores using biotechnologies-Polish case studies. *Physicochemical Problems of Mineral Processing*, 41: 373-386.

d'Hugues, P., Norris, P.R., Hallberg, K.B., Sánchez, F., Langwaldt, J., Grotowski, A., Chmielewski, T. and Groudev, S., 2008. Bioshale FP6 European project: Exploiting black shale ores using biotechnologies? *Minerals Engineering*, 21(1): 111-120.

Dinkla, I.J.T., Gonzalez-Contreras, P., Gahan, C.S., Weijma, J., Buisman, C.J.N., Henssen, M.J.C. and Sandström, Å., 2013. Quantifying microorganisms during biooxidation of arsenite and bioleaching of zinc sulfide. *Minerals Engineering*, 48: 25-30.

Dopson, M. and Lindström, E.B., 1999. Potential role of *Thiobacillus caldus* in arsenopyrite bioleaching. *Applied and Environmental Microbiology*, 65(1): 36-40.

Dove, P.M. and Rimstidt, J.D., 1985. The solubility and stability of scorodite, $FeAsO_4 \cdot 2H_2O$. *American Mineralogist*, 70(7-8): 838-844.

Duquesne, K., Lebrun, S., Casiot, C., Bruneel, O., Personné, J.-C., Leblanc, M., Elbaz-Poulichet, F., Morin, G. and Bonnefoy, V., 2003. Immobilization of arsenite and ferric iron by *Acidithiobacillus ferrooxidans* and its relevance to acid mine drainage. *Applied and Environmental Microbiology*, 69(10): 6165-6173.

Dutrizac, J.E. and Jambor, J.L., 1988. The synthesis of crystalline scorodite, $FeAsO_4 \cdot 2H_2O$. *Hydrometallurgy*, 19(3): 377-384.

Dutrizac, J.E., Jambor, J.L. and Chen, T.T., 1987. The behaviour of arsenic during jarosite precipitation: Reactions at 150°C and the mechanism of arsenic precipitation. *Canadian Metallurgical Quarterly*, 26(2): 103-115.

Ehrlich, H., 1964. Bacterial oxidation of arsenopyrite and enargite. *Economic Geology*, 59(7): 1306-1312.

EPA, 1994. EPA Method 1311. Toxicity Characteristic Leaching Procedure. Test methods for evaluating solid wastes physical/chemical methods. United States Environmental Protection Agency, Washington DC.

Escobar, B., Huenupi, E., Godoy, I. and Wiertz, J.V., 2000. Arsenic precipitation in the bioleaching of enargite by *Sulfolobus* BC at 70 °C. *Biotechnology Letters*, 22(3): 205-209.

Ferguson, J.F. and Gavis, J., 1972. A review of the arsenic cycle in natural waters. *Water Research*, 6(11): 1259-1274.

Fernandez, M.G.M., Mustin, C., de Donato, P., Barres, O., Marion, P. and Berthelin, J., 1995. Occurrences at mineral–bacteria interface during oxidation of arsenopyrite by *Thiobacillus ferrooxidans*. *Biotechnology and Bioengineering*, 46(1): 13-21.

Filippou, D. and Demopoulos, G.P., 1997. Arsenic immobilization by controlled scorodite precipitation. *JOM*, 49(12): 52-55.

Fujita, T., Taguchi, R., Abumiya, M., Matsumoto, M., Shibata, E. and Nakamura, T., 2008a. Effects of zinc, copper and sodium ions on ferric arsenate precipitation in a novel atmospheric scorodite process. *Hydrometallurgy*, 93(1–2): 30-38.

Fujita, T., Taguchi, R., Abumiya, M., Matsumoto, M., Shibata, E. and Nakamura, T., 2008b. Novel atmospheric scorodite synthesis by oxidation of ferrous sulfate solution. Part I. *Hydrometallurgy*, 90(2–4): 92-102.

Fujita, T., Taguchi, R., Abumiya, M., Matsumoto, M., Shibata, E. and Nakamura, T., 2008c. Novel atmospheric scorodite synthesis by oxidation of ferrous sulfate solution. Part II. Effect of temperature and air. *Hydrometallurgy*, 90(2–4): 85-91.

Fujita, T., Taguchi, R., Kubo, H., Shibata, E. and Nakamura, T., 2009. Immobilization of arsenic from novel synthesized scorodite-analysis on solubility and stability. *Materials Transactions*, 50(2): 321-331.

Fujita, T., Fujieda, S., Shinoda, K. and Suzuki, S., 2012. Various arsenic treatments in non-ferrous metallurgy and other potential applications, T.T. Chen Honorary Symposium on Hydrometallurgy, Electrometallurgy and Materials Characterization. John Wiley & Sons, Inc., 397-406.

Fuller, C.C., Davis, J.A. and Waychunas, G.A., 1993. Surface chemistry of ferrihydrite: Part 2. Kinetics of arsenate adsorption and coprecipitation. *Geochimica et Cosmochimica Acta*, 57(10): 2271-2282.

Gentina, J.C. and Acevedo, F., 2013. Application of bioleaching to copper mining in Chile. *Electronic Journal of Biotechnology*, 16(3): 16-16.

Gentina, J. and Acevedo, F., 2016. Copper Bioleaching in Chile. *Minerals*, 6(1): 23.

Giménez, J., Martínez, M., de Pablo, J., Rovira, M. and Duro, L., 2007. Arsenic sorption onto natural hematite, magnetite, and goethite. *Journal of Hazardous Materials*, 141(3): 575-580.

Gomez, M., Becze, L., Bluteau, M., Le Berre, J., Cutler, J. and Demopoulos, G., 2008. Autoclave precipitation and characterization of Fe (III)–AsO_4–SO_4 phases. *Hydrometallurgy*, 8: 1078.

Gomez, M.A., Assaaoudi, H., Becze, L., Cutler, J.N. and Demopoulos, G.P., 2010. Vibrational spectroscopy study of hydrothermally produced scorodite ($FeAsO_4 \cdot 2H_2O$), ferric arsenate sub-hydrate (FAsH; $FeAsO_4 \cdot 0.75H_2O$) and basic ferric arsenate sulfate (BFAS; $Fe[(AsO_4)_{1-x}(SO_4)_x(OH)_x] \cdot wH_2O$). *Journal of Raman Spectroscopy*, 41(2): 212-221.

Gomez, M.A., Becze, L., Celikin, M. and Demopoulos, G.P., 2011a. The effect of copper on the precipitation of scorodite ($FeAsO_4 \cdot 2H_2O$) under hydrothermal conditions: Evidence for a hydrated copper containing ferric arsenate sulfate-short lived intermediate. *Journal of Colloid and Interface Science*, 360(2): 508-518.

Gomez, M.A., Becze, L., Cutler, J.N. and Demopoulos, G.P., 2011b. Hydrothermal reaction chemistry and characterization of ferric arsenate phases precipitated from $Fe_2(SO_4)_3$–As_2O_5–H_2SO_4 solutions. *Hydrometallurgy*, 107(3): 74-90.

Gonzalez, V.E. and Monhemius, A., 1988. The mineralogy of arsenates relating to arsenic impurity control, Arsenic Metallurgy Fundamentals and Applications. The Minerals, *Metals and Materials Society*, 153-166.

Gonzalez-Contreras, P., Weijma, J., Weijden, R.v.d. and Buisman, C.J.N., 2010. Biogenic scorodite crystallization by *Acidianus sulfidivorans* for arsenic removal. *Environmental Science & Technology*, 44(2): 675-680.

Gonzalez-Contreras, P., Weijma, J. and Buisman, C.J.N., 2012a. Kinetics of ferrous iron oxidation by batch and continuous cultures of thermoacidophilic archaea at extremely low pH of 1.1–1.3. *Applied Microbiology and Biotechnology*, 93(3): 1295-1303.

González-Contreras, P., Weijma, J. and Buisman, C.J.N., 2012b. Continuous bioscorodite crystallization in CSTRs for arsenic removal and disposal. *Water Research*, 46(18): 5883-5892.

Gonzalez-Contreras, P., Weijma, J. and Buisman, C.J.N., 2012c. Bioscorodite Crystallization in an airlift reactor for arsenic removal. *Crystal Growth & Design*, 12(5): 2699-2706.

Gräfe, M., Nachtegaal, M. and Sparks, D.L., 2004. Formation of metal−arsenate precipitates at the goethite−water interface. *Environmental Science & Technology*, 38 (24): 6561-6570.

Hallberg, K.B. and Lindström, E.B., 1994. Characterization of *Thiobacillus caldus* sp. nov., a moderately thermophilic acidophile. *Microbiology*, 140(12): 3451-3456.

Harrington, J.M., Fendorf, S.E. and Rosenzweig, R.F., 1998. Biotic generation of arsenic(III) in metal(loid)-contaminated freshwater lake sediments. *Environmental Science & Technology*, 32(16): 2425-2430.

Harris, B., 2003. The removal of arsenic from process solutions: theory and industrial practice. *Hydrometallurgy 2003 Proceedings of the 5th International Symposium*: 1889-1902.

Harvey, M.C., Schreiber, M.E., Rimstidt, J.D. and Griffith, M.M., 2006. Scorodite dissolution kinetics: implications for arsenic release. *Environmental Science & Technology*, 40(21): 6709-6714.

Hawthorne, F., 1976. The hydrogen positions in scorodite. *Acta Crystallographica Section B*, 32(10): 2891-2892.

Hourn, M., Rohner, P., Bartsch, P. and Ngoviky, K., 2005. Benefits of using the Albion process for a North Queensland project and a case study of capital and operating cost benefits versus bacterial oxidation and pressure oxidation. Albion Process, Available at http://www.albionprocess.com/publications.html, 29.

Huang, C.P. and Vane, L.M., 1989. Enhancing As^{5+} removal by a Fe^{2+}-treated activated carbon. *Research Journal of the Water Pollution Control Federation*, 61(9-10): 1596-1603.

Huber, G., Spinnler, C., Gambacorta, A. and Stetter, K.O., 1989. *Metallosphaera sedula* gen, and sp. nov. represents a new genus of aerobic, metal-mobilizing, thermoacidophilic archaebacteria. *Systematic and Applied Microbiology*, 12(1): 38-47.

Huber, G. and Stetter, K.O., 1991. *Sulfolobus metallicus*, sp. nov., a novel strictly chemolithoautotrophic thermophilic archaeal species of metal-mobilizers. *Systematic and Applied Microbiology*, 14(4): 372-378.

Ivarson, K.C., 1973. Microbiological formation of basic ferric sulfates. *Canadian Journal of Soil Science*, 53(3): 315-323.

Jambor, J. and Dutrizac, J., 1998. Occurrence and constitution of natural and synthetic ferrihydrite, a widespread iron oxyhydroxide. *Chemical Reviews*, 98(7): 2549-2586.

Jiang, W., Lv, J., Luo, L., Yang, K., Lin, Y., Hu, F., Zhang, J. and Zhang, S., 2013. Arsenate and cadmium co-adsorption and co-precipitation on goethite. *Journal of Hazardous Materials*, 262, 55-63.

JOGMEC, 2016. Trends in the world of mining 2016: Finland (in Japanese).

Johnson, D.B., 1998. Biodiversity and ecology of acidophilic microorganisms. *FEMS Microbiology Ecology*, 27(4): 307-317.

Johnson, D.B., Joulian, C., d'Hugues, P. and Hallberg, K.B., 2008. *Sulfobacillus benefaciens* sp. nov., an acidophilic facultative anaerobic *Firmicute* isolated from mineral bioleaching operations. *Extremophiles*, 12(6): 789-798.

Kartinen Jr, E.O. and Martin, C.J., 1995. An overview of arsenic removal processes. *Desalination*, 103(1–2): 79-88.

Kato, T. and Miura, Y., 1977. The crystal structures of jarosite and svanbergite. *Mineralogical Journal*, 8(8): 419-430.

Kelly, T.D., Matos, G.R., Buckingham, D., DiFrancesco, C., Porter, K., Berry, C., Crane, M., Goonan, T. and Sznopek, J., 2005. Historical statistics for mineral and material commodities in the United States. Data Series 140, Arsenic Statics. US Geological Survey Reston, VA, United States.

Kim, M.-J. and Nriagu, J., 2000. Oxidation of arsenite in groundwater using ozone and oxygen. *Science of The Total Environment*, 247(1): 71-79.

Kitahama, K., Kiriyama, R. and Baba, Y., 1975. Refinement of the crystal structure of scorodite. *Acta Crystallographica Section B*, 31(1): 322-324.

Klaus, P.R., Jain, A. and Loeppert, R.H., 1998. Arsenite and arsenate adsorption on ferrihydrite: Kinetics, equilibrium, and adsorption envelopes. *Environmental Science & Technology*, 32(3): 344-349.

Koerdt, A., Gödeke, J., Berger, J., Thormann, K.M. and Albers, S.-V., 2010. Crenarchaeal biofilm formation under extreme conditions. *PLOS ONE*, 5(11): e14104.

Krause, E. and Ettel, V.A., 1988. Solubility and stability of scorodite, $FeAsO_4 \cdot 2H_2O$: new data and further discussion. *American Mineralogist*, 73: 850-854.

Krause, E. and Ettel, V.A., 1989. Solubilities and stabilities of ferric arsenate compounds. *Hydrometallurgy*, 22(3): 311-337.

Kubo, H., Abumiya, M. and Matsumoto, M., 2010. Dowa Mining Scorodite Process®—application to copper hydrometallurgy. Copper 2010, GDMB Society for Mining, Metallurgy, Resource and Environmental Technology, Hamburg, Germany, 7: 2947-2958.

Langhans, D., Lord, A., Lampshire, D., Burbank, A. and Baglin, E., 1995. Biooxidation of an arsenic-bearing refractory gold ore. *Minerals Engineering*, 8(1): 147-158.

Langmuir, D., Mahoney, J., MacDonald, A. and Rowson, J., 1999. Predicting arsenic concentrations in the porewaters of buried uranium mill tailings. *Geochimica et Cosmochimica Acta*, 63(19–20): 3379-3394.

Langmuir, D., Mahoney, J. and Rowson, J., 2006. Solubility products of amorphous ferric arsenate and crystalline scorodite ($FeAsO_4 \cdot 2H_2O$) and their application to arsenic behavior in buried mine tailings. *Geochimica et Cosmochimica Acta*, 70(12): 2942-2956.

Le Berre, J.F., Gauvin, R. and Demopoulos, G.P., 2007. Characterization of poorly-crystalline ferric arsenate precipitated from equimolar Fe(III)-As(V) solutions in the pH range 2 to 8. *Metallurgical and Materials Transactions B*, 38(5): 751-762.

Le Berre, J.F., Gauvin, R. and Demopoulos, G.P., 2008. A study of the crystallization kinetics of scorodite via the transformation of poorly crystalline ferric arsenate in weakly acidic solution. *Colloids and Surfaces A: Physicochemical and Engineering Aspects*, 315(1): 117-129.

Lebrun, E., Brugna, M., Baymann, F., Muller, D., Lièvremont, D., Lett, M.-C. and Nitschke, W., 2003. Arsenite oxidase, an ancient bioenergetic enzyme. *Molecular Biology and Evolution*, 20(5): 686-693.

Legal, J.M., Manfait, M. and Theophanides, T., 1991. Applications of FTIR spectroscopy in structural studies of cells and bacteria. *Journal of Molecular Structure*, 242: 397-407.

Leist, M., Casey, R.J. and Caridi, D., 2000. The management of arsenic wastes: problems and prospects. *Journal of Hazardous Materials*, 76(1): 125-138.

Li, B., Chen, Y., Liu, Q., Hu, S. and Chen, X., 2011. Complete genome analysis of *Sulfobacillus acidophilus* strain TPY, isolated from a hydrothermal vent in the Pacific Ocean. *Journal of Bacteriology*, 193(19): 5555-5556.

Lièvremont, D., Bertin, P.N. and Lett, M.-C., 2009. Arsenic in contaminated waters: Biogeochemical cycle, microbial metabolism and biotreatment processes. *Biochimie*, 91(10): 1229-1237.

Maddams, W.F., 1980. The scope and limitations of curve fitting. *Applied Spectroscopy*, 34(3): 245-267.

Mamindy-Pajany, Y., Hurel, C., Marmier, N. and Roméo, M., 2009. Arsenic adsorption onto hematite and goethite. *Comptes Rendus Chimie*, 12(8): 876-881.

Mandal, B.K. and Suzuki, K.T., 2002. Arsenic round the world: a review. *Talanta*, 58(1): 201-235.

Mandl, M., Matulová, P. and Dočekalová, H., 1992. Migration of arsenic (III) during bacterial oxidation of arsenopyrite in chalcopyrite concentrate by *Thiobacillus ferrooxidans*. *Applied Microbiology and Biotechnology*, 38(3): 429-431.

Matschullat, J., 2000. Arsenic in the geosphere — a review. *Science of The Total Environment*, 249(1): 297-312.

Melamud, V., Pivovarova, T., Tourova, T., Kolganova, T., Osipov, G., Lysenko, A., Kondrat'Eva, T. and Karavaiko, G., 2003. *Sulfobacillus sibiricus* sp. nov., a new moderately thermophilic bacterium. *Microbiology*, 72(5): 605-612.

Molnár, L.u., Virčíkova, E. and Lech, P., 1994. Experimental study of As(III) oxidation by hydrogen peroxide. *Hydrometallurgy*, 35(1): 1-9.

Monhemius, A.J. and Swash, P.M., 1999. Removing and stabilizing as from copper refining circuits by hydrothermal processing. *JOM*, 51(9): 30-33.

Moon, D.H., Dermatas, D. and Menounou, N., 2004. Arsenic immobilization by calcium–arsenic precipitates in lime treated soils. *Science of The Total Environment*, 330(1–3): 171-185.

Morishita, S., 2015. As(III) oxidation and immobilization from copper refinery wastewaters using thermo-achidophilic Fe(II)-oxidizing archaeon, *Acidianus brierleyi*. Master thesis, Kyushu University.

Myneni, S.C.B., Traina, S.J., Waychunas, G.A. and Logan, T.J., 1998. Vibrational spectroscopy of functional group chemistry and arsenate coordination in ettringite. *Geochimica et Cosmochimica Acta*, 62(21): 3499-3514.

Ning, R.Y., 2002. Arsenic removal by reverse osmosis. *Desalination*, 143(3): 237-241.

Okibe, N., Gericke, M., Hallberg, K.B. and Johnson, D.B., 2003. Enumeration and characterization of acidophilic microorganisms isolated from a pilot plant stirred-tank bioleaching operation. *Applied and Environmental Microbiology*, 69(4): 1936-1943.

Okibe, N. and Johnson, D., 2001. Bioleaching of pyrite by defined mixed cultures of moderately thermophilic acidophiles. *Process Metallurgy*, 11: 443-452.

Okibe, N. and Johnson, D.B., 2002. Toxicity of flotation reagents to moderately thermophilic bioleaching microorganisms. *Biotechnology Letters*, 24(23): 2011-2016.

Okibe, N. and Johnson, D.B., 2004. Biooxidation of pyrite by defined mixed cultures of moderately thermophilic acidophiles in pH‐controlled bioreactors: Significance of microbial interactions. *Biotechnology and Bioengineering*, 87(5): 574-583.

Okibe, N., Koga, M., Morishita, S., Tanaka, M., Heguri, S., Asano, S., Sasaki, K. and Hirajima, T., 2014. Microbial formation of crystalline scorodite for treatment of As(III)-bearing copper refinery process solution using *Acidianus brierleyi*. *Hydrometallurgy*, 143: 34-41.

Okibe, N., Koga, M., Sasaki, K., Hirajima, T., Heguri, S. and Asano, S., 2013. Simultaneous oxidation and immobilization of arsenite from refinery waste water by thermoacidophilic iron-oxidizing archaeon, *Acidianus brierleyi*. *Minerals Engineering*, 48: 126-134.

Okibe, N., Morishita, S., Tanaka, M., Sasaki, K., Hirajima, T., Hatano, K. and Ohata, A., 2017. Bioscorodite crystallization using *Acidianus brierleyi*: Effects caused by Cu(II) present in As(III)-bearing copper refinery wastewaters. *Hydrometallurgy*, 168: 121-126.

Ondruš, P., Skála, R., Viti, C., Veselovský, F., Novák, F. and Jansa, J., 1999. Parascorodite, $FeAsO_4 \cdot 2H_2O$—a new mineral from Kaňk near Kutná Hora, Czech Republic, *American Mineralogist*, 1439.

Oremland, R.S. and Stolz, J.F., 2005. Arsenic, microbes and contaminated aquifers. *Trends in Microbiology*, 13(2): 45-49.

Paktunc, D. and Bruggeman, K., 2010. Solubility of nanocrystalline scorodite and amorphous ferric arsenate: Implications for stabilization of arsenic in mine wastes. *Applied Geochemistry*, 25(5): 674-683.

Paktunc, D., Dutrizac, J. and Gertsman, V., 2008. Synthesis and phase transformations involving scorodite, ferric arsenate and arsenical ferrihydrite: Implications for arsenic mobility. *Geochimica et Cosmochimica Acta*, 72(11): 2649-2672.

Paktunc, D. and Dutrizac, J.E., 2003. Characterization of arsenate-for-sulfate substitution in synthetic jarosite using X-ray diffraction and X-ray absorption spectroscopy. *The Canadian Mineralogist*, 41(4): 905-919.

Panda, S., Akcil, A., Pradhan, N. and Deveci, H., 2015. Current scenario of chalcopyrite bioleaching: A review on the recent advances to its heap-leach technology. *Bioresource Technology*, 196: 694-706.

Peng, T.-J., Liu, L.-J., Liu, C., Yang, Z.-F., Liu, S.-J. and Jiang, C.-Y., 2015. *Metallosphaera tengchongensis* sp. nov., an acidothermophilic archaeon isolated from a hot spring. *International Journal of Systematic and Evolutionary Microbiology*, 65(2): 537-542.

Pradhan, N., Nathsarma, K.C., Srinivasa Rao, K., Sukla, L.B. and Mishra, B.K., 2008. Heap bioleaching of chalcopyrite: A review. *Minerals Engineering*, 21(5): 355-365.

Ravel, B. and Newville, M., 2005. ATHENA, ARTEMIS, HEPHAESTUS: data analysis for X-ray absorption spectroscopy using IFEFFIT. *Journal of Synchrotron Radiation*, 12(4): 537-541.

Regenspurg, S. and Peiffer, S., 2005. Arsenate and chromate incorporation in schwertmannite. *Applied Geochemistry*, 20 (6): 1226-1239.

Riveros, P.A., Dutrizac, J.E. and Spencer, P., 2001. Arsenic disposal practices in the metallurgical Industry. *Canadian Metallurgical Quarterly*, 40(4): 395-420.

Robins, R.G., 1987. Solubility and stability of scorodite, $FeAsO_4 \cdot 2H_2O$: Discussion. *American Mineralogist*, 72: 842-844.

Ruan, H.D., Frost, R.L., Kloprogge, J.T. and Duong, L., 2002. Infrared spectroscopy of goethite dehydroxylation: III. FT-IR microscopy of in situ study of the thermal transformation of goethite to hematite. *Spectrochimica Acta Part A: Molecular and Biomolecular Spectroscopy*, 58(5): 967-981.

Ruixia, L., Jinlong, G. and Hongxiao, T., 2002. Adsorption of fluoride, phosphate, and arsenate ions on a new type of ion exchange fiber. *Journal of Colloid and Interface Science*, 248(2): 268-274.

Sasaki, K. and Konno, H., 2000. Morphology of jarosite-group compounds precipitated from biologically and chemically oxidized Fe ions. *The Canadian Mineralogist*, 38(1): 45-56.

Savage, K.S., Bird, D.K. and O'Day, P.A., 2005. Arsenic speciation in synthetic jarosite. *Chemical Geology*, 215(1): 473-498.

Schnaitman, C. and Lundgren, D.G., 1965. Organic compounds in the spent medium of *Ferrobacillus ferrooxidans*. *Canadian journal of microbiology*, 11(1): 23-27.

Segerer, A., Neuner, A., Kristjansson, J.K. and Stetter, K.O., 1986. *Acidianus infernus* gen. nov., sp. nov., and *Acidianus brierleyi* Comb. nov.: Facultatively aerobic, extremely acidophilic thermophilic sulfur-metabolizing archaebacteria. *International Journal of Systematic and Evolutionary Microbiology*, 36(4): 559-564.

Sehlin, H.M. and Lindström, E.B., 1992. Oxidation and reduction of arsenic by *Sulfolobus acidocaldarius* strain BC. *FEMS Microbiology Letters*, 93(1): 87-92.

Sherman, D.M. and Randall, S.R., 2003. Surface complexation of arsenic(V) to iron(III) (hydr)oxides: structural mechanism from ab initio molecular geometries and EXAFS spectroscopy. *Geochimica et Cosmochimica Acta*, 67(22): 4223-4230.

Shibata, E., Onodera, N., Nakamura, T. and Abumiya, M., 2015. Method of producing crystalline iron arsenate from solution containing pentavalent arsenic. Japan patent JP2015-003852A.

Shivvers, D.W. and Brock, T.D., 1973. Oxidation of elemental sulfur by *Sulfolobus acidocaldarius*. *Journal of Bacteriology*, 114(2): 706-710.

Sing, K.S., Everett D.H., Haul R.A.W., Moscou L., Pierotti R.A., Rouquerol J., and Siemienewska T., 1985. Reporting physisorption data for gas/solid systems with special reference to the determination of surface area and porosity (Recommendations 1984). *Pure and applied chemistry*, 57(4): 603-619.

Singhania, S., Wang, Q., Filippou, D. and Demopoulos, G.P., 2005. Temperature and seeding effects on the precipitation of scorodite from sulfate solutions under atmospheric-pressure conditions. *Metallurgical and Materials Transactions B*, 36(3): 327-333.

Singhania, S., Wang, Q., Filippou, D. and Demopoulos, G.P., 2006. Acidity, valency and third-ion effects on the precipitation of scorodite from mixed sulfate solutions under atmospheric-pressure conditions. *Metallurgical and Materials Transactions B*, 37(2): 189-197.

Smedley, P.L. and Kinniburgh, D.G., 2002. A review of the source, behaviour and distribution of arsenic in natural waters. *Applied Geochemistry*, 17(5): 517-568.

Smith, A.M.L., Hudson-Edwards, K.A., Dubbin, W.E. and Wright, K., 2006. Dissolution of jarosite [$KFe_3(SO_4)_2(OH)_6$] at pH 2 and 8: Insights from batch experiments and computational modelling. *Geochimica et Cosmochimica Acta*, 70(3): 608-621.

Suzuki, T., Iwasaki, T., Uzawa, T., Hara, K., Nemoto, N., Kon, T., Ueki, T., Yamagishi, A. and Oshima, T., 2002. *Sulfolobus tokodaii* sp. nov. (f. *Sulfolobus* sp. strain 7), a new member of the genus *Sulfolobus* isolated from Beppu Hot Springs, Japan. *Extremophiles*, 6(1): 39-44.

Swash, P. and Monhemius, A., 1995. Synthesis, characterization and solubility testing of solids in the Ca-Fe-AsO_4 system, Sudbury'95, Conference on Mining and the Environment, Sudbury, Ontario, 17-28.

Swash, P., Monhemius, A. and Schaekers, J. (Eds.), 2000. Solubilities of process residues from biological oxidation pretreatments of refractory gold ores. Minor Elements 2000. Society of Mining, Metallurgy, and Exploraton, Littleton, CO, United States, 115-122.

Tanaka, M., Yamaji, Y., Fukano, Y., Shimada, K., Ishibashi, J.-I., Hirajima, T., Sasaki, K., Sawada, M. and Okibe, N., 2015. Biooxidation of gold-, silver, and antimony-bearing highly refractory polymetallic sulfide concentrates, and its comparison with abiotic pretreatment techniques. *Geomicrobiology Journal*, 32(6): 538-548.

Tanaka, M., Hirajima, T., Sasaki, K. and Okibe, N., 2017. Optimization of bioscorodite crystallization for treatment of As(III)-bearing wastewaters. *Solid State Phenomena*, 262: 555-558.

Tanaka, M., 2017. A comparison study of heap bioleaching sites in Chile and Finland for further development of biotechnology for mining. *Evergreen*, 4(4): 1-7.

Tanaka M. and Okibe, N., 2018. Factors to enable crystallization of environmentally-stable bioscorodite from dilute As(III)-contaminated waters. *Minerals*, 8(1): 23.

Tomioka, Y., Hiroyoshi, N. and Tsunekawa, M., 2005. Recent topics on environmental contamination caused by minerals containing arsenic and its remediation—arsenic dissolution and stabilization in mine tailing dumps—. *Resources Processing*, 52(3): 145-150.

Travisany, D., Di Genova, A., Sepúlveda, A., Bobadilla-Fazzini, R.A., Parada, P. and Maass, A., 2012. Draft genome sequence of the *Sulfobacillus thermosulfidooxidans* Cutipay strain, an indigenous bacterium isolated from a naturally extreme mining environment in Northern Chile. *Journal of Bacteriology*, 194(22): 6327-6328.

Tuovinen, O.H., Bhatti, T.M., Bigham, J.M., Hallberg, K.B., Garcia, O. and Lindström, E.B., 1994. Oxidative dissolution of arsenopyrite by mesophilic and moderately thermophilic acidophiles. *Applied and Environmental Microbiology*, 60(9): 3268-3274.

Twidwell, L., 2011. The removal of arsenic, selenium and metals from aqueous solution by iron precipitation and reduction techniques, TMS2011 Annual Meeting, San Diego, CA.

Twidwell, L., Robins, R. and Hohn, J., 2005. The removal of arsenic from aqueous solution by coprecipitation with iron (III). *Arsenic Metallurgy*: 3-24.

Twidwell, L.G. and McCloskey, J.W., 2011. Removing arsenic from aqueous solution and long-term product storage. *JOM*, 63: 94-100.

Valdes, J., Quatrini, R., Hallberg, K., Dopson, M., Valenzuela, P.D. and Holmes, D.S., 2009. Draft genome sequence of the extremely acidophilic bacterium *Acidithiobacillus caldus* ATCC 51756 reveals metabolic versatility in the genus *Acidithiobacillus*. *Journal of Bacteriology*, 191(18): 5877-5878.

Van Aswegen, P.C., Van Niekerk, J. and Olivier, W., 2007. The BIOX™ process for the treatment of refractory gold concentrates, Biomining. Springer, 1-33.

Watanabe, H., Gutleben, C.D. and Seto, J.e., 1994. Sulfate ions on the surface of maghemite and hematite. *Solid State Ionics*, 69(1): 29-35.

Waychunas, G.A., Davis, J.A. and Fuller, C.C., 1995. Geometry of sorbed arsenate on ferrihydrite and crystalline FeOOH: Re-evaluation of EXAFS results and topological factors in predicting sorbate geometry, and evidence for monodentate complexes. *Geochimica et Cosmochimica Acta*, 59(17): 3655-3661.

Waychunas, G.A., Rea, B.A., Fuller, C.C. and Davis, J.A., 1993. Surface chemistry of ferrihydrite: Part 1. EXAFS studies of the geometry of coprecipitated and adsorbed arsenate. *Geochimica et Cosmochimica Acta*, 57(10): 2251-2269.

Weert, G.V. and Droppert, D.J., 1994. Aqueous processing of arsenic trioxide to crystalline scorodite. *JOM*, 46(6): 36-38.

Weijma, J., Gonzàles-Contreras, P. and Buisman, C.N., 2017. Chemical vs. biological crystals, all the same? *Solid State Phenomena*, 559-562.

Welch, S.A., Kirste, D., Christy, A.G., Beavis, F.R. and Beavis, S.G., 2008. Jarosite dissolution II—Reaction kinetics, stoichiometry and acid flux. *Chemical Geology*, 254(1): 73-86.

WHO, 2001. IPCS environmental health criteria 224 arsenic and arsenic compounds. Geneva: International Program on Chemical Safety. World Health Organization.

Wiertz, J.V., Mateo, M. and Escobar, B., 2006. Mechanism of pyrite catalysis of As(III) oxidation in bioleaching solutions at 30 °C and 70 °C. *Hydrometallurgy*, 83(1): 35-39.

William, H., 2004. Producing Copper Nature's Way: Bioleaching. Available at https://www.copper.org/publications/newsletters/innovations/2004/05/producing_copper_natures_way_bioleaching.html.

William, R.R., Loan, M., Morton, J. and Parkinson, G.M., 2004. Arsenic removal from aqueous solution via ferrihydrite crystallization control. *Environmental Science & Technology*, 38(8): 2368-2372.

Zaulochnyi, P., Bulaev, A., Savari, E., Pivovarova, T., Kondratieva, T. and Sedelnikova, G., 2011. Two-stage process of bacterial-chemical oxidation of refractory pyrite-arsenopyrite gold-bearing concentrate. *Applied biochemistry and microbiology*, 47(9): 833-840.

Acknowledgements

First of all, I would like to express my most sincere gratitude to my supervisor, Assoc. Prof. Naoko Okibe for her constant encouragement and guidance. During my master's and PhD course, she spent so much precious time and energy on my research, presentation practice and paper writing. I could not finish this work without her support. It is my honor to be her student.

I also would like to express my deep appreciation to Prof. Tsuyoshi Hirajima and Prof. Keiko Sasaki for their valuable suggestion for this thesis and presentations at conferences. Their comments have provided me helpful directions. I am really grad to study in Mineral Processing, Recycling and Environmental Remediation Laboratory led by them.

I would like to thank Prof. Hiroaki Nakano from Department of Materials Science and Engineering, Kyushu University as a part of my thesis committee, for his invaluable comments and warm encouragements.

My appreciation goes to also Assoc. Prof. Hajime Miki for his technical advices, insightful comments and kind supports in my GA life, and Assist. Prof. Moriyasu Nonaka for technical advices. I also wish to acknowledge our secretary Mrs. Makiko Semba. This study could not be completed without her kind supports.

I would like to express my appreciation to Advanced Graduate Program in Global Strategy for Green Asia for providing me with meaningful opportunities to learn a relationship between technologies and society. I would like to show my appreciation to Assoc. Prof. Junichiro Ishibashi and Mr. Kazuhiko Shimada (Department of Earth and Planetary Sciences, Graduate School of Science, Kyushu University), Dr. Fumio Inagaki, Dr. Tatsuhiko Hoshino, Dr. Akira Ijiri (Japan Agency for Marine-Earth Science and Technology; JAMSTEC), Dr. Himawan Tri Bayu Murti

Petrus, Ms. Wulaningrum Slamet Riyadi (Gadjah Mada University), Dr. Naoaki Kataoka, Dr. Takao Hagino and Mr. Sen Shimamoto (Swing Corporation) for giving me the valuable opportunity of the internship, and for taking care of me.

I am also grateful to Assist. Prof. Takahiro Funatsu, Ms. Miwa Hirashima and Ms. Minako Matsue in GA Program, who gave me kind supports and encouragement.

In biooxidation study, I would like to show my acknowledgment to Sumitomo Metal Mining Co., Ltd. for providing us with arsenopyrite concentrates, cyanide leaching, sample analysis, and giving advice about experimental methods.

In bioscorodite study, I would like to show my acknowledgment to JX Nippon Mining & Metals Co., Ltd. for giving me advice for experimental policy.

The writing of this thesis was made possible through the scholarship provided by the Advanced Graduate Program in Global Strategy for Green Asia, and partial financial supports to Assoc. Prof. Naoko Okibe from JSPS KAKENHI (JP24760689, JP15H02333) and Kurita Water and Environmental Foundation (14A040, 15K002). I would like to acknowledge here the generosity of these organizations.

These acknowledgements would not be complete without mentioning postdoctoral researchers, my seniors, juniors and colleagues in Minepro lab, GA program, and UGM. I spent the majority of time with the members, and shared very enjoyable time with them. Many thanks for sharing your time with me.

Last but not the least, I really appreciate my parents, Hirofumi Tanaka and Mieko Tanaka for their support and warm encouragements.

March, 2018

Masahito Tanaka